

UC Irvine

UC Irvine Electronic Theses and Dissertations

Title

Collagenomics of tissue-engineered cartilage regeneration

Permalink

<https://escholarship.org/uc/item/0qr2z0fb>

Author

Bielajew, Benjamin

Publication Date

2022

Peer reviewed|Thesis/dissertation

UNIVERSITY OF CALIFORNIA

IRVINE

Collagenomics of tissue-engineered cartilage regeneration

DISSERTATION

submitted in partial satisfaction of the requirements for the degree of

DOCTOR OF PHILOSOPHY

in Biomedical Engineering

by

Benjamin Jacob Bielajew

Dissertation Committee:

Distinguished Professor Kyriacos Athanasiou, Chair

Program Manager Jerry Hu

Professor Wendy Liu

2022

Chapter 1 © 2020 Springer Nature

Chapter 2 © 2021 Elsevier Ltd.

Chapter 3 © 2021 SAGE Publications Ltd.

Chapter 4 © 2022 Acta Materialia Inc.

Appendix A © 2020 Acta Materialia Inc.

Appendix B © 2022 Mary Ann Liebert, Inc.

All other materials © 2022 Benjamin Jacob Bielajew

To my parents, Alex Bielajew and Karen Vineberg
for fostering a deep love of science in me from the very beginning

TABLE OF CONTENTS

LIST OF FIGURES	xiii
LIST OF TABLES	xvii
ACKNOWLEDGEMENTS	xix
VITA	xxi
ABSTRACT OF THE DISSERTATION	xxii
INTRODUCTION	1
CHAPTER 1 Collagen: quantification, biomechanics, and role of minor subtypes in cartilage	7
Abstract	7
Introduction	7
Collagens and collagen crosslinks	9
Identification and quantification	12
Traditional assays	12
Quantitative antibody-based assays	14
Collagen imaging and spectroscopy	15
Quantification with mass spectrometry	17
Collagens in cartilage	19
Classification of cartilage	21
Cartilage degeneration and therapies	22
Collagen subtypes in cartilage	24
Collagen and mechanical properties	33
Outlook	35
Characterization in disease states	36

Biomechanical relationships.....	37
Screening for engineered therapeutics.....	37
Collagens for engineering neocartilages	38
References.....	40
CHAPTER 2 Knee orthopaedics as a template for the temporomandibular joint.....	53
Abstract	53
Introduction	53
Pathology	57
The TMJ requires improved diagnostic modalities despite similarities in osteoarthritis progression.....	57
TMJ disorders are more prevalent in women	58
The anatomical challenge of sensory structures near the TMJ versus the knee.....	58
Current clinical practices	59
Divergence of end-stage treatment strategies for osteoarthritis of the knee and TMJ	59
Training disparities between knee and TMJ surgeons.....	60
From incidence to clinic: gender imbalances in physician populations and clinical trials.....	61
Commercial products.....	63
Joint prostheses: successes in the knee and catastrophic setbacks in the TMJ.....	63
The TMJ field trails the progress of tissue engineering in the knee	64
Future directions.....	65
The vicious cycle of translating TMJ research.....	65
Increasing the quantity of rigorous TMJ research.....	66

Bolstering training opportunities for researchers and physicians	68
Narrowing and specifying indications for TMDs toward establishing the commercial landscape for TMJ cartilage products.....	69
Implementing industry guidance for treatment of TMJ cartilages.....	71
Conclusion	72
References.....	73
CHAPTER 3 Methodology to quantify collagen subtypes and crosslinks: application in minipig cartilages	80
Abstract	80
Introduction	81
Methods	83
LC-MS/MS for collagen subtype quantification.....	83
Quantification of collagen crosslinks and hydroxyproline.....	84
Bottom-up proteomics.....	84
Data analysis and statistical analysis	85
Sample preparation.....	86
Results	88
LC-MS assays for collagen subtypes and crosslinks.....	88
Bottom-up proteomics analysis	94
Histology	95
Discussion.....	96
References.....	102

CHAPTER 4 Proteomic, mechanical, and biochemical characterization of cartilage development.....	105
Abstract	105
Introduction	106
Methods	108
Sample collection.....	108
Histology	110
Mechanical testing	110
Photometric biochemical assays for total collagen, GAG, and DNA content.....	110
Fluorophore assisted carbohydrate electrophoresis (FACE)	111
Crosslink quantification and bottom-up proteomics	111
Statistical analysis.....	112
Results	112
Histology	112
Mechanical testing	113
Biochemical content.....	115
Crosslinks analysis	115
Bottom-up proteomics	119
Discussion	119
References.....	124
Supplementary materials	127
CHAPTER 5 Proteomic, mechanical, and biochemical development of tissue-engineered neocartilage.....	129

Abstract	129
Introduction	129
Methods	132
Costal cartilage harvest and isolation	132
Costal chondrocyte expansion and aggregate rejuvenation	132
Neocartilage self-assembly and bioactive factor treatment.....	133
Sample preparation.....	134
Histology	134
Mechanical testing	135
Collagen, GAG, and DNA assays	135
Fluorophore assisted carbohydrate electrophoresis (FACE)	135
Collagen crosslink quantification	136
Bottom-up proteomics	136
Statistical analysis.....	137
Results	137
Neocartilage histology	137
Mechanical properties	139
Biochemical properties.....	141
Crosslink quantification	141
Bottom-up proteomic analysis.....	144
Discussion	144

References.....	150
Supplementary materials.....	153
CHAPTER 6 Long-term safety and efficacy of temporomandibular joint disc regeneration in the Yucatan minipig.....	156
Abstract.....	156
Introduction.....	157
Results.....	160
Tissue-engineered implants approached native tissue values, and the intralaminar perforation surgical technique secured tissue-engineered implants in the Yucatan minipig TMJ disc.....	161
Perforation defects in the TMJ disc healed with tissue-engineered implants.....	163
Tissue-engineered implants facilitated regeneration of mechanically robust repair tissue that reached native TMJ disc tensile properties.....	165
Repair tissue of implant-treated discs mimicked the native TMJ disc biochemical content.....	166
Implantation of tissue-engineered neocartilages resulted in no abnormal systemic effects.....	167
Tissue-engineered implants were well-tolerated immunologically.....	168
Tissue-engineered implants remodeled to a native-like tissue.....	172
Discussion.....	174
Materials and methods.....	180
Tissue engineering of implants.....	180
In vivo experiments.....	182

Presurgical medication and anesthesia.....	182
Surgical implantation and defect creation.....	182
Postoperative medication and animal care.....	184
Animal euthanasia	184
TMJ sample preparation	184
In vitro sample preparation.....	185
Histology and immunohistochemistry	185
Mechanical testing	186
Biochemical testing	187
Mass spectrometry analyses for crosslinks quantification and bottom-up proteomics	187
ICRS scoring.....	187
Statistical analyses	188
References.....	188
Supplementary materials.....	191
CHAPTER 7 Tissue-engineered implants regenerate large perforations in the Yucatan minipig temporomandibular joint disc	208
Abstract.....	208
Introduction	209
Results	211
Tissue-engineered implants were suitable for implantation	211
The intralaminar perforation surgical technique was successful in securing implants in large perforation defects	212
Implants achieved tissue regeneration after 8 weeks; controls did not heal.....	215

Regenerated tissue, only present in implant-treated discs, displayed robust tensile properties	217
Regenerated tissue biochemical and proteomic composition was reminiscent of native TMJ discs	217
Tissue adjacent to perforations in controls deviated from native TMJ disc composition....	221
Implants remodeled, exhibiting biochemical and proteomic contents similar to native TMJ discs	221
Implants exhibited safety, as shown by no adverse systemic response and minimal local response	226
Discussion	229
Materials and methods	233
Tissue engineering of implants.....	233
In vivo experiments	235
Presurgical medication and anesthesia.....	235
Surgical implantation and defect creation.....	236
Postoperative medication and animal care.....	237
Animal euthanasia	237
Sample preparation.....	238
Histology	238
Mechanical testing	238
Biochemical testing	239
Mass spectrometry analyses for crosslinks quantification and bottom-up proteomics	239

Statistical analyses	240
References	240
Supplementary materials	243
CONCLUSIONS AND FUTURE DIRECTIONS.....	248
APPENDIX A Engineering self-assembled neomenisci through combination of matrix augmentation and directional remodeling	254
Abstract	254
Introduction	254
Materials and methods	257
Chondrocyte and meniscus cell isolation	257
Self-assembly and culture of constructs	258
Treatments.....	258
Tissue gross morphology, histology, and macroscopic characterization.....	259
Tensile and compressive testing	259
Analysis of tissue biochemical content	260
Statistical analysis.....	261
Results	261
Gross morphology, histology, and immunohistochemistry	262
Tissue biomechanics	263
Tissue biochemistry	264
Tissue organization.....	264
Discussion	266
References	271

APPENDIX B The effect of neonatal, juvenile, and adult donors on rejuvenated neocartilage functional properties.....	275
Abstract	275
Introduction	276
Materials and methods	280
Costal cartilage harvest and isolation.....	280
Chondrocyte expansion and aggregate rejuvenation	281
Neocartilage self-assembly	282
Sample processing and photometric biochemical analysis.....	282
Pyridinoline mass spectrometry analysis.....	283
Bottom-up mass spectrometry proteomic analysis	284
Mechanical testing and analysis.....	284
Histological processing and staining	285
Statistical analyses	285
Results	285
Gross morphology and histology.....	285
Biochemical and proteomic properties	288
Mechanical properties	288
Discussion	290
References.....	294

LIST OF FIGURES

Chapter 1. Collagen: quantification, biomechanics, and role of minor subtypes in cartilage

Figure 1. Collagen types of the human body	8
Figure 2. Lysyl oxidase pathway	10
Figure 3. Examples of quantitative assays for collagen and collagen crosslinks.....	13
Figure 4. Collagen structure and location in cartilage, and its role in cartilage development.....	20
Figure 5. Functional groups of collagen subtypes in cartilage	25
Figure 6. Broad applications for high-throughput, low-cost collagen quantification	35

Chapter 2. Knee orthopaedics as a template for the temporomandibular joint

Figure 1. Knee and TMJ anatomy and proximity to crucial sensory structures	54
Figure 2. Clinical practices for the knee and TMJ.....	62
Figure 3. The vicious cycle of TMJ translational research	66

Chapter 3. Methodology to quantify collagen subtypes and crosslinks: application in minipig cartilages

Figure 1. The locations of the different cartilages harvested from the Yucatan minipig.....	87
Figure 2. Collagen subtype quantification in the cartilages of the Yucatan minipig	89
Figure 3. Crosslink quantification in the cartilages of the Yucatan minipig.....	91
Figure 4. Histological stains on minipig cartilages	95

Chapter 4. Proteomic, mechanical, and biochemical characterization of cartilage development

Figure 1. Sample collection diagram	108
Figure 2. Representative histology and gross morphology images for porcine articular cartilage of different developmental ages	113
Figure 3. Mechanical results for porcine articular cartilage of different developmental ages....	114
Figure 4. Biochemical results for porcine articular cartilage of different developmental ages...	116
Figure 5. Crosslink quantification results for porcine articular cartilage of different developmental ages.....	117
Figure 6. Bottom-up proteomic results for porcine articular cartilage of different developmental ages.....	118

Chapter 5. Proteomic, mechanical, and biochemical development of tissue-engineered neocartilage

Figure 1. The tissue-engineering process using costal chondrocytes and neocartilage sample preparation..... 133

Figure 2. Histology and gross morphology of neocartilage constructs..... 137

Figure 3. Mechanical properties of neocartilage constructs 138

Figure 4. Biochemical composition of neocartilage constructs..... 140

Figure 5. Collagen crosslink composition of neocartilage constructs 142

Figure 6. Bottom-up proteomics analysis of neocartilage constructs 143

Chapter 6. Long-term safety and efficacy of temporomandibular joint disc regeneration in the Yucatan minipig

Figure 1. Neocartilages were fabricated using the self-assembling process and exhibited robust matrix content for implantation into the TMJ disc..... 160

Figure 2. The intralaminar perforation surgical technique secured tissue-engineered implants in perforation defects 162

Figure 3. Gross morphology and histological cross sections of TMJ discs showed lack of complete healing in controls and repair tissue in implant-treated groups 164

Figure 4. Tensile properties of repair tissue of implant-treated discs were higher compared to fill tissue of controls 165

Figure 5. Collagens in the matrix of repair tissue was reminiscent of native TMJ disc content 166

Figure 6. Heatmap of normalized complete blood count and comprehensive metabolic panel parameters show no abnormal systemic effects..... 169

Figure 7. Immunohistochemical staining for T cells, B cells, and macrophages showed immunogenic tolerance to tissue-engineered implants..... 170

Figure 8. Histological and biochemical properties of neocartilages after implantation showed remodeling toward native TMJ discs 171

Figure 9. Bottom-up proteomic analysis of neocartilages after implantation also showed remodeling toward native TMJ disc content 172

Supplementary Figure 1. Depiction of the surgical placement of the incision, defect, and implant 191

Supplementary Figure 2. Short-term gross morphology of implant-treated TMJ discs..... 192

Supplementary Figure 3. Gross morphology of all discs in the long-term study..... 192

Supplementary Figure 4. Gross morphology and mediolateral histological cross sections of condyles.....	193
Supplementary Figure 5. The synovium of empty defect and implant-treated TMJs.....	194
Supplementary Figure 6. Controls for immunohistochemical staining.....	195
Supplementary Figure 7. TMJ disc sample preparation and excision.....	196

Chapter 7. Tissue-engineered implants regenerate large perforations in the Yucatan minipig temporomandibular joint disc

Figure 1. Tissue-engineered implants were suitable for nonhomologous usage in the TMJ disc	212
Figure 2. The intralaminar perforation technique secured implants in place toward regeneration of large perforation defects.....	213
Figure 3. Control discs and condyles showed degenerative changes compared to implant-treated discs and condyles after 8 weeks.....	214
Figure 4. Implant-treated discs exhibited regeneration in the centrolateral region of the TMJ disc, and controls displayed lack of healing.....	215
Figure 5. Defect perimeter and area after 8 weeks of implantation were higher in controls	216
Figure 6. Regenerated tissue tensile properties approached native tissue values.....	218
Figure 7. Biochemical and crosslink content of regenerated tissue recapitulated native TMJ disc content.....	219
Figure 8. Adjacent tissue to control perforations deviated from native tissue in biochemical and crosslink content.....	220
Figure 9. Histology of neocartilage implanted for 8 weeks displayed similarities to native TMJ discs	222
Figure 10. Biochemical properties of implants after 8 weeks remodeled toward native tissue values	223
Figure 11. Crosslink content after 8 weeks remodeled toward native tissue values.....	224
Figure 12. Proteomic analytes after 8 weeks of implantation further approached native tissue values	225
Figure 13. Heatmap of normalized complete blood count and comprehensive metabolic panel parameters showed no abnormal systemic effects due to implants.....	227
Figure 14. H&E revealed moderate cellular response to TMJ disc implants	228

Appendix A. Engineering self-assembled neomenisci through combination of matrix augmentation and directional remodeling

Figure 1. Gross morphology and histological staining of self-assembled neomenisci261
Figure 2. Mechanical properties of neomenisci263
Figure 3. Biochemical properties of self-assembled neomenisci265
Figure 4. TCL+LPA treatment enhances anisotropy265

Appendix B. The effect of neonatal, juvenile, and adult donors on rejuvenated neocartilage functional properties

Figure 1. Costal cartilage harvest and isolation and the tissue engineering process280
Figure 2. Gross morphology and histology of neocartilage constructs286
Figure 3. Biochemical properties of neocartilage constructs287
Figure 4. Proteomic analysis of neocartilage constructs287
Figure 5. Mechanical properties of neocartilage constructs289

LIST OF TABLES

Chapter 1. Collagen: quantification, biomechanics, and role of minor subtypes in cartilage

Table 1. Classically defined groups of collagen subtypes.....	9
Table 2. The collagen subtypes of cartilage	26

Chapter 2. Knee orthopaedics as a template for the temporomandibular joint

Table 1. Comparison of the knee and TMJ fields	55
--	----

Chapter 3. Methodology to quantify collagen subtypes and crosslinks: application in minipig cartilages

Table 1. Mass spectrometry settings for target analytes.....	84
Table 2. Bottom-up proteomics results on Yucatan minipig cartilages.....	92
Table 3. Comparison of collagen assays.....	97

Chapter 4. Proteomic, mechanical, and biochemical characterization of cartilage development

Supplementary Table 1. Bottom-up proteomics results on porcine knee cartilage.....	127
--	-----

Chapter 5. Proteomic, mechanical, and biochemical development of tissue-engineered neocartilage

Supplementary Table 1. Additional mechanical outcomes of neocartilage constructs	153
Supplementary Table 2. Bottom-up proteomics analytes of neocartilage constructs	153

Chapter 6. Long-term safety and efficacy of temporomandibular joint disc regeneration in the Yucatan minipig

Supplementary Table 1. Osteoarthritis scores of condyles	197
Supplementary Table 2. Tensile properties of intralaminar fusion	197
Supplementary Table 3. Crosslinks in the fill and repair tissues.	197
Supplementary Table 4. Bottom-up proteomics data for all tissues	198
Supplementary Table 5. Raw values for the complete blood count and comprehensive metabolic panel parameters	200
Supplementary Table 6. Crosslinks in the implants after extended culture or implantation.....	207
Supplementary Table 7. Compressive properties of neocartilage.....	207
Supplementary Table 8. Immunohistochemistry parameters	207

Chapter 7. Tissue-engineered implants regenerate large perforations in the Yucatan minipig temporomandibular joint disc

Supplementary Table 1. Intralaminar fusion metrics.....243
Supplementary Table 2. Bottom-up proteomics raw data243
Supplementary Table 3. Dry weight crosslink normalizations and biochemical data for regenerated tissue245
Supplementary Table 4. Dry weight crosslink normalizations and biochemical data for adjacent tissue245
Supplementary Table 5. Compressive properties of implants cultured in vitro245
Supplementary Table 6. Raw complete blood count and complete metabolic panel data.....246

Appendix A. Engineering self-assembled neomenisci through combination of matrix augmentation and directional remodeling

Table 1. Morphological properties of neomenisci262

Appendix B. The effect of neonatal, juvenile, and adult donors on rejuvenated neocartilage functional properties

Table 1. Morphological properties of neocartilage constructs286

ACKNOWLEDGEMENTS

My professional and personal growth throughout graduate school has been truly transformative, and I owe a deep debt of gratitude to the people who have supported me along the way. I would first like to thank Dr. Kyriacos Athanasiou, my advisor and principal investigator, for his excellent mentorship. Dr. Athanasiou ingrained a deep sense of scientific rigor and integrity within me that will never falter. His wisdom and high standards of excellence have truly fueled my passion for biomedical research, and he sets a wonderful example as a professor that I hope to emulate in my future career. I would also like to thank Dr. Jerry Hu for his mentorship. Jerry's creativity and feedback were invaluable. To Dr. Athanasiou and Jerry — I could not have asked for better mentors, and I will always be grateful to both of you.

My first research experience was as a high school student, where I was a summer student in Dr. Felix Feng's laboratory at the University of Michigan. I am very thankful to Dr. Feng, Kari, and Sumin for introducing me to the world of biomedical research. When I was an undergraduate student at the University of Michigan, Dr. Joan Greve's passion for teaching and research inspired me. While I do not think I could ever perform cartwheels as a demonstration of dynamic biomechanics as she did, I will do my best to model Joan's enthusiasm and respect for students. At U of M, I was mentored by Dr. David Kohn and one of his DDS/PhD students, Dr. Genevieve Romanowicz. I am incredibly grateful to Dr. Kohn for supporting me as an undergraduate researcher, and to Genny for teaching me crucial skills such as differentiating mesenchymal stem cells, running samples on high performance liquid chromatography, and cooking delicious food.

Throughout my graduate studies at UCI, several faculty, staff, and institutions were crucial to the success of my work. Dr. Felix Grun and Benjamin Katz of the UCI Mass Spectrometry Facility were indispensable; Dr. Grun's and Ben's infectious passion for analytical chemistry were key to the development of my mass spectrometry methods. I would like to express gratitude to collaborators of our laboratory who I worked with throughout my PhD: Dr. Wendy Liu at UC Irvine,

a member of my dissertation committee, who developed my grantsmanship skills through the immunology and tissue engineering collaborations; Dr. Sriram Eleswarapu at UCLA, who shared exciting directions of medical and biomedical engineering research with me; and Dr. Natalia Vapniarsky-Arzi and Dr. Boaz Arzi at UC Davis, who were crucial to the success of the *in vivo* portions of this dissertation. I would also like to acknowledge the National Institute of Arthritis and Musculoskeletal and Skin Diseases and the National Institute of Dental and Craniofacial Research for funding my research at UC Irvine. Chapters 1, 2, 3, and 4 were published in the journals *Nature Reviews Materials*, *Cell Reports Medicine*, *Cartilage*, and *Acta Biomaterialia*, respectively, and Appendices A and B were published in the journals *Acta Biomaterialia* and *Tissue Engineering Part A*, respectively. All of these journals permit republication of articles in dissertations.

I feel incredibly fortunate to have conducted research in a laboratory with an excellent group of graduate students and postdoctoral scholars. Wendy, Heenam, Rachel, Gaby, Nathan, Jarrett, Evelia, Erik, Gaston, and Ryan, you have taught me so much since I first joined the laboratory, and I am very grateful for our professional and personal relationships. Another fantastic group of people I worked with are the Right To Know and Challenging All Men to Prevent Sexism peer education groups through the UCI CARE office. Rosanna, Melissa, Kaeleigh, Eli, and my RTK/ChAMPS folks, you have taught me so much. Thank you for everything you do.

Finally, I would like to express deep gratitude to my friends and family that kept me balanced and motivated throughout this work. To Daniel, Sam, Jordan, and Johanna, thank you for your long-lasting deep friendship that I will always cherish. To Ryan, Holly, Austin, Evelia, Gaston, Maca, Lila, Chris, and Amy, thank you for making UCI feel like home. To my sisters Rachel, Elizabeth, and Alexandra, thank you for always inspiring me. To my parents Alex and Karen, thank you for being my first teachers, for instilling a passion for science within me ever since I was a young child, and for supporting me ever since. And, finally, to my wife Elise, thank you for being my best friend, and for the love and support that kept me going through the toughest parts of graduate school. I cannot express enough how much I appreciate you.

VITA

Education

2022, Ph.D. in Biomedical Engineering, University of California, Irvine
Dissertation: *Collagenomics of tissue-engineered cartilage regeneration*
2019, M.S. in Biomedical Engineering, University of California, Irvine
2017, B.S.E. in Biomedical Engineering, University of Michigan

Appointments

2019, Teaching Assistant, BME 110C: Biomechanics III, University of California, Irvine
2017-2022, Graduate Student Researcher, Advisor: Kyriacos Athanasiou, University of California, Irvine
2017, Engineering Project Lead, Advisor: Martijn Muller, University of Michigan
2016-2017 Undergraduate Researcher, Advisor: David Kohn, University of Michigan

Field of Study

Biomedical Engineering

Publications

Bielajew BJ*, Donahue RP*, Lamkin EK, Hu JC, Hascall VC, Athanasiou KA. Proteomic, Mechanical, and Biochemical Characterization of Cartilage Development. *Acta Biomaterialia* 2022; online ahead of print. *These authors contributed equally

Bielajew BJ, Hu JC, Athanasiou KA. Methodology to Quantify Collagen Subtypes and Crosslinks: Application in Minipig Cartilages. *Cartilage* 2021; 13(Suppl 2): 1742S-1754S.

Donahue RP*, Nordberg RC*, **Bielajew BJ**, Hu JC, Athanasiou KA. The effect of neonatal, juvenile, and adult donors on rejuvenated neocartilage functional properties. *Tissue Engineering Part A* 2021; online ahead of print. *These authors contributed equally

Bielajew BJ*, Donahue RP*, Espinosa MG*, Arzi B, Wang D, Hatcher DC, Paschos NK, Wong MEK, Hu JC, Athanasiou KA. Knee orthopedics as a template for the temporomandibular joint. *Cell Reports Medicine* 2021; 2(5). *These authors contributed equally

Bielajew BJ, Hu JC, Athanasiou KA. Collagen: quantification, biomechanics and role of minor subtypes in cartilage. *Nature Reviews Materials* 2020; 5(10): 730-747.

Gonzalez-Leon EA, **Bielajew BJ**, Hu JC, Athanasiou KA. Engineering self-assembled neomenisci through combination of matrix augmentation and directional remodeling. *Acta Biomaterialia* 2020; 109: 73-81.

Van der Laan HL, Zajdowicz SL, Kuroda K, **Bielajew BJ**, Davidson TA, Gardinier J, Kohn DH, Chahal S, Chang S, Liu J, Gerszberg J, Scott TF, Clarkson BH. Biological and Mechanical Evaluation of Novel Prototype Dental Composites. *Journal of Dental Research* 2019; 09(1): 91-97.

ABSTRACT OF THE DISSERTATION

Collagenomics of tissue-engineered cartilage regeneration

By

Benjamin Jacob Bielajew

Doctor of Philosophy in Biomedical Engineering

University of California, Irvine, 2022

Distinguished Professor Kyriacos Athanasiou, Chair

Cartilage, the tissue that provides a lubricious surface in diarthrodial joints, does not regenerate when injured or diseased. No treatments for cartilage degeneration succeed at regenerating native cartilage, and most fail in the long term. Tissue-engineered cartilage is a promising therapeutic for cartilage repair and regeneration; this is particularly pertinent for people who have ailments of the temporomandibular joint (TMJ) cartilages — up to 8-16% of the population. However, a deep understanding of the extracellular matrix (ECM) of tissue-engineered cartilage is limited by a dearth of analytic techniques for collagens, the proteins that play essential functional roles in cartilage ECM. Through novel liquid chromatography–mass spectrometry (LC-MS) methods, the global objectives of this work were to: 1) develop methods for the quantification of collagen subtypes and crosslinks, 2) interrogate the temporal changes in collagen subtype and crosslink profiles of native cartilage and tissue-engineered neocartilage during tissue development, and 3) investigate the collagen subtypes and crosslinks of cartilage regeneration through the use of tissue-engineered neocartilage implants in a large animal model.

Toward addressing the dearth of techniques for collagen subtype quantification, novel LC-MS methods were developed to quantify individual collagen subtypes and crosslinks in biological samples, and bottom-up proteomics techniques were used to quantify all proteins in tissue ECM, including collagen subtypes, using the cartilages of the Yucatan minipig as a model. The high-

throughput LC-MS methods for collagen subtype and crosslink quantification are low in cost and operator time and can be translated to any facility that has access to a triple quadrupole mass spectrometer. These novel collagenomic techniques are widely applicable to researchers studying tissue characterization, disease states, and tissue engineering of all collagenous tissues, including cartilage, skin, bone, ligament, tendon, and many others.

The novel collagenomic methods were applied to study the development of native and engineered cartilages. In addition to well-known developmental changes in native cartilage such as total collagen and DNA contents, trends in the collagen subtype and crosslink profiles throughout maturation of knee cartilage were elucidated. The self-assembling process of tissue engineered cartilage was also examined with collagenomic techniques, and many similarities in development between the self-assembled cartilage and native cartilage, such as an increase in collagen type II, were determined. These trends showed evidence that self-assembled engineered cartilage recapitulates aspects of the development of native cartilages.

Toward developing a deeper understanding of cartilage regeneration with self-assembled neocartilage implants, Yucatan minipig TMJ disc perforation models were evaluated. Small perforation (3-mm) and large perforation (6-mm) defects were regenerated with self-assembled neocartilage implants and evaluated at 24 weeks and 8 weeks, respectively. In both *in vivo* studies, treatment with self-assembled neocartilage implants resulted in regenerated fibrocartilaginous repair tissue, an important step toward translating self-assembled cartilage implants to clinical usage. Quantitative collagenomics was used to show that the repair tissue of empty defects in the small perforation group had a collagen subtype profile similar to that of scar tissue (more collagen type III and less collagen type I) than repair tissue of implant-treated TMJ discs, which had a collagen subtype profile of native TMJ disc tissue.

Overall, this work is highly significant in that it introduces novel methods for collagen subtype and crosslink quantification, which are applicable not only to cartilage, but to a wide breadth of tissue fields. Because of the critical roles of major and minor collagens in providing

structure to tissues, collagenomics techniques are particularly relevant to researchers studying tissue characterization, disease states, structure-function relationships, and tissue engineering of cartilage, bone, heart valve, ligament, tendon, blood vessels, and skin. Applying collagenomics techniques to the development of native and engineered cartilages allows for a deeper understanding of the self-assembling process of cartilage tissue engineering beyond traditional benchtop biochemical assays. Finally, showing the fibrocartilaginous collagenomic profile of regenerated cartilage tissue in a large animal model is a major milestone toward translating tissue-engineered cartilage to the clinic for human usage, which can drastically improve the quality of life in millions of patients who suffer from TMJ disorders.

INTRODUCTION

Collagen, the most abundant protein in the human body, provides structure and functionality to the extracellular matrix (ECM) of many different tissues. Due to collagen's critical roles in the biomechanics and disease states of tissues such as cartilage, bone, skin, ligament, tendon, and many others, collagen analysis has long been of high importance to tissue researchers, with techniques having been developed and performed for over a century. Collagen has 28 currently identified subtypes which all have unique roles. While collagen types I, II, and III account for 80-90% of the collagen in the body, the minor collagens, which can be in proportions as low as fractions of a percent of the total collagen content, play major roles in tissue functionality.

Cartilage is a connective tissue that bears mechanical load, cushions the ends of bones, and provides a lubricious surface for joint articulation. Hyaline cartilage is found in the ribs, nose, and the ends of long bones, and has an ECM rich in glycosaminoglycans (GAGs) and collagen type II. Fibrocartilage is found in the knee meniscus, temporomandibular joint (TMJ), intervertebral disc, and pubic symphysis, and contains an ECM that comprises mostly collagen type I. Cartilage also contains up to 12 minor collagens that are critical in cartilage ECM assembly and biomechanics. The collagen matrix of cartilage is essentially a permanent structure; cartilage does not heal itself when damaged or degraded due to many factors including the avascularity, aneurality, and hypocellularity of most cartilages. This contributes to the high prevalence of arthritis, which is diagnosed in nearly one in four US adults. One type is TMJ osteoarthritis, which is common in temporomandibular joint disorders (TMDs), which are reported in 8-16% of the population, and can cause severe, debilitating pain when performing everyday necessary motions such as speaking, chewing, and breathing. Even with this high incidence, the suitability and efficacy of current mid- and late-stage treatments for TMDs remain bleak, with current treatment options such as discectomy leading to degenerative remodeling of the TMJ.

A promising solution to the growing problem of arthritides, such as those of TMDs, is to use tissue-engineered cartilage implants, which have the potential to regenerate biomimetic cartilage and relieve symptoms in the long-term. By implanting engineered neocartilages, cartilage defects can be repaired and regenerated, preventing the osteoarthritic changes. For example, in TMDs, the fibrocartilaginous TMJ disc often undergoes thinning or perforation; in such cases, neocartilage implants are envisioned to restore joint function by regenerating thinned or perforated regions of the TMJ disc, relieving symptoms and preventing further degeneration of the joint. The self-assembling process in cartilage tissue engineering, a scaffold-free approach, is a particularly effective method for engineering robust neocartilages, with tensile and compressive properties of neotissues reaching values on par with native human cartilage. Over the past several years, advancements in self-assembled neocartilage include the usage of growth factors and enzymes to enhance mechanical properties of neocartilage and the usage of passaged and rejuvenated costal chondrocytes as a cell source to generate many neocartilage implants from a small biopsy in an allogeneic, non-homologous approach. Self-assembled neocartilage implants have previously been used in a TMJ disc thinning model in the Yucatan minipig, self-assembled neocartilage implants resulted in lower (better) osteoarthritis scores, more complete defect closure, and greater repair tissue properties than those of untreated controls. With safety and efficacy shown in this large animal model, the self-assembling process in cartilage tissue engineering holds great promise for translation to clinical use in humans, especially for TMJ disc cartilage repair and regeneration.

One barrier to the translation of self-assembled neocartilage implants is the incomplete understanding of the specific biochemical makeup of neocartilage ECM and how it develops over time throughout tissue culture. While routine biochemical analysis includes quantification of collagen, GAGs, and DNA, these three assays account for less than half of neocartilage dry weight (which comprises approximately 15% collagen, 30% GAG, and <1% DNA). Additionally, the most commonly performed collagen assay, the hydroxyproline assay, only estimates general

collagen, and does not quantify individual collagen subtypes. Despite the unique and crucial functional roles of different collagen subtypes, current methods lack in sensitivity, specificity of subtypes, and/or cost effectiveness. This, along with knowing less than half of the composition of neocartilage ECM, necessitates the development and implementation of liquid chromatography–mass spectrometry (LC-MS) proteomic techniques for self-assembled neocartilage. Because the ideal engineered neocartilage implant is biomimetic of native cartilage, proteomic studies can show differences (e.g., in collagen subtype composition) between engineered and native cartilages, and how they change throughout maturation and development, informing future tissue-engineering techniques. Additionally, knowing exactly what specific biomolecules constitute the neocartilage implant ECM and their relative proportions will be important for proving safety in preclinical and clinical trials, and can inform release criteria and quality control measures as this technology is translated toward human clinical use. However, before this is possible, proteomic methods, including quantification of collagen subtypes, must be developed and applied to self-assembled neocartilage implants.

An additional barrier to translation of self-assembled neocartilage implants is that previous animal models using neocartilage implants are limited in analysis techniques of the generated repair tissue. For example, in previous disc thinning models in the TMJ discs of Yucatan minipigs, the collagen subtypes of the repair tissue were not verified to match the profile of native fibrocartilage. To ensure long-term efficacy, it is crucial to know whether the resulting repair tissue is a true regenerated fibrocartilage or an inferior scar tissue. With the advent of quantitative bottom-up proteomic techniques, there is great potential to understand the collagenomics of cartilage regeneration *in vivo*, but because collagen-specific methods are underdeveloped, this has not yet been performed in large animal models of cartilage regeneration.

Toward the overarching goal of using quantitative collagenomic techniques to further translational efforts in cartilage tissue-engineering, the global objectives of this work were: 1) to develop novel quantitative methods for analyzing individual collagen subtypes and collagen

crosslinks, and use these methods to investigate the collagen profiles of cartilages; 2) to interrogate the development of both native cartilage and self-assembled cartilage through quantitative collagenomics; and 3) to employ quantitative collagenomic methods to analyze regenerated cartilage in a clinically relevant, large animal model. To complete these objectives, three Specific Aims were investigated in this work:

Specific Aim 1: To develop novel assays for collagen subtype and crosslink quantification. The objectives of this aim were to develop LC-MS methods for quantification of collagen subtypes and collagen crosslinks, apply these methods to the cartilages of the Yucatan minipig, and perform bottom-up proteomics analysis of these cartilages to quantify the proteome of cartilage ECM. *It was hypothesized that the LC-MS collagen subtyping method can quantify marker peptides of collagen types I and II with high specificity and sensitivity, and that the LC-MS collagen crosslinks assay can quantify mature and immature collagen crosslinks.*

Specific Aim 2: To interrogate the development of native and engineered cartilages through quantitative collagenomic methods. The objectives of this aim were to apply the LC-MS methods developed in Specific Aim 1 to show how the mechanical properties, biochemical properties, collagen crosslinks, and collagen subtypes of native and engineered cartilages change throughout tissue development. *It was hypothesized that the proteome of engineered cartilage development recapitulates developmental changes in native knee cartilage.*

Specific Aim 3: To employ quantitative collagenomic methods to analyze regenerated cartilage in a clinically relevant, large animal model. The objectives of this aim were to use the LC-MS methods developed in Specific Aim 1 to analyze regenerated fibrocartilage in small (3-mm) and large (6-mm) perforations of the TMJ disc of the Yucatan minipig treated with self-assembled neocartilage implants. *It was hypothesized that regenerated tissue would have a collagen subtype profile similar to native TMJ disc, unlike empty-defect controls.*

The Specific Aims have been completed as proposed, as described in this dissertation. All seven chapters in the main body of this dissertation, in addition to the three chapters in the appendix, are original works that have either been already published or are presented as full-sized manuscripts for future publication. A brief description of each chapter is provided below.

Chapters 1 and 2 establish the background that motivates this work. Chapter 1 presents the current state of collagen identification and quantification techniques, and why high-throughput collagen subtype quantification methods must be developed. Chapter 2 compares the pathology, epidemiology, and current clinical practices for the arthritides of the knee and TMJ and describes the criticality of translational efforts for tissue-engineered products to treat TMDs.

Toward achieving Specific Aim 1, Chapter 3 introduces a novel method for high-throughput collagen subtype and collagen crosslink quantification using LC-MS. As an application of this assay, ten cartilages of the Yucatan minipig are analyzed for collagen types I and II and collagen crosslinks. In addition, bottom-up proteomics with label-free quantification is performed on representative samples to quantify all proteins, including the minor collagens, in these cartilages. The methodology introduced in this chapter provides the basis for Specific Aims 2 and 3, and, thus, all remaining chapters in this work.

Chapters 4 and 5 address Specific Aim 2 by investigating the development of native cartilage and self-assembled cartilage, respectively. In Chapter 4, porcine knee cartilage from pigs of different developmental ages (fetal, neonatal, juvenile, mature) are examined for their mechanical properties, biochemical composition, and proteomic makeup. Significant changes in major and minor collagen types throughout tissue maturity are determined. In Chapter 5, the development of self-assembled neocartilage is analyzed with the same methods. In this chapter, it is determined that engineered neocartilage implants recapitulate aspects of the development of native cartilage through temporal trends in mechanics, biochemistry, and proteomics.

Specific Aim 3 is completed in Chapters 6 and 7. In Chapter 6, small (3-mm) perforations are regenerated in the Yucatan minipig TMJ disc using self-assembled neocartilage implants.

Using proteomics, it is shown that implant-treated TMJ discs contain repair tissue with a collagen subtype profile that matches that of native fibrocartilage tissue, while empty defect TMJ discs contain scar tissue with a less fibrocartilaginous collagen subtype profile and inferior mechanical properties. In Chapter 7, the model is scaled up to a large (6-mm) perforation defect, and self-assembled neocartilage implants were again shown to result in regenerated TMJ disc fibrocartilage. While the empty defects do not lead to repair tissue at this defect size, it is shown through bottom-up proteomics that the regenerated tissue has a collagen subtype profile of native TMJ disc fibrocartilage, lending credence to the long-term prospects of self-assembled neocartilage implants for TMJ disc regeneration.

Additional original work is presented in the appendices. Appendix A presents a novel combination of bioactive factors for fibrocartilage tissue engineering of the knee meniscus. Appendix B describes self-assembled neocartilage implants made with different donor chondrocyte ages. While the work in these appendices does not directly address the Specific Aims of this work, they represent other collagenomic applications in the field of cartilage tissue engineering, using the techniques developed in Specific Aim 1.

In summary, this work develops the nascent field of quantitative collagenomics by introducing high-throughput assays for collagen subtype and collagen crosslink quantification, and it advances the translation of tissue-engineered cartilage by investigating the collagenomics of self-assembled neocartilage implants through *in vitro* development and *in vivo* regeneration of TMJ disc defects in the Yucatan minipig.

CHAPTER 1 | Collagen: quantification, biomechanics, and role of minor subtypes in cartilage*

Abstract

Collagen is a ubiquitous biomaterial in vertebrate animals. Although each of its 28 subtypes contributes to the functions of many different tissues in the body, most studies on collagen or collagenous tissues have focussed on only one or two subtypes. With recent developments in analytical chemistry, especially mass spectrometry, significant advances have been made toward quantifying the different collagen subtypes in various tissues; however, high-throughput and low-cost methods for collagen subtype quantification do not yet exist. In this Chapter, we introduce the roles of collagen subtypes and crosslinks, and describe modern assays that enable a deep understanding of tissue physiology and disease states. Using cartilage as a model tissue, we describe the roles of major and minor collagen subtypes in detail; discuss known and unknown structure–function relationships; and show how tissue engineers may harness the functional characteristics of collagen to engineer robust neotissues.

Introduction

Collagens — the most abundant proteins in the body by weight — are the main structural proteins in the extracellular matrix (ECM) of various tissues, including cartilage, bone, blood vessels, skin, and other connective tissues (Figure 1). Collagen has been studied since the 1800s¹. Since then, it (and its crosslinks) been shown to be implicated in tissue biomechanics^{2–4}, and disease states, such as cancer^{5,6}, arthritis^{7,8}, and over 40 hereditary diseases^{9,10}. Collagen is categorized into 28 subtypes, with types I, II, and III, making up 80–90% of the collagen in the human body¹¹. The so-called ‘minor collagens,’ which do not have a set definition, are present in very low amounts but

* Published as: Bielajew BJ, Hu JC, Athanasiou KA. Collagen: quantification, biomechanics and role of minor subtypes in cartilage. *Nature Reviews Materials* 2020; 5 (10): 730-747.

have vital functional roles¹². Despite this, most studies in collagen and collagenous tissues have only focused on general collagen (that is, total collagen without subtype specificity) or just one or two collagen subtypes.

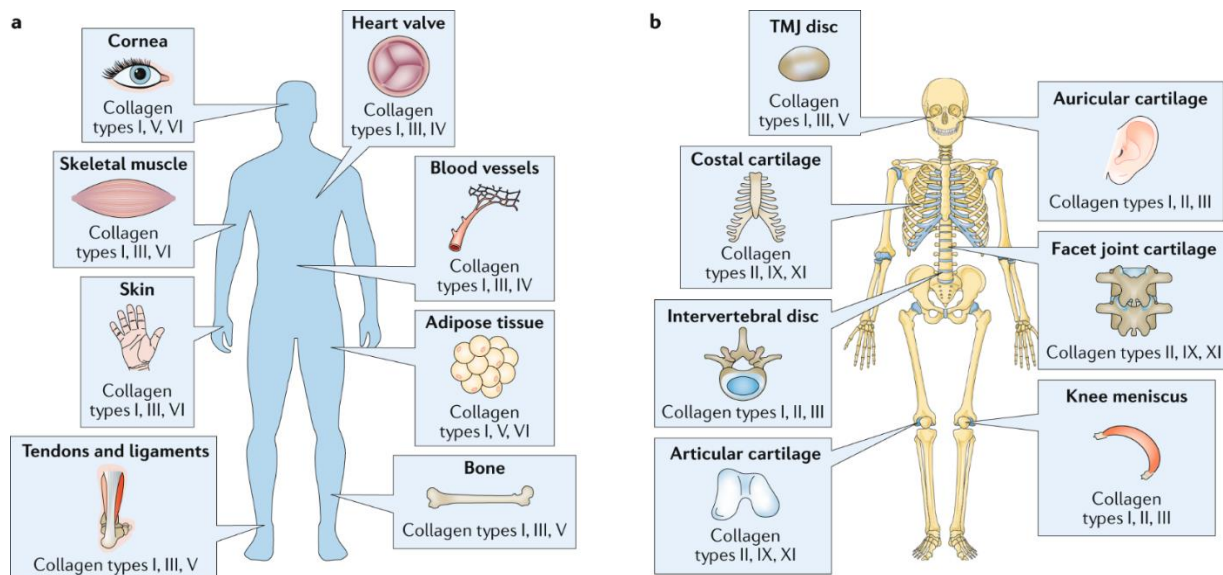


Figure 1. Collagen types of the human body. Different collagen types are found in various tissues all over the body. Three of the most abundant collagen types are displayed for non-cartilage tissues (panel a) and cartilage tissues (panel b). TMJ, temporomandibular joint. The skeleton image in panel b reprinted from https://smart.servier.com/smart_image/skeleton/ CC BY 3.0.

In this Chapter, we first describe the collagen superfamily. We then discuss recent advances in mass spectrometry that allow sensitive quantification of individual collagen subtypes and determination of their role in disease states and tissue biomechanics. Our attention is then turned to the subtypes of cartilage, which have been neglected in the literature. Finally, we describe the need for new studies, in particular those that leverage high-throughput technologies. We urge tissue engineers to take advantage of bottom-up proteomics techniques to better understand the ECM of engineered tissue, potentially unveiling how to engineer stiffer, stronger, and more durable neotissues. A similar approach focusing on all collagen subtypes would lead to a deeper understanding of the roles of minor collagens, and may explain the gap in functionality between engineered implants and native tissues. Outside the scope of this Chapter are collagen assembly, molecular mechanics, or in-depth cellular interactions, which have been reviewed in depth elsewhere^{13–16}.

Collagens and collagen crosslinks

All 28 subtypes of collagen contain specific amino acid sequences that encode one or more triple-helical domains¹⁷. Triple-helical domains consist of a signature repetition of amino acids G-X-Y, with G always representing glycine, X usually representing proline, and Y usually representing hydroxyproline. This repeated sequence creates favourable hydrogen bonding, allowing for three polypeptides, called alpha-chains, to be assembled into a triple-helical collagen protein. The 28 types of collagen are divided into groups based on the location, size, and distribution of triple-helical domains; these groups are summarized in Table 1. Collagens may consist of three of the same alpha-chain or of different alpha-chains. For example, collagen type I usually consists of two α_1 chains and one α_2 chain¹⁸, collagen type II consists of three α_1 chains¹⁹, and collagen type IX consists of α_1 , α_2 , and α_3 chains²⁰. Even though collagen types I and II are the most abundant, minor collagens, which account for less than 10% of the total collagen content, have important roles in collagenous tissues, as described later.

Table 1. Classically defined groups of collagen subtypes. Classically, collagen subtypes are grouped according to their structure.

Group name	Key features	Collagen types
Fibril-forming collagens	Long triple-helical domains for fibril formation	I, II, III, V, XI, XXIV, XXVII
Fibril-associated collagens with interrupted triple helices (FACITs)	Do not form fibrils, but associate with fibril surfaces	IX, XII, XIV, XVI, XIX, XX, XXI, XXII
Network-forming collagens	Form repeating patterns	IV, VIII, X
Membrane collagens	Span the cell membrane	XIII, XXIII, XXV
Multiplexins	Have many non-collagenous domains, but are not FACITs	XV, XVIII
Others	Do not belong to any of the above categories	VI, VII, XXVIII

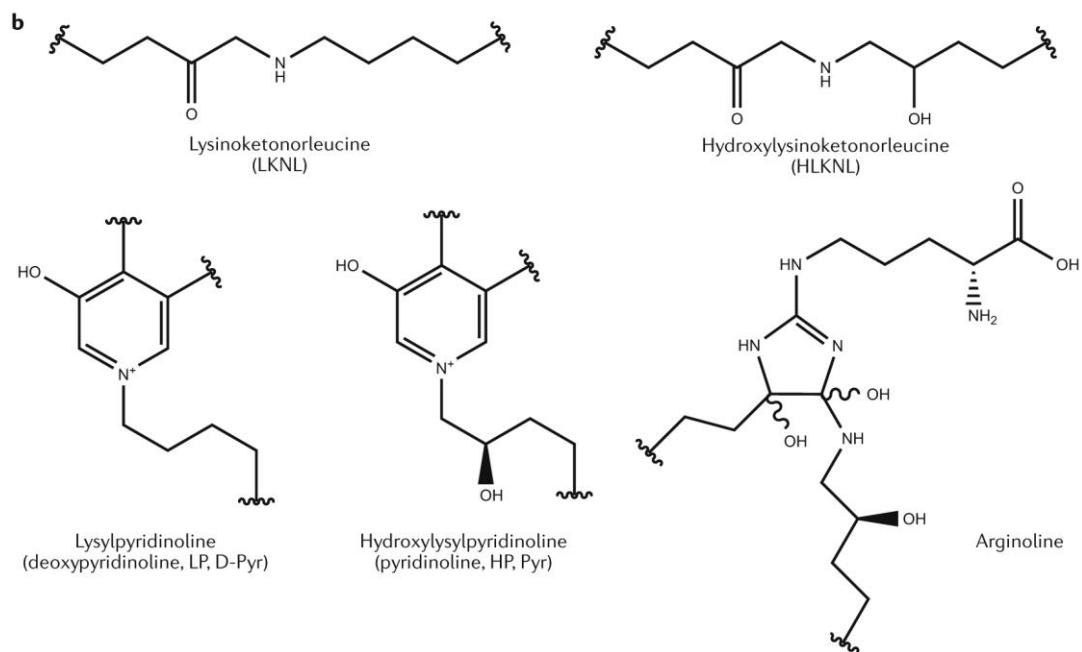
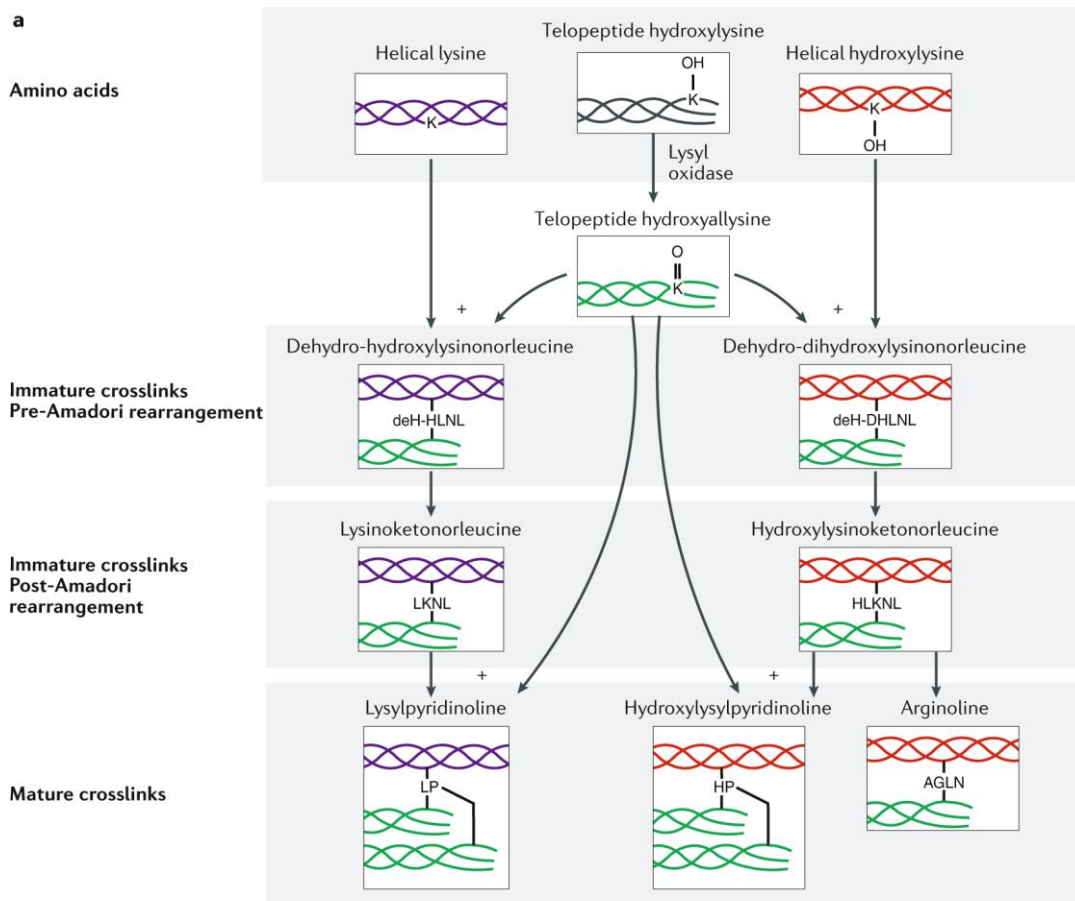


Figure 2. Lysyl oxidase pathway. (a) The enzymatic pathway for the formation of pyridinoline and arginine crosslinks. The initial process of hydroxylysine to hydroxyallysine is catalysed by lysyl oxidase, which is necessary for the cascade of reactions shown in the pathway. (b) Structural formulas of the immature and mature crosslinks.

Collagen types I, II, III, V, XI, and IX form covalent enzymatic collagen crosslinks, which strengthen and mature the collagen network²¹. The formation pathway of these collagen crosslinks is displayed in Figure 2. The first step is catalysed by lysyl oxidase (LOX), and involves deamination of specific hydroxylysines in the collagen amino acid sequence to form hydroxyallysine²². Hydroxyallysine reacts with lysine or hydroxylysine in another collagen alpha-chain to form the divalent crosslinks dehydro-dihydroxylysinonorleucine (deH-DHLNL) and dehydro-hydroxylysinonorleucine (deH-HLNL). These crosslinks undergo a spontaneous Amadori rearrangement to the more stable hydroxylysinoketonorleucine (HLKLN) and lysinoketonorleucine (LKNL), respectively^{23,24}. These molecules are also known as immature, reducible, or intermediate crosslinks. Because HLKLN and LKNL are destroyed upon hydrolysis, they are analysed in their borohydride-reduced forms, dihydroxylysinonorleucine (DHLNL) and hydroxylysinonorleucine (HLNL).²⁵ HLKLN and LKNL react with another hydroxyallysine to connect to a third alpha-chain of collagen, forming the trivalent crosslinks hydroxylysylpyridinoline (HP) and lysylpyridinoline (LP), respectively²⁶. HP and LP, which are also called pyridinoline and deoxypyridinoline, are known as mature or non-reducible crosslinks. More recently, another ketoimine maturation, arginoline, was found to form when ketoimines undergo oxidation and free arginine addition; arginoline exists in approximately equimolar amounts to HP in articular cartilage²⁷. Pyrrole crosslinks, which are created by telopeptide lysines, are discussed in detail elsewhere²¹. There are also non-enzymatic crosslinks, by which lysines or hydroxylysines in helical collagen react with sugars like glucose or ribose to form glucosepane and pentosidine through the Maillard reaction. These crosslinks are known as advanced glycation end-products (AGEs) and are associated with aging and disease states²⁸.

HP and LP are important for the tensile properties of collagenous tissues, and the amount of HP varies greatly in connective tissues. In the knee, the cruciate ligaments have 3–5 times as much HP per collagen mass than the collateral ligaments, and articular cartilage has about twice the relative HP content than the knee meniscus³. In bovine sternomandibularis muscle and nuchal

ligament, the relative HP content was shown to increase with animal age²⁹; however, the HP content in human intervertebral discs was shown to decrease with age³⁰. Moreover, HP and LP are excreted during bone resorption and collagen degradation, and may be used as urinary biomarkers for diseases such as osteoporosis³¹ and osteogenesis imperfecta³², and for cancer metastasis³³.

Identification and quantification

Methods for identification and quantification of collagen and its subtypes have been in iterative development for over a century^{34,35}. Collagen analysis is relevant to fields such as tissue engineering, tissue characterization, drug development and delivery, and biomechanics. Although several methods currently exist for collagen identification and quantification, all lack in sensitivity, specificity, and/or cost effectiveness. Next-generation high-throughput assays may enable the highly sensitive parallel processing of several samples in a short time, with individual subtype specificity. We provide an overview of existing and next-generation methods in this section, covering traditional and antibody-based assays, imaging, mass spectrometry, and promising proteomics approaches. A summary of the quantitative assays for collagen subtypes and crosslinks is displayed in Figure 3.

Traditional assays

Because hydroxyproline content is highly correlated to the collagen content, the hydroxyproline assay has been frequently used to quantify collagen in biological samples. Since its establishment in the mid-20th century, this procedure has been improved and simplified through many iterations^{36–38}. This method has been cited as the ‘gold standard’ collagen quantification assay^{39,40}. Although this assay is relatively simple and low cost, it does not discriminate between collagen types or other non-collagen molecules that contain hydroxyproline, such as elastin, which is present in many collagenous tissues⁴¹. Moreover, the hydroxyproline content varies among different collagen subtypes; for example, collagen type VI contains less hydroxyproline

per chain than fibrillar types⁴². Therefore, although the hydroxyproline assay may be sufficient for estimating overall collagen, additional analysis is needed for highly sensitive or type-specific collagen quantification.

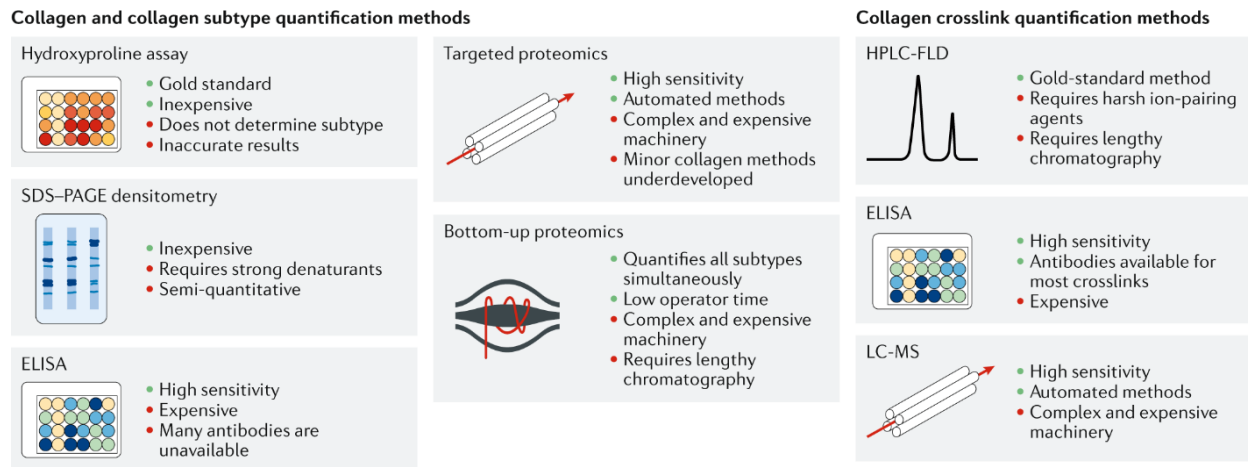


Figure 3. Examples of quantitative assays for collagen and collagen crosslinks. Several assays for quantification of collagen subtypes and crosslinks are displayed. The advantages and disadvantages of each assay are denoted. ELISA, enzyme-linked immunosorbent assay; HPLC-FLD, high-performance liquid chromatography with fluorescence detection; LC-MS, liquid chromatography-mass spectrometry; SDS-PAGE, sodium dodecyl sulfate-polyacrylamide gel electrophoresis.

Another assay used to identify collagens is sodium dodecyl sulfate-polyacrylamide gel electrophoresis (SDS-PAGE), which separates molecules by molecular weight and charge. Because the molecular weights of many collagen alpha-chains are documented, they can be identified using a prepared ladder of proteins⁴³. Nevertheless, separating the alpha-chains is challenging and requires strong denaturants⁴⁴. Semi-quantification of protein in gel bands from SDS-PAGE is possible via densitometric analysis⁴⁵. Although SDS-PAGE alone does not confirm the identity of proteins, they can be identified through antibody binding in a Western Blot.

High-performance liquid chromatography (HPLC) with fluorescence detection (HPLC-FLD) has been used for the identification and quantification of HP and LP since the mid-1980s. This method uses reverse-phase chromatography with ion-pairing agents⁴⁶. This was extended to quantify the AGE pentosidine and, using post-column derivatization, quantify immature crosslinks HLKLN and LKLN⁴⁷. While HPLC-FLD has been a gold standard assay for collagen

crosslink quantification for many years, its lengthy chromatography and usage of harsh ion-pairing agents are significant disadvantages.

Quantitative antibody-based assays

Enzyme-linked immunosorbent assay (ELISA) is a plate-based assay to quantify target molecules based on antigen recognition and thus can be used to measure individual collagen subtypes or crosslinks. Commercial ELISA kits exist for several collagen subtypes, and ELISA has been developed for crosslinks such as HP⁴⁸, LP⁴⁹, and pentosidine⁵⁰. ELISA's drawbacks include its high cost and requirement for separate runs for different molecules (for example, different collagen types, different collagen crosslinks, or collagen from different biological species). Antibodies specific to minor collagen types for many species are not readily available. Identifying or quantifying different collagen types in the same sample is not possible, and because different collagen types have a high degree of sequence homology, careful attention is needed when choosing custom epitopes for collagen subtypes.

Protein microarrays are emerging technologies that can characterize proteins in a parallel and high-throughput manner. This technique consists of several parallel, miniaturized assays on a small plate — a concept originally used in the DNA microarray⁵¹. ECM protein microarrays can be used to profile cell adhesion to different collagen subtypes⁵² but have not been used for collagen quantification. Similar immunoassays may also be multiplexed with magnetic bead-based technologies, which may allow for parallel quantification of different collagen types⁵³. Although magnetic bead-based assays for human collagen types I, II, IV, and VI assays are available, poor concurrence of quantitative values between bead-based assays and ELISAs were demonstrated, and results from different vendors were not consistent⁵⁴. The DNA microarray, in combination with SOMAmers (small off-rate modified aptamers), can be used to quantify proteins in the SOMAscan assay⁵⁵. This assay can target collagen subtype fragments in human blood⁵⁶ and can be multiplexed, but it is not yet fully developed for tissue homogenate.

Collagen imaging and spectroscopy

Visible light, fluorescence, and many other microscopy techniques allow for visualization of bulk collagen, collagen types, and organization parameters, such as fiber or fibril size, and spacing. For light microscopy, histochemical techniques, such as Van Gieson's stain (which was developed in the late 19th century), are still commonly used. Collagens are acidophilic and can be stained with eosin. Other stains include picosirius red, methyl blue, and water blue. Although these stains give appealing visualizations of fibrillar collagen, they have been noted to give inaccurate results based on non-random sampling or sample inhomogeneity. Furthermore, these stains are not collagen-specific⁵⁷; for example, they have been noted to stain other matrix components, such as tenascin⁵⁸ and amyloid⁵⁹. Moreover, fibrillar collagen stains do not differentiate among collagen subtypes^{60,61}, necessitating the use of additional methods.

Immunohistochemistry (IHC) and immunofluorescence (IF) enable targeted labelling of individual collagen types through antibody-binding. As with ELISA, the availability of antibodies for minor collagens or for particular species can pose a challenge, and collagen sequence homology may induce cross-reactivity. Some examples of these techniques are IHC to show the location of collagen type X in avian tissues⁶² and IF to show co-distribution of collagen types XII and XIV with cartilage oligomeric matrix protein (COMP)⁶³.

Imaging techniques are particularly useful for examining collagen architecture and organization. Several imaging modalities may be used for quantifying the alignment of fibrillar collagens. These include transmission polarized light microscopy⁶⁴, second-harmonic generation⁶⁵, and liquid crystal-based polarization microscopy⁶⁶. Diffusion tensor imaging, which can measure the differences in water diffusion across collagen fibers, has been used to evaluate the orientation of collagen fibrils in engineered cardiovascular tissues⁶⁷. Electron microscopy (EM) techniques, including scanning electron microscopy (SEM), transmission electron microscopy (TEM), and environmental scanning electron microscopy (ESEM) may be used for visualization of collagen fibers and fibrils. For example, TEM has been used to visualize fibril diameter and

spacing⁶⁸, as well as size and organization⁶⁹; SEM was used to measure the diameter of collagen fibers in normal and degraded articular cartilage⁷⁰; and ESEM has been used to study the morphology and wetting behaviour of sponges made from collagen type I⁷¹.

Some imaging techniques are also useful for discerning among collagen types. For example, immunoelectron microscopy, which uses electron microscopy to label specific proteins, has been used to visualize the location of collagen subtypes, such as types XIII⁷², XV⁷³, and XXVII⁷⁴. Moreover, fluorescence lifetime imaging microscopy (FLIM) can be used to differentiate between collagen types I and III⁷⁵. FLIM has also been used to correlate collagen content to fluorescence lifetime in native cartilage with varying amounts of collagen depletion⁷⁶. This same technique was used in a study of tissue-engineered cartilage to correlate fluorescence lifetime to ultimate tensile strength⁷⁷. A similar FLIM technique was used to quantify crosslinking in collagen hydrogels⁷⁸. Because these FLIM systems can be used in sterile conditions without damaging engineered tissue, they may be used for quality control or release criteria for engineered implants, without the need to manufacture extra implants for destructive analysis.

Spectroscopic techniques, including Fourier-transform infrared (FTIR) spectroscopy, Raman spectroscopy, and time-resolved laser-induced fluorescence spectroscopy (TR-LIFS) may be used for analysing collagen or collagen subtypes. In one study, the spectral characteristics of FTIR, such as the amide I band profile and area, were compared among different types of tendons, and correlated to pyridinoline crosslinking and fiber organization⁷⁹. In another example of FTIR spectroscopy, highly discriminant absorption bands for individual collagen subtypes were determined⁸⁰. Raman spectroscopy is emerging as a technique to characterize ECM, including the collagen of engineered and native cartilages, both in localized regions and throughout the entire tissue depth^{81,82}. Raman spectroscopy has also recently been used to show changes in collagen secondary structure after damage from burning⁸³, and to discriminate between collagen types I and IV in skin⁸⁴. TR-LIFS has been used to characterize

collagen types I, II, III, IV, and V in vitro⁸⁵, and was used to assess collagen type I in arterial plaques to diagnose atherosclerosis⁸⁶.

Quantification with mass spectrometry

Mass spectrometry (MS) techniques have been developed for the identification and quantification of proteins, including collagen subtypes. To identify or quantify collagen subtypes with MS, collagen proteins or peptides must be ionized and then analysed in a mass spectrometer. Ionization techniques include matrix-assisted laser desorption/ionization (MALDI) or electrospray ionization (ESI). Liquid chromatography (LC) is frequently used in conjunction with ESI to separate analytes out of complex mixtures. After ionization, analytes are separated by their mass-to-charge ratio in time-of-flight (TOF), quadrupole, or ion-trap mass spectrometers. MS techniques can be used to quantify overall collagen and collagen crosslinks, individual collagen subtypes with targeted methods, or many collagen subtypes at once in bottom-up proteomics methods.

Quantification of overall collagen and collagen crosslinks

LC and multiple reaction monitoring (MRM) — an MS technique that quantifies fragmentation product ions from parent ions — can be used to quantify hydroxyproline in hydrolysed tissues as an estimation of total collagen content⁸⁷, similar to the photometric hydroxyproline assay described above, but with higher sensitivity and specificity. MALDI-TOF can also be used to quantify the amount of glycine-proline-hydroxyproline tripeptide as an estimation of total collagen content⁸⁸. In addition to estimating total collagen, LC-MS has been used for measuring collagen crosslinks. In one example, LC-MS MRM was used to quantify HP, LP, DHLNL, HLNL, and pentosidine in mouse cervical tissue during pregnancy using a reverse-phase chromatography column and ion-pairing agent⁸⁹. Another technique uses selected ion monitoring rather than MRM, and foregoes ion pairing by using a silica hydride column; this method quantified HP and LP in skin and urine samples⁹⁰. LC-MS is more sensitive and accurate than HPLC-FLD for several

compounds⁹¹⁻⁹³, although a thorough comparison between LC-MS and HPLC-FLD for collagen crosslink quantification has not been performed.

Quantification of targeted collagen subtypes

Aside from measuring small molecules, such as hydroxyproline, mass spectrometry methods can be used to detect intact proteins or specific marker peptides. For example, in an early study, whole fibrils of collagen types I, III, and V were identified with MALDI-TOF; however, because enzymatic digestion was not carried out, they formed large polymeric structures, making reproducible quantification difficult⁹⁴. More recently, MRM has been used to quantify peptides resulting from cyanogen bromide and trypsin cleavage of collagen types I, II, III, IV, and V in placenta and cartilage samples⁹⁵. MRM has also been used to measure the release of collagen type II and III in human articular cartilage after mechanical injury and cytokine treatment⁹⁶, and to identify collagen type I in trypsin digests of leather to determine the animal source⁹⁷. Within mass spectrometry systems, a number of quantitative approaches exist, including isobaric tags for relative and absolute quantitation (iTRAQ)⁹⁸, stable isotope labelling by amino acids in cell culture (SILAC)⁹⁹, tandem mass tags (TMT)¹⁰⁰, oxygen-18 stable isotope labelling¹⁰¹, and label-free methods based on peak intensity or spectral count¹⁰². Prior to targeted analysis, operators must determine variables, such as retention time, ionization voltages, and the masses of ions, and careful attention must be paid to ensure complete and reproducible enzymatic digestion and chromatography. Although such techniques are promising for quantifying individual collagen subtypes, methods for most minor collagen subtypes are yet to be developed; collagen is part of the insoluble ECM, does not digest easily in trypsin¹⁰³, and the low quantity of minor collagens relative to other tissue components render them difficult for targeted analysis.

Bottom-up proteomics approaches

The resolving power of modern ion-trap and Orbitrap mass spectrometers allows for quantification of many trypsinized proteins within a single run. After trypsin digestion, bottom-up proteomics

analysis, also called shotgun proteomics, may be used for identification and quantification of many different proteins, including collagen subtypes. These proteins may be quantified with the aforementioned tagging methods or with label-free methods, such as intensity-based absolute quantification (iBAQ)¹⁰⁴ or MaxLFQ¹⁰⁵.

Bottom-up approaches are useful for characterizing proteins relevant to disease states, such as cancer, or quantifying ECM components in native tissues. For example, bottom-up proteomics was used to quantify collagen types I, II, III, V, VI, IX, X, XI, and XII relative to a reference sample in different types of cartilage¹⁰⁶ and compare collagen types I, II, III, VI, XI, and XII in osteoarthritic and healthy cartilage¹⁰⁷. Bottom-up approaches also revealed the peptide sequences of collagen types I, III, IV, V, and IX in renal cell carcinoma¹⁰⁸ and increased deposition of collagen types X, XII, XIV, and XV in colorectal cancer and colorectal liver metastasis compared to healthy tissue,¹⁰⁹ which may serve as potential biomarkers. By quantifying native tissue compositions and determining variations in disease states, new understandings of ECM remodelling through disease progression may be achieved toward developing new treatments. However, although bottom-up proteomics datasets give a great amount of information, they are more costly and slower than most targeted approaches.

Modern assays to quantify collagen subtypes are applicable to all collagen-containing tissues in the body. In the remainder of this Chapter, cartilage will be used as a model tissue. We describe the role of each collagen subtype in cartilage and outline future directions for collagen subtype quantification.

Collagens in cartilage

Cartilage is a family of collagenous tissues with major structural and mechanical roles in the body. Depending on the anatomical location, cartilage's functions include bearing load, providing shape, cushioning, and lubricating diarthrodial joints. Cartilage contains an ECM rich in glycosaminoglycans (GAGs) and up to 15 types of collagen. Several of these are displayed in

Figure 4, which shows these collagen subtypes' structure, location, and roles in cartilage formation. The combination of collagens and other ECM molecules gives cartilage biomechanical properties in compression, shear, and tension that are unlike any other soft tissues. However, because cartilage is largely avascular and aneural, its lack of inherent healing poses significant medical problems when it is injured or diseased¹¹⁰. In this section, we briefly describe the different classifications of cartilage, its degeneration and promising therapies, and the role of each collagen type in cartilage.

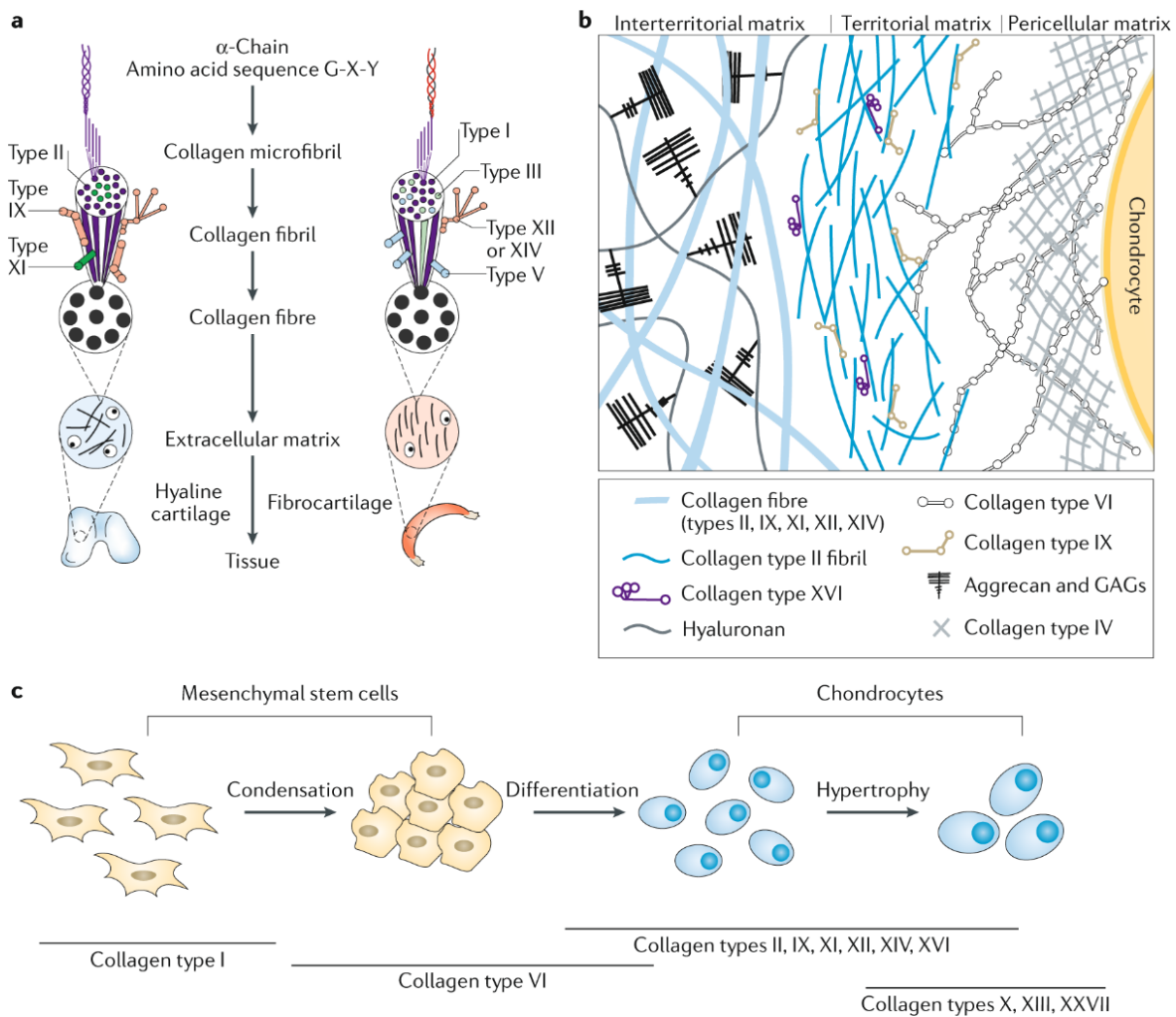


Figure 4. Collagen structure and location in cartilage, and its role in cartilage development. (a) Heterofibrils of different collagen types compose the structure of the cartilage extracellular matrix (ECM). Hyaline and fibrocartilage ECMs are shown as examples. (b) The locations of different collagen types in hyaline cartilage ECM. Many other ECM molecules are present but not shown. (c) Different collagens are involved in the process of cartilage formation during embryonic development. Collagen type I is expressed by mesenchymal stem cells. Collagen type VI accumulates during condensation and is then replaced by collagen type II and minor collagens as the cells differentiate and deposit chondrogenic ECM. GAGs, glycosaminoglycans.

Classification of cartilage

Cartilage is categorized into hyaline cartilage, fibrocartilage, and elastic cartilage (collectively termed cartilages). This classification is based on the presence of major collagens or elastin in the ECM. For example, the ECM of hyaline cartilage contains mostly collagen type II, whereas the fibrocartilage ECM contains mostly collagen type I. Hyaline cartilage is the most abundant type of cartilage in the body and can be further classified as articular or non-articular, based on whether the cartilage is found on the surface of articulating bones. Articular cartilage distributes forces generated in musculoskeletal movement and provides a low-friction surface to facilitate movement in diarthrodial joints^{111,112}. Non-articular hyaline cartilage is found in locations such as the ends of ribs, nose, larynx, and in tracheal rings.

Fibrocartilage is distinct from hyaline cartilage owing to the presence of collagen type I and the lower GAG content. It is also 5–20 times stiffer than hyaline cartilage in tension and at least five times less stiff in compression^{113,114}. Fibrocartilage is found in the knee meniscus, the temporomandibular joint, intervertebral discs, and the pubic symphysis. Some cartilages in articulating joints, such as the mandibular condyle cartilage, are classified as fibrocartilage^{115,116}. Fibrocartilage can also be created as repair tissue when hyaline articular cartilage is damaged; however, this repair mechanism is ineffective for long-term replacement¹¹⁷.

Elastic cartilage is distinct from other cartilages as it contains elastin, a highly crosslinked protein that makes this type of cartilage flexible. Elastic cartilage is primarily found in the ear and epiglottis. Although septal cartilage of the nose contains elastin, this is categorized as hyaline cartilage¹¹⁸. Elastic cartilage is more cellular and has different mechanical properties to hyaline cartilage and fibrocartilage¹¹⁹. The main collagen types in elastic cartilage are types I and II^{120,121}.

Cartilage degeneration and therapies

Arthritides are degenerative diseases of cartilage that affect over 30 million US adults according to the US Centers for Disease Control and Prevention. Osteoarthritis, which is often associated with aging or injury, leads to cartilage that has different mechanical properties than its healthy counterpart: for example, the tensile modulus can decrease by as much as 90% and the compressive modulus also decreases¹²². Osteoarthritis transforms the collagen in articular cartilage from mostly type II to a mixture of types I, II, and III; osteoarthritis can induce a 100-fold upregulation in collagen type I¹²³, fivefold downregulation of collagen type II¹²⁴, and sixfold increased deposition of collagen type III¹²⁵. The collagen type II in articular cartilage has negligible turnover, and the low regenerative capacity of cartilage may partly come from this inability to repair and replace collagen¹²⁶.

For treatment of cartilage pathologies, arthroscopic debridement, the surgical removal of damaged cartilage, used to be commonly performed¹²⁷ but was shown to not relieve symptoms¹²⁸. Osteochondral autografts and allograft plugs may be used for small chondral defects, although matching the surface shape from the implant to the defect remains a challenge¹²⁹. The dense collagenous matrix in cartilage can impede tissue–tissue integration, hindering the effectiveness of graft approaches¹³⁰. Surgical interventions for cartilage defects also include microfracture and matrix-assisted autologous chondrocyte implantation (MACI), although both may lead to fibrocartilage repair tissue and long-term degeneration^{131,132}. Microfracture specifically leads to repair tissue that contains collagen type I, unlike healthy articular cartilage¹³³. Minor collagens in repair tissue from microfracture or MACI have not been identified or quantified.

Fibrocartilage disorders, such as those of the knee meniscus, temporomandibular joint (TMJ) disc, and intervertebral disc can originate from a variety of aetiologies. Tears in the knee meniscus are common injuries among athletes, and often occur alongside knee-ligament injuries, which can severely limit mobility¹³⁴. TMJ pain afflicts approximately 10% of the adult population¹³⁵, with a disproportionately high occurrence in premenopausal women¹³⁶. The intervertebral disc

shows age-related degeneration earlier than any other connective tissue in the body¹³⁷, and is strongly associated with back pain, which has a lifetime prevalence rate of 49–80%^{138,139}. Surgical removal procedures, such as meniscectomy and discectomy, offer short-term relief, but lead to worsening of symptoms and eventual fibrocartilage degeneration^{140–143}.

There are currently no therapies to repair or regenerate either hyaline cartilage or fibrocartilage that are effective in the long-term¹⁴⁴. Because cartilages lack intrinsic healing, tissue-engineering techniques are potential therapies¹⁴⁵. Tissue-engineered cartilage, or neocartilage, has the potential to fill defects or regenerate damaged tissues to restore function^{146,147}. To do this, neocartilage implants must meet the mechanical demands imposed upon the native tissue¹⁴⁸. A systematic approach to designing neocartilage starts from delineating quantitative design criteria, such as the specific biomechanical and biochemical properties of the native tissue to serve as gold standards¹⁴⁹. Biomechanical properties include compressive and tensile moduli, and biochemical properties include the quantity of collagen and collagen crosslinks. Although a major effort in the field of cartilage tissue engineering is to mimic the structure and mechanics of native cartilage, most current attempts to create mimetic neocartilage fall short. Quantification of minor collagens would form the foundation of a systematic approach toward engineering biomimetic cartilages.

Cartilage tissue engineers frequently use scaffolds, such as collagen or synthetic materials, for cell seeding^{150–152}. Collagen scaffolds are naturally occurring biomaterials that support cell adhesion, are degradable, and can have a low or pro-healing immune response^{153,154}. Collagen can also be blended with natural (for example, silk, hyaluronic acid) or synthetic polymers (for example, poly(lactic acid), poly(L-lactide-co-glycolic acid)) to improve the mechanical properties and support a chondrogenic phenotype in both primary and stem cells¹⁵⁵. 3D woven composite scaffolds can recapitulate certain biomechanical properties of native cartilage, such as anisotropy, viscoelasticity, and tension–compression nonlinearity¹⁵⁶. Although these attributes may help neocartilage formation, collagen and synthetic scaffolds do not

recapitulate the variety and distribution of different collagen subtypes and crosslinks of native tissues. It remains unknown whether scaffolds are sufficiently biomimetic to effectively regenerate damaged and diseased tissues.

Collagen subtypes in cartilage

For this Chapter, we define types I and II as major collagens in cartilages because they account for a majority of the collagen mass (for example, mature articular cartilage collagen is about 90% type II¹⁵⁷, and knee meniscus collagen is about 90% type I¹⁵⁸). The remaining collagen types (III, IV, V, VI, IX, X, XI, XII, XIII, XIV, XVI, XXII, and XXVII) make up the minor collagens in cartilage. It may appear daunting at first for cartilage researchers to consider these 15 collagen types simultaneously. Thus, we recommend organizing collagens not by the classical categorization, but by their functions in cartilage, as described in Figure 5a. For example, in tissue engineering, this system may make it easier to design criteria without an extensive background in collagen biochemistry.

Although the main collagens in cartilage are frequently identified and quantified with histological stains or ELISA methods, minor collagens are rarely identified in engineered cartilage, likely because of their low quantity and lesser-known roles; however, these minor collagens are necessary for the function of cartilage¹⁵⁹. For example, knockouts of many minor collagens result in lethal phenotypes (Figure 5b). In this section, we describe the function of each major and minor subtype (for example, for supporting collagen fibrils, maintaining chondrocytes, and forming interfaces between cartilages and other tissues) while noting its importance for cartilage tissue mechanics. A summary of all collagen subtypes in cartilages, including the alpha-chain isoforms, location, description, and structure, is provided in Table 2.

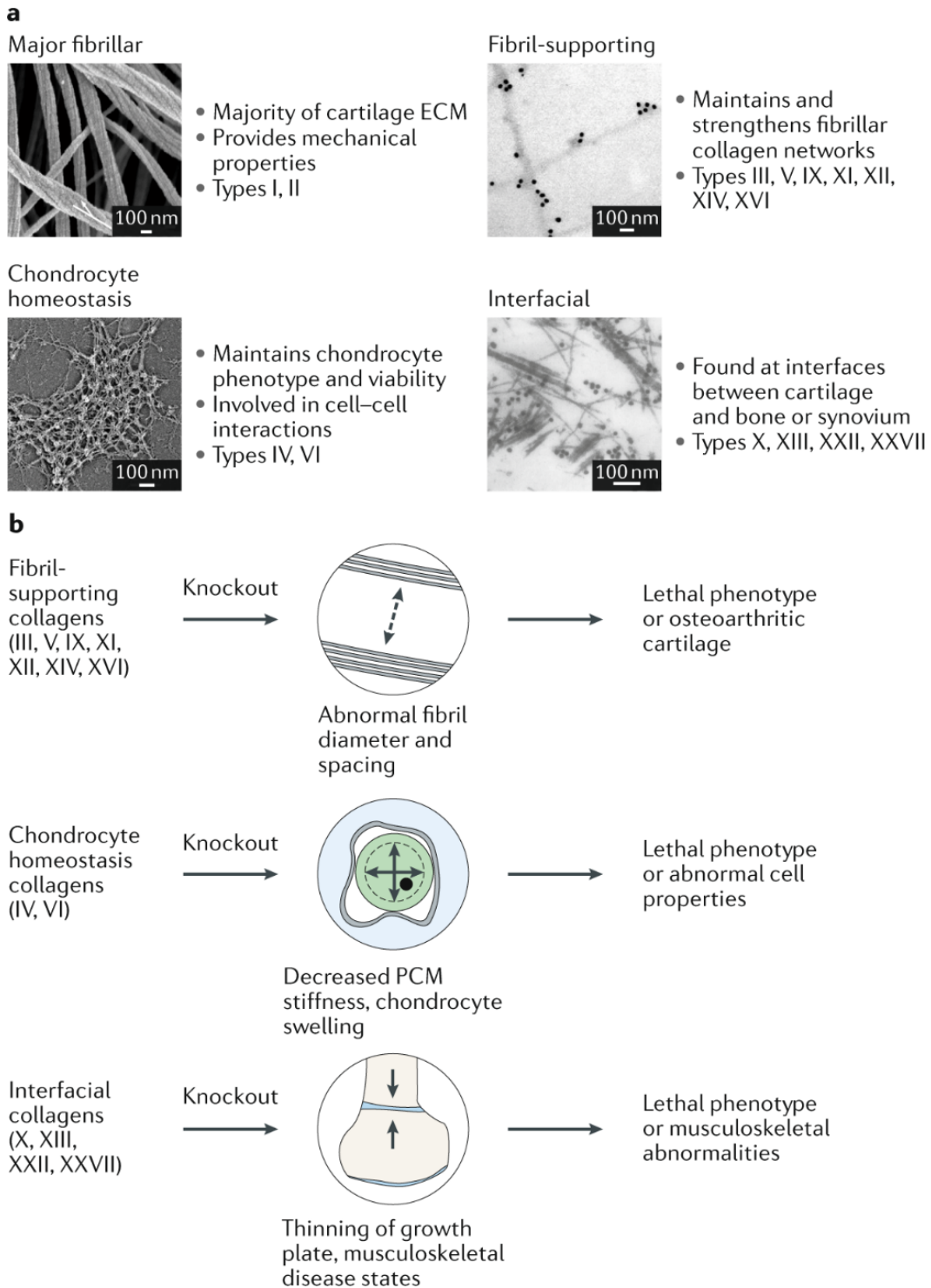



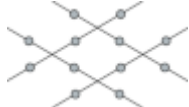



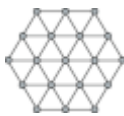

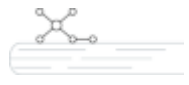

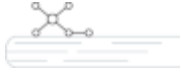



Figure 5. Functional groups of collagen subtypes in cartilage. (a) Scanning electron microscopy image of collagen fibers in knee articular cartilage (the white arrow indicates twisting of fibrils in the axial direction) (top left); immunogold electron microscopy (EM) image of labelled collagen IX (top right); rotary shadowing EM showing a collagen type VI network (bottom left); and immunogold EM image of labelled collagen type X (bottom right). (b) Knocking out different types of minor collagens can cause lethal or abnormal phenotypes in cartilage and other musculoskeletal tissues. ECM, extracellular matrix; PCM, pericellular matrix. Panel a, top left image from ref.167; top right image from ref.248; bottom left image from ref.249, bottom right image from ref.250.

Table 2. The collagen subtypes of cartilage. All collagen subtypes present in cartilage tissues are described. E, Elastic; F, fibrocartilage; H, hyaline; ECM, extracellular matrix; PCM, pericellular matrix; TM, territorial matrix. Refer to the subsections under 'Collagen subtypes in cartilage' for information about the isoforms.

Collagen subtype	Cartilage location	Description	Structure	Refs
I	ECM (E,F)	Main fibrillar type of fibrocartilage and elastic cartilages		111,114,121
II	ECM (E,F,H)	Main fibrillar type of hyaline, fibrocartilage, and elastic cartilages		3,111,112
III	ECM (E,F,H)	<ul style="list-style-type: none"> Fibrillar type co-assembling with collagen type I Involved in repair response with collagen type II 		124,179,180
IV	PCM (H)	<ul style="list-style-type: none"> Tetrameric network in PCM of articular cartilage Potential involvement in chondrocyte homeostasis 		201–204
V	ECM (E,F)	Fibrillar type co-assembling with collagen type I		181–183
VI	PCM (E,F,H)	Regulation of PCM properties and mechanotransduction		205–207
IX	ECM (E,F,H)	<ul style="list-style-type: none"> Forms crosslinks with collagen type II Forms collagen type II-IX-XI heterofibrils 		184,185
X	Deep zone (H)	<ul style="list-style-type: none"> Produced by hypertrophic chondrocytes Marker of endochondral ossification 		62,208
XI	ECM (E,F,H)	<ul style="list-style-type: none"> Involved with fibrillogenesis of collagen type II Forms collagen type II-IX-XI heterofibrils 		157,189
XII	ECM (E,F,H)	<ul style="list-style-type: none"> Codistributed with collagen types I and II May contribute to fibril alignment and stabilization 		192–194
XIII	Deep zone (H)	Involved with endochondral ossification		210,211

XIV	ECM (E,F,H)	<ul style="list-style-type: none"> Involved in fibrillogenesis of collagen types I and II 		196,197
XVI	TM (H)	<ul style="list-style-type: none"> Associates with collagen type II fibrils May stabilize larger collagen fibrils 		198–200
XXII	Synovial junction (H)	<ul style="list-style-type: none"> Associates with collagen type VI Role in cartilage understudied 	Not yet determined	212,213
XXVII	Deep zone (H)	<ul style="list-style-type: none"> Associated with endochondral ossification Structural role in PCM of growth plate cartilage 	Not yet determined	215–217

Major fibrillar collagens (I, II)

Collagen type I comprises a large portion of the ECM of many connective tissues, lending stiffness to skin, tendon, ligament, bone, and fibrocartilage. For example, collagen type I accounts for about 85% of dry weight of the TMJ disc¹⁶⁰. Its spatial distribution can vary among different cartilages. For example, the collagen type I content in the outer annulus of the intervertebral disc is over 80% by dry weight, but drops to about 70% in the inner annulus¹⁶¹. Similarly, in the knee meniscus, the outer red-red zone of the tissue is approximately 80% collagen type I by dry weight; however, in the inner white-white zone, this proportion drops by over half¹¹⁴. Collagen type I is also found in elastic cartilage, giving structure and mechanical properties to the tissue alongside collagen type II and elastin¹²¹. Collagen type I in hyaline articular cartilage can indicate damage or pathology, and it can be found when ineffective fibrocartilage repair tissue fills a defect, eventually leading to osteoarthritis¹¹⁰. Collagen type I is usually found in the heterotrimer $\alpha_1\alpha_2$ (a triple helix of two α_1 chains and one α_2 chain) but is also found in the $\alpha_1\alpha_1\alpha_1$ homotrimer (three α_1 chains) in fetal tissues, fibrosis, and cancer; this isomer is not found in healthy non-fetal tissues¹⁶².

Collagen type II represents 90–95% of the collagen in hyaline cartilage¹¹². It is found in the isoform $\alpha_1\alpha_1\alpha_1$, and in hyaline cartilage, is interwoven with proteoglycan aggregates consisting of hyaluronic acid, aggrecan core protein, and GAGs. The collagen network formed by collagen

type II is a crosslinked polymer that also contains collagen types IX, XI, XII, and XIV. This collagen network and its crosslinks are highly correlated with tensile stiffness and strength³, but also have roles in articular cartilage compression¹⁶³. Collagen type II is also present in fibrocartilage and elastic cartilage ECM, making up the majority of the inner white-white zone of the knee meniscus, as well as a portion of the TMJ disc, intervertebral disc, and auricular cartilage^{114,121,161,164}.

The major fibrillar collagens form a hierarchical structure. Collagen molecules, which are about 300-nm long and about 1.5 nm in diameter, are axially staggered by a multiple of approximately 67 nm, which creates a characteristic 'D-period' or 'D-band'¹⁶⁵. D-periodic molecular segments pack together in a quasi-hexagonal lattice to form collagen microfibrils¹⁶⁶. In hyaline cartilage, collagen II microfibrils surround collagen type XI microfibrils to form thin fibrils, with a diameter of about 20 nm (Ref. ¹⁶⁷). These fibrils grow laterally, organizing like ropes threaded with thin fibrils, to form fibril bundles or fibers with diameters from 40 to 200 nm (Ref.¹⁶⁸). In fibrocartilage, collagen type I can form fibrils by itself, but it can also form heterofibrils with collagens III and V^{169,170}. The fibril size in fibrocartilage can vary greatly by location, from 35-nm fibrils at the meniscus surface to 120-nm fibrils below¹⁷¹. Collagen fibrils with a diameter 100–150 nm have been observed in the intervertebral disc¹⁷², and thinner fibrils (20–40-nm diameter) were found in human fetal intervertebral discs¹⁷³.

Why collagen type II, not type I, makes up most of the hyaline cartilage ECM, and is almost absent from other parts of the body, remains an important question. There is ample evidence that fibrocartilage, which is abundant in collagen type I, is ineffective at replacing hyaline cartilage as a repair tissue^{174,175}. The repaired fibrocartilage is mechanically weaker and more permeable than articular cartilage, and degrades over two years^{110,176}. When articular cartilage is compressed, osmotic swelling pressure from GAGs provides compressive resistance, and this swelling is restrained by the collagen type II network¹⁷⁷. Collagen type II has a larger molecular spacing than collagen type I due to glycosylated hydroxylysine residues, allowing it to contain 50–100% more water than collagen type I¹⁷⁸. The ability of collagen type II to hold more water may be significant

for restraining osmotic swelling and dissipating compressive forces, and, thus, explain why this collagen type is uniquely present in hyaline cartilage¹⁷⁸.

Fibril-supporting collagens (III, V, IX, XI, XII, XIV, XVI)

Collagen type III is found in the ECM of various musculoskeletal tissues, organs, and skin, and has the isoform $\alpha 1_3$. It is essential for normal collagen type I fibrillogenesis, organizing and regulating the diameter of type I fibrils¹⁷⁹. Collagen type III is found alongside collagen type I in fibrocartilages, although it accounts for less than 10% of the overall collagen content¹⁵⁸. In articular cartilage, collagen type III is also crosslinked to collagen type II, which superimposes it onto collagen type II-IX-XI copolymers¹⁸⁰. Moreover, collagen type III can add additional cohesion or strength when a collagen type II network is damaged. For example, one study found a sixfold upregulation of collagen type III in osteoarthritic hip cartilage compared to control¹²⁵, although this may be due to co-polymerization with collagen type I, which is also present in osteoarthritic cartilage¹²⁴. Although global knockout of collagen type III results in perinatal lethality from rupture of major blood vessels¹⁷⁹, cartilage mechanics have not been studied in knockouts.

Collagen type V is found in the ECM of bone, cartilage, and corneal stroma. The major isoform of collagen type V is $\alpha 1_2\alpha 2$, which co-assembles with collagen type I¹⁸¹, where type I fibrils are co-polymerized on a template of collagen type V¹⁸². Global collagen type V mouse knockouts are embryonic lethal, and a conditional knockout in the cornea showed that collagen type V is necessary for fibrillogenesis; the knockout mice produced normal amounts of collagen type I, but with increased fibril and abnormal structure¹⁸³. This implies that collagen type V increases the mechanical strength in tissues containing collagen type I (for example, fibrocartilage, tendon, and skin). However, potentially because of the neonatal lethality of global collagen type V knockouts, the relationship between collagen type V and tissue mechanics has not been determined.

Collagen type IX, which has the isoform $\alpha 1\alpha 2\alpha 3$, is found in articular cartilage, where it forms LOX-mediated crosslinks with collagen type II fibrils to stabilize and strengthen the ECM.

Collagen type IX, alongside collagen type XI, is colocalized with collagen type II fibrils¹⁸⁴. All three alpha-chains of collagen type IX contain intermolecular crosslinking sites, where they form covalent bonds with other collagen type IX molecules, or with collagen type II¹⁸⁵. The quantity of collagen type IX decreases with cartilage age, starting at over 10% of the overall collagen content in fetal articular cartilage and dropping to about 1% in adult articular cartilage¹⁵⁷. This collagen type is also necessary for the maturation of cartilage during fracture repair, as shown in a global knockout study¹⁸⁶. Knockouts lead to degenerative joint disease resembling osteoarthritis¹⁸⁷; however, the mechanics of collagen type IX-deficient cartilage have not been tested.

Collagen type XI has the isoform $\alpha1\alpha2\alpha3$ and is broadly distributed in many tissues. In articular cartilage, it crosslinks with itself in fibrils that also contain collagen types II and IX, and is involved with fibrillogenesis by maintaining the spacing and diameter of collagen type II fibrils¹⁵⁷. The $\alpha3$ chain of collagen type XI has the same primary structure as the $\alpha1$ chain of collagen type II.¹⁸⁸ In articular cartilage, collagen type XI was shown to trimerize with collagen type V in the isoforms $\alpha1(XI)\alpha1(V)\alpha3(XI)$ and $\alpha1(XI)\alpha2(V)_2$ ¹⁸⁹. This means it would be more accurate to describe collagen types V and XI as a single type, collagen V/XI¹⁹⁰. A collagen type XI $\alpha1$ global knockout mouse model was neonatal lethal, with thick banded collagen fibrils in cartilage ECM¹⁹¹. Like collagen type IX, collagen type XI decreases with age, accounting for over 10% of overall collagen in fetal articular cartilage and about 3% in adult articular cartilage¹⁵⁷.

Collagen type XII is codistributed with collagen type I in bone, ligament, tendon, fibrocartilage, muscle, and skin, and codistributed with collagen type II in articular cartilage¹⁹². It has the isoform $\alpha1_3$ and is associated with fibril formation, cell adhesion, fibrosis, and osteogenesis. One study on passaged chondrocytes showed that collagen type XII is present in cartilage-forming chondrocytes, but not in the other dedifferentiated chondrocytes, indicating that this collagen subtype is necessary to support the formation of hyaline cartilage¹⁹³. It may contribute to fibril organization, alignment, and stabilization, helping the matrix bear load¹⁹⁴. Collagen type XII expression is localized to the growth plate and the surface of articular cartilage,

and has been found in juvenile but not embryonic rib hyaline cartilage¹⁹⁴. Children with collagen type XII mutations show muscle weakness and joint hyperlaxity¹⁹⁵, but cartilage effects have not been reported.

Collagen type XIV has the isoform $\alpha 1_3$. A global knockout mouse model of collagen type XIV resulted in deteriorated mechanical properties of skin and tendon, and showed that this collagen type has a role in fibrillogenesis and regulating fibril diameter¹⁹⁶. In this study, collagen fibrils were thicker, and mature fibrils did not form; however, the resulting effects on cartilage mechanics were not tested. Collagen type XIV has also been identified as a binding partner of COMP⁶³, and mutations of ECM proteins matrilin-3 and COMP decreased the relative amount of collagen type XIV in cartilage, indicating that these proteins stabilize collagen type XIV¹⁹⁷.

Collagen type XVI has the isoform $\alpha 1_3$ and is found in the territorial matrix of hyaline cartilage in a population of thin collagen type II fibrils, which also contains collagen type IX (but without colocalization of types IX and XVI)¹⁹⁸. The role of collagen type XVI is not well understood, but it is hypothesized to stabilize ECM by connecting and organizing large fibrillar networks¹⁹⁹. It binds to integrins, fibronectin, and fibrillin-1 and -2, participating in intermolecular interactions, organization, and maintenance²⁰⁰. Knockout studies of collagen type XVI have not been performed.

Chondrocyte-homeostasis collagens (IV, VI)

Collagen type IV is the main component of the basement membrane in articular cartilage and has $\alpha 1_2\alpha 2$ isoform. It forms a tetrameric network in the pericellular matrix (PCM) of articular cartilage, where it is involved in maintaining the viability and phenotype of articular chondrocytes²⁰¹. Collagen type IV expression is decreased in damaged cartilage and clinically failed repair tissue²⁰². It contains anti-angiogenic domains, suggesting that it may have an important role in cartilage homeostasis by arresting tumour growth in vivo²⁰³. Owing to its role in the basement membrane, global knockout mouse models are embryonic lethal²⁰⁴. Although collagen type IV

seems to have an important role in cartilage PCM, the specific mechanisms must be further investigated to understand how this collagen type maintains healthy chondrocyte properties.

Collagen type VI makes up about 1% of total collagen in adult articular cartilage, where it is mainly found in the PCM¹⁵⁷. It has been hypothesized to have important roles in mediating cell–cell and intermolecular interactions²⁰⁵. It was originally thought to have a single isoform of $\alpha1\alpha2\alpha3$, but the $\alpha3$ chain can be switched for an $\alpha4$, $\alpha5$, or $\alpha6$ chain²⁰⁶. In a global knockout model, a lack of collagen type VI resulted in swelling cells and decreased stiffness of the PCM, indicating that it regulates PCM and cellular properties²⁰⁷.

Interfacial collagens (X, XIII, XXII, XXVII)

Collagen type X, which has the isoform $\alpha1_3$, creates a hexagonal network that is limited locally to hypertrophic cartilage and close to the calcified zone of the cartilage. Because collagen type X is only found at this boundary between cartilage and bone, we classify it as an interfacial collagen. Although it is not produced by most chondrocytes, about 45% of hypertrophic chondrocyte collagen production is collagen type X⁶². It is highly correlated spatially and temporally with endochondral ossification, making it a biomarker of cartilage hypertrophy²⁰⁸. A collagen type X global knockout study showed that without collagen type X, mice exhibited 14% lethality, whereas the rest had dwarfism and growth-plate compression²⁰⁹.

Collagen type XIII, which has the isoform $\alpha1_3$, is the only collagen in cartilage that spans the cell membrane. It is observed in the perichondrium, hypertrophic and proliferative cartilage, and in many other tissues²¹⁰. A transgenic mouse overexpressing collagen type XIII showed abnormally high bone mass; collagen type XIII was strongly expressed before mineralization started, suggesting that this collagen type has important roles in endochondral ossification²¹¹.

Collagen type XXII, which has the isoform $\alpha1_3$, is expressed at junctions between many different types of tissues, including the muscle attachment sites of ribs and the junction of articular cartilage and synovial fluid, where it associates with microfibrils, such as fibrillins, or collagen type

VI²¹². It has been shown to bind to collagen-binding integrins in the myotendinous junction, especially $\alpha 2\beta 1$ and $\alpha 11\beta 1$ ²¹³; however, its function in articular cartilage remains largely understudied and unknown. Although knockouts in mammals have not been performed, global knockdown of collagen type XXII in zebrafish resulted in muscular dystrophy²¹⁴.

Collagen type XXVII, like collagen type X, is found near the osteochondral junction and is associated with endochondral ossification²¹⁵. It has the isoform $\alpha 1_3$ and has a structural role in the PCM of growth-plate cartilage²¹⁶. Collagen type XXVII is much less abundant than the other types of fibril-forming collagens, and its function is not well understood²¹⁷. Mutations in the collagen type XXVII gene lead to Steel syndrome — a disease involving skeletal abnormalities, such as dislocations, short stature, and scoliosis²¹⁸.

Collagen and mechanical properties

The structure of collagen subtypes and crosslinks affects the function of the cartilage tissue. For the purpose of this Chapter, the 'structure' of matrix components refers to measurable physical properties, such as the quantity of collagen, quantity of crosslinks, and the spatial distribution and homogeneity of the collagen network. The function of cartilage refers to the measurable material characteristics of the overall tissue, such as the tensile stiffness, viscoelastic measures (such as the aggregate modulus), and the lubricity of the cartilage surface.

Some structure–function relationships in cartilages have been well characterized, particularly those between the quantity of GAGs and compressive stiffness²¹⁹, and between the quantity of collagen crosslinks and tensile stiffness^{3,220}. Relationships that correlate collagen content to compressive properties and Poisson's ratio in articular cartilage have also been described¹⁴. Structure–function relationships of specific collagen subtypes are yet to be explicitly defined, but some may be inferred from previous work; because most of the collagen of fibrocartilage is collagen type I, and most of the collagen of hyaline cartilage is collagen type II, it can be assumed that non subtype-specific structure–function relationships are mostly due to

these two collagen types. Collagen type VI knockout models showed a structure–function relationship between the amount of collagen type VI and PCM stiffness²⁰⁷. Because full knockouts of collagen types are often neonatal lethal, and collagens form heterofibrils of more than one collagen type, it may be difficult to determine the influence of individual collagen subtypes on the mechanical properties. Nonetheless, the vital roles of minor collagens (for example, in fibril assembly) suggest that their relative contribution to cartilage biomechanics is far greater than their relative proportion of mass in cartilage ECM.

Because the goal of cartilage tissue engineering is functional restoration of diseased or damaged cartilage, the engineered tissue must have similar functional properties to native cartilage. With defined structure–function relationships, certain structural measurements can serve as quality-control measures or design criteria for engineering cartilage. For example, specific GAG or measurements of collagen subtype can be used to assess tissue quality. If these structural analyses are nondestructive, they could be used as preliminary benchmarks prior to implantation. For example, native-like amounts of collagen types IV and VI can be indicative of healthy chondrocytes and PCM suitable for implantation. The presence of collagen type II at 50–60% by dry weight and with crosslinks similar to those of native tissue, would indicate a tissue with native-like tensile properties. Understanding the structure–function relationships of different collagen subtypes would give insight to further develop the cartilage tissue-engineering process and may hold the key to further strengthening neocartilages. For example, quantifying interfacial collagens may indicate how well an osteochondral implant can maintain healthy subchondral bone, and quantification of fibril-supporting collagens can inform tissue engineers whether the ECM is mature and robust.

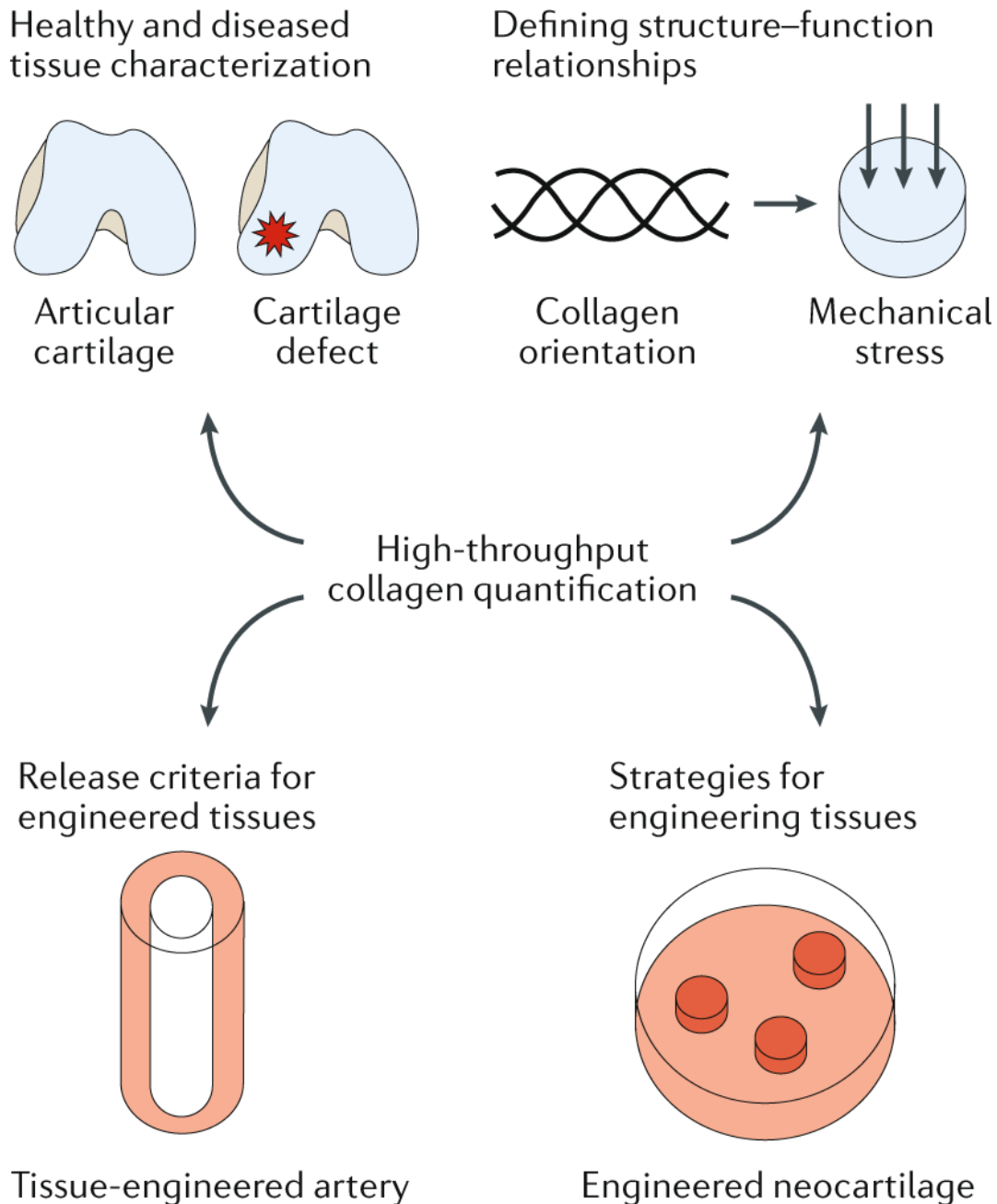


Figure 6. Broad applications for high-throughput, low-cost collagen quantification. The development of next-generation assays for collagen-subtype quantification will impact many different fields of biomedical engineering. Examples are shown for healthy and diseased tissues, structure–function relationships, tissue-engineering release criteria and tissue-engineering strategies.

Outlook

Although bottom-up proteomics allows the simultaneous analysis of many collagen types, and targeted MRM techniques offer fast analysis of individual collagen types, no methods exist for high-throughput quantification of both major and minor collagen subtypes. The development of

such a method would be an important milestone for understanding the distributions and roles in all tissue types of minor collagens. Ideally, this would be low-cost and allow for processing of many samples quickly, while keeping operator time to a minimum. Because collagen has roles throughout the body, characterization studies on a multitude of tissues will not only deepen our understanding of ECM composition, tissue disease states, and structure–function relationships, but also lead to design criteria for engineered tissues (Figure 6).

Characterization in disease states

Although shotgun proteomics has increased our understanding of the collagen profile of cartilages and other musculoskeletal tissues^{221–223}, sufficiently powered studies to characterize the collagen subtypes of these native tissues must be performed. If highly sensitive targeted or bottom-up LC-MS methods for all minor collagens can be performed in a short (for example, 5- or 10-minute) run, this would allow the analysis of collagens in tissues from different ages, sexes, and species to provide a more comprehensive understanding of the biochemical makeup of healthy native tissues. Once these values are defined, screening efforts can show how cellular phenotype and tissue proteome change through disease or injury. For example, MRM was recently used to show that collagen types II, III, and VI were deposited in greater amounts in osteoarthritic articular cartilage than in the control articular cartilage²²⁴, and label-free, bottom-up proteomics was used in an in vitro lung fibrosis model to quantify the relative amounts of collagen types I–VIII, XII, XV, XVI, and XVIII²²⁵. In recent years, machine learning has become increasingly important for analysing large datasets in biomedicine^{226–228}. Proteomic datasets with thousands of quantified peptides are excellent candidates for machine-learning algorithms, which may lead to new discoveries of biomarkers for prediction or early detection of many different diseases. In the coming years, quantitative assessments of collagen subtypes in healthy and diseased tissues will be of the utmost importance in understanding the ECM of native tissue and how it remodels through degeneration and disease.

Biomechanical relationships

Several structure–function relationships between biochemical and biomechanical properties are yet to be defined for cartilages, particularly those of minor collagens. Knockout or mutation mouse studies have been completed for collagen types IX²²⁹, XI²³⁰, and XIV¹⁹⁶, but only one study has tested the resultant effects on cartilage mechanics; this knockout study of collagen type VI found a reduced Young’s modulus of the PCM but not of the bulk cartilage²³¹. The quantity, spatial distribution, homogeneity, and assembly of other minor collagens have yet to be tied to the functional properties of cartilage.

Defined structure–function relationships are largely limited to compressive and tensile moduli, which do not constitute the full picture. Cartilages are viscoelastic and lubricious, making it necessary to understand correlations with functional properties such as instantaneous and relaxation moduli, permeability, and tribological properties. Once high-throughput quantification methods for minor collagens are developed, it may be possible to draw correlations between specific collagen subtypes and these and other additional functional properties. For example, well-defined correlations between tensile stiffness and major fibrillar collagens exist but are not yet complemented by studies on fibril-supporting collagens. Collagen type VI has been shown to correlate to PCM stiffness, but collagen type IV has not. It is not known if the presence of interfacial collagens could be correlated to integration strength, or if collagen type XXII at the interface with synovial fluid could have a role in cartilage lubricity. These relationships, if determined experimentally, would further help to elucidate the roles of minor collagens in different tissues.

Screening for engineered therapeutics

Minor collagens and collagen subtype quantification are absent from tissue engineering, perhaps owing to the lack of robust and high-throughput methods for collagen subtype quantification. Although the hydroxyproline assay is frequently used to estimate overall collagen, individual

collagen subtypes are rarely quantified, and relatively little attention has been paid to minor collagens in engineered tissues. For example, collagen type XIV is only mentioned in two tissue-engineering studies: one identified mRNA²³² and the other identified the protein with LC-MS²³³. Collagen subtype identification is present in some tissue-engineering studies. For example, IF has been used to identify collagen types I and III in cultured fibroblasts for engineering ligaments²³⁴; IHC has been used to visualize collagen types I and II in mesenchymal stem cell-seeded scaffolds for engineering of intervertebral discs²³⁵; collagen type III mRNA has been identified in engineered arterial grafts²³⁶; and TR-LIFS has been used to assess the relative expression of collagen types I, III, IV, and V in osteogenic ECM from adipose-derived stem cells²³⁷. However, the lack of subtype specificity for collagen histological stains and the non-quantitative nature of collagen IHC and IF techniques inhibit a deep understanding of the role of minor collagens in engineered tissues. Ideally, engineered tissues are fully biomimetic, exhibiting the same quantities of all collagen subtypes in native tissues. With the advent of new high-throughput collagen quantification technologies, all tissue engineers will be able to measure the biomimicry of their tissues on a collagen subtype level; the quality of engineered cartilages, bones, heart valves, ligaments, tendons, blood vessels, and skin will particularly depend on their major and minor collagen content.

Collagens for engineering neocartilages

Tissue engineers have put much effort in harnessing major fibrillar collagens to improve the mechanical properties of neocartilage, for example, by using tensile stimulation to increase the alignment of collagen fibrils²³⁸. Spectroscopic techniques are promising for quantitative and non-destructive measurement of collagen in cartilage tissue engineering. For example, TR-LIFS was used to measure collagen type II²³⁹ and diffuse fiber-optic Raman spectroscopy with hydroxyproline assay was used assess collagen deposition²⁴⁰ in engineered cartilage.

Compared with the tissue-engineering research on total or major collagens, relatively little has focusses specifically on minor collagens. Some tissue-engineering studies using primary chondrocytes or stem cells quantified collagen type IX with ELISA²⁴¹, and identified collagen type XI²⁴², and types VI, IX, XI, XII, and XIV with mass spectrometry²³³. However, no studies have determined if specific collagen types in engineered cartilage ECM are similar to those in native tissues. Similarly, there has been no attempt to promote deposition of minor collagens for engineered cartilages. We suggest that, because different collagen types are expressed by mesenchymal stem cells and differentiated chondrocytes during fetal development, tissue engineers could use these collagen types as markers of neocartilage development. For example, the self-assembling process in cartilage tissue engineering is reminiscent of mesenchymal condensation²⁴³ and follows the pattern of collagen type VI being remodelled and replaced by collagen type II²⁴⁴.

Collagen crosslinks have been the subject of some cartilage tissue-engineering studies and could be used to better characterize engineered tissues. For example, the deposition of HP crosslinks in engineered cartilage has been enhanced via hypoxia²⁴⁵, endogeneous LOX²⁴⁶, and mechanical stimulation with centrifugation²⁴⁷. HP is the only crosslink identified in engineered cartilages. A study on the presence of HLKLN, arginoline, or AGEs would better describe the quantity of different crosslinks in engineered cartilages.

The need for different collagen subtypes in engineered cartilages is indicated by their functional roles. The fibril-supporting collagens maintain and regulate fibrils of collagen types I and II, and, thus, should be used to assemble fibrils with correct spacing and diameter. Although chondrocyte-homeostasis collagens do not directly affect the strength of cartilage ECM, they interact with chondrocytes and maintain healthy tissue. Interfacial collagens are particularly important for osteochondral implants. Endochondral ossification continues until about age 18 for females and 21 for males;²⁴⁸ thus, these collagens are needed to produce implants that ossify and grow with the patient. A lack of minor collagens accounts for neonatal lethality or inferior

cartilage tissue. Therefore, native-like amounts of all minor collagens are necessary in engineered cartilages. A better understanding and new methods for identifying novel biochemical and biophysical stimuli to enhance the deposition of collagen crosslinks and specific collagen subtypes are the next key steps toward strong, durable, and biomimetic cartilages.

References

- 1 Whitslar, W. H. A Study of the Chemical Composition of the Dental Pulp. *Am J Dent Sci* **23**, 350–355 (1889).
- 2 Lin, S. & Gu, L. Influence of Crosslink Density and Stiffness on Mechanical Properties of Type I Collagen Gel. *Materials* **8**, 551–560 (2015).
- 3 Eleswarapu, S. V., Responde, D. J. & Athanasiou, K. A. Tensile Properties, Collagen Content, and Crosslinks in Connective Tissues of the Immature Knee Joint. *PLoS One* **6**, e26178 (2011).
- 4 Brüel, A., Ortoft, G. & Oxlund, H. Inhibition of cross-links in collagen is associated with reduced stiffness of the aorta in young rats. *Atherosclerosis* **140**, 135–145 (1998).
- 5 Fang, M., Yuan, J., Peng, C. & Li, Y. Collagen as a double-edged sword in tumor progression. *Tumour Biol.* **35**, 2871–2882 (2014).
- 6 Xu, S. *et al.* The role of collagen in cancer: from bench to bedside. *J. Transl. Med.* **17**, 309 (2019).
- 7 Poole, A. R. *et al.* Type II collagen degradation and its regulation in articular cartilage in osteoarthritis. *Ann. Rheum. Dis.* **61 Suppl 2**, ii78–81 (2002).
- 8 Landewé, R. B. M. *et al.* Arthritis instantaneously causes collagen type I and type II degradation in patients with early rheumatoid arthritis: a longitudinal analysis. *Ann. Rheum. Dis.* **65**, 40–44 (2006).
- 9 Kuivaniemi, H., Tromp, G. & Prockop, D. J. Mutations in collagen genes: causes of rare and some common diseases in humans. *The FASEB Journal* vol. 5 2052–2060 (1991).
- 10 Arseni, L., Lombardi, A. & Orioli, D. From Structure to Phenotype: Impact of Collagen Alterations on Human Health. *Int. J. Mol. Sci.* **19**, (2018).
- 11 Soroushova, A. *et al.* The Collagen Suprafamily: From Biosynthesis to Advanced Biomaterial Development. *Adv. Mater.* **31**, e1801651 (2019).
- 12 Kadler, K. E., Hill, A. & Canty-Laird, E. G. Collagen fibrillogenesis: fibronectin, integrins, and minor collagens as organizers and nucleators. *Curr. Opin. Cell Biol.* **20**, 495–501 (2008).
- 13 Shoulders, M. D. & Raines, R. T. Collagen structure and stability. *Annu. Rev. Biochem.* **78**, 929–958 (2009).
- 14 Responde, D. J., Natoli, R. M. & Athanasiou, K. A. Collagens of articular cartilage: structure, function, and importance in tissue engineering. *Crit. Rev. Biomed. Eng.* **35**, 363–411 (2007).
- 15 Lin, K. *et al.* Advanced Collagen-Based Biomaterials for Regenerative Biomedicine. *Advanced Functional Materials* vol. 29 1804943 (2019).
- 16 Chang, S.-W. & Buehler, M. J. Molecular biomechanics of collagen molecules. *Materials Today* vol. 17 70–76 (2014).
- 17 Ricard-Blum, S. The collagen family. *Cold Spring Harb. Perspect. Biol.* **3**, a004978 (2011).
- 18 Sharma, U. *et al.* Structural basis of homo- and heterotrimerization of collagen I. *Nat. Commun.* **8**, 14671 (2017).

- 19 An, B. *et al.* Definition of the native and denatured type II collagen binding site for fibronectin using a recombinant collagen system. *J. Biol. Chem.* **289**, 4941–4951 (2014).
- 20 Pihlajamaa, T. *et al.* Characterization of recombinant human type IX collagen. Association of alpha chains into homotrimeric and heterotrimeric molecules. *J. Biol. Chem.* **274**, 22464–22468 (1999).
- 21 Eyre, D. R., Weis, M. A. & Wu, J.-J. Advances in collagen cross-link analysis. *Methods* **45**, 65–74 (2008).
- 22 Siegel, R. C. Biosynthesis of collagen crosslinks: increased activity of purified lysyl oxidase with reconstituted collagen fibrils. *Proc. Natl. Acad. Sci. U. S. A.* **71**, 4826–4830 (1974).
- 23 Barnard, K., Light, N. D., Sims, T. J. & Bailey, A. J. Chemistry of the collagen cross-links. Origin and partial characterization of a putative mature cross-link of collagen. *Biochem. J* **244**, 303–309 (1987).
- 24 Robins, S. Fibrillogenesis and Maturation of Collagens. *Dynamics of Bone and Cartilage Metabolism* 41–53 (2006) doi:10.1016/b9-78-012088-5/62650-0030.
- 25 Avery, N. C., Sims, T. J. & Bailey, A. J. Quantitative Determination of Collagen Cross-links. *Methods in Molecular Biology* 103–121 (2009) doi:10.1007/978-1-59745-413-1_6.
- 26 Saito, M. & Marumo, K. Effects of Collagen Crosslinking on Bone Material Properties in Health and Disease. *Calcif. Tissue Int.* **97**, 242–261 (2015).
- 27 Eyre, D. R., Weis, M. A. & Wu, J.-J. Maturation of collagen Ketoimine cross-links by an alternative mechanism to pyridinoline formation in cartilage. *J. Biol. Chem.* **285**, 16675–16682 (2010).
- 28 Willett, T. L., Kandel, R., De Croos, J. N. A., Avery, N. C. & Grynblas, M. D. Enhanced levels of non-enzymatic glycation and pentosidine crosslinking in spontaneous osteoarthritis progression. *Osteoarthritis Cartilage* **20**, 736–744 (2012).
- 29 Steinhart, H., Bosselmann, A. & Moeller, C. Determination of Pyridinolines in Bovine Collagenous Tissues. *Journal of Agricultural and Food Chemistry* vol. 42 1943–1947 (1994).
- 30 Tan, C. I., Kent, G. N., Randall, A. G., Edmondston, S. J. & Singer, K. P. Age-related changes in collagen, pyridinoline, and deoxypyridinoline in normal human thoracic intervertebral discs. *J. Gerontol. A Biol. Sci. Med. Sci.* **58**, B387–93 (2003).
- 31 Delmas, P. D., Schlemmer, A., Gineyts, E., Riis, B. & Christiansen, C. Urinary excretion of pyridinoline crosslinks correlates with bone turnover measured on iliac crest biopsy in patients with vertebral osteoporosis. *J. Bone Miner. Res.* **6**, 639–644 (1991).
- 32 Lindert, U. *et al.* Urinary pyridinoline cross-links as biomarkers of osteogenesis imperfecta. *Orphanet J. Rare Dis.* **10**, 104 (2015).
- 33 Takeuchi, S., Arai, K., Saitoh, H., Yoshida, K. & Miura, M. Urinary pyridinoline and deoxypyridinoline as potential markers of bone metastasis in patients with prostate cancer. *J. Urol.* **156**, 1691–1695 (1996).
- 34 Siegfried, M. Reticulin and collagen. *The Journal of Physiology* vol. 28 319–324 (1902).
- 35 Tebb, M. C. & Christine Tebb, M. Reticulin and collagen. *The Journal of Physiology* vol. 27 463–472 (1902).
- 36 Neuman, R. E. & Logan, M. A. The determination of hydroxyproline. *J. Biol. Chem.* **184**, 299–306 (1950).
- 37 Reddy, G. K. & Enwemeka, C. S. A simplified method for the analysis of hydroxyproline in biological tissues. *Clin. Biochem.* **29**, 225–229 (1996).
- 38 Cissell, D. D., Link, J. M., Hu, J. C. & Athanasiou, K. A. A Modified Hydroxyproline Assay Based on Hydrochloric Acid in Ehrlich's Solution Accurately Measures Tissue Collagen Content. *Tissue Eng. Part C Methods* **23**, 243–250 (2017).

- 39 Caetano, G. F., Fronza, M., Leite, M. N., Gomes, A. & Frade, M. A. C. Comparison of collagen content in skin wounds evaluated by biochemical assay and by computer-aided histomorphometric analysis. *Pharm. Biol.* **54**, 2555–2559 (2016).
- 40 Kliment, C. R., Englert, J. M., Crum, L. P. & Oury, T. D. A novel method for accurate collagen and biochemical assessment of pulmonary tissue utilizing one animal. *Int. J. Clin. Exp. Pathol.* **4**, 349–355 (2011).
- 41 Stoilov, I., Starcher, B. C., Mecham, R. P. & Broekelmann, T. J. Measurement of elastin, collagen, and total protein levels in tissues. in *Methods in Cell Biology* 133–146 (2018).
- 42 Khan, T. *et al.* Metabolic dysregulation and adipose tissue fibrosis: role of collagen VI. *Mol. Cell. Biol.* **29**, 1575–1591 (2009).
- 43 Wu, J. *et al.* Extraction and isolation of type I, III and V collagens and their SDS-PAGE analyses. *Trans. Tianjin Univ.* **17**, 111–117 (2011).
- 44 Hayashi, T. & Nagai, Y. Separation of the α Chains of Type I and III Collagens by SDS-Polyacrylamide Gel Electrophoresis. *J. Biochem.* **86**, 453–459 (1979).
- 45 Vincent, S. G., Cunningham, P. R., Stephens, N. L., Halayko, A. J. & Fisher, J. T. Quantitative densitometry of proteins stained with coomassie blue using a Hewlett Packard scanjet scanner and Scanplot software. *Electrophoresis* **18**, 67–71 (1997).
- 46 Eyre, D. R., Koob, T. J. & Van Ness, K. P. Quantitation of hydroxypyridinium crosslinks in collagen by high-performance liquid chromatography. *Anal. Biochem.* **137**, 380–388 (1984).
- 47 Saito, M., Marumo, K., Fujii, K. & Ishioka, N. Single-column high-performance liquid chromatographic-fluorescence detection of immature, mature, and senescent cross-links of collagen. *Anal. Biochem.* **253**, 26–32 (1997).
- 48 Robins, S. P., Stewart, P., Astbury, C. & Bird, H. A. Measurement of the cross linking compound, pyridinoline, in urine as an index of collagen degradation in joint disease. *Ann. Rheum. Dis.* **45**, 969–973 (1986).
- 49 Robins, S. P. *et al.* Direct, enzyme-linked immunoassay for urinary deoxypyridinoline as a specific marker for measuring bone resorption. *J. Bone Miner. Res.* **9**, 1643–1649 (1994).
- 50 Taneda, S. & Monnier, V. M. ELISA of pentosidine, an advanced glycation end product, in biological specimens. *Clin. Chem.* **40**, 1766–1773 (1994).
- 51 Sutandy, F. X. R., Reymond Sutandy, F. X., Qian, J., Chen, C.-S. & Zhu, H. Overview of Protein Microarrays. *Current Protocols in Protein Science* vol. 72 27.1.1–27.1.16 (2013).
- 52 Kuschel, C. *et al.* Cell adhesion profiling using extracellular matrix protein microarrays. *BioTechniques* vol. 40 523–531 (2006).
- 53 Baker, H. N., Murphy, R., Lopez, E. & Garcia, C. Conversion of a capture ELISA to a Luminex xMAP assay using a multiplex antibody screening method. *J. Vis. Exp.* (2012) doi:10.3791/4084.
- 54 Elshal, M. F. & McCoy, J. P. Multiplex bead array assays: performance evaluation and comparison of sensitivity to ELISA. *Methods* **38**, 317–323 (2006).
- 55 Kim, C. H. *et al.* Stability and reproducibility of proteomic profiles measured with an aptamer-based platform. *Sci. Rep.* **8**, 8382 (2018).
- 56 Coghlan, R. F. *et al.* A degradation fragment of type X collagen is a real-time marker for bone growth velocity. *Sci. Transl. Med.* **9**, (2017).
- 57 Koolmees, P. A. & Bijker, P. G. Histometric and chemical methods for determining collagen in meats. *Vet. Q.* **7**, 84–90 (1985).
- 58 Grimm, P. C. *et al.* Computerized image analysis of Sirius Red-stained renal allograft biopsies as a surrogate marker to predict long-term allograft function. *J. Am. Soc. Nephrol.* **14**, 1662–1668 (2003).
- 59 Brigger, D. & Muckle, R. J. Comparison of Sirius red and Congo red as stains for amyloid in animal tissues. *J. Histochem. Cytochem.* **23**, 84–88 (1975).

- 60 Coelho, P. G. B., Souza, M. V. de, Conceição, L. G., Vitoria, M. I. V. & Bedoya, S. A. O. Evaluation of dermal collagen stained with picosirius red and examined under polarized light microscopy. *An. Bras. Dermatol.* **93**, 415–418 (2018).
- 61 Nagai, M. *et al.* Alteration of cartilage surface collagen fibers differs locally after immobilization of knee joints in rats. *J. Anat.* **226**, 447–457 (2015).
- 62 Schmid, T. M. & Linsenmayer, T. F. Immunohistochemical localization of short chain cartilage collagen (type X) in avian tissues. *J. Cell Biol.* **100**, 598–605 (1985).
- 63 Agarwal, P. *et al.* Collagen XII and XIV, new partners of cartilage oligomeric matrix protein in the skin extracellular matrix suprastructure. *J. Biol. Chem.* **287**, 22549–22559 (2012).
- 64 Yakovlev, D. D. *et al.* Quantitative mapping of collagen fiber alignment in thick tissue samples using transmission polarized-light microscopy. *J. Biomed. Opt.* **21**, 71111 (2016).
- 65 Chen, X., Nadiarynk, O., Plotnikov, S. & Campagnola, P. J. Second harmonic generation microscopy for quantitative analysis of collagen fibrillar structure. *Nat. Protoc.* **7**, 654–669 (2012).
- 66 Keikhosravi, A. *et al.* Quantification of collagen organization in histopathology samples using liquid crystal based polarization microscopy. *Biomed. Opt. Express* **8**, 4243–4256 (2017).
- 67 Ghazanfari, S., Driessen-Mol, A., Strijkers, G. J., Baaijens, F. P. T. & Bouten, C. V. C. The evolution of collagen fiber orientation in engineered cardiovascular tissues visualized by diffusion tensor imaging. *PLoS One* **10**, e0127847 (2015).
- 68 Starborg, T., Lu, Y., Kadler, K. E. & Holmes, D. F. Chapter 17 Electron Microscopy of Collagen Fibril Structure In Vitro and In Vivo Including Three-Dimensional Reconstruction. *Methods in Cell Biology* 319–345 (2008) doi:10.1016/s0091-679x(08)00417-2.
- 69 Starborg, T. *et al.* Using transmission electron microscopy and 3View to determine collagen fibril size and three-dimensional organization. *Nat. Protoc.* **8**, 1433–1448 (2013).
- 70 Changoor, A. *et al.* Structural characteristics of the collagen network in human normal, degraded and repair articular cartilages observed in polarized light and scanning electron microscopies. *Osteoarthritis Cartilage* **19**, 1458–1468 (2011).
- 71 Ruozi, B. *et al.* Intact collagen and atelocollagen sponges: Characterization and ESEM observation. *Materials Science and Engineering: C* vol. 27 802–810 (2007).
- 72 Snellman, A. *et al.* A short sequence in the N-terminal region is required for the trimerization of type XIII collagen and is conserved in other collagenous transmembrane proteins. *The EMBO Journal* vol. 19 5051–5059 (2000).
- 73 Manferdini, C. *et al.* Immunoelectron microscopic localization of Collagen type XV during human mesenchymal stem cells mineralization. *Connect. Tissue Res.* **59**, 42–45 (2018).
- 74 Plumb, D. A. *et al.* Collagen XXVII is developmentally regulated and forms thin fibrillar structures distinct from those of classical vertebrate fibrillar collagens. *J. Biol. Chem.* **282**, 12791–12795 (2007).
- 75 Ranjit, S. *et al.* Imaging Fibrosis and Separating Collagens using Second Harmonic Generation and Phasor Approach to Fluorescence Lifetime Imaging. *Sci. Rep.* **5**, 13378 (2015).
- 76 Haudenschild, A. K. *et al.* Nondestructive fluorescence lifetime imaging and time-resolved fluorescence spectroscopy detect cartilage matrix depletion and correlate with mechanical properties. *Eur. Cell. Mater.* **36**, 30–43 (2018).
- 77 Haudenschild, A. K. *et al.* Non-destructive detection of matrix stabilization correlates with enhanced mechanical properties of self-assembled articular cartilage. *Journal of Tissue Engineering and Regenerative Medicine* vol. 13 637–648 (2019).
- 78 Sherlock, B. E. *et al.* Nondestructive assessment of collagen hydrogel cross-linking using time-resolved autofluorescence imaging. *J. Biomed. Opt.* **23**, 1 (2018).
- 79 Vidal, B. de C. & Mello, M. L. S. Collagen type I amide I band infrared spectroscopy. *Micron* **42**, 283–289 (2011).

- 80 Belbachir, K., Noreen, R., Gouspillou, G. & Petibois, C. Collagen types analysis and differentiation by FTIR spectroscopy. *Anal. Bioanal. Chem.* **395**, 829–837 (2009).
- 81 Bergholt, M. S., Serio, A. & Albro, M. B. Raman Spectroscopy: Guiding Light for the Extracellular Matrix. *Front Bioeng Biotechnol* **7**, 303 (2019).
- 82 Albro, M. B. *et al.* Raman spectroscopic imaging for quantification of depth-dependent and local heterogeneities in native and engineered cartilage. *NPJ Regen Med* **3**, 3 (2018).
- 83 Ye, H. *et al.* Burn-related Collagen Conformational Changes in ex vivo Porcine Skin using Raman Spectroscopy. *Sci. Rep.* **9**, 19138 (2019).
- 84 Nguyen, T. T. *et al.* Characterization of Type I and IV Collagens by Raman Microspectroscopy: Identification of Spectral Markers of the Dermo-Epidermal Junction. *Spectroscopy: An International Journal* vol. 27 421–427 (2012).
- 85 Marcu, L., Cohen, D., Maarek, J.-M. I. & Grundfest, W. S. Characterization of type I, II, III, IV, and V collagens by time-resolved laser-induced fluorescence spectroscopy. *Optical Biopsy III* (2000) doi:10.1117/12.382720.
- 86 Sun, Y. *et al.* Development of a dual-modal tissue diagnostic system combining time-resolved fluorescence spectroscopy and ultrasonic backscatter microscopy. *Rev. Sci. Instrum.* **80**, 065104 (2009).
- 87 Colgrave, M. L., Allingham, P. G., Tyrrell, K. & Jones, A. Multiple Reaction Monitoring for the Accurate Quantification of Amino Acids: Using Hydroxyproline to Estimate Collagen Content. *Methods Mol. Biol.* **2030**, 33–45 (2019).
- 88 Nimptsch, A. *et al.* Quantitative analysis of denatured collagen by collagenase digestion and subsequent MALDI-TOF mass spectrometry. *Cell Tissue Res.* **343**, 605–617 (2011).
- 89 Yoshida, K. *et al.* Quantitative evaluation of collagen crosslinks and corresponding tensile mechanical properties in mouse cervical tissue during normal pregnancy. *PLoS One* **9**, e112391 (2014).
- 90 Naffa, R. *et al.* Rapid analysis of pyridinoline and deoxypyridinoline in biological samples by liquid chromatography with mass spectrometry and a silica hydride column. *Journal of Separation Science* vol. 42 1482–1488 (2019).
- 91 Kovacevic, I., Pokrajac, M., Miljkovic, B., Jovanovic, D. & Prostran, M. Comparison of liquid chromatography with fluorescence detection to liquid chromatography-mass spectrometry for the determination of fluoxetine and norfluoxetine in human plasma. *J. Chromatogr. B Analyt. Technol. Biomed. Life Sci.* **830**, 372–376 (2006).
- 92 Lin, H., Goodin, S., Strair, R. K., DiPaola, R. S. & Gounder, M. K. Comparison of LC-MS Assay and HPLC Assay of Busulfan in Clinical Pharmacokinetics Studies. *ISRN Analytical Chemistry* vol. 2012 1–5 (2012).
- 93 Santa, T. Recent advances in analysis of glutathione in biological samples by high-performance liquid chromatography: a brief overview. *Drug Discov. Ther.* **7**, 172–177 (2013).
- 94 Dreisewerd, K., Rohlfing, A., Spottke, B., Urbanke, C. & Henkel, W. Characterization of whole fibril-forming collagen proteins of types I, III, and V from fetal calf skin by infrared matrix-assisted laser desorption ionization mass spectrometry. *Anal. Chem.* **76**, 3482–3491 (2004).
- 95 Pataridis, S., Eckhardt, A., Mikulikova, K., Sedlakova, P. & Miksik, I. Determination and Quantification of Collagen Types in Tissues Using HPLC-MS/MS. *Curr. Anal. Chem.* **5**, 316–323 (2009).
- 96 Wang, Y. *et al.* Quantitative proteomics analysis of cartilage response to mechanical injury and cytokine treatment. *Matrix Biol.* **63**, 11–22 (2017).
- 97 Kumazawa, Y., Taga, Y., Iwai, K. & Koyama, Y.-I. A Rapid and Simple LC-MS Method Using Collagen Marker Peptides for Identification of the Animal Source of Leather. *J. Agric. Food Chem.* **64**, 6051–6057 (2016).

- 98 Wiese, S., Reidegeld, K. A., Meyer, H. E. & Warscheid, B. Protein labeling by iTRAQ: A new tool for quantitative mass spectrometry in proteome research. *PROTEOMICS* vol. 7 1004–1004 (2007).
- 99 Lanucara, F. & Eyers, C. E. Mass spectrometric-based quantitative proteomics using SILAC. *Methods Enzymol.* **500**, 133–150 (2011).
- 100 Zhang, L. & Elias, J. E. Relative Protein Quantification Using Tandem Mass Tag Mass Spectrometry. *Methods in Molecular Biology* 185–198 (2017) doi:10.1007/978-1-4939-6747-6_14.
- 101 Ye, X., Luke, B., Andresson, T. & Blonder, J. 18O stable isotope labeling in MS-based proteomics. *Brief. Funct. Genomic. Proteomic.* **8**, 136–144 (2009).
- 102 Zhu, W., Smith, J. W. & Huang, C.-M. Mass spectrometry-based label-free quantitative proteomics. *J. Biomed. Biotechnol.* **2010**, 840518 (2010).
- 103 Dresner, E. & Schubert, M. THE COMPARATIVE SUSCEPTIBILITY TO COLLAGENASE AND TRYPSIN OF COLLAGEN, SOLUBLE COLLAGENS AND RENAL BASEMENT MEMBRANE. *Journal of Histochemistry & Cytochemistry* vol. 3 360–368 (1955).
- 104 Krey, J. F. *et al.* Accurate label-free protein quantitation with high- and low-resolution mass spectrometers. *J. Proteome Res.* **13**, 1034–1044 (2014).
- 105 Cox, J. *et al.* Accurate proteome-wide label-free quantification by delayed normalization and maximal peptide ratio extraction, termed MaxLFQ. *Mol. Cell. Proteomics* **13**, 2513–2526 (2014).
- 106 Önnarfjord, P., Khabut, A., Reinholt, F. P., Svensson, O. & Heinegård, D. Quantitative proteomic analysis of eight cartilaginous tissues reveals characteristic differences as well as similarities between subgroups. *J. Biol. Chem.* **287**, 18913–18924 (2012).
- 107 Lourido, L. *et al.* Quantitative proteomic profiling of human articular cartilage degradation in osteoarthritis. *J. Proteome Res.* **13**, 6096–6106 (2014).
- 108 Frantzi, M. *et al.* Discovery and validation of urinary biomarkers for detection of renal cell carcinoma. *J. Proteomics* **98**, 44–58 (2014).
- 109 van Huizen, N. A. *et al.* Up-regulation of collagen proteins in colorectal liver metastasis compared with normal liver tissue. *J. Biol. Chem.* **294**, 281–289 (2019).
- 110 Huey, D. J., Hu, J. C. & Athanasiou, K. A. Unlike Bone, Cartilage Regeneration Remains Elusive. *Science* **338**, 917–921 (2012).
- 111 Athanasiou, K. A., Darling, E. M., Hu, J. C., DuRaine, G. D. & Hari Reddi, A. *Articular Cartilage*. (CRC Press, 2017).
- 112 Sophia Fox, A. J., Bedi, A. & Rodeo, S. A. The Basic Science of Articular Cartilage: Structure, Composition, and Function. *Sports Health: A Multidisciplinary Approach* **1**, 461–468 (2009).
- 113 Almarza, A. J. & Athanasiou, K. A. Design Characteristics for the Tissue Engineering of Cartilaginous Tissues. *Ann. Biomed. Eng.* **32**, 2–17 (2004).
- 114 Makris, E. A., Hadidi, P. & Athanasiou, K. A. The knee meniscus: structure-function, pathophysiology, current repair techniques, and prospects for regeneration. *Biomaterials* **32**, 7411 (2011).
- 115 Kuroda, S. *et al.* Biomechanical and biochemical characteristics of the mandibular condylar cartilage. *Osteoarthritis Cartilage* **17**, 1408–1415 (2009).
- 116 Singh, M. & Detamore, M. S. Biomechanical properties of the mandibular condylar cartilage and their relevance to the TMJ disc. *J. Biomech.* **42**, 405–417 (2009).
- 117 Mithoefer, K., McAdams, T., Williams, R. J., Kreuz, P. C. & Mandelbaum, B. R. Clinical efficacy of the microfracture technique for articular cartilage repair in the knee: an evidence-based systematic analysis. *Am. J. Sports Med.* **37**, 2053–2063 (2009).
- 118 Bos, E. J. *et al.* Structural and Mechanical Comparison of Human Ear, Alar, and Septal Cartilage. *Plast Reconstr Surg Glob Open* **6**, e1610 (2018).

- 119 Griffin, M. F., Premakumar, Y., Seifalian, A. M., Szarko, M. & Butler, P. E. M. Biomechanical Characterisation of the Human Auricular Cartilages; Implications for Tissue Engineering. *Ann. Biomed. Eng.* **44**, 3460–3467 (2016).
- 120 Naumann, A. *et al.* Immunochemical and mechanical characterization of cartilage subtypes in rabbit. *J. Histochem. Cytochem.* **50**, 1049–1058 (2002).
- 121 Madsen, K., von der Mark, K., van Menxel, M. & Friberg, U. Analysis of collagen types synthesized by rabbit ear cartilage chondrocytes in vivo and in vitro. *Biochem. J* **221**, 189–196 (1984).
- 122 Setton, L. A., Elliott, D. M. & Mow, V. C. Altered mechanics of cartilage with osteoarthritis: human osteoarthritis and an experimental model of joint degeneration. *Osteoarthritis Cartilage* **7**, 2–14 (1999).
- 123 Miosge, N., Hartmann, M., Maelicke, C. & Herken, R. Expression of collagen type I and type II in consecutive stages of human osteoarthritis. *Histochem. Cell Biol.* **122**, 229–236 (2004).
- 124 Lahm, A. *et al.* Changes in content and synthesis of collagen types and proteoglycans in osteoarthritis of the knee joint and comparison of quantitative analysis with Photoshop-based image analysis. *Arch. Orthop. Trauma. Surg.* **130**, 557–564 (2010).
- 125 Hosseininia, S. *et al.* Evidence for enhanced collagen type III deposition focally in the territorial matrix of osteoarthritic hip articular cartilage. *Osteoarthritis Cartilage* **24**, 1029 (2016).
- 126 Heinemeier, K. M. Type II Collagen; Designed to Last a Lifetime? *Osteoarthritis and Cartilage* vol. 25 S5 (2017).
- 127 Owings, M. F. & Kozak, L. J. Ambulatory and inpatient procedures in the United States, 1996. *Vital Health Stat.* **13** 1–119 (1998).
- 128 Moseley, J. B. *et al.* A Controlled Trial of Arthroscopic Surgery for Osteoarthritis of the Knee. *N. Engl. J. Med.* **347**, 81–88 (2002).
- 129 Koh, J. L., Wirsing, K., Lautenschlager, E. & Zhang, L.-O. The effect of graft height mismatch on contact pressure following osteochondral grafting: a biomechanical study. *Am. J. Sports Med.* **32**, 317–320 (2004).
- 130 Khan, I. M., Gilbert, S. J., Singhrao, S. K., Duance, V. C. & Archer, C. W. Cartilage integration: evaluation of the reasons for failure of integration during cartilage repair. A review. *Eur. Cell. Mater.* **16**, 26–39 (2008).
- 131 Makris, E. A., Gomoll, A. H., Malizos, K. N., Hu, J. C. & Athanasiou, K. A. Repair and tissue engineering techniques for articular cartilage. *Nat. Rev. Rheumatol.* **11**, 21–34 (2014).
- 132 Zhang, Z. *et al.* Matrix-induced autologous chondrocyte implantation for the treatment of chondral defects of the knees in Chinese patients. *Drug Des. Devel. Ther.* **8**, 2439–2448 (2014).
- 133 Frisbie, D. D. *et al.* Early events in cartilage repair after subchondral bone microfracture. *Clin. Orthop. Relat. Res.* 215–227 (2003).
- 134 Barber, F. A. What is the terrible triad? *Arthroscopy* **8**, 19–22 (1992).
- 135 LeResche, L. Epidemiology of temporomandibular disorders: implications for the investigation of etiologic factors. *Crit. Rev. Oral Biol. Med.* **8**, 291–305 (1997).
- 136 Murphy, M. K., MacBarb, R. F., Wong, M. E. & Athanasiou, K. A. Temporomandibular disorders: a review of etiology, clinical management, and tissue engineering strategies. *Int. J. Oral Maxillofac. Implants* **28**, e393–414 (2013).
- 137 Urban, J. P. G. & Roberts, S. Degeneration of the intervertebral disc. *Arthritis Res. Ther.* **5**, 120–130 (2003).
- 138 Luoma, K. *et al.* Low Back Pain in Relation to Lumbar Disc Degeneration. *Spine* vol. 25 487–492 (2000).

- 139 Maniadas, N. & Gray, A. The economic burden of back pain in the UK. *Pain* vol. 84 95–103 (2000).
- 140 Ha, A. Y., Shalvoy, R. M., Voisinnet, A., Racine, J. & Aaron, R. K. Controversial role of arthroscopic meniscectomy of the knee: A review. *World J. Orthop.* **7**, 287–292 (2016).
- 141 Miloro, M. & Henriksen, B. Discectomy as the primary surgical option for internal derangement of the temporomandibular joint. *J. Oral Maxillofac. Surg.* **68**, 782–789 (2010).
- 142 Thorlund, J. B. *et al.* Patient reported outcomes in patients undergoing arthroscopic partial meniscectomy for traumatic or degenerative meniscal tears: comparative prospective cohort study. *BMJ* **356**, j356 (2017).
- 143 Illien-Jünger, S. *et al.* Detrimental effects of discectomy on intervertebral disc biology can be decelerated by growth factor treatment during surgery: a large animal organ culture model. *Spine J.* **14**, 2724–2732 (2014).
- 144 Kwon, H. *et al.* Surgical and tissue engineering strategies for articular cartilage and meniscus repair. *Nat. Rev. Rheumatol.* **15**, 550–570 (2019).
- 145 Makris, E. A., Gomoll, A. H., Malizos, K. N., Hu, J. C. & Athanasiou, K. A. Repair and tissue engineering techniques for articular cartilage. *Nat. Rev. Rheumatol.* **11**, 21–34 (2014).
- 146 Higashioka, M. M., Chen, J. A., Hu, J. C. & Athanasiou, K. A. Building an anisotropic meniscus with zonal variations. *Tissue Eng. Part A* **20**, 294–302 (2014).
- 147 Cao, Y., Vacanti, J. P., Paige, K. T., Upton, J. & Vacanti, C. A. Transplantation of chondrocytes utilizing a polymer-cell construct to produce tissue-engineered cartilage in the shape of a human ear. *Plast. Reconstr. Surg.* **100**, 297–302; discussion 303–4 (1997).
- 148 Little, C. J., Bawolin, N. K. & Chen, X. Mechanical properties of natural cartilage and tissue-engineered constructs. *Tissue Eng. Part B Rev.* **17**, 213–227 (2011).
- 149 Salinas, E. Y., Hu, J. C. & Athanasiou, K. A Guide for Using Mechanical Stimulation to Enhance Tissue-Engineered Articular Cartilage Properties. *Tissue Eng. Part B Rev.* **24**, 345–358 (2018).
- 150 Pulkkinen, H. J. *et al.* Repair of osteochondral defects with recombinant human type II collagen gel and autologous chondrocytes in rabbit. *Osteoarthritis and Cartilage* vol. 21 481–490 (2013).
- 151 Matsiko, A., Levingstone, T. J., O'Brien, F. J. & Gleeson, J. P. Addition of hyaluronic acid improves cellular infiltration and promotes early-stage chondrogenesis in a collagen-based scaffold for cartilage tissue engineering. *Journal of the Mechanical Behavior of Biomedical Materials* vol. 11 41–52 (2012).
- 152 Munir, N. & Callanan, A. Novel phase separated polycaprolactone/collagen scaffolds for cartilage tissue engineering. *Biomed. Mater.* **13**, 051001 (2018).
- 153 Corradetti, B. *et al.* Immune tuning scaffold for the local induction of a pro-regenerative environment. *Sci. Rep.* **7**, 17030 (2017).
- 154 Boehler, R. M., Graham, J. G. & Shea, L. D. Tissue engineering tools for modulation of the immune response. *Biotechniques* **51**, 239–40, 242, 244 passim (2011).
- 155 Irawan, V., Sung, T.-C., Higuchi, A. & Ikoma, T. Collagen Scaffolds in Cartilage Tissue Engineering and Relevant Approaches for Future Development. *Tissue Eng Regen Med* **15**, 673–697 (2018).
- 156 Moutos, F. T. & Guilak, F. Composite scaffolds for cartilage tissue engineering. *Biorheology* vol. 45 501–512 (2008).
- 157 Eyre, D. Collagen of articular cartilage. *Arthritis Res.* **4**, 30–35 (2002).
- 158 Eyre, D. R. & Wu, J. J. Collagen of fibrocartilage: a distinctive molecular phenotype in bovine meniscus. *FEBS Lett.* **158**, 265–270 (1983).
- 159 Luo, Y. *et al.* The minor collagens in articular cartilage. *Protein Cell* **8**, 560–572 (2017).

- 160 Johns, D. E. & Athanasiou, K. A. Design characteristics for temporomandibular joint disc
tissue engineering: learning from tendon and articular cartilage. *Proc. Inst. Mech. Eng. H*
221, 509–526 (2007).
- 161 Eyre, D. R. & Muir, H. Types I and II collagens in intervertebral disc. Interchanging radial
distributions in annulus fibrosus. *Biochem. J* **157**, 267–270 (1976).
- 162 Han, S. *et al.* Molecular mechanism of type I collagen homotrimer resistance to
mammalian collagenases. *J. Biol. Chem.* **285**, 22276–22281 (2010).
- 163 Li, L. P., Herzog, W., Korhonen, R. K. & Jurvelin, J. S. The role of viscoelasticity of collagen
fibers in articular cartilage: axial tension versus compression. *Med. Eng. Phys.* **27**, 51–57
(2005).
- 164 Aryaei, A., Vapniarsky, N., Hu, J. C. & Athanasiou, K. A. Recent tissue engineering
advances for the treatment of temporomandibular joint disorders. *Curr. Osteoporos. Rep.*
14, 269 (2016).
- 165 Bozec, L., van der Heijden, G. & Horton, M. Collagen fibrils: nanoscale ropes. *Biophys. J.*
92, 70–75 (2007).
- 166 Orgel, J. P. R. O., San Antonio, J. D. & Antipova, O. Molecular and structural mapping of
collagen fibril interactions. *Connect. Tissue Res.* **52**, 2–17 (2011).
- 167 Holmes, D. F. & Kadler, K. E. The 10+4 microfibril structure of thin cartilage fibrils. *Proc.*
Natl. Acad. Sci. U. S. A. **103**, 17249–17254 (2006).
- 168 Gottardi, R. *et al.* Supramolecular Organization of Collagen Fibrils in Healthy and
Osteoarthritic Human Knee and Hip Joint Cartilage. *PLoS One* **11**, e0163552 (2016).
- 169 Eryilmaz, E., Teizer, W. & Hwang, W. In Vitro Analysis of the Co-Assembly of Type-I and
Type-III Collagen. *Cellular and Molecular Bioengineering* vol. 10 41–53 (2017).
- 170 Gelse, K. Collagens—structure, function, and biosynthesis. *Advanced Drug Delivery*
Reviews vol. 55 1531–1546 (2003).
- 171 Petersen, W. & Tillmann, B. Collagenous fibril texture of the human knee joint menisci.
Anat. Embryol. **197**, 317–324 (1998).
- 172 Inoue, H. & Takeda, T. Three-dimensional observation of collagen framework of lumbar
intervertebral discs. *Acta Orthop. Scand.* **46**, 949–956 (1975).
- 173 Hickey, D. S. & Hukins, D. W. Collagen fibril diameters and elastic fibres in the annulus
fibrosus of human fetal intervertebral disc. *J. Anat.* **133**, 351–357 (1981).
- 174 Armiento, A. R., Alini, M. & Stoddart, M. J. Articular fibrocartilage - Why does hyaline
cartilage fail to repair? *Adv. Drug Deliv. Rev.* **146**, 289–305 (2019).
- 175 Karuppall, R. Current concepts in the articular cartilage repair and regeneration. *J Orthop*
14, A1–A3 (2017).
- 176 Zhang, L., Hu, J. & Athanasiou, K. A. The Role of Tissue Engineering in Articular Cartilage
Repair and Regeneration. *Critical Reviews™ in Biomedical Engineering* vol. 37 1–57
(2009).
- 177 Han, E., Chen, S. S., Klisch, S. M. & Sah, R. L. Contribution of proteoglycan osmotic
swelling pressure to the compressive properties of articular cartilage. *Biophys. J.* **101**,
916–924 (2011).
- 178 Grynepas, M. D., Eyre, D. R. & Kirschner, D. A. Collagen type II differs from type I in native
molecular packing. *Biochim. Biophys. Acta* **626**, 346–355 (1980).
- 179 Liu, X., Wu, H., Byrne, M., Krane, S. & Jaenisch, R. Type III collagen is crucial for collagen
I fibrillogenesis and for normal cardiovascular development. *Proc. Natl. Acad. Sci. U. S.*
A. **94**, 1852 (1997).
- 180 Wu, J.-J., Weis, M. A., Kim, L. S. & Eyre, D. R. Type III collagen, a fibril network modifier
in articular cartilage. *J. Biol. Chem.* **285**, 18537–18544 (2010).
- 181 Birk, D. E., Fitch, J. M., Babiarz, J. P. & Linsenmayer, T. F. Collagen type I and type V are
present in the same fibril in the avian corneal stroma. *J. Cell Biol.* **106**, 999–1008 (1988).

- 182 Wenstrup, R. J. *et al.* Type V collagen controls the initiation of collagen fibril assembly. *J. Biol. Chem.* **279**, 53331–53337 (2004).
- 183 Sun, M. *et al.* Collagen V is a dominant regulator of collagen fibrillogenesis: dysfunctional regulation of structure and function in a corneal-stroma-specific Col5a1-null mouse model. *J. Cell Sci.* **124**, 4096–4105 (2011).
- 184 Olsen, B. R. Collagen IX. *Int. J. Biochem. Cell Biol.* **29**, 555–558 (1997).
- 185 Eyre, D. R., Pietka, T., Weis, M. A. & Wu, J.-J. Covalent cross-linking of the NC1 domain of collagen type IX to collagen type II in cartilage. *J. Biol. Chem.* **279**, 2568–2574 (2004).
- 186 Opolka, A. *et al.* Collagen IX is indispensable for timely maturation of cartilage during fracture repair in mice. *Matrix Biology* vol. 26 85–95 (2007).
- 187 Fässler, R. *et al.* Mice lacking alpha 1 (IX) collagen develop noninflammatory degenerative joint disease. *Proc. Natl. Acad. Sci. U. S. A.* **91**, 5070–5074 (1994).
- 188 Oxford, J. T., Doege, K. J., Horton, W. E., Jr & Morris, N. P. Characterization of type II and type XI collagen synthesis by an immortalized rat chondrocyte cell line (IRC) having a low level of type II collagen mRNA expression. *Exp. Cell Res.* **213**, 28–36 (1994).
- 189 Wu, J.-J., Weis, M. A., Kim, L. S., Carter, B. G. & Eyre, D. R. Differences in chain usage and cross-linking specificities of cartilage type V/XI collagen isoforms with age and tissue. *J. Biol. Chem.* **284**, 5539–5545 (2009).
- 190 Fichard, A., Kleman, J.-P. & Ruggiero, F. Another look at collagen V and XI molecules. *Matrix Biol.* **14**, 515–531 (1995).
- 191 Fernandes, R. J., Weis, M., Scott, M. A., Seegmiller, R. E. & Eyre, D. R. Collagen XI chain misassembly in cartilage of the chondrodysplasia (cho) mouse. *Matrix Biol.* **26**, 597–603 (2007).
- 192 Chiquet, M., Birk, D. E., Bönnemann, C. G. & Koch, M. Collagen XII: Protecting bone and muscle integrity by organizing collagen fibrils. *Int. J. Biochem. Cell Biol.* **53**, 51–54 (2014).
- 193 Taylor, D. W. *et al.* Collagen type XII and versican are present in the early stages of cartilage tissue formation by both redifferentating passaged and primary chondrocytes. *Tissue Eng. Part A* **21**, 683–693 (2015).
- 194 Gregory, K. E., Keene, D. R., Tufa, S. F., Lunstrum, G. P. & Morris, N. P. Developmental distribution of collagen type XII in cartilage: association with articular cartilage and the growth plate. *J. Bone Miner. Res.* **16**, 2005–2016 (2001).
- 195 Zou, Y. *et al.* Recessive and dominant mutations in COL12A1 cause a novel EDS/myopathy overlap syndrome in humans and mice. *Human Molecular Genetics* vol. 23 2339–2352 (2014).
- 196 Ansorge, H. L. *et al.* Type XIV Collagen Regulates Fibrillogenesis: PREMATURE COLLAGEN FIBRIL GROWTH AND TISSUE DYSFUNCTION IN NULL MICE. *J. Biol. Chem.* **284**, 8427–8438 (2009).
- 197 Bell, P. A. *et al.* Analysis of the cartilage proteome from three different mouse models of genetic skeletal diseases reveals common and discrete disease signatures. *Biol. Open* **2**, 802–811 (2013).
- 198 Kassner, A. *et al.* Discrete integration of collagen XVI into tissue-specific collagen fibrils or beaded microfibrils. *Matrix Biol.* **22**, 131–143 (2003).
- 199 Grässel, S. & Bauer, R. J. Collagen XVI in health and disease. *Matrix Biol.* **32**, 64–73 (2013).
- 200 Kassner, A. *et al.* Molecular structure and interaction of recombinant human type XVI collagen. *J. Mol. Biol.* **339**, 835–853 (2004).
- 201 Kvist, A. J. *et al.* The major basement membrane components localize to the chondrocyte pericellular matrix--a cartilage basement membrane equivalent? *Matrix Biol.* **27**, 22–33 (2008).

- 202 Foldager, C. B. *et al.* Collagen Type IV and Laminin Expressions during Cartilage Repair
and in Late Clinically Failed Repair Tissues from Human Subjects. *Cartilage* **7**, 52–61
(2016).
- 203 Sudhakar, A. *et al.* Human alpha1 type IV collagen NC1 domain exhibits distinct
antiangiogenic activity mediated by alpha1beta1 integrin. *J. Clin. Invest.* **115**, 2801–2810
(2005).
- 204 Poschl, E. Collagen IV is essential for basement membrane stability but dispensable for
initiation of its assembly during early development. *Development* **131**, 1619–1628 (2004).
- 205 Pfaff, M. *et al.* Integrin and Arg-Gly-Asp dependence of cell adhesion to the native and
unfolded triple helix of collagen type VI. *Exp. Cell Res.* **206**, 167–176 (1993).
- 206 Gara, S. K. *et al.* Three novel collagen VI chains with high homology to the alpha3 chain.
J. Biol. Chem. **283**, 10658–10670 (2008).
- 207 Zelenski, N. A. *et al.* Type VI Collagen Regulates Pericellular Matrix Properties,
Chondrocyte Swelling, and Mechanotransduction in Mouse Articular Cartilage. *Arthritis &
Rheumatology* **67**, 1286–1294 (2015).
- 208 Shen, G. The role of type X collagen in facilitating and regulating endochondral ossification
of articular cartilage. *Orthod. Craniofac. Res.* **8**, 11–17 (2005).
- 209 Gress, C. J. & Jacenko, O. Growth plate compressions and altered hematopoiesis in
collagen X null mice. *J. Cell Biol.* **149**, 983–993 (2000).
- 210 Sund, M. *et al.* Distinct expression of type XIII collagen in neuronal structures and other
tissues during mouse development. *Matrix Biol.* **20**, 215–231 (2001).
- 211 Ylönen, R. *et al.* Type XIII collagen strongly affects bone formation in transgenic mice. *J.
Bone Miner. Res.* **20**, 1381–1393 (2005).
- 212 Koch, M. *et al.* A Novel Marker of Tissue Junctions, Collagen XXII. *J. Biol. Chem.* **279**,
22514–22521 (2004).
- 213 Zwolanek, D. *et al.* Collagen XXII binds to collagen-binding integrins via the novel motifs
GLQGER and GFKGER. *Biochem. J* **459**, 217–227 (2014).
- 214 Charvet, B. *et al.* Knockdown of col22a1 gene in zebrafish induces a muscular dystrophy
by disruption of the myotendinous junction. *Development* **140**, 4602–4613 (2013).
- 215 Hjorten, R. *et al.* Type XXVII collagen at the transition of cartilage to bone during
skeletogenesis. *Bone* **41**, 535–542 (2007).
- 216 Plumb, D. A. *et al.* Collagen XXVII organises the pericellular matrix in the growth plate.
PLoS One **6**, e29422 (2011).
- 217 Exposito, J.-Y., Valcourt, U., Cluzel, C. & Lethias, C. The fibrillar collagen family. *Int. J.
Mol. Sci.* **11**, 407–426 (2010).
- 218 Gonzaga-Jauregui, C. *et al.* Mutations in COL27A1 cause Steel syndrome and suggest a
founder mutation effect in the Puerto Rican population. *Eur. J. Hum. Genet.* **23**, 342–346
(2015).
- 219 Pfeiffer, E., Vickers, S. M., Frank, E., Grodzinsky, A. J. & Spector, M. The effects of
glycosaminoglycan content on the compressive modulus of cartilage engineered in type II
collagen scaffolds. *Osteoarthritis Cartilage* **16**, 1237–1244 (2008).
- 220 Rieppo, J. *et al.* Structure-function relationships in enzymatically modified articular
cartilage. *Cells Tissues Organs* **175**, 121–132 (2003).
- 221 Lee, J.-H. & Cho, J.-Y. Proteomics approaches for the studies of bone metabolism. *BMB
Rep.* **47**, 141–148 (2014).
- 222 Sato, N. *et al.* Proteomic Analysis of Human Tendon and Ligament: Solubilization and
Analysis of Insoluble Extracellular Matrix in Connective Tissues. *J. Proteome Res.* **15**,
4709–4721 (2016).
- 223 Deshmukh, A. S. *et al.* Deep proteomics of mouse skeletal muscle enables quantitation of
protein isoforms, metabolic pathways, and transcription factors. *Mol. Cell. Proteomics* **14**,
841–853 (2015).

- 224 Hosseininia, S., Önerfjord, P. & Dahlberg, L. E. Targeted proteomics of hip articular
cartilage in OA and fracture patients. *J. Orthop. Res.* **37**, 131–135 (2019).
- 225 Merl-Pham, J. *et al.* Quantitative proteomic profiling of extracellular matrix and site-specific
collagen post-translational modifications in an in vitro model of lung fibrosis. *Matrix Biology
Plus* vol. 1 100005 (2019).
- 226 Ko, J. *et al.* Machine learning to detect signatures of disease in liquid biopsies – a user’s
guide. *Lab on a Chip* vol. 18 395–405 (2018).
- 227 Saha, S. *et al.* Automated detection and classification of early AMD biomarkers using deep
learning. *Sci. Rep.* **9**, 10990 (2019).
- 228 Banaei, N. *et al.* Machine learning algorithms enhance the specificity of cancer biomarker
detection using SERS-based immunoassays in microfluidic chips. *RSC Advances* vol. 9
1859–1868 (2019).
- 229 Van Camp, G. *et al.* A new autosomal recessive form of Stickler syndrome is caused by a
mutation in the COL9A1 gene. *Am. J. Hum. Genet.* **79**, 449–457 (2006).
- 230 Hafez, A. *et al.* Col11a1 Regulates Bone Microarchitecture during Embryonic
Development. *J Dev Biol* **3**, 158–176 (2015).
- 231 Alexopoulos, L. G., Youn, I., Bonaldo, P. & Guilak, F. Developmental and osteoarthritic
changes in Col6a1-knockout mice: biomechanics of type VI collagen in the cartilage
pericellular matrix. *Arthritis Rheum.* **60**, 771–779 (2009).
- 232 Bayer, M. L. *et al.* Release of tensile strain on engineered human tendon tissue disturbs
cell adhesions, changes matrix architecture, and induces an inflammatory phenotype.
PLoS One **9**, e86078 (2014).
- 233 Pu, X. & Oxford, J. T. Proteomic Analysis of Engineered Cartilage. *Methods Mol. Biol.*
1340, 263–278 (2015).
- 234 Fawzi-Grancher, S., De Isla, N., Faure, G., Stoltz, J. F. & Muller, S. Optimisation of
biochemical condition and substrates in vitro for tissue engineering of ligament. *Ann.
Biomed. Eng.* **34**, 1767–1777 (2006).
- 235 Richardson, S. M. *et al.* The differentiation of bone marrow mesenchymal stem cells into
chondrocyte-like cells on poly-L-lactic acid (PLLA) scaffolds. *Biomaterials* **27**, 4069–4078
(2006).
- 236 Kurobe, H. *et al.* Development of small diameter nanofiber tissue engineered arterial
grafts. *PLoS One* **10**, e0120328 (2015).
- 237 Ashjian, P. *et al.* Noninvasive in situ evaluation of osteogenic differentiation by time-
resolved laser-induced fluorescence spectroscopy. *Tissue Eng.* **10**, 411–420 (2004).
- 238 Lee, J. K. *et al.* Tension stimulation drives tissue formation in scaffold-free systems. *Nat.
Mater.* **16**, 864–873 (2017).
- 239 Kutsuna, T. *et al.* Noninvasive evaluation of tissue-engineered cartilage with time-resolved
laser-induced fluorescence spectroscopy. *Tissue Eng. Part C Methods* **16**, 365–373
(2010).
- 240 Bergholt, M. S., Albro, M. B. & Stevens, M. M. Online quantitative monitoring of live cell
engineered cartilage growth using diffuse fiber-optic Raman spectroscopy. *Biomaterials*
140, 128–137 (2017).
- 241 Riesle, J., Hollander, A. P., Langer, R., Freed, L. E. & Vunjak-Novakovic, G. Collagen in
tissue-engineered cartilage: types, structure, and crosslinks. *J. Cell. Biochem.* **71**, 313–
327 (1998).
- 242 Murdoch, A. D., Hardingham, T. E., Eyre, D. R. & Fernandes, R. J. The development of a
mature collagen network in cartilage from human bone marrow stem cells in Transwell
culture. *Matrix Biol.* **50**, 16–26 (2016).
- 243 Lee, J. K., Link, J. M., Hu, J. C. Y. & Athanasiou, K. A. The Self-Assembling Process and
Applications in Tissue Engineering. *Cold Spring Harb. Perspect. Med.* **7**, pii: a025668
(2017).

- 244 Ofek, G. *et al.* Matrix development in self-assembly of articular cartilage. *PLoS One* **3**,
e2795 (2008).
- 245 Makris, E. A., Hu, J. C. & Athanasiou, K. A. Hypoxia-induced collagen crosslinking as a
mechanism for enhancing mechanical properties of engineered articular cartilage.
Osteoarthritis Cartilage **21**, 634–641 (2013).
- 246 Makris, E. A., Responde, D. J., Paschos, N. K., Hu, J. C. & Athanasiou, K. A. Developing
functional musculoskeletal tissues through hypoxia and lysyl oxidase-induced collagen
cross-linking. *Proc. Natl. Acad. Sci. U. S. A.* **111**, E4832–41 (2014).
- 247 Yan, D. *et al.* The impact of low levels of collagen IX and pyridinoline on the mechanical
properties of in vitro engineered cartilage. *Biomaterials* **30**, 814–821 (2009).
- 248 Setiawati, R. & Rahardjo, P. Bone Development and Growth. *Osteogenesis and Bone
Regeneration* 13 (2018) doi:10.5772/intechopen.82452.
- 249 Budde, B. *et al.* Altered integration of matrilin-3 into cartilage extracellular matrix in the
absence of collagen IX. *Mol. Cell. Biol.* **25**, 10465–10478 (2005).
- 250 Zhang, R.-Z. *et al.* Recessive COL6A2 C-globular missense mutations in Ullrich congenital
muscular dystrophy: role of the C2a splice variant. *J. Biol. Chem.* **285**, 10005–10015
(2010).
- 251 Schmid, T. M. & Linsenmayer, T. F. Immunoelectron microscopy of type X collagen:
Supramolecular forms within embryonic chick cartilage. *Developmental Biology* vol. 138
53–62 (1990).

CHAPTER 2 | Knee orthopaedics as a template for the temporomandibular joint*

Abstract

Although the knee joint and temporomandibular joint (TMJ) experience similar incidence of cartilage ailments, the knee orthopaedics field has greater funding and more effective end-stage treatment options. Translational research has resulted in the development of tissue-engineered products for knee cartilage repair, but the same is not true for TMJ cartilages. Here, we examine the anatomy and pathology of the joints, compare current treatments and products for cartilage afflictions, and explore ways to accelerate the TMJ field. We examine disparities such as a 6-fold higher article count and 2,000-fold higher total joint replacement frequency in the knee compared to the TMJ, despite similarities in osteoarthritis incidence. Using knee orthopaedics as a template, basic and translational research will drive the development and implementation of clinical products for the TMJ. With more funding opportunities, training programs, and federal guidance, millions of people afflicted with TMJ disorders could benefit from novel, life-changing therapeutics.

Introduction

The knee joint and temporomandibular joint (TMJ) are two of the most used joints in the body. They are both diarthrodial joints consisting of a fibrocartilaginous disc between two articular surfaces (Figure 1)^{1,2}. The knee comprises two joints, the tibiofemoral joint and the patellofemoral joint, which perform flexion, extension, and rotation of the lower legs. The knee is essential for walking, running, and jumping³. The TMJ is one of the most complex joints in the body and performs crucial activities such as chewing, speaking, and breathing⁴. Both joints are critical for performing many day-to-day movements, where they withstand large, repeated forces.

* Published as: Bielajew BJ[†], Donahue RP[†], Espinosa MG[†], Arzi B, Wang D, Hatcher DC, Paschos NK, Wong MEK, Hu JC, Athanasiou KA. Knee orthopaedics as a template for the temporomandibular joint. *Cell Reports Medicine* 2021; 2(5). [†]equal contribution

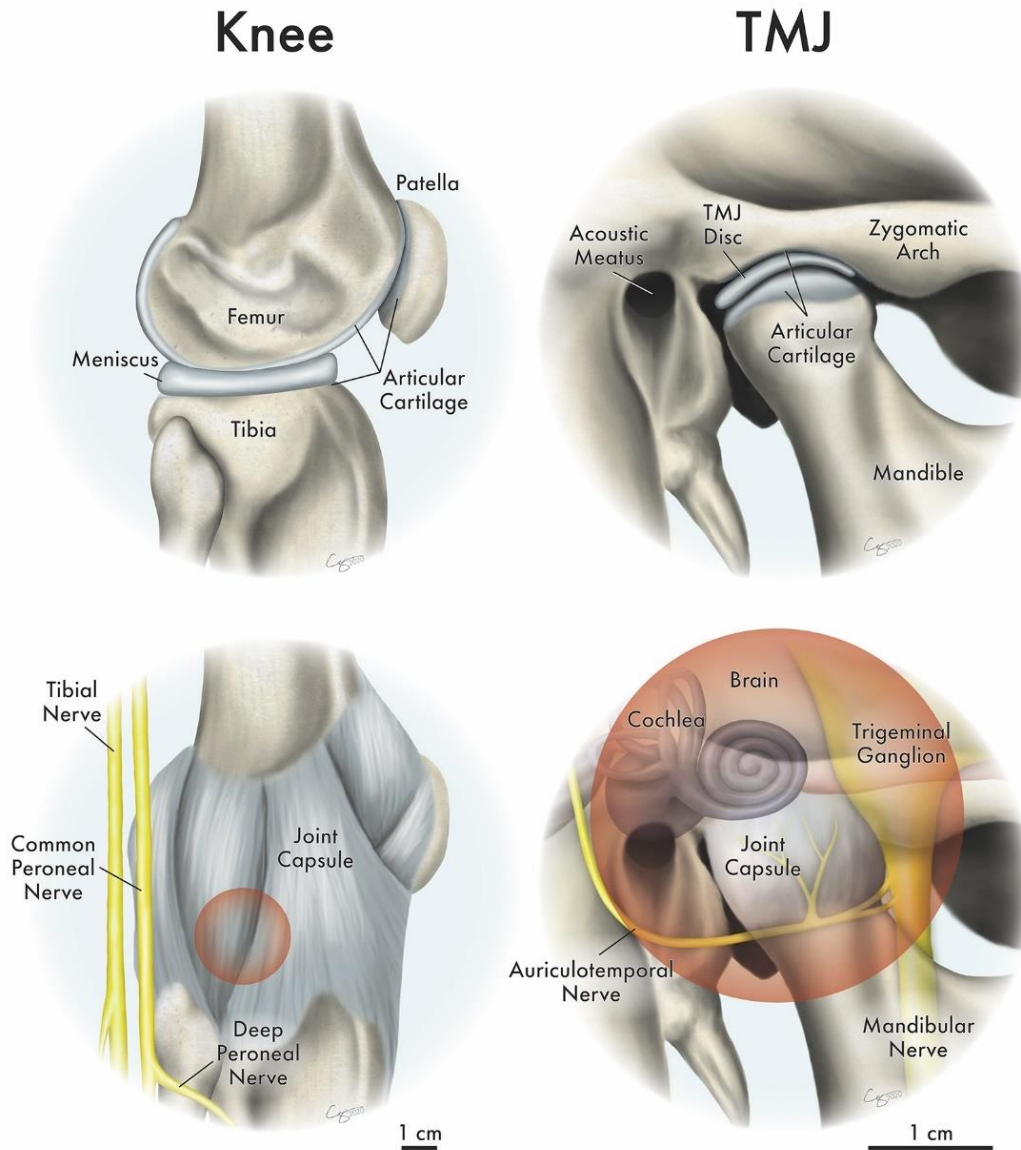


Figure 1. Knee and TMJ anatomy and proximity to crucial sensory structures. (Top) Both the knee and TMJ are diarthrodial joints with two articular surfaces and an interpositional fibrocartilage. Specifically, the meniscus is situated between the tibia and the femur in the knee, and the TMJ disc is situated between the zygomatic arch and the mandible. (Bottom) Within a 3-cm sphere (red circle representation in 2D space) centered around the meniscus and the TMJ disc, the knee has no crucial sensory structures, although the TMJ has numerous structures present, including components of the inner ear, the brain, the trigeminal ganglion, and the mandibular and auriculotemporal nerves.

While there are analogous structures in the knee and TMJ (Figure 1), there are some biomechanical and biochemical differences between the two joints. When performing simple motions, the knee withstands comparatively large forces; light jogging can put over four times the body's weight (e.g., 3080-3600 N) on the knee^{5,6}, compared to the TMJ, which experiences forces equivalent to the body's weight (e.g., 770-900 N) when biting^{5,7}. While compression and shear

are major loading types in both joints⁸, tensile loading plays a greater role in the TMJ than the knee⁹. The knee meniscus contains zonal differences in collagen type I and II ratios, while the TMJ disc is almost completely composed of collagen type I¹⁰. While both articular surfaces contain growth plates, the mandibular condyle contains a unique fibrous zone¹¹, unlike the articular cartilages of the knee which are completely hyaline. Despite these differences, the two joints manifest pathologies and disorders leading to pain and dysfunction.

Table 1. Comparison of the knee and TMJ fields. Despite similar incidence of osteoarthritis, the TMJ lags behind in research output, grant funding, cell-based products, and practicing physicians.

	Knee	TMJ
Osteoarthritis incidence	~14% ¹³	8-16% ¹⁶
Professional membership	AAOS membership: 39,195 ¹¹⁶	AAOMS membership: 11,436 ¹¹⁷
PubMed articles*	1,852 (in 2019)	288 (in 2019)
R01s (research project grant)**	33 (in 2019)	6 (in 2019)
R21s (exploratory/developmental research project grant)**	9 (in 2019)	1 (in 2019)
Cell-based therapeutics in development or clinical trials (worldwide)***	18 ⁵⁷	1****
Projected number of joint replacement procedures in 2020 (U.S. only)	882,000-1,783,000 ¹¹⁸ (range of 2020 projections from a variety of historical data)	709 ¹¹⁹ (2020 projection from historic data from 2005-2014)
<p>* PubMed was searched using the following keyword schemes: [(((tibiofemoral) OR (knee)) AND ((cartilage) OR (meniscus)))] [(((temporomandibular) OR (jaw)) AND ((cartilage) OR (meniscus) OR (disc) OR (disk)))]</p> <p>** NIH RePORTER was searched using the following keyword schemes limited to project abstracts: [(((tibiofemoral) OR (knee)) AND ((cartilage) OR (meniscus)))] [(((temporomandibular) OR (jaw)) AND ((cartilage) OR (meniscus) OR (disc) OR (disk)))]</p> <p>*** Related to treating cartilage, meniscus, and disc pathologies.</p> <p>**** Based on searches based in clinicaltrials.gov across all countries.</p>		

Approximately 25% of adults have some sort of cartilage affliction¹². Arthritides, diseases involving joint inflammation and cartilage degeneration, frequently occur from overuse, aging, trauma, or pathology. Osteoarthritis (OA) is the most common form, with the knee being one of the most frequently affected joints; about 14% of the adult U.S. population is afflicted by knee OA¹³. Other disorders of the knee joint include meniscus tears, common in young athletes¹⁴, resulting in the development of OA in the knee; one study showed that 85% of patients with medial

meniscus tears also developed OA¹⁵. Although epidemiological studies of OA incidence in the TMJ are not extensive, one article indicates evidence of TMJ-OA in 8-16% of the population¹⁶. Temporomandibular disorders (TMDs), an umbrella term to describe a wide variety of TMJ pathologies, includes TMJ-OA (also referred to as degenerative joint disease) as well as other ailments such as disc pathologies and myofascial dysfunction. Joint disorders also involve changes to muscles, ligaments, tendons, and bones; this Chapter will be focused primarily on the cartilages of the knee joint and the TMJ.

Although the joints have similar anatomy and OA incidence, the knee and TMJ fields display stark differences in primary research, funding, cell-based products in development, and total joint replacement procedures (Table 1). Compared to the TMJ, the knee has a greater quantity of basic and translational research, resulting in more product development and marketed treatments. For example, the knee has a 5.5-fold higher amount of R01 research project grants from the National Institutes of Health (NIH) compared to the TMJ in 2019. The NIH is part of the U.S. Department of Health and Human Services and is the largest biomedical research agency in the world. It is broken down into 27 institutes and centers which fund scientific grants. There is also a major difference in the amount of end-stage surgical procedures performed on knee and TMJ patients; the knee has approximately a 2,000-fold higher frequency of total joint replacements compared to the TMJ. The dearth of TMJ research presents a pressing challenge toward developing novel cartilage therapies, but, by bolstering primary and translational research of the TMJ, new products for its cartilages may be developed¹⁷. The lack of translational advancement for the TMJ represents a chokepoint in the development of safe and effective therapeutics for people afflicted by TMDs, which, according to the TMJ Association, totals over 35 million adults in the U.S.¹⁸ In this Chapter, we compare the pathologies, anatomical challenges, clinical practices, and products for the cartilages of the two joints within the U.S. medical system and call for improved treatment options for specific TMJ indications. By using the knee

orthopaedics field as a template to follow in translational pathways, TMJ experts can drive the implementation of new cartilage therapies for millions of TMD patients.

Pathology

The TMJ requires improved diagnostic modalities despite similarities in osteoarthritis progression

Knee and TMJ OA pathologies have several similarities. This disease involves mechanical and biochemical degradation of cartilage, subchondral bone, and synovium¹⁹. Pain is the most common OA symptom, which can range from barely noticeable to severe and debilitating²⁰. Other symptoms include joint stiffness and reduced function or range of motion, and, with severe TMJ-OA, changes in occlusion. Knee OA is traditionally diagnosed with radiography, and early damage can be detected using magnetic resonance imaging (MRI)²¹. For TMJ-OA, panoramic radiography has a low sensitivity for diagnosis²². Cone beam computed tomography (CBCT), a widely used imaging modality, is used as a more reliable diagnostic technique²³. and MRI can be used to assess different signs of dysfunction²⁴. Dynamic MRI scoring algorithms, similar to those used to evaluate cardiac wall motion²⁵, can be used for the TMJ, for example, to assess the causes of reduced joint mobility. Reduced mobility is often caused by a displaced disc²⁶, but capsule and ligament pathology may also play a role; these are not routinely examined with imaging. An unusual caveat with TMJ imaging is that radiographic signs alone may not be associated with pain; one study performed CBCT imaging on TMJs of healthy adults with no TMJ complaints, and nearly 40% of the TMJs showed degenerative changes²⁷. Conversely, TMJ pain may not be associated with radiographic signs of disease²⁸. For determining the source of pain in the TMJ, positron emission tomography paired with a computed tomography scan (PET/CT) is being used to image inflammation and bone changes in the TMJ and may be useful for diagnosing TMJ-OA²⁹. While knee OA is similar in nature to TMJ-OA, additional assessment tools are needed to improve the accuracy of OA diagnosis correlating with symptoms in the TMJ³⁰, thus, improving indications for TMJ repair.

TMJ disorders are more prevalent in women

Women experience higher levels of knee pain than men³¹, with about a 1.6-fold higher incidence of knee OA³². This difference is likely caused by biomechanical, hormonal, and neural differences³³, but a better understanding is needed. Epidemiological studies on gender differences in TMJ-OA are not extensive, but the higher prevalence of TMDs in women has been widely documented; TMDs are up to four times more prevalent in women than men, with women presenting more severe symptoms³⁴. There is evidence of increased amounts of hormone receptors in the TMJ discs of women with TMDs³⁵, but there is conflicting literature showing relationships between TMD prevalence and estrogen levels³⁶. This coincides with a high proportion of young TMD patients compared to knee OA patients^{37,38}. An earlier onset of TMJ-OA challenges the “overuse phenomenon” — that OA occurs when functional demands exceed the adaptive capacity of the cartilage³⁹. One stark example of age and gender bias in TMDs is the incidence of idiopathic condylar resorption of the TMJ. This disease occurs nine times more frequently in women than men and rarely develops after the age of 20⁴⁰. In these young patients, TMDs may profoundly affect facial growth, occlusion, and airway dimensions⁴¹. Given the severe, unexplained gender discrepancy in the TMJ, which has been called the “TMJ gender paradox,^{42”} deeper understanding of what drives the higher TMD occurrence in young women remains a major milestone for the field.

The anatomical challenge of sensory structures near the TMJ versus the knee

A major difference between the joints is the location relative to vital structures, which affects joint symptoms, treatment effectiveness, surgical approaches, and adverse events. In the knee, the tibial, peroneal, and saphenous nerves are near the joint (Figure 1), but nerve damage is rare during knee surgery. The TMJ is near multiple important sensory nerves, parts of the inner ear, and the brain (Figure 1). The TMJ’s sensory nerves innervate surrounding masticatory muscles, and spasms in these muscles might be associated with TMJ pain⁴³. One study on 501 TMD

patients showed that 60 also had trigeminal neuritis, a condition causing severe, chronic pain⁴⁴. TMJ disc displacement may compress the mandibular nerve, causing neuropathic pain⁴⁵. People with TMDs are more likely to have severe tinnitus and vertigo, potentially due to the TMJ's proximity to the inner ear⁴⁶. The complex anatomy and associated symptoms can complicate diagnosis and make treatment difficult⁴⁷, and the outcome of patients with neural and joint symptoms is inconsistent, often resulting in unsuccessful treatments⁴⁸. As shown in Figure 1, a 3 cm sphere centered on the TMJ disc contains major nerve structures, the inner ear, and the brain, while the same sphere centered on the knee meniscus contains no major sensory structures. In addition to the aforementioned lack of diagnostic modalities, a major hurdle in performing surgery is the TMJ's close proximity to the brain⁴⁹, illustrating the anatomical challenge of diagnosing and treating cartilage disorders of the TMJ compared to the knee.

Current clinical practices

Divergence of end-stage treatment strategies for osteoarthritis of the knee and TMJ

The treatment strategies for knee and TMJ cartilage pathologies are similar at first glance (Figure 2A). Both the American Academy of Orthopaedic Surgeons (AAOS) and the American Association of Oral and Maxillofacial Surgeons (AAOMS) list physical therapy, analgesics, and mechanical stabilizers as conservative treatment options for OA^{50,51}. These relatively noninvasive, early-stage therapies are often undertaken by a variety of providers, such as physicians and physical therapists or, for the TMJ, dentists and dental specialists. If such therapies prove ineffective, frequently, orthopaedic and oral and maxillofacial (OMF) surgeons employ injection-based therapies^{52,53}. There are greater differences between surgical treatment options. Few late-stage TMD patients are referred to an OMF surgeon, indicated by the small number of TMJ surgeries performed. Only 5% of TMD patients are considered candidates for surgery⁵⁴, despite a lack of positive outcomes with non-surgical approaches. This is reflected in the decline of TMJ surgeries; the number of TMJ arthroscopic surgeries has steadily decreased since the 1990s⁵⁵.

This is in contrast to total knee arthroplasties, which are projected to increase by up to 800% by 2050⁵⁶. The declining trend in the TMJ field may be attributed to a number of causes, such as disagreement over the suitability or efficacy of surgical approaches⁵⁵. Conversely, knee cartilages have well-defined treatment algorithms. For example, focal defects are treatable with widely accepted surgical techniques⁵⁷. In the U.S., Current Procedural Terminology (CPT) codes are used to report medical or dental services provided by a physician to insurance companies for reimbursement or payment. A higher specificity of knee treatments is shown in a higher quantity of CPT codes compared to the TMJ. For example, TMJ arthroplasty has only three CPT codes while knee arthroplasty has ten^{58,59}. Knee treatment is covered by medical insurance, while TMDs can be covered under either medical or dental insurance. It is clear that TMD patients need greater access to effective, end-stage treatments with indications that are well-vetted among OMF surgeons with specialized training in the TMJ.

Training disparities between knee and TMJ surgeons

Quality surgical treatment is directly related to physician training. OMF and orthopaedic surgery training consists of four years of dental or medical school followed by residency (Figure 2B). OMF surgery residency lengths and degree requirements vary significantly across countries; this is reviewed elsewhere⁶⁰. In the U.S., OMF surgery residency may either be a four-year program (single degree) or an MD-granting six-year program (dual degree). Dual degree programs make up to 46% of the residency programs⁶¹. One measure of surgical training is resident case log volume throughout the duration of the program (Figure 2B). Regardless of residency duration, the Commission on Dental Accreditation (CODA) requires that OMF residents log 175 major procedures in their final year⁶². A survey of senior OMF residents in the U.S. showed that only ~3.5% of these cases involve TMJ arthroscopic or open joint procedures⁶³. Most TMJ-specific treatments performed by residents were injection-based⁶³. At programs lacking OMF residencies, TMDs may be covered by plastic surgery or otorhinolaryngology residencies, but TMDs are not a

focus. In general, orthopaedic surgery residents log 200-600 cases in the final year^{64,65}, and, in 2019, knee-specific arthroscopy and open joint surgery accounted for ~16%⁶⁶. Following their five-year residency, most orthopaedic surgeons complete a fellowship year⁶⁷, and those interested in knee cartilage typically choose a sports medicine or arthroplasty fellowship. While the CODA-accredited endoscopic maxillofacial fellowship provides more substantial TMJ-related training⁶⁸, fellowships are not as popular among OMF surgeons.⁶⁹ If better end-stage treatment options are to become available, there will be a greater need for TMJ specialization to meet the surgical needs of TMD patients.

From incidence to clinic: gender imbalances in physician populations and clinical trials

Gender imbalances are present in the demographics of knee and TMJ patients and the surgeons that treat them, and these disparities have a clinical impact on the treatment of knee- and TMJ-related ailments. Because there are significantly more women who experience OA and TMDs, it is important to account for gender-based differences in treatment development. For example, women report more pain before and after total knee arthroplasty when compared to men⁷⁰. Similarly, the percentage of women reporting orofacial pain at routine dental visits was triple that of men⁷¹. While some have focused on psychosocial factors to explain this difference⁷²⁻⁷⁴, it is important to consider the ample evidence showing that women's analgesic response is physiologically different from men's⁷⁵. Interestingly, a recent review noted that physicians are more likely to recommend greater pain intervention for patients of the same gender⁷⁶. This is important, given that most knee and TMJ OA patients are female, while orthopaedic and OMF surgeons are predominantly male (Figure 2C). In the last decade, approximately half of medical and dental school graduates were women, but the percentage of female residents in both orthopaedic and OMF surgery programs has only been about 15%^{77,78}. This imbalance is greater within professional societies; women make up only 6.5% and 8.0% of the AAOS and AAOMS

membership, respectively^{79,80}. Reducing this disparity among orthopaedic and OMF practitioners will help ensure that gender-based differences are not overlooked in patient treatment.

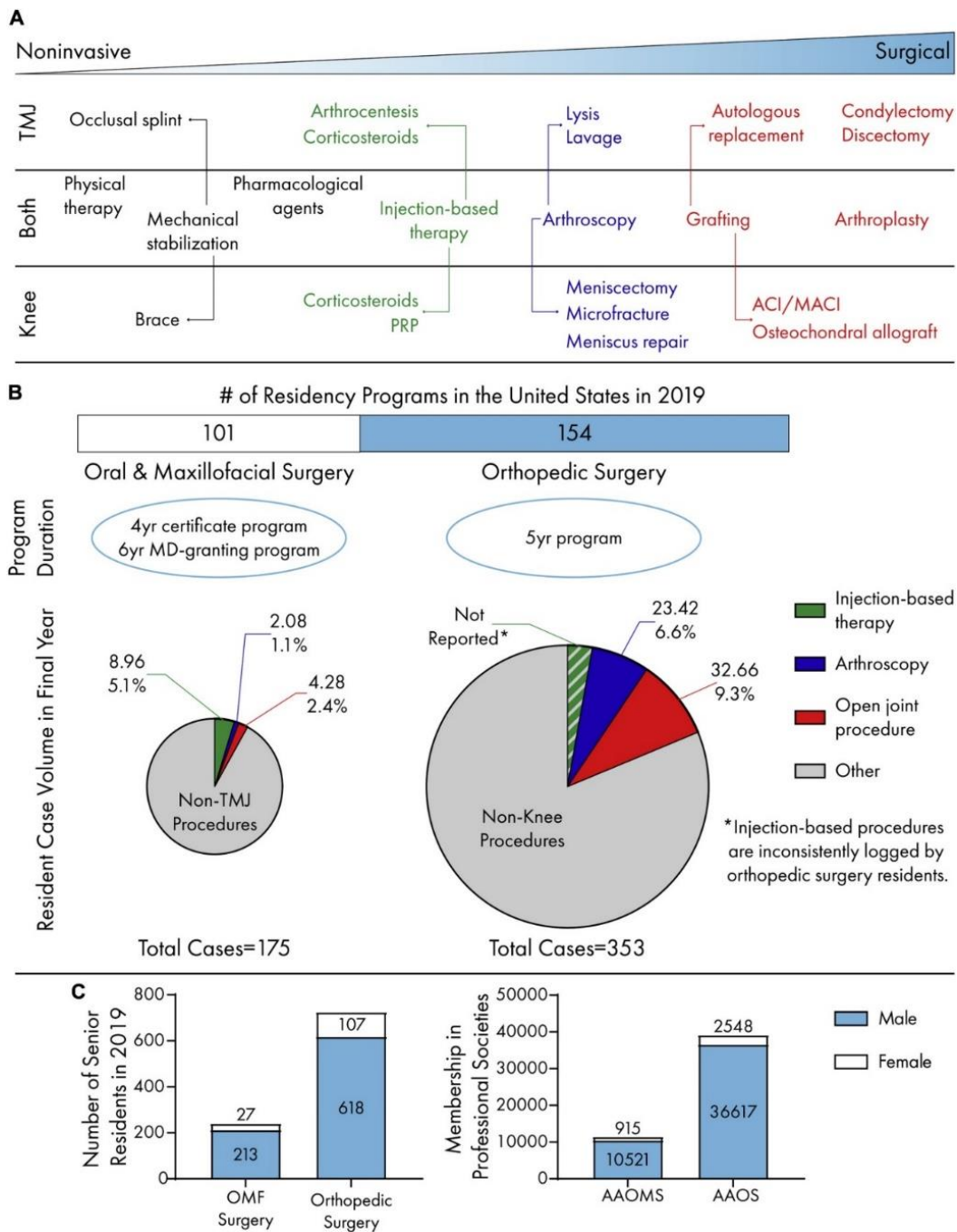


Figure 2. Clinical practices for the knee and TMJ. (A) The cartilages of knee and TMJ share similar treatment pathways. Progressing from noninvasive to surgical approaches, conservative treatment is often indicated prior to end-stage surgeries, such as grafting (e.g., fat and rib) for the TMJ and osteochondral allografts for the knee. (B) Orthopedic surgery leads oral and maxillofacial surgery in residency program quantity. Oral and maxillofacial surgery residents are exposed to a lower quantity and percentage of total cases in open joint and arthroscopic procedures compared to orthopedic residents. (C) Males are overrepresented in both senior resident numbers and professional society memberships in AAOMS and AAOS.

Potential therapeutics must go through preclinical and clinical trials to gain regulatory approval. Potential product sponsors must consider careful design of such trials, specifically, the gender of the participants. With a vast majority of people experiencing TMDs being women, the NIH's policy on "sex as a biological variable" is particularly relevant^{81,82}. This strongly encourages researchers to consider gender-based differences throughout the translational process. Unfortunately, meta-analytic studies have shown that gender differences in clinical trials are underreported⁸³. Translational scientists must consider how gender disparities in knee and TMJ OA patients may not only affect the demographics of clinical trials but, subsequently, the landscape of commercial products.

Commercial products

Joint prostheses: successes in the knee and catastrophic setbacks in the TMJ

Partial or total joint replacement is the current solution for patients with cartilage pathologies that fail to improve with less invasive treatments. The first hemiarthroplastic knee device, a tibial plateau prosthesis, was designed by McKee in 1957^{84,85}. In 1963, Christensen published on a fossa-eminence prosthesis for TMJ hemiarthroplasty⁸⁶. These devices paved the way for the development of total joint implants in the U.S. The early total knee devices include the Freeman-Swanson knee and the Geomedic knee⁸⁵. In the 1970s and '80s, the Oxford knee and the New Jersey Low-Contact-Stress knee significantly improved mobility and are still used⁸⁷. Today, there are over a dozen knee replacement manufacturers collectively offering a wide range of customization options^{87,88}.

Unlike the knee, TMJ prosthesis development has been slow and controversial. In 1983, the U.S. Food and Drug Administration (FDA), the regulatory body responsible for determining safety and efficacy of therapeutics, cleared Vitek's Proplast-Teflon implant for TMJ disc replacement, despite evidence of fragmentation with similar Teflon-based hip replacements⁸⁹. Given the joint's proximity to the brain, the implant's failure led to catastrophic outcomes, such as

particulate migration and cranial breaching^{90,91}. By 1990, the FDA rescinded clearance of the implant and issued a recall a year later⁹². In 1993, the FDA reclassified all TMJ prostheses as Class III, a designation reserved for devices posing the greatest risk⁹³, requiring more rigorous premarket approval and stifling production of all TMJ implants. Currently, there are only four FDA-approved TMJ implants⁹⁴. Nexus makes both a partial and total metallic joint, and Zimmer-Biomet and TMJ Concepts make metal/polymer total joint replacements⁸⁹. This is in stark contrast to the hundreds of total joint replacement systems available for the knee⁸⁵.

The TMJ field trails the progress of tissue engineering in the knee

An important measure of an implant's success is its long-term performance and lifetime. Approximately 82% of total knee replacements survive 25 years⁹⁵. Although most surveillance studies for TMJ implants are ongoing, Zimmer-Biomet reports that implant survival is 86% after 10 years⁹⁶. The average age of a TMJ implant recipient is only 34.9 years compared to 67.5 years for knee implant recipients^{38,97}. Assuming an implant lifetime of 20 years and an average life expectancy of 78.6 years in the U.S.⁹⁸, a TMJ patient is likely to need two revision surgeries; a knee patient is unlikely to need any. This disparity underscores the TMD patient's dire need for high quality, long-lasting replacement options for treatment of late-stage, degenerative TMDs. Tissue engineering offers a promising long-term alternative to alloplastic implants, thus, potentially eliminating the need for revision surgeries.

In 2016, the FDA approved matrix-induced autologous chondrocyte implantation (MACI), a two-surgery process utilizing expanded cells seeded on a porcine collagen membrane, for the repair of knee cartilage defects⁹⁹. Several more tissue-engineered products, such as NOVOCART 3D for articular cartilage and Chondrogen for the meniscus, are currently proceeding through the regulatory pipeline⁵⁷. Some tissue-engineered products employ an allogeneic approach; one example, Revaflex, reports encouraging results in clinical trials^{57,100}. Given this established precedent, continued development of tissue-engineered products for the knee cartilages will

proceed. Development of cell-based therapeutics for the TMJ cartilages is still in its nascent stage, with only one clinical trial based in Brazil¹⁰¹. Although autologous grafts (e.g., fat, rib) for the TMJ offer a tissue-based option^{102,103}, there are still no approved, tissue-engineered products for the TMJ cartilages in the U.S.

Future directions

The vicious cycle of translating TMJ research

Tissue engineering can potentially offer long-term solutions for knee and TMJ cartilage ailments. With multiple products, either approved or in trials, tissue engineering toward regeneration of knee cartilages is poised to be a major early success of regenerative medicine, acting as a template for other joints such as the TMJ. Although the knee and TMJ fields had similar start points in the 1950s and '60s with joint replacement devices, the catastrophic failure of the Proplast-Teflon prostheses affects the TMJ field to this day. The knee field enjoys much success in terms of quantity of research output, funding, marketed products, and regulatory guidance, while the TMJ field is relatively stagnant in nearly all areas. Low research output, especially in translational science, leads to fewer innovative therapeutics that make it to clinical trials. The resulting dearth of products for TMJ cartilages limits commercial success, disincentivizing financial and regulatory support, feeding back into the vicious cycle as a lack of precedent (Figure 3). By increasing research output, bolstering training opportunities, narrowing and specifying indications for TMJ cartilages, establishing a commercial TMJ landscape, and publishing guidance documents, the field can accelerate translational research to break the vicious cycle.

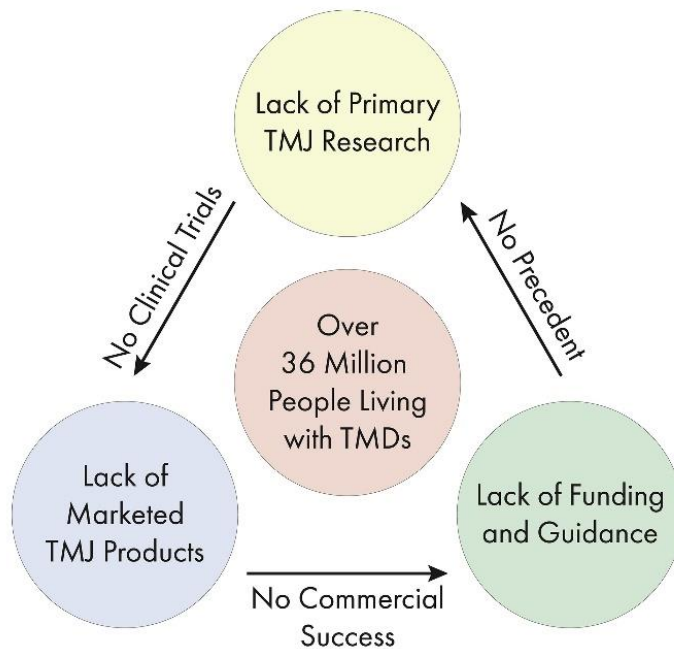


Figure 3. The vicious cycle of TMJ translational research. Primary research is lacking in the TMJ field, leading to little translation and resulting human clinical trials. Without clinical trials, approved, marketed products do not exist, resulting in little to no commercial market for TMJ products. This disincentivizes regulatory and funding agencies from publishing guidance and providing funding for the TMJ field, feeding back into the loop and resulting in a lack of precedent for researchers.

Increasing the quantity of rigorous TMJ research

There is a critical need for increased basic and translational research output to energize the TMJ field. Within the U.S., the number of TMJ-related, NIH-funded grants drastically trails those of the knee (Table 1), illustrating the need to further mature the TMJ field. In a recent report, the National Academies of Science, Engineering, and Medicine recommended bolstering different aspects of TMJ research¹⁰⁴. For example, the report calls for the creation of a national collaborative research consortium and expansion of TMJ research. For orthopaedics, the Orthopedic Research Society (ORS) helps facilitate these activities through their annual meeting. This meeting brings together orthopaedic surgeons, biologists, engineers, and other experts across various fields. This fosters a collaborative environment for those within orthopaedics, both researchers and practitioners, to discuss interdisciplinary research and form collaborations. While the TMJ Bioengineering Conference occurs every two years and achieves the same goal as the ORS annual meeting on

a smaller scale, the TMJ field is more fragmented. There are multiple different symposiums, such as the meetings of the American Society of TMJ Surgeons, the AAOMS, the American College of Oral and Maxillofacial Surgeons, and the American Academy of CranioMaxillofacial Surgeons that discuss the TMJ, but the field does not have one meeting that brings together experts from different fields at the same scale of ORS. One can consider a TMJ meeting, modeled after ORS, where researchers and clinicians meet to discuss current treatment issues and how interdisciplinary approaches can be developed toward relieving TMJ ailments. Additionally, ORS may consider cosponsoring a TMJ-specific meeting to bring together researchers, orthopaedic surgeons, and OMF surgeons to discuss how treatments and approaches in the knee cartilages could be transferred to the TMJ. By using orthopaedic meetings as a template, the TMJ field can accelerate the basic and translational research toward clinical trials to develop effective TMJ therapeutics.

Without a large quantity of interdisciplinary research, the TMJ field will not be able to establish a base to propel itself forward. One of the major issues is that TMDs disproportionately affect up to 17% of all American women^{18,34}. Understanding fundamental science will shape the approach of translational research, such as in the design of preclinical animal studies. Although basic science and translational research have already resulted in a steady rise of TMJ-related publications since 2006¹⁰⁵, federal bodies such as the National Institute of Dental and Craniofacial Research (NIDCR), NIH, and FDA still push for increased research¹⁰⁴. This will not only lead to increased output but also maintain a high standard of scientific rigor, as those bodies require that grant applications and manuscripts undergo peer-review. On average, an R01 grant from the NIH leads to 7.36 published research articles with almost 300 citations¹⁰⁶. Similar to ORS sponsoring a combined meeting, the NIDCR and institutes such as the National Institute of Arthritis and Musculoskeletal and Skin Diseases (NIAMS), two U.S. NIH institutes which the TMJ and knee commonly fall under, may consider publishing dual requests for applications that study the knee and TMJ cartilages under one grant. These could focus on transferring the knee knowledge,

equipment, and protocols to the cartilages of the TMJ, providing incentive for established musculoskeletal researchers to extend a branch into the TMJ field. By increasing grant funding through various channels such as the NIH, TMJ research output will be closer to the level of the knee field.

Bolstering training opportunities for researchers and physicians

As research output rises, more trained researchers and surgeons will be needed. The NIH F-series of grants is targeted toward students and postdoctoral fellows to support both individuals (e.g., salary, stipend, tuition) as well as their proposed research. The funding success rates of the NIDCR grants for pre- (F31) and post-doctoral (F32) candidates are 70% and 35% in 2019, respectively¹⁰⁷. Considering both of these success rates trend in the top third of all NIH institutes¹⁰⁷, the NIDCR is commended for their commitment to funding junior researchers. However, total funds disbursed by the NIDCR ranked in the bottom half of all NIH institutes¹⁰⁷. Compared to the NIDCR, the NIAMS F31 and F32 success rates were lower in 2019, about 18% for both mechanisms¹⁰⁷. Although the number of candidates funded were similar for each mechanism, the total number of applicants for NIAMS fellowships was drastically larger than those of the NIDCR¹⁰⁷; thus, the NIDCR could improve their outreach and advertising of such mechanisms. A mechanism to bridge postdoctoral scientists to their early career (e.g., junior faculty) is the K99/R00 grant which includes both a mentored and independent research phase. In 2019, the K99 application numbers were comparable between the NIDCR and NIAMS, but the NIDCR maintained a higher success rate of 36.8% compared to 20.0%¹⁰⁷. Clearly, the NIDCR is committed to developing researchers' careers in the craniofacial, dental, and TMJ fields. By maintaining high success rates, increasing funding disbursed, and bolstering outreach efforts for these awards, the NIDCR will increase the number of trainees pursuing a TMJ-related career.

As discussed above, orthopaedic surgery residents gain exceptional experience in open joint surgeries and arthroscopy of the knee (~16% of cases)⁶⁶, compared to the equivalent for the

TMJ (~3.5%) for OMF residents⁶³. Development of reliable diagnostic modalities and clear treatment algorithms to address specific pathology will increase TMJ surgery case volume for OMF residents, thus, better equipping future surgeons for implementing new therapeutics. An additional option would be to develop a TMJ-specific surgical fellowship for OMF residents, modeled after fellowships for orthopaedic surgeons. Lastly, as the field matures, the need for dual degree clinician-researchers will grow, which is expected to spur the development of novel therapeutics. The dual degree F30 fellowship success rate for the NIDCR in 2019 was in excess of 80%¹⁰⁷, indicating that the institute is committed to developing clinician-researchers and their ideas toward therapeutics. Early career medical professionals might bridge their careers into research with a K08 clinical investigator award, which provides these individuals with an intensive, research career development experience. In contrast to the F30 mechanism, the K08 success rate for the NIDCR (25.0%) trails that of NIAMS (56.3%) although they maintain relatively similar applicant numbers¹⁰⁷. Encouragement of clinician-researchers to apply for funding at the success rate of the F30 award and continuing to increase success rates at the K08 level will grow and sustain the number of TMJ physicians and translation of novel therapeutics.

Narrowing and specifying indications for TMDs toward establishing the commercial landscape for TMJ cartilage products

As researchers and clinical practitioners continue to grow the field in number and research output, there will be a push to narrow and specify indications for the TMJ-specific conditions amenable to surgical management. Currently, the term TMD encompasses many different conditions, including muscle and joint problems¹⁰⁸. This has led to confusion in the field today that causes conflicting paradigms for treating certain indications. Toward solving this, the National Academies' report recently recommended establishing a national TMD registry to track incidences, indications, and treatment pathways toward establishing best practices¹⁰⁴. A template for the TMJ field may be the AAOS American Joint Replacement Registry that has recorded procedural data,

post-operative data, and patient-reported outcome measures on over 2,000,000 joint replacement procedures for the knee and hip since 2009¹⁰⁹. Continued clinical research output, specifically retrospective and meta-analytic studies on certain indications, will additionally improve the clinical body of knowledge.

Establishing specific indications for TMDs is crucial to a healthy market for the TMJ field; without a clear indication, there is no commercial product. Due to a lack of indications, it is not clear how TMJ tissue-engineered products might be implemented¹¹⁰. By establishing indications, more TMJ scientists and clinicians will attempt to translate technologies, therapeutics, and devices from the benchtop to the bedside. In the knee, MACI is indicated for patients with symptomatic, full-thickness knee cartilage defects who have failed conservative treatments¹¹¹. The TMJ market would benefit from using MACI and other knee cartilage therapeutics as a template for TMJ tissue-engineered products. As translation occurs for various TMJ therapeutics, additional CPT codes and surgical procedures will likely be needed. Historically, only 5% of TMDs are candidates for surgical intervention¹¹². These few surgical cases only include three CPT codes for TMJ arthroplasty, compared to ten for knee arthroplasty. As therapeutics are developed, specifically those for late-stage pathology, it is likely that the number of CPT codes and surgical TMD cases will increase^{58,59}. CPT codes for these indications will need to be sufficiently supported by science for third party reimbursors to support payment for the procedures. Furthermore, additional CPT codes specifying indications for late-stage pathology may further bolster medical insurance support (i.e., as compared to dental insurance). Additionally, following the specificity seen in CPT codes for the knee as a template, progress is also needed in delineating CPT codes for early-stage TMDs to support non-surgical treatment. Finally, specific terminology delineating between the various muscle and joint problems would be a step toward dismantling the umbrella term “TMD.” This would clarify communication among researchers, physicians, and patients, improving granularity in treatment algorithms, and garnering support for TMDs for treatment under medical insurance as opposed to dental insurance. A recent example of this is the

recommendation provided by the International Research Diagnostic Criteria for Temporomandibular Disorders Consortium Network and Orofacial Pain Special Interest Group which attempts to delineate among the various myogenous and arthrogeous conditions¹¹³, but this report has been deemed to fall short¹⁰⁸. Additional work is needed in order to delineate the term further and identify appropriate indications. As more entrepreneurial ventures are established, a larger market for therapeutics indicated for specific, end-stage TMDs will arise, laying the groundwork for the TMJ commercial landscape.

Implementing industry guidance for treatment of TMJ cartilages

As scientific entrepreneurs establish TMJ startup companies, they will look to regulatory agencies for guidance. The FDA has previously given specific guidance for products intended to repair or replace knee cartilage, with specific recommendations to establish safety and efficacy¹¹⁴. Analogous FDA guidance for the TMJ is necessary if new cartilage products are to emerge; to this end, the knee cartilage guidance document may serve as a template for the TMJ. Specific considerations, such as proximity to crucial sensory structures, the mechanical loading environment of the joint, and appropriate animal models, should be included. Defining regulatory jurisdiction would also be helpful by delineating various types of therapeutics (e.g., drug, biologic, device, or combination product), not only for the TMJ but also the knee. Autologous materials have been used in the past for the TMJ¹⁷, but recent animal studies suggest that allogeneic approaches are also safe¹¹⁵. Assays required to show safety for allogeneic approaches compared to autologous approaches may be considered. Due to the dearth of precedent for both the knee and TMJ, the FDA might consider providing early communication and advice through existing designations and programs, such as Breakthrough and Fast Track designations and Priority Review and Accelerated Approval programs, as applicable to product sponsors. Additionally, establishing regulatory guidance in the benchtop and preclinical phases of the translational paradigm would be useful. For example, for NIH-funded grants with animal studies, perhaps the

FDA and the appropriate NIH institute could collaborate to provide early regulatory advice to the principal investigator. This guidance and support would undoubtedly improve the success of translational TMJ research.

Conclusion

The nature of translational research is inherently arduous, with many choke points frequently leading to a vicious cycle (Figure 3). However, there are just as many possibilities to break this cycle. As the NIDCR moves forward with funding various projects, they should consider funding TMJ cartilage-specific grants to encourage focused research in the field. While current support at the R-series level is insufficient (Table 1), early career researchers are well funded through F-series mechanisms, which bodes well for the future of the TMJ field. Increasing funding and outreach for such mechanisms while maintaining success rates would be beneficial to the field. For surgical trainees, bolstering the number of TMJ cases encountered throughout residency, developing TMJ surgical fellowships, and encouraging clinicians to apply for F30/K08 awards will increase the supply of TMJ-specific OMF surgeons to perform technically challenging cartilage procedures and explore the clinical efficacy of new therapeutics. Clarification of indications and treatments for TMDs through a national registry will be of great value to entrepreneurs attempting to translate technologies. By doing so, markets for such technologies will arise so that additional CPT codes specific to cartilage indications will be established, enabling additional insurance coverage for TMDs. Finally, guidance published by the FDA will enable translational studies to support safety and efficacy of TMJ cartilage products, especially tissue-engineered implants. These documents should include specific considerations for TMJ cartilages such as proximity to crucial structures and timely guidance for nascent products. Similar approaches and suggestions have resulted in the development and translation of tissue-engineered products for knee cartilages and can thrust the TMJ field forward. With knee orthopaedics as a template, the TMJ

field can make great strides toward ameliorating the symptoms that millions of TMD patients experience on a day-to-day basis, drastically improving their quality of life.

References

- 1 Bordoni, B. & Varacallo, M. in *StatPearls* (StatPearls Publishing, 2019).
- 2 Makris, E. A., Hadidi, P. & Athanasiou, K. A. The knee meniscus: structure-function, pathophysiology, current repair techniques, and prospects for regeneration. *Biomaterials* **32**, 7411-7431, doi:10.1016/j.biomaterials.2011.06.037 (2011).
- 3 Gupton, M., Imonugo, O. & Terreberry, R. R. in *StatPearls* (2020).
- 4 Lee, Y.-H. *et al.* Emerging Potential of Exosomes in Regenerative Medicine for Temporomandibular Joint Osteoarthritis. *Int. J. Mol. Sci.* **21**, doi:10.3390/ijms21041541 (2020).
- 5 Fryar, C. D., Kruszon-Moran, D., Gu, Q. & Ogden, C. L. Mean Body Weight, Height, Waist Circumference, and Body Mass Index Among Adults: United States, 1999-2000 Through 2015-2016. *Natl Health Stat Report*, 1-16 (2018).
- 6 D'Lima, D. D., Fregly, B. J., Patil, S., Steklov, N. & Colwell, C. W., Jr. Knee joint forces: prediction, measurement, and significance. *Proc. Inst. Mech. Eng. H* **226**, 95-102, doi:10.1177/09544119111433372 (2012).
- 7 Pizolato, R. A., Gaviao, M. B., Berretin-Felix, G., Sampaio, A. C. & Trindade Junior, A. S. Maximal bite force in young adults with temporomandibular disorders and bruxism. *Braz Oral Res* **21**, 278-283, doi:10.1590/s1806-83242007000300015 (2007).
- 8 Patel, J. M., Wise, B. C., Bonnevie, E. D. & Mauck, R. L. A Systematic Review and Guide to Mechanical Testing for Articular Cartilage Tissue Engineering. *Tissue Eng Part C Methods* **25**, 593-608, doi:10.1089/ten.TEC.2019.0116 (2019).
- 9 Allen, K. D. & Athanasiou, K. A. A surface-regional and freeze-thaw characterization of the porcine temporomandibular joint disc. *Ann Biomed Eng* **33**, 951-962, doi:10.1007/s10439-005-3872-6 (2005).
- 10 Bielajew, B. J., Hu, J. C. & Athanasiou, K. A. Collagen: quantification, biomechanics and role of minor subtypes in cartilage. *Nat Rev Mater* **5**, 730-747, doi:10.1038/s41578-020-0213-1 (2020).
- 11 Singh, M. & Detamore, M. S. Biomechanical properties of the mandibular condylar cartilage and their relevance to the TMJ disc. *J Biomech* **42**, 405-417, doi:10.1016/j.jbiomech.2008.12.012 (2009).
- 12 Huey, D. J., Hu, J. C. & Athanasiou, K. A. Unlike bone, cartilage regeneration remains elusive. *Science* **338**, 917-921, doi:10.1126/science.1222454 (2012).
- 13 Lawrence, R. C. *et al.* Estimates of the prevalence of arthritis and other rheumatic conditions in the United States. Part II. *Arthritis Rheum.* **58**, 26-35, doi:10.1002/art.23176 (2008).
- 14 Masini, B. D. *et al.* Epidemiology of Isolated Meniscus Tears in Young Athletes. *Orthopaedic Journal of Sports Medicine* **3**, 2325967115S2325960010, doi:10.1177/2325967115s00107 (2015).
- 15 Badlani, J. T., Borrero, C., Golla, S., Harner, C. D. & Irrgang, J. J. The effects of meniscus injury on the development of knee osteoarthritis: data from the osteoarthritis initiative. *Am. J. Sports Med.* **41**, 1238-1244, doi:10.1177/0363546513490276 (2013).
- 16 Kalladka, M. *et al.* Temporomandibular joint osteoarthritis: diagnosis and long-term conservative management: a topic review. *J. Indian Prosthodont. Soc.* **14**, 6-15, doi:10.1007/s13191-013-0321-3 (2014).

- 17 Donahue, R. P., Hu, J. C. & Athanasiou, K. A. Remaining Hurdles for Tissue-Engineering the Temporomandibular Joint Disc. *Trends Mol. Med.* **25**, 241-256, doi:10.1016/j.molmed.2018.12.007 (2019).
- 18 The TMJ Association. *TMD Basics*, <<http://www.tmj.org/Page/34/17>> (2017).
- 19 Glyn-Jones, S. *et al.* Osteoarthritis. *The Lancet* **386**, 376-387, doi:10.1016/s0140-6736(14)60802-3 (2015).
- 20 Heidari, B. Knee osteoarthritis prevalence, risk factors, pathogenesis and features: Part I. *Caspian J Intern Med* **2**, 205-212 (2011).
- 21 Braun, H. J. & Gold, G. E. Diagnosis of osteoarthritis: Imaging. *Bone* **51**, 278-288, doi:10.1016/j.bone.2011.11.019 (2012).
- 22 Im, Y.-G. *et al.* Diagnostic accuracy and reliability of panoramic temporomandibular joint (TMJ) radiography to detect bony lesions in patients with TMJ osteoarthritis. *J Dent Sci* **13**, 396-404, doi:10.1016/j.jds.2018.08.006 (2018).
- 23 Honey, O. B. *et al.* Accuracy of cone-beam computed tomography imaging of the temporomandibular joint: comparisons with panoramic radiology and linear tomography. *Am. J. Orthod. Dentofacial Orthop.* **132**, 429-438, doi:10.1016/j.ajodo.2005.10.032 (2007).
- 24 Tomas, X. *et al.* MR imaging of temporomandibular joint dysfunction: a pictorial review. *Radiographics* **26**, 765-781, doi:10.1148/rg.263055091 (2006).
- 25 Daly, C. & Kwong, R. Y. Cardiac MRI for myocardial ischemia. *Methodist Debaquey Cardiovasc J* **9**, 123-131, doi:10.14797/mdcj-9-3-123 (2013).
- 26 Maini, K. & Dua, A. in *StatPearls* (2020).
- 27 Bakke, M., Petersson, A., Wiesel, M., Svanholt, P. & Sonnesen, L. Bony deviations revealed by cone beam computed tomography of the temporomandibular joint in subjects without ongoing pain. *J Oral Facial Pain Headache* **28**, 331-337, doi:10.11607/ofph.1255 (2014).
- 28 Talmaceanu, D. *et al.* Imaging modalities for temporomandibular joint disorders: an update. *Clujul Med* **91**, 280-287, doi:10.15386/cjmed-970 (2018).
- 29 Lee, J. W., Lee, S. M., Kim, S. J., Choi, J. W. & Baek, K. W. Clinical utility of fluoride-18 positron emission tomography/CT in temporomandibular disorder with osteoarthritis: comparisons with 99mTc-MDP bone scan. *Dentomaxillofac Radiol* **42**, 29292350, doi:10.1259/dmfr/29292350 (2013).
- 30 Monasterio, G. *et al.* Osteoarthritis of the Temporomandibular Joint: Clinical and Imagenological Diagnosis, Pathogenic Role of the Immuno- Inflammatory Response, and Immunotherapeutic Strategies Based on T Regulatory Lymphocytes. *Temporomandibular Joint Pathology - Current Approaches and Understanding*, doi:10.5772/intechopen.72496 (2018).
- 31 Glass, N. *et al.* Examining sex differences in knee pain: the multicenter osteoarthritis study. *Osteoarthritis Cartilage* **22**, 1100-1106, doi:10.1016/j.joca.2014.06.030 (2014).
- 32 Srikanth, V. K. *et al.* A meta-analysis of sex differences prevalence, incidence and severity of osteoarthritis. *Osteoarthritis Cartilage* **13**, 769-781, doi:10.1016/j.joca.2005.04.014 (2005).
- 33 Boyan, B. D. *et al.* Addressing the gaps: sex differences in osteoarthritis of the knee. *Biol. Sex Differ.* **4**, 4, doi:10.1186/2042-6410-4-4 (2013).
- 34 Poveda Roda, R., Bagan, J. V., Díaz Fernández, J. M., Hernández Bazán, S. & Jiménez Soriano, Y. Review of temporomandibular joint pathology. Part I: classification, epidemiology and risk factors. *Med. Oral Patol. Oral Cir. Bucal* **12**, E292-298 (2007).
- 35 Abubaker, A. O., Omar Abubaker, A., Raslan, W. F. & Sotereanos, G. C. Estrogen and progesterone receptors in temporomandibular joint discs of symptomatic and asymptomatic persons: A preliminary study. *Journal of Oral and Maxillofacial Surgery* **51**, 1096-1100, doi:10.1016/s0278-2391(10)80448-3 (1993).

- 36 Berger, M. *et al.* Association between estrogen levels and temporomandibular disorders: a systematic literature review. *Prz Menopauzalny* **14**, 260-270, doi:10.5114/pm.2015.56538 (2015).
- 37 Stewart, C. L. & Standish, S. M. Osteoarthritis of the TMJ in teenaged females: report of cases. *J Am Dent Assoc* **106**, 638-640, doi:10.14219/jada.archive.1983.0108 (1983).
- 38 Shan, L., Shan, B., Suzuki, A., Nouh, F. & Saxena, A. Intermediate and Long-Term Quality of Life After Total Knee Replacement: A Systematic Review and Meta-Analysis. *JBJS* **97**, 156-168, doi:10.2106/jbjs.M.00372 (2015).
- 39 Haskin, C. L., Milam, S. B. & Cameron, I. L. Pathogenesis of degenerative joint disease in the human temporomandibular joint. *Crit Rev Oral Biol Med* **6**, 248-277, doi:10.1177/10454411950060030601 (1995).
- 40 Wolford, L. M. Idiopathic condylar resorption of the temporomandibular joint in teenage girls (cheerleaders syndrome). *Proc (Bayl Univ Med Cent)* **14**, 246-252, doi:10.1080/08998280.2001.11927772 (2001).
- 41 Hatcher, D. C. Cone beam computed tomography: craniofacial and airway analysis. *Dent Clin North Am* **56**, 343-357, doi:10.1016/j.cden.2012.02.002 (2012).
- 42 Detamore, M. S., Athanasiou, K. A. & Mao, J. A call to action for bioengineers and dental professionals: directives for the future of TMJ bioengineering. *Ann Biomed Eng* **35**, 1301-1311, doi:10.1007/s10439-007-9298-6 (2007).
- 43 Tanaka, E., Detamore, M. S. & Mercuri, L. G. Degenerative disorders of the temporomandibular joint: etiology, diagnosis, and treatment. *J Dent Res* **87**, 296-307, doi:10.1177/154405910808700406 (2008).
- 44 Dupont, J. S., Jr. The prevalence of trigeminal neuritis with TMD. *Cranio* **21**, 180-184, doi:10.1080/08869634.2003.11746248 (2003).
- 45 Sims, A. B., Clark, V. P. & Cooper, M. S. Suppression of movement disorders by jaw realignment. *Pain Med.* **13**, 731-732, doi:10.1111/j.1526-4637.2012.01364.x (2012).
- 46 Edvall, N. K. *et al.* Impact of Temporomandibular Joint Complaints on Tinnitus-Related Distress. *Front. Neurosci.* **13**, 879, doi:10.3389/fnins.2019.00879 (2019).
- 47 Paparo, F., Fatone, F. M. G., Ramieri, V. & Cascone, P. Anatomic relationship between trigeminal nerve and temporomandibular joint. *Eur. Rev. Med. Pharmacol. Sci.* **12**, 15-18 (2008).
- 48 Pedullà, E. *et al.* Neuropathic pain in temporomandibular joint disorders: case-control analysis by MR imaging. *AJNR Am. J. Neuroradiol.* **30**, 1414-1418, doi:10.3174/ajnr.A1575 (2009).
- 49 *Complications of Temporomandibular Joint Surgery.* (Springer International Publishing, 2017).
- 50 Brown, G. A. AAOS clinical practice guideline: treatment of osteoarthritis of the knee: evidence-based guideline, 2nd edition. *J. Am. Acad. Orthop. Surg.* **21**, 577-579, doi:10.5435/JAAOS-21-09-577 (2013).
- 51 Bouloux, G., Koslin, M. G., Ness, G. & Shafer, D. Temporomandibular Joint Surgery. *J. Oral Maxillofac. Surg.* **75**, e195-e223, doi:10.1016/j.joms.2017.04.027 (2017).
- 52 Meneses, S. R. F. *et al.* Clinical algorithms to aid osteoarthritis guideline dissemination. *Osteoarthritis Cartilage* **24**, 1487-1499, doi:10.1016/j.joca.2016.04.004 (2016).
- 53 American Society of Temporomandibular Joint Surgeons. Guidelines for diagnosis and management of disorders involving the temporomandibular joint and related musculoskeletal structures. *Cranio* **21**, 68-76 (2003).
- 54 Dimitroulis, G. Management of temporomandibular joint disorders: A surgeon's perspective. *Aust. Dent. J.* **63 Suppl 1**, S79-S90, doi:10.1111/adj.12593 (2018).
- 55 Dimitroulis, G. The role of surgery in the management of disorders of the temporomandibular joint: a critical review of the literature: Part 2. *Int. J. Oral Maxillofac. Surg.* **34**, 231-237, doi:10.1016/j.ijom.2004.06.006 (2005).

- 56 Inacio, M. C. S., Paxton, E. W., Graves, S. E., Namba, R. S. & Nemes, S. Projected increase in total knee arthroplasty in the United States – an alternative projection model. *Osteoarthritis Cartilage* **25**, 1797-1803, doi:10.1016/j.joca.2017.07.022 (2017).
- 57 Kwon, H. *et al.* Surgical and tissue engineering strategies for articular cartilage and meniscus repair. *Nat. Rev. Rheumatol.* **15**, 550-570, doi:10.1038/s41584-019-0255-1 (2019).
- 58 UnitedHealthcare Oxford. *Surgical and Non-Surgical Treatment of Temporomandibular Joint Disorders*, <<https://www.oxhp.com/providers/toolsResources/practicalResources/policy/tmd.html>> (2005).
- 59 Zimmer Biomet. Knee Systems Coding Reference Guide. (2019).
- 60 Kumar, S. Training Pathways in Oral and Maxillofacial Surgery Across the Globe-A Mini Review. *J Maxillofac Oral Surg* **16**, 269-276, doi:10.1007/s12663-017-1020-0 (2017).
- 61 American Association of Oral and Maxillofacial Surgeons. OMS Residency Training Programs. (2020).
- 62 Commission on Dental Accreditation. Accreditation Standards for Advanced Dental Education Programs in Oral and Maxillofacial Surgery. 43 (2018).
- 63 Momin, M., Miloro, M., Mercuri, L. G., Munaretto, A. & Markiewicz, M. R. Senior Oral and Maxillofacial Surgery Resident Confidence in Performing Invasive Temporomandibular Joint Procedures. *J. Oral Maxillofac. Surg.* **75**, 2091.e2091-2091.e2010, doi:10.1016/j.joms.2017.06.037 (2017).
- 64 Accreditation Council for Graduate Medical Education. ACGME Program Requirements for Graduate Medical Education in Orthopaedic Surgery. (2019).
- 65 Baskies, M. A., Ruchelsman, D. E., Capeci, C. M., Zuckerman, J. D. & Egol, K. A. Operative Experience in an Orthopaedic Surgery Residency Program: The Effect of Work-Hour Restrictions. *The Journal of Bone and Joint Surgery-American Volume* **90**, 924-927, doi:10.2106/jbjs.g.00918 (2008).
- 66 Accreditation Council for Graduate Medical Education. Orthopaedic Surgery Case Logs National Data Report. (2019).
- 67 Daniels, A. H. & DiGiovanni, C. W. Is subspecialty fellowship training emerging as a necessary component of contemporary orthopaedic surgery education? *J. Grad. Med. Educ.* **6**, 218-221, doi:10.4300/JGME-D-14-00120.1 (2014).
- 68 Commission on Dental Accreditation. Accreditation Standards for Clinical Fellowship Training Programs in Oral and Maxillofacial Surgery. (2017).
- 69 Fattahi, T. & Fernandes, R. Fellowship training and academic careers. *Oral Maxillofac. Surg. Clin. North Am.* **20**, 11-15, doi:10.1016/j.coms.2007.09.003 (2008).
- 70 Perruccio, A. V. *et al.* Sex-Modified Effects of Depression, Low Back Pain, and Comorbidities on Pain After Total Knee Arthroplasty for Osteoarthritis. *Arthritis Care Res (Hoboken)* **72**, 1074-1080, doi:10.1002/acr.24002 (2020).
- 71 Haggman-Henrikson, B. *et al.* Increasing gender differences in the prevalence and chronification of orofacial pain in the population. *Pain*, doi:10.1097/j.pain.0000000000001872 (2020).
- 72 Keogh, E. & Herdenfeldt, M. Gender, coping and the perception of pain. *Pain* **97**, 195-201, doi:10.1016/s0304-3959(01)00427-4 (2002).
- 73 Edwards, R. R., Smith, M. T., Stonerock, G. & Haythornthwaite, J. A. Pain-related catastrophizing in healthy women is associated with greater temporal summation of and reduced habituation to thermal pain. *Clin J Pain* **22**, 730-737, doi:10.1097/01.ajp.0000210914.72794.bc (2006).
- 74 Pincus, T., Burton, A. K., Vogel, S. & Field, A. P. A systematic review of psychological factors as predictors of chronicity/disability in prospective cohorts of low back pain. *Spine (Phila Pa 1976)* **27**, E109-120, doi:10.1097/00007632-200203010-00017 (2002).

- 75 Paller, C. J., Campbell, C. M., Edwards, R. R. & Dobs, A. S. Sex-based differences in pain perception and treatment. *Pain Med* **10**, 289-299, doi:10.1111/j.1526-4637.2008.00558.x (2009).
- 76 Bartley, E. J. & Fillingim, R. B. Sex differences in pain: a brief review of clinical and experimental findings. *Br J Anaesth* **111**, 52-58, doi:10.1093/bja/aet127 (2013).
- 77 Chambers, C. C., Ihnow, S. B., Monroe, E. J. & Suleiman, L. I. Women in Orthopaedic Surgery: Population Trends in Trainees and Practicing Surgeons. *J Bone Joint Surg Am* **100**, e116, doi:10.2106/JBJS.17.01291 (2018).
- 78 Kolokythas, A. & Miloro, M. Why Do Women Choose to Enter Academic Oral and Maxillofacial Surgery? *J Oral Maxillofac Surg* **74**, 881-888, doi:10.1016/j.joms.2016.01.004 (2016).
- 79 DeMaio, M. *Making the Case (Again) for Gender Equity*, <<https://www.aaos.org/aaosnow/2019/jun/youraaos/youraaos05>> (2019).
- 80 Drew, S. J. *President's Editorial*, <<https://www.acoms.org/news/407850/Presidents-Editorial.htm>> (2018).
- 81 National Institutes of Health. *Consideration of Sex as a Biological Variable in NIH-funded Research*, <<https://grants.nih.gov/grants/guide/notice-files/not-od-15-102.html>> (2015).
- 82 Office of Research on Women's Health. *NIH Policy on Sex as a Biological Variable*, <<https://orwh.od.nih.gov/sex-gender/nih-policy-sex-biological-variable>>
- 83 Nolan, M. R. & Nguyen, T. L. Analysis and reporting of sex differences in phase III medical device clinical trials-how are we doing? *J Womens Health (Larchmt)* **22**, 399-401, doi:10.1089/jwh.2013.4400 (2013).
- 84 McKeever, D. C. Tibial Plateau Prosthesis. *Clin. Orthop. Relat. Res.* **18**, 86-95 (1960).
- 85 Carr, B. C. & Goswami, T. Knee implants – Review of models and biomechanics. *Mater. Des.* **30**, 398-413, doi:10.1016/j.matdes.2008.03.032 (2009).
- 86 Christensen, R. W. The correction of mandibular ankylosis by arthroplasty and the insertion of a cast vitallium glenoid fossa: a new technique. A preliminary report of three cases. *Am. J. Orthop.* **5**, 16-24 (1963).
- 87 Hamelynck, K. J. The history of mobile-bearing total knee replacement systems. *Orthopedics* **29**, S7-12 (2006).
- 88 Wen, J. in *Orthopedic Design & Technology* (2017).
- 89 Mercuri, L. G. Temporomandibular joint replacement devices - dark past to challenging future. *Stomatological Disease and Science* **2019**, doi:10.20517/2573-0002.2018.25 (2019).
- 90 Chuong, R. & Piper, M. A. Cerebrospinal fluid leak associated with proplast implant removal from the temporomandibular joint. *Oral Surg. Oral Med. Oral Pathol.* **74**, 422-425, doi:10.1016/0030-4220(92)90286-y (1992).
- 91 Kulber, D. A., Davos, I. & Aronowitz, J. A. Severe cutaneous foreign body giant cell reaction after temporomandibular joint reconstruction with Proplast-Teflon. *J. Oral Maxillofac. Surg.* **53**, 719-722; discussion 722-713, doi:10.1016/0278-2391(95)90182-5 (1995).
- 92 Cowley, T. A delicate balance: The food and drug administration (FDA) and the reform of the medical device approval process. (2011).
- 93 Ingawale, S. & Goswami, T. Temporomandibular joint: disorders, treatments, and biomechanics. *Annals of biomedical engineering* **37**, 976-996 (2009).
- 94 Food and Drug Administration. *Temporomandibular Joint (TMJ) Implants*, <<https://www.fda.gov/medical-devices/temporomandibular-disorders-tmd-devices/temporomandibular-joint-tmj-implants>> (2019).
- 95 Evans, J. T. *et al.* How long does a knee replacement last? A systematic review and meta-analysis of case series and national registry reports with more than 15 years of follow-up. *Lancet* **393**, 655-663, doi:10.1016/S0140-6736(18)32531-5 (2019).

- 96 Center for Devices and Radiological Health. *PS110004: 522 Postmarket Surveillance Studies*, <https://www.accessdata.fda.gov/scripts/cdrh/cfdocs/cfPMA/pss.cfm?t_id=41&c_id=394> (2016).
- 97 Johnson, N., Roberts, M., Doi, S. & Batstone, M. Total temporomandibular joint replacement prostheses: a systematic review and bias-adjusted meta-analysis. *International journal of oral and maxillofacial surgery* **46**, 86-92 (2017).
- 98 Arias, E. United States Life Tables, 2017. *Natl Vital Stat Rep* **68**, 1-66 (2019).
- 99 Food and Drug Administration. FDA approves first autologous cellularized scaffold for the repair of cartilage defects of the knee. (2016).
- 100 McCormick, F. *et al.* Treatment of Focal Cartilage Defects With a Juvenile Allogeneic 3-Dimensional Articular Cartilage Graft. *Operative Techniques in Sports Medicine* **21**, 95-99, doi:10.1053/j.otsm.2013.03.007 (2013).
- 101 Faculdade de Medicina de Petrópolis Faculdade Arthur Sá Earp Neto. *Nasal Septum Autologous Chondrocytes Transplantation for Condylar Resorption After Orthognathic Surgery*, <<https://clinicaltrials.gov/ct2/show/study/NCT03137914>> (2017).
- 102 Thangavelu, A., Thiruneelakandan, S., Prasath, C. H. & Chatterjee, D. Fate of Free Fat Dermis Graft in TMJ Interpositional Gap Arthroplasty: A Long Term MRI Study. *J. Maxillofac. Oral Surg.* **14**, 321-326, doi:10.1007/s12663-014-0672-2 (2015).
- 103 Sharma, H., Chowdhury, S., Navaneetham, A., Upadhyay, S. & Alam, S. Costochondral Graft as Interpositional material for TMJ Ankylosis in Children: A Clinical Study. *Journal of Maxillofacial and Oral Surgery* **14**, 565-572, doi:10.1007/s12663-014-0686-9 (2015).
- 104 The National Academies of Sciences, Engineering, and Medicine. Temporomandibular Disorders (TMD): From Research Discoveries to Clinical Treatment. (2020).
- 105 Almarza, A. *et al.* State of TMJ Bioengineering: Working Together Toward Improving Clinical Outcomes. *J Biomech Eng*, doi:10.1115/1.4044090 (2019).
- 106 Li, D. & Agha, L. Big names or big ideas: Do peer-review panels select the best science proposals? *Science* **348**, 434-438, doi:10.1126/science.aaa0185 (2015).
- 107 National Institutes of Health. Research Project Grants and Other Mechanisms: Competing applications, awards, success rates, and funding, by Institute/Center, mechanism/funding source, and activity code. (2019).
- 108 Laskin, D. M. Temporomandibular Disorders: A Term Whose Time Has Passed! *J Oral Maxillofac Surg* **78**, 496-497, doi:10.1016/j.joms.2019.11.038 (2020).
- 109 American Academy of Orthopaedic Surgeons. *The AAOS American Joint Replacement Registry*, <<https://www.aaos.org/registries/registry-program/american-joint-replacement-registry>> (
- 110 Salash, J. R. *et al.* Potential Indications for Tissue Engineering in Temporomandibular Joint Surgery. *J Oral Maxillofac Surg* **74**, 705-711, doi:10.1016/j.joms.2015.11.008 (2016).
- 111 Erickson, B. J., Strickland, S. M. & Gomoll, A. H. Indications, Techniques, Outcomes for Matrix Induced Autologous Chondrocyte Implantation (MACI). *Operative Techniques in Sports Medicine* **26**, 175-182, doi:10.1053/j.otsm.2018.06.002 (2018).
- 112 Dolwick, M. F. & Dimitroulis, G. Is there a role for temporomandibular joint surgery? *Br J Oral Maxillofac Surg* **32**, 307-313, doi:10.1016/0266-4356(94)90052-3 (1994).
- 113 Schiffman, E. *et al.* Diagnostic Criteria for Temporomandibular Disorders (DC/TMD) for Clinical and Research Applications: recommendations of the International RDC/TMD Consortium Network* and Orofacial Pain Special Interest Groupdagger. *J Oral Facial Pain Headache* **28**, 6-27, doi:10.11607/jop.1151 (2014).
- 114 Center for Biologics Evaluation and Research, Food and Drug Administration,. Preparation of IDEs and INDs for Products Intended to Repair or Replace Knee Cartilage. (2011).
- 115 Vapniarsky, N. *et al.* Tissue engineering toward temporomandibular joint disc regeneration. *Sci Transl Med* **10**, doi:10.1126/scitranslmed.aaq1802 (2018).

- 116 American Academy of Orthopaedic Surgeons. 2019 Annual Report. (2019).
- 117 American Association of Oral and Maxillofacial Surgeons. *About AAOMS*, <<https://www.aaoms.org/about>> (2020).
- 118 Singh, J. A., Yu, S., Chen, L. & Cleveland, J. D. Rates of Total Joint Replacement in the United States: Future Projections to 2020-2040 Using the National Inpatient Sample. *J Rheumatol* **46**, 1134-1140, doi:10.3899/jrheum.170990 (2019).
- 119 Onoriobe, U. *et al.* How Many Temporomandibular Joint Total Joint Alloplastic Implants Will Be Placed in the United States in 2030? *J Oral Maxillofac Surg* **74**, 1531-1538, doi:10.1016/j.joms.2016.04.011 (2016).

CHAPTER 3 | Methodology to quantify collagen subtypes and crosslinks: application in minipig cartilages*

Abstract

This study develops assays to quantify collagen subtypes and crosslinks with liquid chromatography-mass spectrometry (LC-MS), and characterizes the cartilages in the Yucatan minipig. For collagen subtyping, liquid chromatography-tandem mass spectrometry (LC-MS/MS) analysis was performed on tissues digested in trypsin. For collagen crosslinks, LC-MS analysis was performed on hydrolysates. Samples were also examined histologically and with bottom-up proteomics. Ten cartilages (femoral condyle, femoral head, facet joint, floating rib, true rib, auricular cartilage, annulus fibrosus, two meniscus locations, and TMJ disc) were analyzed. The collagen subtyping assay quantified collagen types I and II. The collagen crosslink assay quantified mature and immature crosslinks. Collagen subtyping revealed that collagen type I predominates in fibrocartilages and collagen type II in hyaline cartilages, as expected. Elastic cartilage and fibrocartilages had more mature collagen crosslink profiles than hyaline cartilages. Bottom-up proteomics revealed a spectrum of ratios between collagen types I and II, and quantified 42 proteins, including 24 collagen alpha-chains and 12 minor collagen types. The novel assays developed in this work are sensitive, inexpensive, and use a low operator time relative to other collagen analysis methods. Unlike the current collagen assays, these assays quantify collagen subtypes and crosslinks without an antibody-based approach or lengthy chromatography. They apply to any collagenous tissue, with broad applications in tissue characterization and tissue engineering. For example, a novel finding of this work was the presence of a large quantity of collagen type III in the white-white knee meniscus, and a spectrum of hyaline and fibrous cartilages.

* Published as: Bielajew BJ, Hu JC, Athanasiou KA. Methodology to Quantify Collagen Subtypes and Crosslinks: Application in Minipig Cartilages. *Cartilage* 2021; 13(Suppl 2): 1742S-1754S.

Introduction

Collagen is the most abundant protein in the mammalian body and is the foundation of the extracellular matrix (ECM) of connective tissues¹. Collagen is better described as a superfamily of proteins consisting of 28 currently discovered subtypes, each of which is a trimer consisting of three alpha-chains that associate into supercoiled triple helices². The main fibrillar collagen subtypes, collagen types I and II, make up a large majority of collagens found in different tissues all over the body¹. A primary barrier to determining the collagen composition of biological tissues is that high-throughput and low-cost methods for collagen subtype quantification remain a major challenge¹. The traditional method of collagen quantification, the hydroxyproline assay, does not discriminate among collagen subtypes³. Other methods, such as enzyme-linked immunosorbent assay, can be prohibitively expensive or unavailable depending on the animal species or collagen subtype¹. Some imaging methods, such as immunohistochemistry, can be used to visualize different collagen subtypes, but these are non-quantitative¹.

In this work, we introduce a liquid chromatography-tandem mass spectrometry (LC-MS/MS) assay that uses multiple reaction monitoring⁴ to quantify collagen types I and II. This assay is inexpensive compared to antibody-based methods and applicable to collagenous tissues from human, bovine, porcine, and murine sources. Enzymatic collagen crosslinks, such as the mature trivalent crosslink pyridinoline (PYR) and the immature divalent crosslink dihydroxylysinonorleucine (DHLNL) play important roles in the mechanical properties of collagenous tissues^{5,6}. Recent work has introduced the use of diamond hydride chromatography for collagen crosslink quantification⁷, and, in this experiment, this chromatography method is used on an LC-MS with high sensitivity and specificity. As a demonstration of these two novel assays, ten cartilages of the Yucatan minipig are analyzed. This animal model was selected because it is a well-recognized model for cartilage repair studies^{8,9}.

Cartilages are classified into one of three categories: hyaline cartilage, fibrocartilage, and elastic cartilage, based on the composition of the tissue's ECM. Traditionally, cartilages are

classified by the types of fibrillar proteins within the tissue. Hyaline cartilage, found on the ends of bones (articular cartilage) and in the ribs, nose, and trachea, is mostly collagen type II by dry weight¹⁰. Fibrocartilage, found in the knee meniscus, temporomandibular joint (TMJ), and annulus fibrosus, has an ECM that contains mostly collagen type I by dry weight¹¹. Elastic cartilage, found in the auricle of the ear and in the epiglottis, has an ECM that contains both collagen types I and II, as well as a substantial portion of elastin¹².

Previous tissue engineering studies have shown that it is possible to engineer a spectrum of hyaline and fibrous cartilages, based on the ratio of collagen types I and II¹³; i.e., more hyaline cartilage having more collagen type II and less collagen type I, and more fibrous cartilage having more collagen type I and less collagen type II. While there has been evidence of higher collagen type II in the white-white portion of the knee meniscus compared to the red-red meniscus¹⁴, it is not known if a wide spectrum of collagen ratios exist in native cartilages. Prior work has shown that femoral condylar cartilage contains higher PYR crosslinks compared to knee meniscus in the immature knee joint⁵, but it is unknown if this trend holds true for other cartilages, or for mature joints.

The objectives of this work are to develop high-throughput LC-MS assays to analyze collagen subtypes and crosslinks, to use these assays to characterize ten cartilages of the Yucatan minipig, and to use bottom-up proteomics to quantitatively characterize the proteome of these minipig cartilages. The hypotheses of this work are that: 1) the LC-MS/MS collagen subtyping assay can quantify marker peptides of collagen types I and II in a specific and sensitive manner, and 2) the LC-MS collagen crosslinks assay can quantify PYR, DHLNL, and hydroxyproline. Using minipig cartilages as examples, it is expected that: 1) the novel collagen subtyping assay will show a majority of collagen type I in fibrocartilages and a majority of collagen type II in hyaline cartilages, 2) the collagen crosslinks assay will different crosslink ratios in hyaline cartilages than fibrocartilages, and 3) bottom-up proteomics will reveal different ratios of collagen

types I and II in different cartilages within the traditional hyaline and fibrous classifications, revealing a spectrum of cartilage tissues.

Methods

LC-MS/MS for collagen subtype quantification

A Waters ACQUITY UPLC I-Class core system coupled to a Waters Quattro Premier XE triple quadrupole mass spectrometer was used for the collagen subtype LC-MS/MS assay. For all liquid chromatography in this study, solvent A was 0.1% (v/v) formic acid in water, and solvent B was 0.1% (v/v) formic acid in acetonitrile. Liquid chromatography gradient settings were as follows: initial 3% B, 2 min 40% B, 3 min 97% B, 4 min 3% B, 5 min 3% B, total run time 5 min. An ACQUITY UPLC BEH C18 column was used with a flow rate of 300 μ L/min for reverse-phase separation. Target peptides of collagen were selected under the following criteria: susceptible to digestion from trypsin, not found in any other protein aside from one specific collagen subtype, found in human, bovine, porcine, and murine tissues, and mass between 800 and 1800 Da. Briefly, PeptideRank was used for *in silico* prediction of tryptic peptides for collagen subtypes with the best ionization characteristics¹⁵. Peptides were checked with NCBI BLASTp to ensure uniqueness and identical sequence across human, bovine, porcine, and murine proteomes. The set of determined peptides is summarized in Table 1. After a peptide was selected, a custom synthesis of the peptide standard was ordered from GenScript. MRM methods were developed by diluting peptide standards to 10 μ g/mL in solvent A, then optimizing cone voltage (CV) and collision energy (CE) to \pm 1V on repeated 5 μ L injections. Standard curves were prepared by 3x serial dilution of a 10 μ g/mL mix of the col1 α 1 and col2 α 1 peptide standards. LOD and LOQ were calculated based on a signal-to-noise ratio of 3 (LOD) or 10 (LOQ), calculated based on injections of the lowest concentration standard.

Quantification of collagen crosslinks and hydroxyproline

Liquid chromatography gradient settings were as follows: initial 90% B, 1 min 90% B, 2 min 20% B, 4 min 20% B, 5 min 90% B, 10 min 90% B, total run time 10 min. A Cogent Diamond Hydride 2.0 HPLC column was used with a flow rate of 400 μ L/min for aqueous normal phase separation, coupled to a Waters ACQUITY QDa mass spectrometer. PYR standard was ordered from BOC Sciences, DHLNL standard was ordered from Santa Cruz Biotechnology, and hydroxyproline (OHP) and pyridoxine (PDX) standards were ordered from Sigma Aldrich. Quantification methods were developed by diluting PYR, DHLNL, OHP, and PDX standards to 1 μ g/mL in solvent A, then optimizing CV to \pm 1V on repeated 5 μ L injections. Standard curves were prepared by 3x serial dilution of a 1 μ g/mL mix of PYR, DHLNL, and PDX and 10 μ g/mL of OHP. PDX was used as an internal standard. LOD and LOQ were calculated as described above.

Table 1. Mass spectrometry settings for target analytes. Triple quadrupole and single quadrupole settings are described for quantification of collagen subtypes and crosslinks. Bolded **P** represents hydroxyproline. CV, cone voltage; CE, collision energy; PYR, pyridinoline; DHLNL, dihydroxylysinoxorleucine.

Analyte	Peptide sequence	Mass (Da)	Parent m/z	Daughter m/z	CV (V)	CE (V)
Col1 α 1	GVQGPPGPAGPR	1104.58	553.93	668.2	27	30
Col2 α 1	GIVGLPGQR	911.53	457.3	474.46	21	13
Hydroxyproline	n/a	131.13	132.17	n/a	6	n/a
PYR	n/a	428.19	215.21	n/a	6	n/a
DHLNL	n/a	307.34	308.30	n/a	6	n/a
Pyridoxine	n/a	169.18	170.08	n/a	6	n/a

Bottom-up proteomics

For all bottom-up proteomics samples, the same peptide digest used for the collagen I and II LC-MS/MS assay was used. For each tissue, digests from all seven animals were combined into one representative sample. The peptide digests were subjected to LC-MS/MS analysis using a Thermo Fischer Scientific UltiMate 3000 RSLC system coupled on-line to a Thermo Fischer

Scientific Orbitrap Fusion Lumos mass spectrometer. Liquid chromatography gradient was as follows: 4% to 25% solvent B over 57 min. A 50 cm x 75 μ m I.D. Acclaim® PepMap RSLC column was used at a flow rate of 300 nL/min for reverse-phase separation. Each cycle consisted of one full Fourier transform scan mass spectrum (375–1500 m/z, resolution of 60,000 at m/z 400) followed by 15 data-dependent MS/MS acquired in the linear ion trap with collision-induced dissociation with normalized collision energy of 25%. Target ions already selected for MS/MS were dynamically excluded for 30s. Identification and label-free quantification was carried out using MaxQuant, as previously described¹⁶. Briefly, raw files were searched using MaxQuant (v. 1.6.0.16) against a FASTA containing the *sus scrofa* proteome obtained from the SwissProt open-source database (version from December 2020) along with *sus scrofa* collagen proteins from TrEMBL. The first search peptide tolerance was set to 20 ppm, with main search peptide tolerance set to 4.5 ppm. The protein, peptide, and peptide spectrum match level false discovery rates were all 1% as determined by a target-decoy approach. For quantification, intensities were determined as the full peak volume over the retention time profile. The degree of uniqueness required for peptides to be included in quantification was “Unique plus razor peptides.” The resulting label-free quantification (LFQ) values calculated through MaxQuant were used for comparing protein relative abundance among different samples. The proteomics data have been deposited to the ProteomeXchange Consortium via the PRIDE partner repository with the dataset identifier PXD025482.

Data analysis and statistical analysis

For collagen type I and II and for collagen crosslinks, MassLynx v4.1 software with QuanLynx was used to calculate area-under-curve measurements for all MRM peaks for interpolation into the standard curve. The resulting ng/mL result was multiplied by the sample volume and appropriate dilution factor to quantify the analyte quantity in the sample. Any analyte quantity below the LOQ was set to zero. For crosslinks, the resulting mass of each crosslink was

normalized to dry weight or the amount of hydroxyproline in the hydrolysate. For peptides, the peptide mass was converted to protein mass. For collagen type II, the peptide mass (M_{pep}) is multiplied by the mass ratio of the alpha-chain to the peptide (k) to calculate the mass of collagen type II in the digest (M_{Col2}):

$$M_{Col2} = kM_{pep}$$

For collagen type I, protein mass is calculated based on the quantification of the col1 α 1 peptide; because collagen type I is a heterotrimer which has two col1 α 1 chains and one col1 α 2 chain, the mass may be calculated, assuming the molar ratio of col1 α 1 to col1 α 2 is 2:1. Here, k is the mass ratio of a col2 α 1 molecule to the col2 α 1 target peptide, and A is the molar ratio of one col1 α 2 molecule to two col1 α 1 molecules as calculated by their amino acid sequences and post-translational modifications:

$$M_{Col1} = M_{Col1\alpha1} + M_{Col1\alpha2} = (1 + A) M_{Col1\alpha1} = (1 + A)(kM_{pep})$$

For collagen type II, $k = 105.09$. For collagen type I, $k = 86.01$ and $A = 0.49$. Molecular weights of the collagen proteins were calculated after cleavage of the N-terminal propeptides. Protein masses were normalized to sample dry weight.

Statistical analysis was performed in JMP Pro 14. *Post hoc* Tukey tests were used after performing one-way ANOVAs. Statistical significance ($p < 0.05$) is indicated with a connecting-letters report on all bar graphs; bars not sharing the same letter are significantly different from each other. All graphs were generated in GraphPad Prism 8.

Sample preparation

Ten cartilage tissues from the Yucatan minipig were analyzed: knee meniscus (both red-red portion and white-white portion separately), temporomandibular joint disc (center region), annulus fibrosus of the intervertebral disc (L5/S1 or L6/S1 joint), auricular (ear) cartilage, femoral head cartilage, femoral condyle cartilage, costal cartilages of the true rib (rib 1) and floating rib (rib 14), and facet joint cartilage (Figure 1). Cartilage pieces were excised from N=7 skeletally mature (5-

6 month old) Yucatan minipigs which were previously culled for reasons unrelated to this study. For histological analysis, 5-mm biopsies from three representative pieces of each cartilage type were fixed in formalin, embedded in paraffin, sectioned to 5 μm thickness, and stained with hematoxylin and eosin (H&E) or picosirius red (PR) as previously described¹⁷. Two 1.5-mm biopsy samples (0.5-1 mg wet weight) from each cartilage piece were washed in ultrapure water, dabbed dry, weighed for wet weight, lyophilized, and weighed again for dry weight. One biopsy sample was used for the collagen subtyping assay and bottom-up proteomics, and the other was used for the crosslinks assay.

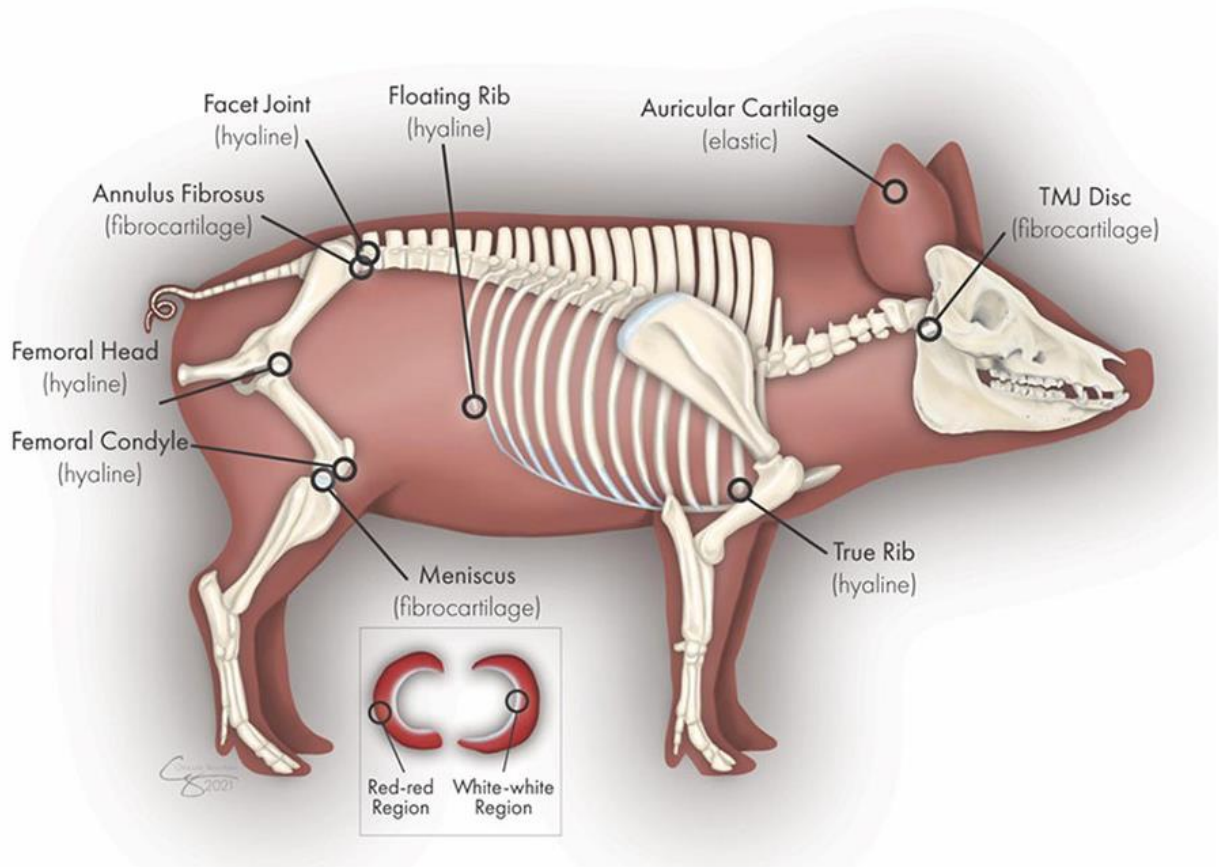


Figure 1. The locations of the different cartilages harvested from the Yucatan minipig. The locations of all cartilages included in this study are illustrated on a Yucatan minipig skeleton. Illustration by Chrisoula Skouritakis. TMJ, temporomandibular joint.

For collagen subtyping and bottom-up proteomics, samples were washed twice in 10 mM ammonium citrate and twice in 50 mM ammonium bicarbonate, then mass spectrometry-grade

trypsin was added in a 1:20 (w/w) ratio of trypsin to sample dry weight, and samples were digested at 65°C in 200 µL of 50 mM ammonium bicarbonate. After digestion, samples were filtered through 100 kDa molecular weight cut-off centrifugal filters and diluted 1:1 in 0.1% formic acid, yielding a transparent, colorless peptide digest solution. For the crosslinks assay, biopsy samples were submerged in 1 mM NaOH containing NaBH₄ (1% weight to sample weight) for 2 hours at room temperature, washed overnight in ultrapure water, then hydrolyzed in 6N HCl at 105°C for 18 hours in a heat block. HCl was evaporated, and samples were resuspended in 400 µL of 0.1% formic acid, then filtered through 100k molecular weight cut-off centrifugal filters and diluted 20:1 in 0.1% formic acid, yielding a transparent, colorless hydrolysate.

Results

LC-MS assays for collagen subtypes and crosslinks

The determined parameters required for running the LC-MS/MS assays for collagen subtype and crosslink quantification are displayed in Table 1. The collagen subtyping assay quantified col1α1 and col2α1 marker peptides in biological tissues in a 5-minute chromatography gradient, and the collagen crosslinks assay quantified PYR, DHLNL, and hydroxyproline in a 10-minute chromatography gradient. For the col1α1 marker peptide, the limit of detection (LOD) was 40.7 ng/mL, and limit of quantification (LOQ) was 135.7 ng/mL. For the col2α1 marker peptide, the LOD was 9.5 ng/mL, and the LOQ was 31.9 ng/mL. For a 200 µg dry weight (DW) sample, these LOQs correspond to a quantifiable amount of collagen at approximately 3.5% collagen type I / DW and 0.7% collagen type II / DW. Both marker peptides' standard curves yielded a strong goodness of fit ($R^2 > 0.99$). To translate the assay result of peptide ng/mL to a protein/DW, complete digestion of the tissue is necessary. The technique of single-step high-temperature trypsin digestion at 65°C rather than the standard 37°C yielded peptide digests that were transparent, colorless, and absent of any undigested tissue (with the exception of mineralized tissues), indicating that digestion was complete. For collagen crosslinks, the LOD and LOQ of

hydroxyproline were 2.7 and 8.9 ng/mL, LOD and LOQ of PYR were 6.5 and 21.5 ng/mL, and LOD and LOQ of DHLNL were 0.6 and 2.0 ng/mL, respectively. This degree of sensitivity was sufficient to quantify PYR, DHLNL, and hydroxyproline in all tested tissues.

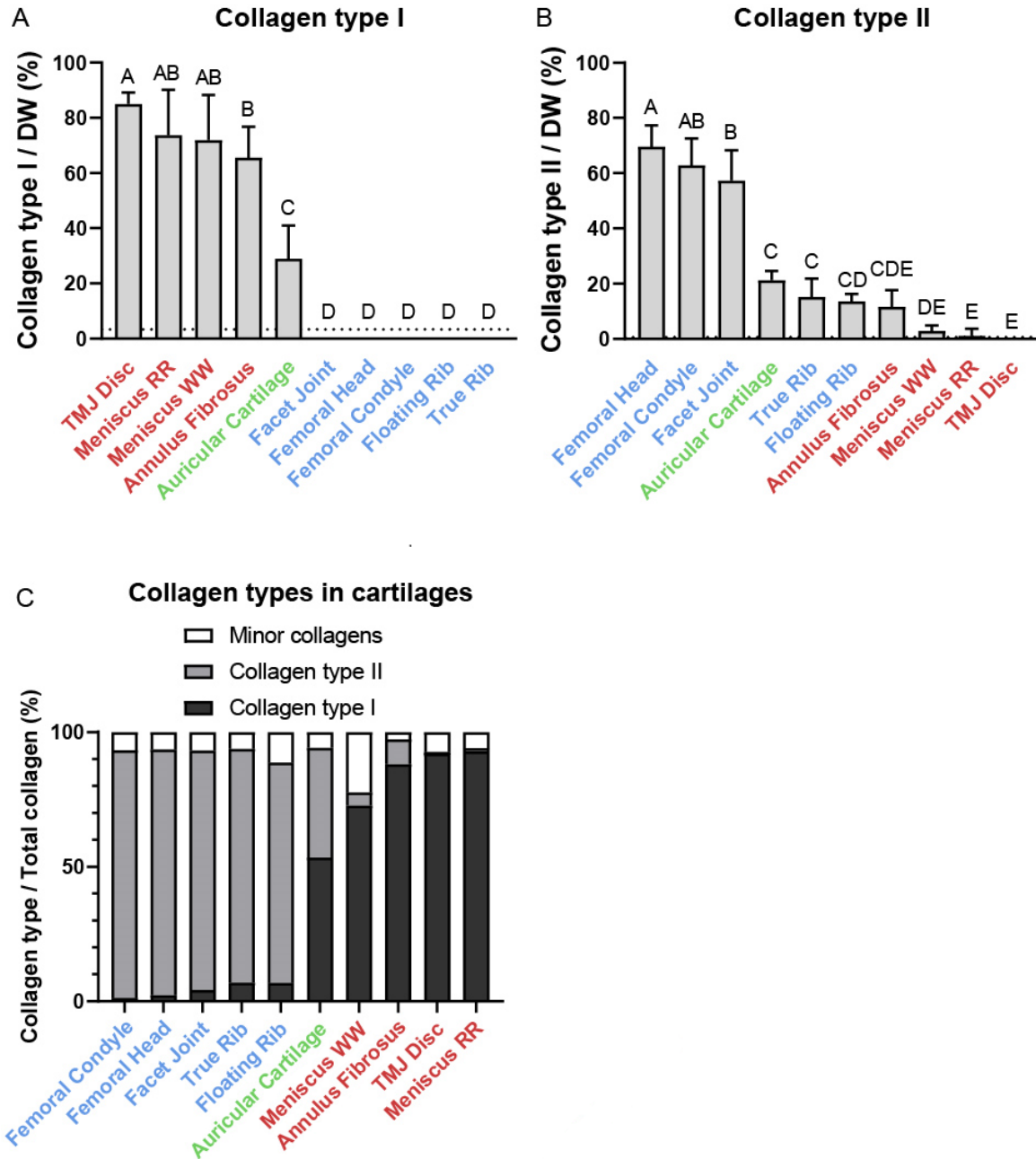


Figure 2. Collagen subtype quantification in the cartilages of the Yucatan minipig. (A) Collagen type I normalized to dry weight. (B) Collagen type II normalized to dry weight. Dashed lines: limits of quantification of the LC-MS/MS assay. (C) Bottom-up proteomics analysis of collagens. Hyaline, elastic, and fibrocartilage x-axis labels are marked with blue, green, and red colors, respectively. LC-MS, liquid chromatography-mass spectrometry; DW, dry weight; TMJ, temporomandibular joint; RR, red-red; WW, white-white.

Collagens in minipig cartilages

Collagen types I and II were quantified in ten tissues via LC-MS/MS high-throughput quantification (Figure 2 A-B); data are presented as collagen mass per dry weight (DW). For collagen type I, the fibrocartilages had the highest amount per DW. TMJ disc had the highest content out of the fibrocartilages, at $85.1\% \pm 4.0\%$ per DW. All hyaline cartilages (true rib, floating rib, femoral condyle, femoral head, facet joint) had a quantity of collagen type I that was below the limit of quantification (LOQ). The articular cartilages (femoral head, femoral condyle, facet joint) had the highest amount of collagen type II per DW ($69.5\% \pm 7.8\%$, $62.8\% \pm 9.7\%$, $57.3\% \pm 11.1\%$, respectively); the femoral head cartilage had significantly ($p=0.02$) higher collagen type II than facet joint cartilage. None of the fibrocartilages had significantly different amounts of collagen type II per DW, and in all TMJ disc samples, the amount of collagen type II was below the LOQ. For the hyaline costal cartilages, collagen type II per DW was significantly lower than other hyaline cartilages; this is due to a high degree of calcification of rib cartilages in the skeletally mature pigs.

Cartilage crosslinks

The mature (PYR) and immature (DHLNL) crosslink contents of the cartilages are depicted in Figure 3. Normalized to hydroxyproline, the highest PYR content was found in the auricular cartilage (62.0 ± 13.0 mmol/mol), while most fibrocartilages such as the red-red meniscus (19.6 ± 6.6 mmol/mol) had higher mean PYR than hyaline cartilage such as the femoral condyle (8.1 ± 2.2 mmol/mol). Normalized to hydroxyproline, there were no significant differences in DHLNL content among all cartilage types. Normalized to dry weight, all elastic and fibrocartilages except for annulus fibrosus have significantly more PYR than hyaline cartilages. For example, red-red meniscus has the highest PYR/DW at 2420 ± 568 ng/mg, while true rib cartilage has the lowest PYR/DW at 609 ± 381 ng/mg. A similar pattern was found with DHLNL/DW, where most fibrocartilages had higher mean DHLNL/DW than hyaline cartilages, except for annulus fibrosus. For example, TMJ disc (692 ± 163 ng/mg) had significantly more DHLNL/DW than true rib ($242 \pm$

106 ng/mg). The molar ratio of PYR to DHLNL (Figure 3E) was highest in the auricular cartilage (10.4 ± 2.3 mol/mol) and had a higher mean in all fibrocartilages than hyaline cartilages, but this difference was only significant for annulus fibrosus (4.0 ± 2.0 mol/mol).

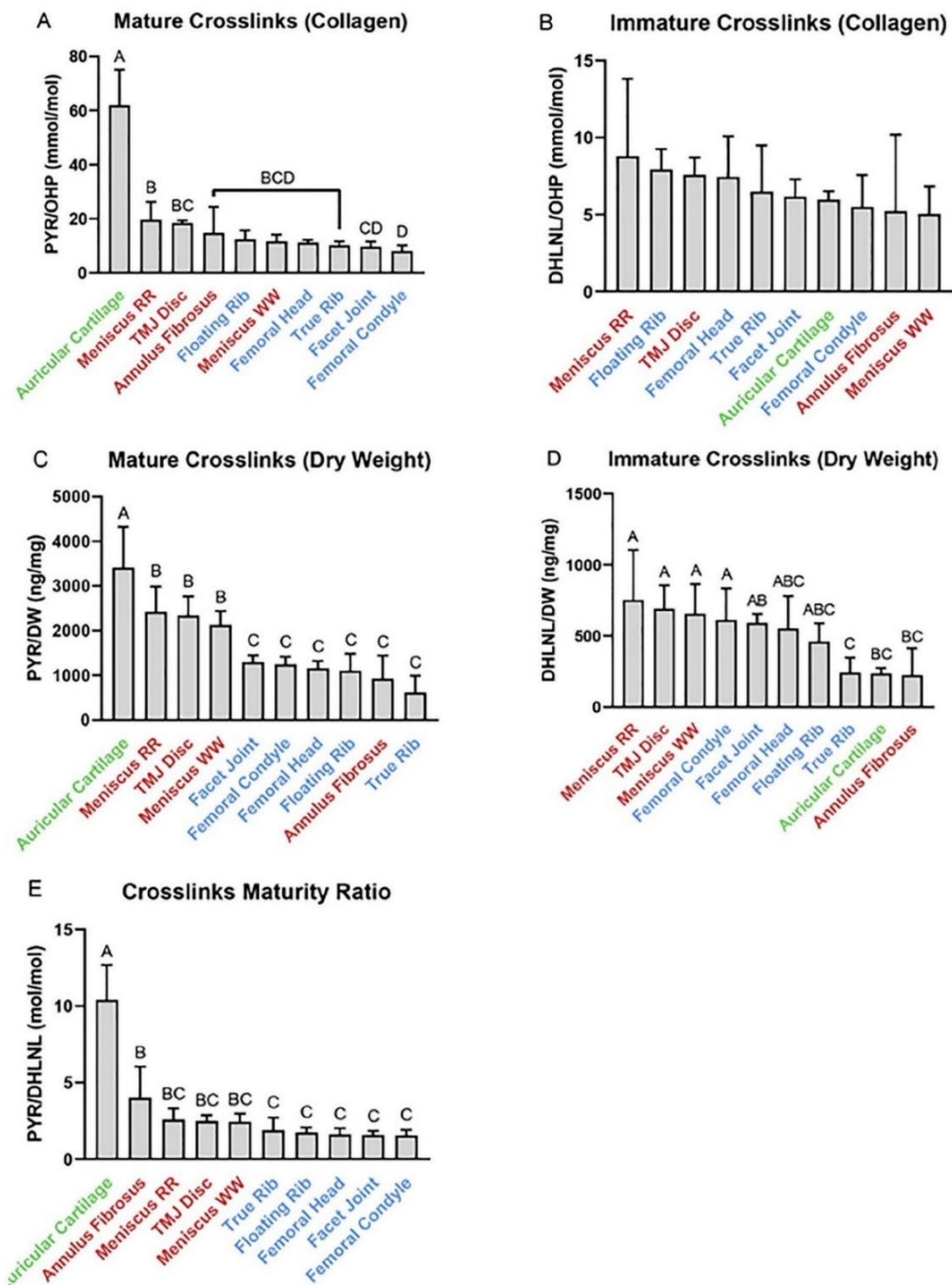


Figure 3. Crosslink quantification in the cartilages of the Yucatan minipig. (A, C) Mature crosslinks (PYR) normalized to hydroxyproline and dry weight, respectively. (B, D) Immature crosslinks (DHLNL) normalized to hydroxyproline and dry weight, respectively. (E) Maturity ratio, or the molar ratio of PYR to DHLNL. Hyaline, elastic, and fibrocartilage x-axis labels are marked with blue, green, and red colors, respectively. DHLNL, dihydroxylysinonorleucine; PYR, pyridinoline; OHP, hydroxyproline; TMJ, temporomandibular joint; DW, dry weight.

Table 2. Bottom-up proteomics results on Yucatan minipig cartilages. All results are reported as percentage protein per total protein. FC, femoral condyle; FH, femoral head; FJ, facet joint cartilage; TR, true rib; FR, floating rib; AC, auricular (ear) cartilage; AF, annulus fibrosus; MW, meniscus white-white region; TD, temporomandibular joint disc; MR, meniscus red-red region. Only proteins that comprise greater than 0.01% of total protein content are included.

Gene	Protein Name	Protein / Total Protein (%)									
		FC	FH	FJ	TR	FR	AC	AF	MW	TD	MR
PGCA	Aggrecan core protein	0.15	0.21	0.18	0.00	0.45	0.04	0.02	0.03	0.00	0.00
PGS1	Biglycan	0.09	0.18	0.13	0.00	0.00	0.08	0.01	0.02	0.00	0.00
CILP1	Cartilage intermediate layer protein 1	0.13	0.14	0.12	0.00	0.00	0.00	0.02	0.06	0.00	0.00
COL1A1	Collagen type I alpha 1	1.11	2.17	3.65	6.34	6.38	34.45	60.01	50.71	63.71	61.32
COL1A2	Collagen type I alpha 2	0.11	0.08	0.51	0.46	0.31	18.08	27.58	21.46	28.53	30.17
COL2A1	Collagen type II alpha 1	91.06	89.87	87.20	84.60	80.90	40.14	9.21	4.81	1.15	0.58
COL3A1	Collagen type III alpha 1	4.42	3.21	3.36	0.32	0.02	3.84	1.56	19.68	4.19	5.76
COL4A1	Collagen type IV alpha 1	0.07	0.09	0.05	0.79	0.32	0.03	0.02	0.00	0.00	0.00
COL4A2	Collagen type IV alpha 2	0.02	0.01	0.01	0.30	0.26	0.01	0.00	0.00	0.00	0.00
COL4A3	Collagen type IV alpha 3	0.05	0.07	0.03	0.04	0.15	0.03	0.04	0.04	0.08	0.05
COL4A4	Collagen type IV alpha 4	0.00	0.00	0.00	0.00	0.00	0.01	0.01	0.01	0.10	0.02
COL4A5	Collagen type IV alpha 5	0.01	0.02	0.01	0.44	0.32	0.03	0.05	0.07	0.08	0.15
COL5A1	Collagen type V alpha 1	0.07	0.04	0.09	0.03	0.01	0.05	0.09	0.42	0.16	0.25
COL5A2	Collagen type V alpha 2	0.07	0.03	0.07	0.01	3.10	0.06	0.08	0.30	0.09	0.09
COL5A3	Collagen type V alpha 3	0.15	0.47	0.14	0.02	0.02	0.14	0.05	0.62	0.23	0.14

COL6A2	Collagen type VI alpha 2	0.06	0.09	0.08	0.01	0.01	0.16	0.05	0.10	0.04	0.05
COL6A3	Collagen type VI alpha 3	0.10	0.18	0.14	0.00	0.00	0.17	0.17	0.33	0.19	0.19
COL9A1	Collagen type IX alpha 1	0.21	0.26	0.37	0.88	0.76	0.00	0.00	0.00	0.02	0.06
COL9A2	Collagen type IX alpha 2	0.14	0.16	0.25	0.79	0.33	0.00	0.02	0.25	0.22	0.02
COL10A1	Collagen type X alpha 1	0.00	0.00	0.00	0.17	0.98	0.03	0.01	0.00	0.00	0.04
COL11A1	Collagen type XI alpha 1	0.40	0.43	0.73	1.15	1.61	0.47	0.23	0.11	0.07	0.10
COL11A2	Collagen type XI alpha 2	0.58	0.70	1.05	1.02	2.03	0.48	0.10	0.05	0.10	0.06
COL12A1	Collagen type XII alpha 1	0.04	0.22	0.13	0.01	0.00	0.07	0.06	0.03	0.07	0.08
COL15A1	Collagen type XV alpha 1	0.00	0.00	0.00	0.00	0.00	0.00	0.04	0.06	0.18	0.08
COL16A1	Collagen type XVI alpha 1	0.15	0.19	0.09	0.03	0.02	0.07	0.01	0.00	0.01	0.00
COL27A1	Collagen type XXVII alpha 1	0.05	0.09	0.06	0.07	0.28	0.04	0.07	0.08	0.08	0.19
COL28A1	Collagen type XXVIII alpha 1	0.00	0.00	0.00	0.00	0.89	0.00	0.00	0.00	0.00	0.00
CUBN	Cubilin	0.00	0.00	0.00	0.00	0.00	0.11	0.25	0.01	0.12	0.27
COX6C	Cytochrome c oxidase subunit 6C	0.00	0.00	0.00	0.17	0.14	0.00	0.00	0.00	0.00	0.00
PGS2	Decorin	0.16	0.11	0.14	0.09	0.11	0.11	0.07	0.10	0.10	0.05
FMOD	Fibromodulin	0.02	0.03	0.03	0.05	0.00	0.03	0.01	0.02	0.01	0.01
G3P	Glyceraldehyde-3- phosphate dehydrogenase	0.02	0.16	0.08	0.01	0.00	0.01	0.02	0.01	0.01	0.00
HBA	Hemoglobin subunit alpha	0.00	0.15	0.05	0.00	0.00	0.01	0.02	0.01	0.01	0.00
H4	Histone H4	0.04	0.04	0.08	0.03	0.02	0.05	0.01	0.01	0.01	0.02
HPLN1	Hyaluronan and proteoglycan link protein 1	0.10	0.14	0.30	0.13	0.11	0.16	0.03	0.04	0.00	0.01

MFGM	Lactadherin	0.07	0.13	0.23	0.08	0.10	0.10	0.02	0.08	0.00	0.00
MYG	Myoglobin	0.00	0.01	0.15	0.00	0.00	0.00	0.01	0.00	0.00	0.00
MYH7	Myosin-7	0.00	0.01	0.00	1.75	0.03	0.00	0.00	0.00	0.00	0.00
ROCK2	Rho-associated protein kinase 2	0.01	0.03	0.02	0.01	0.00	0.17	0.01	0.19	0.23	0.01
TENA	Tenascin	0.14	0.09	0.11	0.01	0.00	0.01	0.00	0.05	0.03	0.05
KSYK	Tyrosine-protein kinase SYK	0.03	0.01	0.04	0.03	0.14	0.02	0.00	0.00	0.05	0.03
VIME	Vimentin	0.02	0.02	0.02	0.00	0.03	0.57	0.00	0.00	0.01	0.02

Bottom-up proteomics analysis

A full list of relative proportions of all quantified proteins with greater than 0.1% protein per total protein can be found in Table 2. Collagen results are summarized in Figure 2C. In hyaline cartilages, collagen type II predominates over collagen type I, varying from a 12-fold difference (floating rib) to a 74-fold difference (femoral condyle). In auricular cartilage, collagen type I and II are very close, with about a 1.3-fold higher amount of collagen type I. This is consistent with a 1.4-fold higher amount of collagen type I in auricular cartilage, as found via high-throughput subtyping (Figures 1A and 1B). All fibrocartilages have much higher collagen type I than type II, ranging from a 9.5-fold difference in the annulus fibrosus to a 157-fold difference in the red-red meniscus. In most cartilages, minor collagens (those aside from collagen types I and II) account for a small proportion of total collagen, ranging from 2.7% in the annulus fibrosus to 12.7% in the floating rib. The exception is the white-white meniscus which contained 28.8%, most of which comes from collagen type III; the white-white meniscus contained 24.7% collagen type III per total collagen, the highest among any cartilages tested. The most prominent minor collagens were collagen types III, IX, XI, and XVI in the hyaline cartilages, and types III, V, VI, and XI in elastic and fibrocartilages. Other proteins that were found in the ECM include aggrecan core protein,

hyaluronan and proteoglycan link protein 1, biglycan, cartilage intermediate layer protein 1, and decorin.

Histology

Histological stains on all cartilages are shown in Figure 4. H&E histology was used to visualize cells and ECM. Fibrocartilages stained more heavily with eosin than hyaline and elastic cartilages and showed anisotropic collagen organization. Histological results were consistent with literature in morphology and staining intensities; for example, hyaline and elastic cartilages stained less with eosin staining and more with hematoxylin due to higher quantities of glycosaminoglycans (GAGs) in the tissues¹⁸. The true rib morphology had a fragmented appearance in areas of high calcification. PR staining, similar to H&E staining, stained more intensely for collagen in the fibrocartilages, and appeared fibrous and anisotropic. PR staining intensity was lower in the non-fibrous cartilages, and there was less organization of collagen fibers.

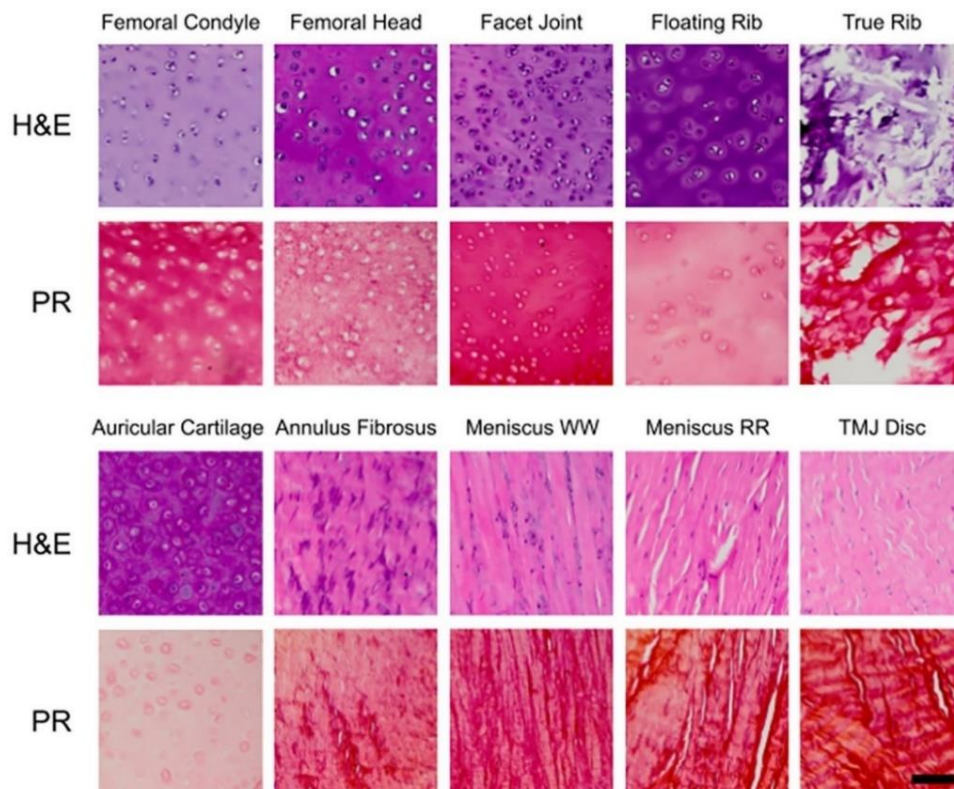


Figure 4. Histological stains on minipig cartilages. Histology of ten Yucatan minipig cartilages is shown. H&E, hematoxylin and eosin; PR, picrosirius red; TMJ, temporomandibular joint. Scale bar, 100 μ m.

Discussion

In this experiment, we developed and optimized two LC-MS assays for quantification of collagen subtypes and collagen crosslinks, and confirmed the hypotheses LC-MS can be used as a sensitive, specific, quantification method for collagen subtypes and crosslinks in biological tissues. With the parameters detailed in Table 1, researchers with access to mass spectrometers can run these assays. The collagen subtyping assay has advantages over other collagen assays; it is specific to collagen subtype, can be run with a 5-minute chromatography gradient, and does not require expensive antibodies. The collagen crosslinks assay can simultaneously detect hydroxyproline and crosslinks (immature and mature) in a 10-minute gradient; this assay offers researchers an additional low-cost and low-operator time technique to study biological tissues.

To demonstrate these novel tools, ten different cartilages of the Yucatan minipig were analyzed with the collagen subtype and crosslink quantification assays. The collagen subtyping assay accurately showed a majority of collagen type I in fibrocartilages and a majority of collagen type II in hyaline cartilages, and the crosslinks assay showed that the collagen of hyaline cartilages contains more crosslinks than the collagen of fibrocartilages. A bottom-up proteomics analysis was also performed, and the proteomes, quantified in Table 2, will allow cartilage researchers and clinicians to better understand the matrix that comprises these tissues. With bottom-up proteomics analysis, evidence that hyaline and fibrous cartilages exist on a spectrum was supported by the quantification of the ratio of collagen types I and II. Notably, the fibrocartilage of the knee meniscus revealed regional differences between the white-white and red-red region, although this difference is substantially less than what has been reported in other work, as described below. Overall, this study provides: 1) a basis for researchers to simultaneously quantify collagen types I and II in a high-throughput manner, 2) relative quantities of the 42 most abundant proteins found in ten cartilages, and 3) evidence for a spectrum of native hyaline and fibrous cartilages.

Table 3. Comparison of collagen assays. The price and operator time of different collagen assays are described.

Method	Price (approx.)*	Operator time (hr)*	Notes
Hydroxyproline Assay	\$50	6	Not specific to different types of collagen
ELISA	\$500 (One collagen type)	6	Antibodies for many minor collagen types unavailable
Label-free Orbitrap-based Quantification	\$4,000 (All collagen types)	2 (36 hr machine time)	Low-throughput for large sample sets
Label-free LC-MS/MS With Multiple Reaction Monitoring	\$40 (Targeted collagen types)	2 (3 hr machine time)	Requires additional method development for minor collagens
*For 36 samples. Prices are estimated based on reagent costs and machine usage rates at the High-end Mass Spectrometry Facility and the Mass Spectrometry Facility at the University of California, Irvine.			

Determining collagen content is a vital step for characterization of biological tissues and products. The currently practiced methods for collagen quantification are described in Table 3, which shows that the LC-MS/MS collagen subtype quantification technique developed in this work is more cost-effective and specific than other options; the novel subtyping assay is a fraction of the cost of ELISA or Orbitrap-based label-free quantification. While some previous work has been done toward developing MS assays for quantitative collagen subtyping¹⁹, the high-throughput method used in this study is faster (5-minute chromatography versus 60-minute), eliminates a lengthy salt cutting procedure, and employs a single-step high-temperature trypsin digestion rather than a combination of trypsin and highly toxic cyanogen bromide²⁰. Although some cartilage types in this sample set yielded collagen readings below the LOQ (collagen type I in hyaline cartilages and collagen type II in TMJ disc), it is possible that these collagen types can be

quantified with the same assay on a different instrument; more recent mass spectrometer models have been advertised to greatly improve the signal-to-noise ratio compared to older models, such as the one used in this study. With these newer models, the target peptide approach can be used to quantify minor collagen subtypes simultaneously with collagen types I and II in a high-throughput and low-cost manner. The work presented in this study is relevant to tissue engineers, who may use collagen content as a benchmark due its role in mechanical properties of tissues such as cartilages²¹, blood vessels²², ligaments⁵, and skin²³. Collagen quantification is important in other fields as well; collagen content has been correlated to malignancy of various cancers²⁴, and it is used in many products in the cosmetics industry^{25,26} and food and beverage industry²⁷.

While collagen crosslink quantification assays have recently seen improvements in the development of silica hydride-based chromatography and mass spectrometry⁷, the assay in this study features an improvement in using a 10-minute chromatography gradient for a low assay runtime compared to commonly used crosslinks assays (30-45 minutes). This collagen crosslink assay, like the collagen subtype quantification assay, is applicable to collagenous tissues all over the body. A novel aspect of this work is the usage of a maturity ratio for cartilages. While other groups have looked at the ratio of immature and mature crosslinks in collagenous tissues⁶, this is the first study that compares this ratio across different types of cartilage. This study showed that fibrocartilages have a greater maturity ratio than hyaline cartilages. Whether or not this is due to rates of collagen turnover in these cartilages, mechanical demands of the tissue, or other factors is yet to be determined.

The bottom-up proteomics method in this study provided quantitative evidence that a spectrum of hyaline and fibrocartilages exist in the Yucatan minipig, shown in the ratio of collagen type I to collagen type II. In hyaline cartilage, the ratio of collagen type II to collagen type I varies from about 74:1 in femoral condyle to about 12:1 in floating rib. In fibrocartilage, the ratio of collagen type I to collagen type II ranges from over 150:1 in the red-red meniscus to less than 10:1 in the annulus fibrosus. Auricular cartilage, the only elastic cartilage in this data set, contains

roughly the same amount of collagen types I and II. This wide array of ratios suggests the existence of a spectrum of fibrous and hyaline cartilage rather than discrete categories.

A spectrum of cartilage properties also appears not only in the collagen ratios, but also in the collagen crosslinks. As shown in Figure 3A and 3C, fibrocartilages had greater quantities of mature crosslinks per hydroxyproline and dry weight than hyaline cartilages. It is possible that this may arise from the way that collagen type II crosslinks to collagen type XI in hyaline cartilage ECM²⁸, given that the bottom-up proteomics revealed 0.99-3.6% collagen type XI per protein in the hyaline cartilages. Collagen type I can crosslink to collagen type V²⁹, and collagen type V was less abundant, at 0.21-1.34% in the fibrocartilages, so it is possible that more crosslinks are formed between collagen types I and V than between II and XI. The difference in crosslinking may also arise from differences in the structure of the collagen molecules. One study has reported that a higher amount of glycosylated hydroxylysine residues in collagen type II results in a larger molecular spacing compared to collagen type I, allowing collagen type II to contain 50-100% more water than collagen type I, and this property may allow collagen type II to resist osmotic swelling from GAGs in cartilage ECM to dissipate compressive loading³⁰. This increased spacing, which is needed for a collagen network that better resists osmotic swelling, may reduce the efficiency of collagen crosslink kinematics. Additional experiments will need to be performed to fully understand the differences in crosslinking between hyaline cartilages and fibrocartilages.

When damage to hyaline articular cartilage results in fibrocartilage formation, either via bleeding from subchondral bone or from microfracture procedures, a fibrocartilage repair tissue is formed in the defect that contains both collagen types I and II³¹, which fails mechanically in the long term³². The failure of this fibrocartilage repair tissue may be in part due to the aforementioned role of collagen II in dissipating compressive forces; if the ECM of the repair tissue is of the wrong composition, it may not stand up to the large, repeated forces withstood by hyaline articular cartilage. While current methods for repair of cartilage defects are unsuccessful in the long term,

tissue engineering is a promising strategy to generate biomimetic cartilage implants for cartilage regeneration³³.

Because different types of collagen are implicated in the loading capabilities of cartilage tissues, engineered cartilages must be designed to match the ECM of the cartilage that they are designed to replace. The bottom-up proteomics analysis of the cartilages in this study can be used to define gold standard ratios of collagen types I and II in engineered cartilages. Tissue engineering studies using the self-assembling process have engineered a spectrum of fibrous and hyaline neocartilages by varying the time of three-dimensional aggregate culture¹³, although collagen types I and II were not quantified. Other studies have used different ratios of cell sources (e.g., meniscus fibroblasts and articular chondrocytes) to achieve different ratios of collagen types³⁴. Additional studies to fine-tune these techniques and generate specific collagen type I:II ratios must be completed to replace different cartilages around the body. While the minipig is a promising animal model for cartilage repair^{8,9} and has been used in attempts at cartilage regeneration using tissue-engineered implants³⁵, a thorough characterization on the hyaline-fibrocartilage spectrum of human cartilage must also be completed to determine engineering specifications for tissue-engineered cartilage in humans, because interspecies differences in collagen content have been noted³⁶. Additionally, the Yucatan minipigs in this study were all skeletally mature. Because the collagen and crosslink content of cartilage changes with age and disease^{37,38}, additional characterization of cartilages at different ages will be needed for a diverse patient population.

The relative proportion of collagen types I and II in the knee meniscus is supported by conflicting literature. An early study claimed that collagen of the porcine meniscus is completely type I³⁹, but a subsequent study claimed that the white-white portion of the bovine meniscus is 60% collagen type II and 40% collagen type I¹⁴. This idea that the white-white meniscus contains abundant collagen type II, and, thus, is reminiscent of hyaline articular cartilage, has become accepted in the meniscus field^{33,40}. A more recent proteomics analysis on various cartilages

reveals over a 12-fold ratio of collagen type I to collagen type II in the human knee meniscus⁴¹, although the region was not specified. The bottom-up proteomics analysis in our study revealed a 15-fold ratio of collagen type I to type II in the white-white region, and a greater than 150-fold ratio in the red-red region. While there is indeed a stark difference in this ratio between the two regions, these data, in conjunction with the histological staining (Figure 4) suggest that the white-white meniscus of the Yucatan minipig is indeed a true fibrocartilage, with a substantially dissimilar ECM from hyaline cartilage. The white-white meniscus also had the highest amount of collagen type III out of any of the cartilages studied. To our knowledge, this is the first study that reports a high amount of collagen type III in the white-white meniscus. One study has shown that collagen type III is intensely expressed at the surfaces of the meniscus⁴²; because the white-white region is exceedingly thin compared to the red-red region, the higher quantity of collagen type III could be a result of this high surface area to volume ratio. Another study has highlighted that collagen type III plays a crucial structural role in meniscus ECM by maintaining fibril spacing and diameter⁴³, but did not quantify the amount of collagen type III in the tissue. Collagen type III comprises up to 20% of the protein in cartilages, suggesting that collagen type III should be considered a major collagen type, along with collagen types I and II. This finding warrants further investigation into the mechanical roles of collagen type III in cartilages. A study on human cartilages will be important to determine the ECM characteristics of the human meniscus, particularly the quantity of collagen types I, II, and III in different regions.

In this study, we developed LC-MS assays to quantify collagen subtypes and crosslinks in biological tissues. These assays are inexpensive, require a low operator time, and can be modified to quantify minor collagen types and their crosslinks. As a demonstration of these assays, they were applied to the cartilages of the Yucatan minipig, a promising animal model for cartilage repair. Collagen types I and II, along with the crosslinks PYR and DHLNL, were quantified in hyaline, elastic, and fibrocartilages. Bottom-up proteomics revealed a spectrum of collagen ratios in these tissues, thus, showing the existence of a hyaline-fibrocartilage spectrum

in native cartilage. This is one of many potential ways that the high-throughput collagen subtyping developed in this work can be used for characterization of collagenous tissues, informing best practices for tissue engineers and surgeons as they develop treatment strategies.

References

- 1 Bielajew, B. J., Hu, J. C. & Athanasiou, K. A. Collagen: quantification, biomechanics and role of minor subtypes in cartilage. *Nature Reviews Materials* (2020) doi:10.1038/s41578-020-0213-1.
- 2 Ricard-Blum, S. & Ruggiero, F. The collagen superfamily: from the extracellular matrix to the cell membrane. *Pathol. Biol.* **53**, 430–442 (2005).
- 3 Cissell, D. D., Link, J. M., Hu, J. C. & Athanasiou, K. A. A Modified Hydroxyproline Assay Based on Hydrochloric Acid in Ehrlich's Solution Accurately Measures Tissue Collagen Content. *Tissue Eng. Part C Methods* **23**, 243–250 (2017).
- 4 Yocum, A. K. & Chinnaiyan, A. M. Current affairs in quantitative targeted proteomics: multiple reaction monitoring-mass spectrometry. *Brief. Funct. Genomic. Proteomic.* **8**, 145–157 (2009).
- 5 Eleswarapu, S. V., Responde, D. J. & Athanasiou, K. A. Tensile properties, collagen content, and crosslinks in connective tissues of the immature knee joint. *PLoS One* **6**, e26178 (2011).
- 6 Yoshida, K. *et al.* Quantitative evaluation of collagen crosslinks and corresponding tensile mechanical properties in mouse cervical tissue during normal pregnancy. *PLoS One* **9**, e112391 (2014).
- 7 Naffa, R. *et al.* Rapid analysis of pyridinoline and deoxypyridinoline in biological samples by liquid chromatography with mass spectrometry and a silica hydride column. *Journal of Separation Science* vol. 42 1482–1488 (2019).
- 8 Goetz, J. E. *et al.* A clinically realistic large animal model of intra-articular fracture that progresses to post-traumatic osteoarthritis. *Osteoarthritis Cartilage* **23**, 1797–1805 (2015).
- 9 Vapniarsky, N. *et al.* The Yucatan Minipig Temporomandibular Joint Disc Structure-Function Relationships Support Its Suitability for Human Comparative Studies. *Tissue Eng. Part C Methods* **23**, 700–709 (2017).
- 10 Fox, A. J. S., Sophia Fox, A. J., Bedi, A. & Rodeo, S. A. The Basic Science of Articular Cartilage: Structure, Composition, and Function. *Sports Health: A Multidisciplinary Approach* vol. 1 461–468 (2009).
- 11 Eyre, D. R. & Wu, J. J. Collagen of fibrocartilage: a distinctive molecular phenotype in bovine meniscus. *FEBS Lett.* **158**, 265–270 (1983).
- 12 Madsen, K., von der Mark, K., van Menxel, M. & Friberg, U. Analysis of collagen types synthesized by rabbit ear cartilage chondrocytes in vivo and in vitro. *Biochem. J* **221**, 189–196 (1984).
- 13 Murphy, M. K., Masters, T. E., Hu, J. C. & Athanasiou, K. A. Engineering a fibrocartilage spectrum through modulation of aggregate redifferentiation. *Cell Transplant.* **24**, 235–245 (2015).
- 14 Cheung, H. S. Distribution of type I, II, III and V in the pepsin solubilized collagens in bovine menisci. *Connect. Tissue Res.* **16**, 343–356 (1987).
- 15 Qeli, E. *et al.* Improved prediction of peptide detectability for targeted proteomics using a rank-based algorithm and organism-specific data. *J. Proteomics* **108**, 269–283 (2014).
- 16 Cox, J. & Mann, M. MaxQuant enables high peptide identification rates, individualized p.p.b.-range mass accuracies and proteome-wide protein quantification. *Nat. Biotechnol.* **26**, 1367–1372 (2008).

- 17 Brown, W. E., Huey, D. J., Hu, J. C. & Athanasiou, K. A. Functional self-assembled neocartilage as part of a biphasic osteochondral construct. *PLoS One* **13**, e0195261 (2018).
- 18 Chiu, L. & Waldman, S. Nanomaterials for cartilage tissue engineering. in *Nanomaterials and regenerative medicine* 417–451 (IAPC Publishing, 2016).
- 19 Pataridis, S., Eckhardt, A., Mikulikova, K., Sedlakova, P. & Miksik, I. Determination and Quantification of Collagen Types in Tissues Using HPLC-MS/MS. *Current Analytical Chemistry* vol. 5 316–323 (2009).
- 20 PubChem. Cyanogen bromide. <https://pubchem.ncbi.nlm.nih.gov/compound/10476>.
- 21 Haudenschild, A. K. *et al.* Nondestructive fluorescence lifetime imaging and time-resolved fluorescence spectroscopy detect cartilage matrix depletion and correlate with mechanical properties. *European Cells and Materials* vol. 36 30–43 (2018).
- 22 Latimer, C. A., Nelson, M., Moore, C. M. & Martin, K. E. Effect of collagen and elastin content on the burst pressure of human blood vessel seals formed with a bipolar tissue sealing system. *J. Surg. Res.* **186**, 73–80 (2014).
- 23 Oxlund, H. & Andreassen, T. T. The roles of hyaluronic acid, collagen and elastin in the mechanical properties of connective tissues. *J. Anat.* **131**, 611–620 (1980).
- 24 Fang, M., Yuan, J., Peng, C. & Li, Y. Collagen as a double-edged sword in tumor progression. *Tumor Biology* vol. 35 2871–2882 (2014).
- 25 De Boule, K., Swinberghe, S., Engman, M. & Shoshani, D. Lip augmentation and contour correction with a ribose cross-linked collagen dermal filler. *J. Drugs Dermatol.* **8**, 1–8 (2009).
- 26 Avila Rodríguez, M. I., Rodríguez Barroso, L. G. & Sánchez, M. L. Collagen: A review on its sources and potential cosmetic applications. *J. Cosmet. Dermatol.* **17**, 20–26 (2018).
- 27 León-López, A. *et al.* Hydrolyzed Collagen—Sources and Applications. *Molecules* **24**, (2019).
- 28 Wu, J. J. & Eyre, D. R. Structural analysis of cross-linking domains in cartilage type XI collagen. Insights on polymeric assembly. *J. Biol. Chem.* **270**, 18865–18870 (1995).
- 29 Niyibizi, C. & Eyre, D. R. Structural characteristics of cross-linking sites in type V collagen of bone. Chain specificities and heterotypic links to type I collagen. *Eur. J. Biochem.* **224**, 943–950 (1994).
- 30 Grynepas, M. D., Eyre, D. R. & Kirschner, D. A. Collagen type II differs from type I in native molecular packing. *Biochimica et Biophysica Acta (BBA) - Protein Structure* vol. 626 346–355 (1980).
- 31 Armiento, A. R., Alini, M. & Stoddart, M. J. Articular fibrocartilage - Why does hyaline cartilage fail to repair? *Adv. Drug Deliv. Rev.* **146**, 289–305 (2019).
- 32 Solheim, E., Hegna, J. & Inderhaug, E. Long-Term Survival after Microfracture and Mosaicplasty for Knee Articular Cartilage Repair: A Comparative Study Between Two Treatments Cohorts. *Cartilage* **11**, 71–76 (2020).
- 33 Kwon, H. *et al.* Surgical and tissue engineering strategies for articular cartilage and meniscus repair. *Nat. Rev. Rheumatol.* **15**, 550–570 (2019).
- 34 Aufderheide, A. C. & Athanasiou, K. A. Assessment of a bovine co-culture, scaffold-free method for growing meniscus-shaped constructs. *Tissue Eng.* **13**, 2195–2205 (2007).
- 35 Vapniarsky, N. *et al.* Tissue engineering toward temporomandibular joint disc regeneration. *Sci. Transl. Med.* **10**, (2018).
- 36 Chiu, L. L. Y., Giardini-Rosa, R., Weber, J. F., Cushing, S. L. & Waldman, S. D. Comparisons of Auricular Cartilage Tissues from Different Species. *Ann. Otol. Rhinol. Laryngol.* **126**, 819–828 (2017).
- 37 Lu, W. *et al.* Dopamine delays articular cartilage degradation in osteoarthritis by negative regulation of the NF- κ B and JAK2/STAT3 signaling pathways. *Biomed. Pharmacother.* **119**, 109419 (2019).
- 38 Li, Y., Wei, X., Zhou, J. & Wei, L. The Age-Related Changes in Cartilage and Osteoarthritis. *Biomed Res. Int.* **2013**, (2013).

- 39 Eyre, D. R. & Muir, H. The distribution of different molecular species of collagen in fibrous, elastic and hyaline cartilages of the pig. *Biochem. J* **151**, 595–602 (1975).
- 40 Makris, E. A., Hadidi, P. & Athanasiou, K. A. The knee meniscus: structure-function, pathophysiology, current repair techniques, and prospects for regeneration. *Biomaterials* **32**, 7411–7431 (2011).
- 41 Önnerfjord, P., Khabut, A., Reinholt, F. P., Svensson, O. & Heinegård, D. Quantitative proteomic analysis of eight cartilaginous tissues reveals characteristic differences as well as similarities between subgroups. *J. Biol. Chem.* **287**, 18913–18924 (2012).
- 42 Mine, T., Ihara, K., Kawamura, H., Date, R. & Umehara, K. Collagen expression in various degenerative meniscal changes: an immunohistological study. *J. Orthop. Surg.* **21**, 216–220 (2013).
- 43 Wang, C. *et al.* Type III collagen is a key regulator of the collagen fibrillar structure and biomechanics of articular cartilage and meniscus. *Matrix Biol.* **85-86**, 47–67 (2020).

CHAPTER 4 | Proteomic, mechanical, and biochemical characterization of cartilage development*

Abstract

The objective of this work is to examine the development of porcine cartilage by analyzing its mechanical properties, biochemical content, and proteomics at different developmental stages. Cartilage from the knees of fetal, neonatal, juvenile, and mature pigs was analyzed using histology, mechanical testing, biochemical assays, and bottom-up proteomics. Mature cartilage has 2.2-times the collagen per dry weight of fetal cartilage, and fetal cartilage has 2.1-times and 17.9-times the glycosaminoglycan and DNA per dry weight of mature cartilage, respectively. Tensile and compressive properties peak in the juvenile stage, with a tensile modulus 4.7-times that of neonatal. Proteomics analysis reveals increases in collagen types II and III, while collagen types IX, XI, and XIV, and aggrecan decrease with age. For example, collagen types IX and XI decrease 9.4-times and 5.1-times respectively from fetal to mature. Mechanical and biochemical measurements have their greatest developmental changes between the neonatal and juvenile stages, where mechanotransduction plays a major role. Bottom-up proteomics serves as a powerful tool for tissue characterization, showing results beyond those of routine biochemical analysis. For example, proteomic analysis shows significant drops in collagen types IX, XI, and XIV throughout development, which shows insight into the permanence of cartilage's matrix. Changes in overall glycosaminoglycan content compared to aggrecan and link protein indicate non-enzymatic degradation of aggrecan structures or hyaluronan in mature cartilage. In addition to tissue characterization, bottom-up proteomics techniques are critical in tissue engineering efforts toward repair or regeneration of cartilage in animal models.

* Published as: Bielajew BJ[†], Donahue RP[†], Lamkin EK, Hu JC, Hascall VC, Athanasiou KA. Proteomic, Mechanical, and Biochemical Characterization of Cartilage Development. *Acta Biomaterialia* 2022; online ahead of print. [†]equal contribution

Introduction

Cartilage does not heal, and current clinical treatments for cartilage degeneration are palliative, not reparative. This motivates cartilage tissue engineering, which aims to design neotissues for cartilage repair or replacement. Many researchers have attempted to engineer neocartilages by recapitulating aspects of cartilage development, including the self-assembling process, which is reminiscent of mesenchymal condensation^{1,2}. Toward ensuring that developmentally accurate neocartilage is produced, developing native cartilage must be characterized — especially its mechanical properties as a function of its biochemical and proteomic content. Through these characterizations, design criteria for tissue-engineered cartilages may be established such that the neocartilage implants are capable of bearing loads experienced by adults in daily activities. Additionally, tissue engineering strategies that mimic developmental processes will be informed by a characterization of these structure-function relationships over developmental time points from fetal to mature tissue.

The extracellular matrix (ECM) content and mechanics of cartilage change during development and aging³. Knee articular cartilage forms as a result of endochondral ossification during embryonic development. During this process, mesenchymal condensation occurs which results in an interzone region at the future joint. Chondrogenesis of mesenchymal progenitor cells in the perichondrium region of the interzone leads to formation of early cartilage tissues which will later develop into mature cartilage⁴. This process continues into postnatal development where cartilage continues to mature. Collagens and glycosaminoglycans (GAGs), two main ECM components of cartilage, change in quantity and type throughout this process^{5,6}. For example, collagen type II, the principal collagen subtype of hyaline cartilage, is known to increase with tissue maturity^{2,5}, but it is not known how other minor collagen subtypes develop. Along with these biochemical changes, mechanical properties of cartilage are altered throughout development⁷⁻⁹. For example, human cartilage reaches peak stiffness between 30 and 50 years of age¹⁰. After cartilage is fully developed, further age-related ECM changes occur, including proteolytic

degradation and other post-translational modifications¹¹. Biochemical changes alter mechanical properties of the cartilage; for example, cartilage shear modulus has a strong negative correlation with age and osteoarthritis grade¹². These age-related changes can result in cartilage degeneration and pathology, affecting approximately nearly 1 in 4 US adults¹³. A promising solution to these age-related degenerative changes is tissue engineering, which is poised to provide a long-term regenerative solution to cartilage ailments toward improving pain and function and enhancing quality of life for patients.

Toward informing design criteria for neocartilage, characterization studies have investigated the biochemical and mechanical properties of cartilage. For example, healthy human articular cartilage has an aggregate modulus of 0.08-2 MPa and tensile modulus of 5-25 MPa, depending on tissue location and depth³. These properties arise from the biochemical makeup of cartilage, mainly being composed of collagen type II and GAGs. Cartilage contains 50-75% collagen by dry weight (DW) and 15-30% GAG by DW, including chondroitin sulfate (CS)³. However, the subtypes of collagens and GAGs are rarely quantified, especially in developmental studies. This study investigates the proteomic development of cartilage ECM using bottom-up proteomics for the first time, as well as isomers of CS (chondroitin-6-sulfate, CS6, and chondroitin-4-sulfate, CS4), via fluorophore-assisted carbohydrate electrophoresis (FACE), in addition to biochemical and mechanical characterization.

Prior to the development of human tissue-engineered therapeutics, preclinical studies must be done in animal models. There are many accepted animal models for cartilage. For example, the sheep and horse are suggested by the U.S. Food and Drug Administration for preclinical studies that aim to repair or replace knee cartilage due to the biochemical and mechanical similarities to human cartilage¹⁴. In developmental biology, the porcine model has long been used due to its similarity to human development¹⁵; this is best illustrated by its use in anatomy courses from the high school to graduate levels. The porcine model has recently emerged as a model for knee cartilage studies due to its cartilage biomechanics¹⁶. Additionally,

minipigs have been used for their lower terminal weight, which offers practical and financial advantages for long-term studies, including easier handling and less food intake¹⁷. Here, the porcine model is investigated due to its well-studied developmental pathway and suitability as a cartilage preclinical animal model.

The objective of this work is to interrogate the development of knee articular cartilage by analyzing the mechanics, biochemical content, and proteomics of knee articular cartilage from different aged pigs. The hypothesis of this work is that age-dependent changes in the mechanical, biochemical, and proteomic properties will be observed. Specifically, as a function of developmental age, increases in the tensile and compressive mechanical properties, increases in collagen, and decreases in GAG and DNA will be observed. Increases and decreases in proteomic biomarkers will also be observed; however, the specific targets are not known *a priori*. Toward this objective, a wide breadth of characterization analyses were performed on the cartilage of pigs ranging from fetal to 2+ years, including compressive and tensile mechanical testing; photometric collagen, GAG, and DNA assays; mass spectrometry for collagen crosslinks; FACE for CS isomers; and bottom-up proteomic approaches for cartilage proteins.

Methods

Sample collection

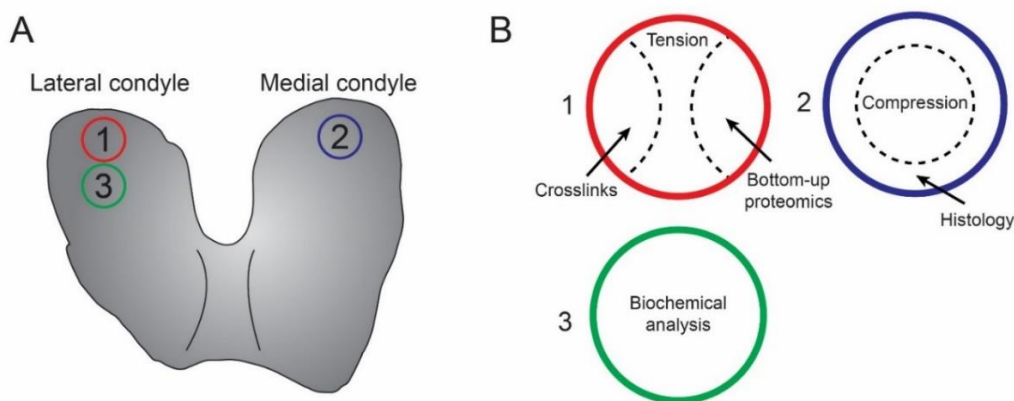


Figure 1. Sample collection diagram. This illustration shows the (A) lateral and medial condyles with punch locations (not to scale) and (B) sample locations within each punch.

Fresh-frozen whole fetal and neonatal pigs (*Sus scrofa domesticus*, Yorkshire cross, female and male) were purchased from Nebraska Scientific. According to the provided growth chart, the pigs were determined to be of 80d, 90d, or 100d gestational age, or stillborn (neonatal). Knees from juvenile (5-6 month old) and mature (2-3 year old) pigs (*Sus scrofa domesticus*, Yorkshire cross, female and castrated male), culled for purposes unrelated to this research, were purchased from Corona Cattle, Inc. For fetal and neonatal pigs, unilateral (only the right) knee joints were used, and for juvenile and mature pigs, bilateral knee joints were used. Prior to sample collection, juvenile and mature knees were fresh-frozen *en bloc* and subsequently thawed to ensure consistency with fetal and neonatal groups. Knee joint capsules were then opened, and macroscopic joint health of patellofemoral joints was checked to ensure that they were absent of osteoarthritic changes such as osteophytes and cartilage fibrillation or defects. A total of 44 knees were used, as follows: 7 knees from fetal 80d, 7 knees from fetal 90d, 7 knees from fetal 100d, 7 knees from neonatal, 8 knees from juvenile, and 8 knees from mature pigs. Osteochondral samples were taken from three locations on the condyles with disposable 3 mm diameter biopsy punches as depicted in Figure 1, and subchondral bone was then trimmed off at the tidemark with a scalpel blade. The center of the condyle was defined as the intersection of midpoints of the height and width of each condyle. Punch 1 from the center of the lateral condyle was cut into a dog-bone shape (approximately 0.5 mm width by 1.0 mm thickness) for tensile testing, and the removed portions were used for crosslinks and bottom-up proteomics analyses. Punch 2 from the center of the medial condyle was used for compression testing and histology, with a 2 mm diameter sample (full-thickness, approximately 1 mm in height) from the center used for stress-relaxation test, and the remaining portion used for histology. Punch 3 was taken adjacent to punch 1 as shown in Figure 1, and this full-thickness sample was used for the biochemical analysis, including the collagen, GAG, DNA, and FACE assays. Mechanical testing samples were stored in phosphate-buffered saline after collection and tested within 24 hours.

Histology

Hematoxylin and eosin (H&E), picosirius red (PR), and safranin O (SO) histological stains were performed. A full-thickness slice of cartilage was fixed in 10% neutral buffered formalin, processed, embedded in paraffin, sectioned to 5 μm thickness, mounted on microscopy slides, and stained with H&E, PR, or SO, as previously described¹⁸. For all stains, all samples were stained simultaneously to ensure consistency. Representative images were taken at 20x magnification on a brightfield microscope. All histology slides were reviewed by a histopathologist to ensure quality of staining.

Mechanical testing

Tensile and compressive mechanical testing was performed, as previously described¹⁷. Briefly, dog-bone shaped specimens were glued to paper tabs for uniaxial tensile tests. Tabs were gripped in a uniaxial testing machine with a gauge length of 1.55 mm, and samples were subjected to a pull-to-failure test at 1% strain per second. A custom MATLAB code was used to determine the tensile Young's modulus and ultimate tensile strength (UTS) from the engineering stress-strain curves which were generated from force-displacement curves. For compressive stress-relaxation tests, 2 mm diameter tissue punches were subjected to 15 preloading cycles of 5% strain followed by application of 10% and 20% strain held for 600 and 900 seconds, respectively, until relaxation equilibrium. The loading rate was 10% strain per second. The force-displacement curves were fit to a standard linear solid model using a custom MATLAB code to obtain instantaneous modulus and relaxation modulus at both strain levels.

Photometric biochemical assays for total collagen, GAG, and DNA content

Hydration was measured by comparing the wet weight (WW) to the post-lyophilization DW. Cartilage was digested overnight with papain, and photometric biochemical assays were performed, as previously described¹⁹. Briefly, overall collagen content (COL) was measured with a modified hydroxyproline assay²⁰. GAG content was measured with a dimethylmethylene blue

assay kit, and DNA was measured with a PicoGreen assay kit. The resulting COL, GAG, and DNA values were normalized to both WW and DW.

Fluorophore assisted carbohydrate electrophoresis (FACE)

Aliquots of the papain digests (50 μ L) were lyophilized and subjected to a series of ethanol precipitations and digestion with chondroitinase ABC. The digested disaccharides were fluorescently derivatized with 2-aminoacridone and separated using FACE, as previously described²¹. CS6 and CS4 contents were quantified using ImageJ software measurements of band integrated optical density with CS6 and CS4 standards, and CS6 content was divided by CS4 content to obtain the CS6/CS4 ratio.

Crosslink quantification and bottom-up proteomics

Collagen crosslink quantification and bottom-up proteomics were performed, as previously described²². Briefly, cartilage pieces \sim 1 mg in WW from the lateral condyle punch were used for both assays. For crosslinks, cartilage pieces were hydrolyzed in HCl, and hydrolysates were subjected to aqueous normal phase chromatography and mass spectrometry with a Waters ACQUITY QDa quadrupole mass spectrometer to quantify pyridinoline (PYR), dihydroxylysinonorleucine (DHLNL), hydroxyproline (OHP), and internal standard pyridoxine. For bottom-up proteomics, cartilage pieces were digested in trypsin then subjected to reverse-phase chromatography and tandem mass spectrometry on a Thermo Fisher Scientific Orbitrap Fusion Lumos mass spectrometer, then label-free quantification was performed with MaxQuant²³ to quantify all identified proteins, normalized to total protein content. Total protein content was determined by dividing the COL/DW from the hydroxyproline assay by the sum of all collagen proteins per total protein, yielding total protein per DW.

Statistical analysis

Experimental data were analyzed with a one-way analysis of variance (ANOVA) with the factor being tissue age followed by a *post hoc* Tukey's honestly significant difference test. A sample size of 7-8 per group (i.e., one from each knee) was used for mechanical testing, biochemical analysis, and crosslink quantification. For bottom-up proteomics, three randomly selected samples per group were used. Normality was verified by a Shapiro-Wilk test. Statistical analyses were performed in JMP Pro 14, and graphs were generated in GraphPad Prism 9. In all bar graphs, bars represent the mean \pm standard deviation, and statistical significance is represented with a connecting letters report; bars that do not share a letter are significantly different from each other. Reported p-values presented in the text refer to multiple pairwise comparisons, all of which are described by the stated p-value inequality. For example, $p < 0.0001$ means that all pairwise comparisons yielded p-values below 0.0001.

Results

Histology

Representative histological images from each cartilage age are shown in Figure 2. H&E staining shows the relative hypercellularity of fetal and neonatal cartilage compared to juvenile and mature, which is consistent with DNA content. Throughout cartilage development, the number of cells decreased and spacing among cells increased. PR staining showed a more intense red staining on the juvenile and mature cartilage than the other groups, which is consistent with the quantitative hydroxyproline assay. All cartilages stained intensely for GAGs with SO.

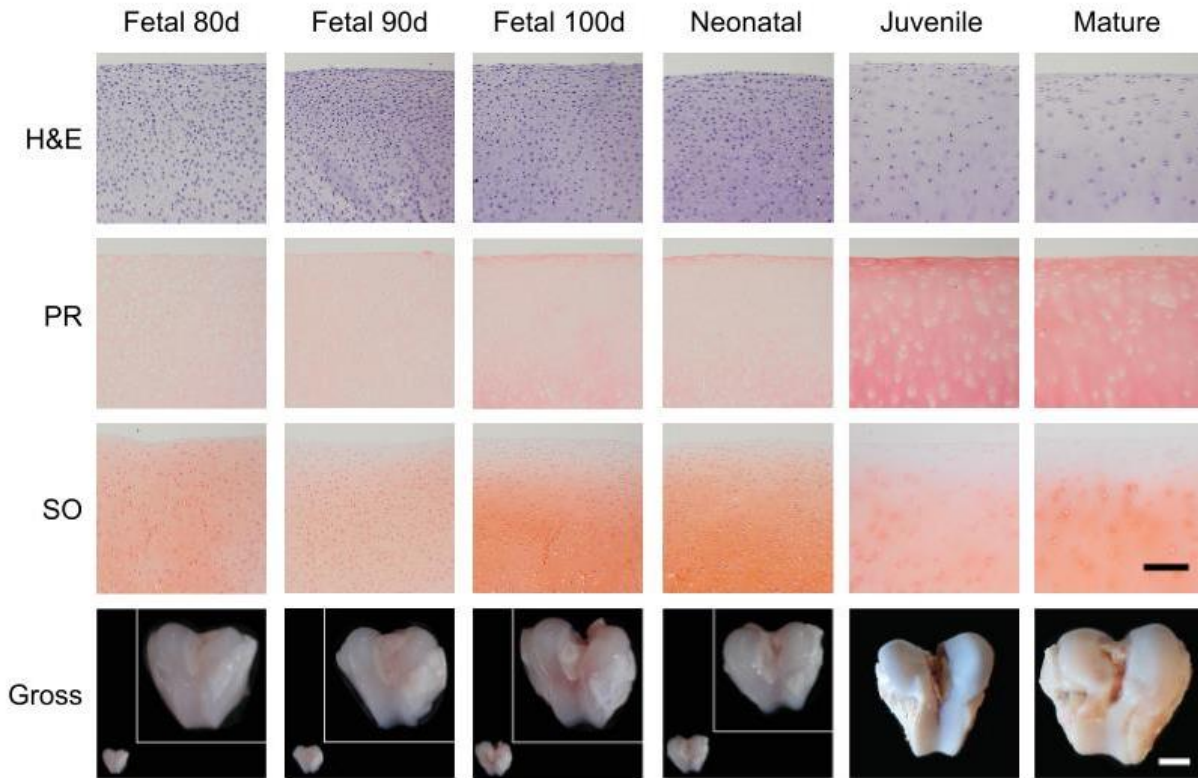


Figure 2. Representative histology and gross morphology images for porcine articular cartilage of different developmental ages. Fetal and neonatal gross morphology images are shown in actual size (bottom left) and zoomed in (inset). Juvenile and mature are shown in actual size. Scale bars: histology, 100 μ m, gross morphology, 2 cm. H&E, hematoxylin and eosin. PR, picrosirius red. SO, safranin O.

Mechanical testing

The mechanical testing results are depicted in Figure 3. For compressive properties, the juvenile cartilage had the highest instantaneous and relaxation moduli ($p < 0.01$). For the 10% instantaneous modulus, the juvenile cartilage was 1.5-times that of neonatal cartilage and 3.0-times that of mature cartilage. The other compressive measurements had similar results, with the juvenile cartilage having between 1.4- and 6.9-times the moduli of all other groups. In tensile testing, the juvenile cartilage had the highest tensile Young's modulus of 37.2 ± 20.1 MPa, significantly higher than any of the other groups ($p < 0.0001$). This stiffness was 10.5-times that of the fetal 80d cartilage, 4.7-times that of neonatal cartilage, and 3.1-times that of mature cartilage. The juvenile cartilage also had the highest UTS at 15.6 ± 7.1 MPa ($p < 0.0001$), over double that of any other cartilage. The fetal tissues had the lowest UTS, with means ranging from 0.6-1.0 MPa.

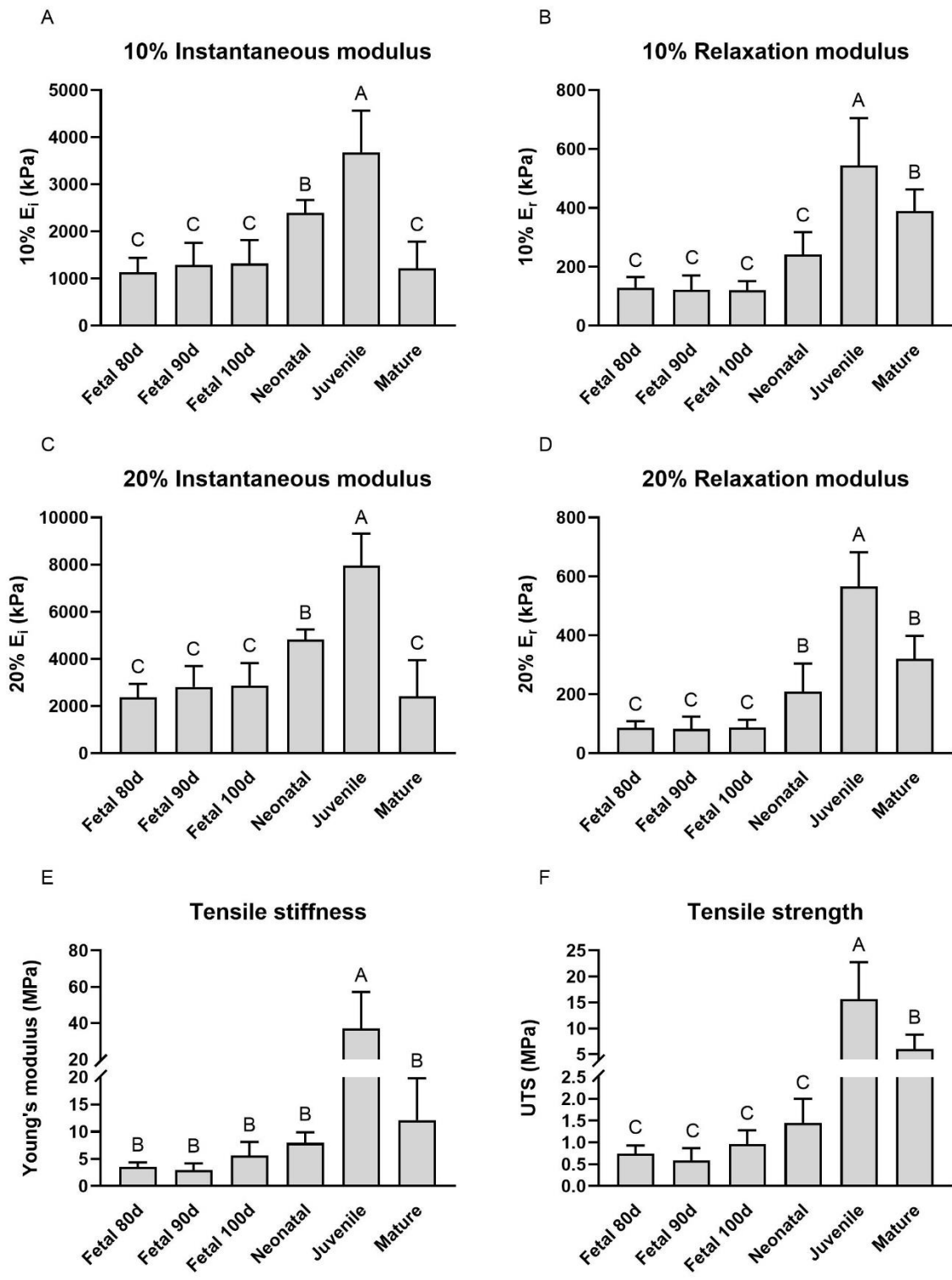


Figure 3. Mechanical results for porcine articular cartilage of different developmental ages. These graphs show the (A) 10% instantaneous modulus, (B) 10% relaxation modulus, (C) 20% instantaneous modulus, (D) 20% relaxation modulus, (E) tensile stiffness, and (F) tensile strength. E_i , instantaneous modulus. E_r , relaxation modulus. UTS, ultimate tensile strength. Bars that do not share a letter are significantly different from each other.

Biochemical content

The biochemical analysis results are shown in Figure 4. COL/DW and COL/WW were significantly greater in the juvenile and mature tissues than in fetal or neonatal tissues ($p < 0.0001$). Juvenile and mature cartilages contained about 2.2-times the COL/DW of fetal and neonatal cartilages. While there were no significant differences in GAG/WW among the different age groups, GAG/DW was significantly lower in the juvenile and mature tissues than in the fetal or neonatal tissues ($p < 0.01$), dropping about 1.6-times from neonatal to juvenile. DNA/WW and DNA/DW were significantly lower in juvenile and mature tissues than in fetal or neonatal tissues ($p < 0.01$). The fetal 80d cartilage had 12.0-times the DNA/DW of juvenile cartilage, and 17.9-times the DNA/DW of the mature cartilage. The hydration of the juvenile and mature tissues was significantly less than that of the younger tissues ($p < 0.01$), dropping from a maximum of $87.0 \pm 0.7\%$ in the fetal 90d cartilage to a minimum of $75.2 \pm 3.8\%$ in the mature cartilage. The CS6/CS4 ratio was significantly higher in the mature cartilage than the other ages ($p < 0.001$), at 1.85 ± 1.29 , while the other tissues ranged from 0.10 ± 0.03 (fetal 90d) to 0.37 ± 0.10 (juvenile).

Crosslinks analysis

The crosslink quantification results are shown in Figure 5. There were no significant differences among any tissue ages for PYR/DW or DHLNL/DW. The fetal 80d group had significantly more PYR/OHP than other groups ($p < 0.01$) at 12.0 ± 2.1 mmol/mol, but there were no other significant differences among groups, and there were no differences in DHLNL/OHP. The fetal 80d cartilage contained 1.9-times the PYR/OHP of juvenile cartilage, and 1.6-times that of mature cartilage. The maturity ratio, which compares the molar amounts of PYR and DHLNL, did not have any significant differences among tissue ages. The highest mean PYR/DHLNL was in the fetal 80d cartilage (1.4 ± 0.4 mol/mol), while the lowest mean PYR/DHLNL was in the mature cartilage (1.0 ± 0.2 mol/mol), but this difference was not significant.

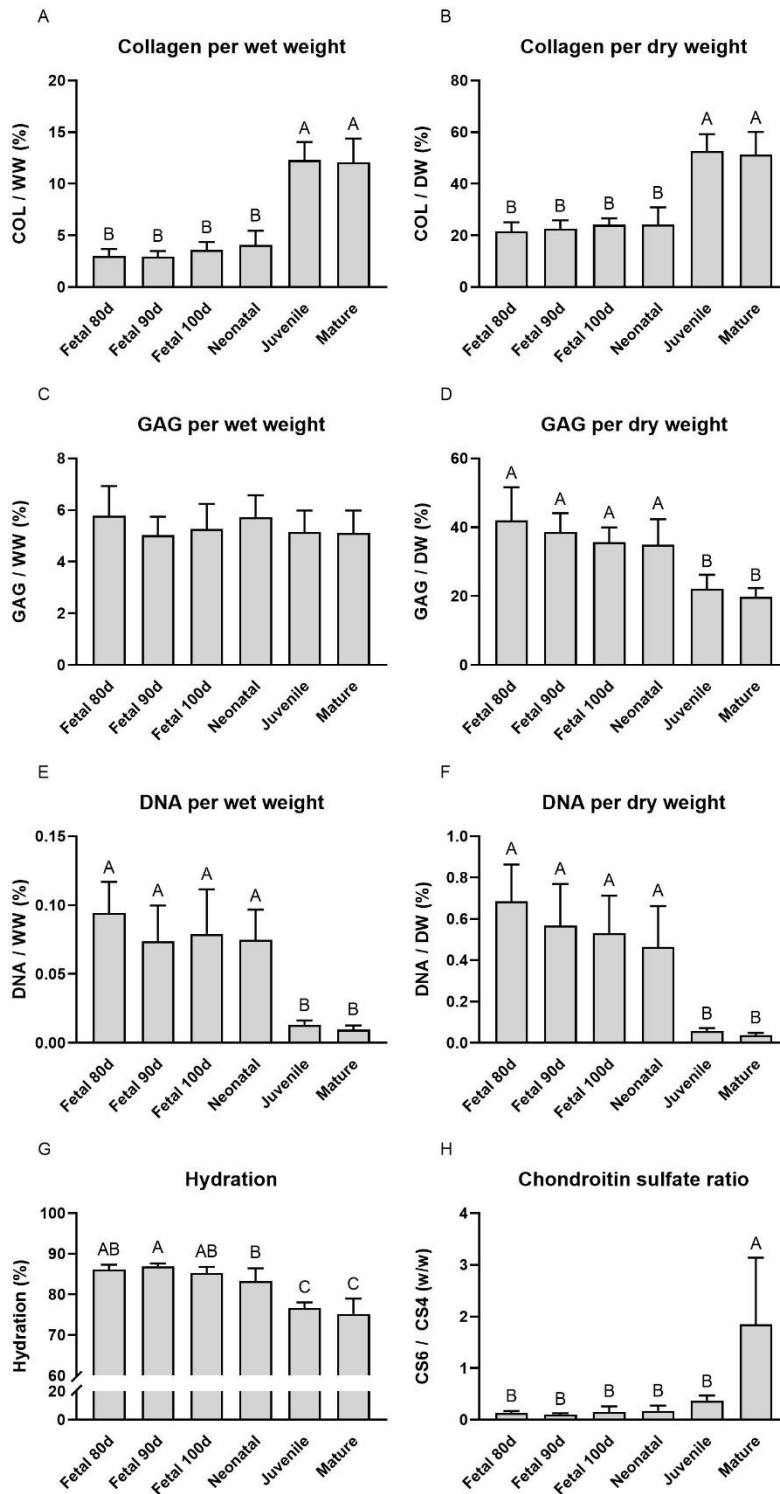


Figure 4. Biochemical results for porcine articular cartilage of different developmental ages. (A, B) Collagen per wet weight and dry weight, respectively. (C, D) Glycosaminoglycan per wet weight and dry weight, respectively. (E, F) DNA per wet weight and dry weight, respectively. (G) Hydration of tissue. (H) Ratio of chondroitin 6-sulfate to chondroitin 4-sulfate. COL, collagen. WW, wet weight. DW, dry weight. GAG, glycosaminoglycan. CS6, chondroitin-6-sulfate. CS4, chondroitin-4-sulfate. Bars that do not share a letter are significantly different from each other.

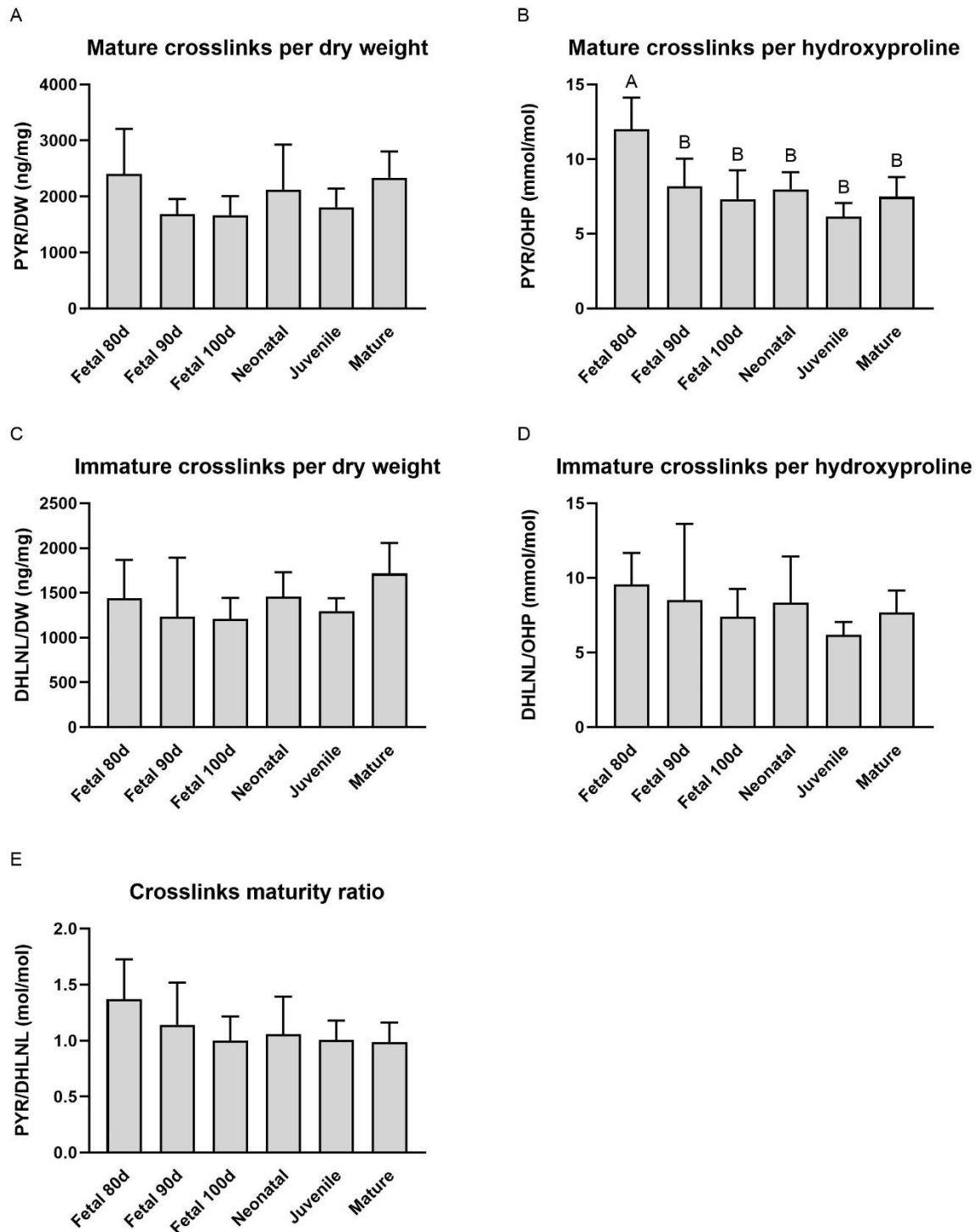


Figure 5. Crosslink quantification results for porcine articular cartilage of different developmental ages. (A, B) Mature pyridinoline crosslinks normalized to dry weight and hydroxyproline, respectively. (C, D) Immature dihydroxylysinoxorleucine crosslinks normalized to dry weight and hydroxyproline, respectively. (E) Crosslinks maturity ratio, calculated as the molar ratio of pyridinoline to dihydroxylysinoxorleucine. PYR, pyridinoline. DW, dry weight. OHP, hydroxyproline. DHLNL, dihydroxylysinoxorleucine. Bars that do not share a letter are significantly different from each other.

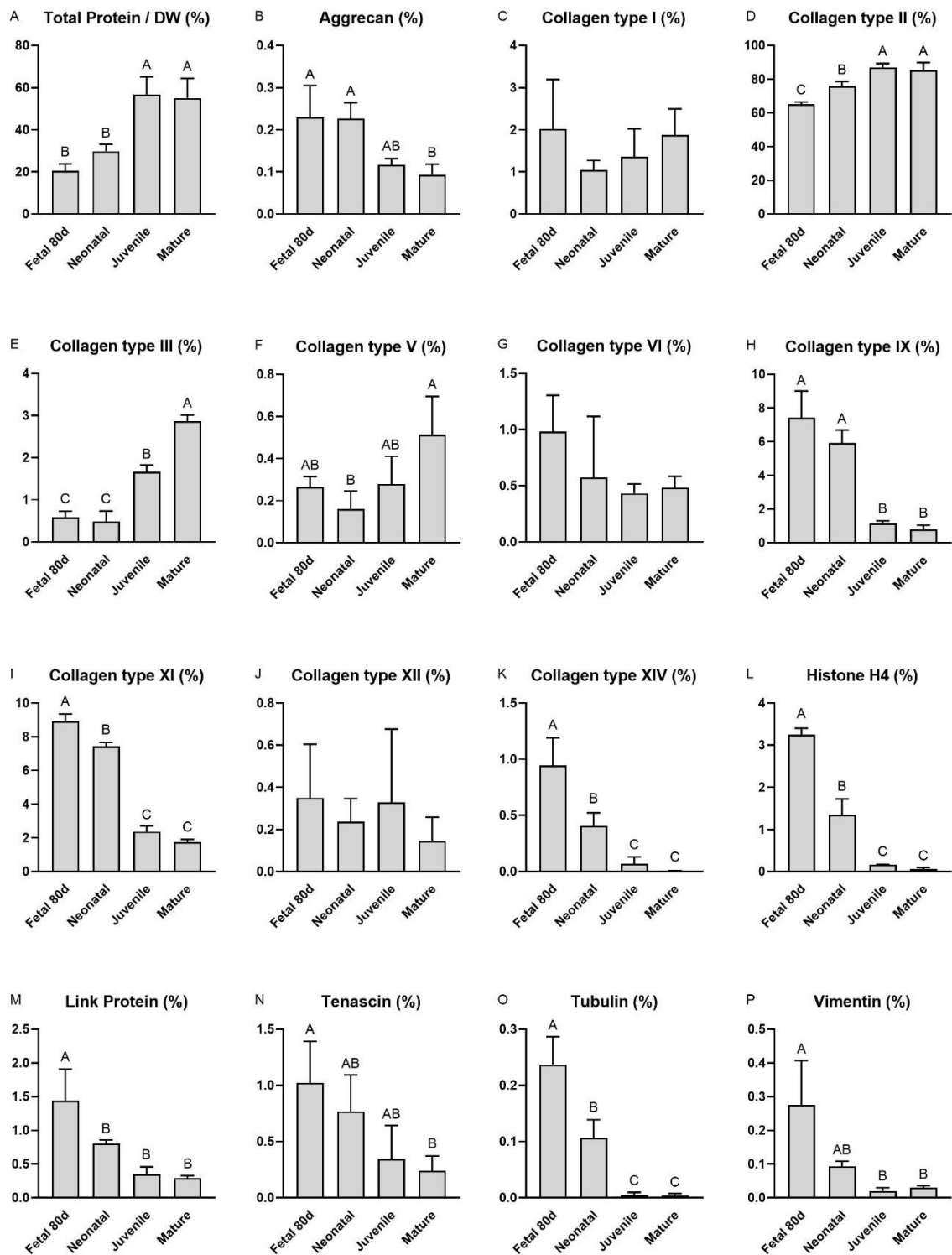


Figure 6. Bottom-up proteomic results for porcine articular cartilage of different developmental ages. Orbitrap results showing (A) total protein content and (B-P) 15 different proteins of interest in different ages of porcine cartilage. All proteins are normalized to total protein content and calculated as a percentage. A table containing averaged data from the four ages can be found in Supplementary Table 1. DW, dry weight. Bars that do not share a letter are significantly different from each other.

Bottom-up proteomics

Over 400 individual proteins were quantified through the bottom-up proteomics approach, which were narrowed down to 42 proteins, including 13 collagen types, that had an intensity of >0.1% per protein in at least one sample. Of the 42 proteins, 15 selected analytes of interest are shown in Figure 6 (the larger list of 42 proteins is presented in Supplementary Table 1). Significant differences were found in several proteomic targets. Collagen types II and III increased with age; aggrecan, collagen types IX, XI, XIV, histone H4, link protein, tenascin, tubulin, and vimentin decreased with age; and collagen types I, VI, and XII did not significantly change with age.

Discussion

In this study, the objective was to elucidate the mechanical, biochemical, and proteomic changes in cartilage throughout development by analyzing knee cartilage from fetal, neonatal, juvenile, and mature pigs. The hypotheses that there will be age-dependent increases in collagen and mechanical properties, as well as age-dependent decreases in GAG and DNA were confirmed. The proteomics analysis revealed that as cartilage ages, its collagen profile shows increases in types II and III and decreases in types IX, XI, and XIV. Aggrecan core protein and link protein, both associated with the GAG bottlebrush structure²⁴, decrease with age. Some intracellular proteins, such as histones, decrease with age, which is expected given the measured decrease in DNA with age. Some collagen types, such as types I, VI, and XII did not change throughout development. As described below, the proteomics analysis yielded insights into cartilage development because of the quantification of individual collagen subtypes, GAG structural components, and cellular proteins, beyond what can be accomplished in traditional assays for collagen, GAG, and DNA.

Throughout cartilage development, mechanical properties increased from fetal to juvenile, then decreased between juvenile and mature time points. The greatest changes occurred between neonatal and juvenile cartilage in most mechanical and biochemical measurements.

Specifically, when comparing neonatal to juvenile tissues, the tensile Young's modulus increased 4.7-times, the 20% relaxation modulus increased 2.7-times, the COL/DW increased 2.2-times, and the DNA/DW decreased 8.2-times. With this developmental stage occurring in the few months following birth, it is likely that mechanotransduction and hormones are major drivers of cartilage developmental changes. Once neonates begin to walk, cartilage loading and strain increase, which can lead to ECM synthesis through osmo-mechanosensitive ion channels²⁵. Growth hormone, which stimulates growth of articular chondrocytes and contributes to cartilage growth and maturity²⁶, circulates at high levels in neonatal pigs²⁷. Maximum mechanical properties occurred at the juvenile stage; from juvenile to mature cartilage, tensile Young's modulus decreased by 3.1-times, and 20% relaxation modulus decreased 1.8-times. However, these changes were not reflected in biochemical properties; collagen, GAG, and DNA had no significant differences between juvenile and mature cartilages. One potential explanation for the decreases in mechanical properties is that farm pigs have been characterized as a model of spontaneously occurring osteoarthritis, where 80-week-old pigs exhibit more lameness and higher chondropathy scores than juvenile pigs, and these degenerative changes worsen as the pigs age to 3-4 years²⁸. The mature pigs used in the present study were 2-3 years old, and even though the joints were undamaged to the naked eye, the mechanical properties may be signs of a pre-osteoarthritic state. Rapid weight gain, which is caused by selective breeding and intensive feeding²⁹, may have led to excessive force and wear on the articular cartilage of the mature pigs, leading to degenerative states that were not detectable via gross observation. Future studies should closely consider not only the biomechanics of weight bearing regions of porcine stifle joint cartilage due to differences compared to humans^{30,31} but also the phenotype of chondrocytes within the matrix through RNA sequencing to gain further insight into this pre-osteoarthritic state.

The existence of different CS isomeric forms and the prevalence and ratios of these isomers in different tissue ECMs suggests tissue specific functionality³². Of particular interest is the CS6/CS4 ratio in maturing cartilage. Changes in this ratio may be due to ECM remodeling

through cartilage development, or may be an indicator of disease and aging. In previous studies, mature porcine cartilage was shown to contain a very small ratio of CS6/CS4, and a decrease in this ratio is correlated with tissue maturation^{2,33}. However, FACE analysis for this study showed lower CS6/CS4 ratios in less developed tissues and a significant increase in mature samples. This inconsistency with previous experiments may be a result of the previously discussed pre-osteoarthritic state of the mature cartilage, because, as osteoarthritic cartilage degrades, GAGs are cleaved from cartilage ECM and released into synovial fluid³⁴, which may lead to different sulfation ratios with GAG turnover. With the pre-osteoarthritic state of the mature cartilage in this work, it is likely that many of these GAGs are cleaved from the surface of the cartilage, because the surface zone stains less with SO with increasing age (Figure 2). Further investigation into CS6/CS4 ratios, especially at different cartilage depths, in developmental and disease states is needed to fully understand the spike in the CS6/CS4 ratio for the mature cartilage in this study.

Bottom-up proteomic techniques have recently received attention as critical tools in tissue characterization, capable of simultaneous quantification of hundreds of proteins³⁵, and been used to show signaling pathways of osteoarthritic diseases³⁶, to compare different cartilages^{22,37}, and to compare the proteome of neocartilage engineered from different aged chondrocytes³⁸. While developmental proteomic studies have been performed in mice³⁹, this study was novel in that it used bottom-up proteomics to show developmental changes in a clinically relevant large animal model for the first time. The hydroxyproline assay showed an increase in overall collagen throughout development, and the proteomics analysis showed that the collagen types that increase are mostly collagen types II and III, which increased by factors of 1.3 and 4.8, respectively, from fetal to mature. Other types of collagen such as types IX and XI, and XIV decreased throughout tissue maturity; types IX and XI dropped by factors of 9.4 and 5.1, respectively, and type XIV dropped from 0.95% in fetal cartilage to <0.01% in mature cartilage (Supplementary Table 1). Collagen types IX and XI are known to decrease with age as finer fibrils mature to thicker and more variably sized fibrils in mature cartilage⁴⁰, but the same was not known

of collagen type XIV. Collagen type XIV is involved in fibrillogenesis by regulating collagen fibril diameter⁴¹. Using values reported in Supplementary Table 1 and Figure 6, the sums of the means reported for collagen types IX, XI, and XIV were 17.3% for fetal, 13.8% for neonatal, 3.6% for juvenile, and 2.6% for mature cartilage; the higher proportion of these collagen subtypes in younger tissue indicates that they are critical for collagen development in cartilage, where fibrils assemble into mature fibers of mainly collagen type II. Radiocarbon dating shows that the collagen matrix of articular cartilage has little to no turnover, and once the collagen type II matrix matures, it is essentially a permanent structure⁴². The drop in collagen types IX, XI, and XIV shown here may either be a cause or an effect of this permanence; either the cartilage loses the tools to rebuild its collagen structure during tissue maturation, or these tools are degraded and replaced as they become no longer needed. The application of bottom-up proteomics techniques to elucidate developmental changes in the collagen profile of cartilage is a novel, exciting aspect of this study that can also be applied to the full cartilage proteome.

The bottom-up proteomics data offer additional insights in non-collagen proteins as well. For example, the amount of aggrecan core protein per total protein dropped 2.6-times from fetal to mature cartilage. This was similar to the 2.1-times drop in GAG/DW across the same ages. This may indicate that entire proteoglycan structures consisting of aggrecan and GAGs are removed from the ECM with aging. Age-related enzymatic degradation of GAG structures typically involve depletion of CS and cleavage of aggrecan without removal of link protein⁴³. It is likely that the changes seen here are a result of mostly non-enzymatic breakdown of aggrecan structures or hyaluronan, as these pathways remove link protein⁴³, and link protein dropped by 5.0-times from fetal to mature, more than the drop in aggrecan. Interestingly, vimentin, an intermediate filament protein, dropped 9.3-times from fetal to mature cartilage, less than the decreases in cellularity seen in the 17.9-times drop in DNA/DW and 54.2-times drop in Histone H4. Thus, the cells that remain in maturing cartilage tissue deposit increasing amounts of vimentin with age. Vimentin intermediate filaments have previously been shown to increase in chondrocytes that

experience more mechanical stress⁴⁴; thus, the increase in vimentin per cell shown here (Vimentin/DNA increased 5.2-times from fetal to mature) is likely a result of increases in loading as the animals gain weight and their knees experience greater forces. As cartilage matures, protein markers such as collagen types II and III increased, mirroring the increases in mechanical properties throughout development; however, despite the significant drop-off in mechanics from juvenile to mature cartilage described above, no significant differences were found between these two ages in any proteomic targets except for an increase in collagen type III. It is clear that this pre-osteoarthritic state cannot be sufficiently described by individual biochemical or proteomic biomarkers, and additional studies on cartilage proteomics will be crucial in studying age-related changes that both strengthen cartilage throughout development and weaken it with aging. Proteomic characterization of structural and cellular components of cartilage and other tissues can provide a deeper understanding of tissue development beyond what is offered by routine benchtop assays for collagen, GAG, and DNA, which is of particular use to researchers in the fields of tissue characterization and tissue engineering.

Porcine animal models have recently shown promise as large animal models for cartilage tissue engineering due to similarities in cartilage thickness, and, in the case of the Yucatan minipig, low mature animal weight and mild temperament^{17,46,47}. While the pigs in this study are not Yucatan minipigs, as used more commonly in orthotopic cartilage large animal studies, the developmental states between the Yorkshire cross breed and the Yucatan minipig breed would likely be conserved between fetal and juvenile states. Because minipigs gain weight less rapidly and typically are on a more controlled diet within closed research herds, the age-related spontaneous pre-osteoarthritic state may not translate. However, tissue engineers may use the results of this work as benchmarks for preclinical porcine studies. Because of cartilage's role as a mechanical tissue, ideal neocartilages will match the mechanical properties of native cartilage, and the results of this study offer comparison points for tensile and compressive properties. Furthermore, through the elucidation of temporal changes in mechanics, biochemistry, and

proteomics, tissue engineers can attempt to mimic the developmental processes of cartilage using tissue engineering techniques toward further improving the mechanical properties of neocartilage. For example, in addition to collagen type II, tissue engineers may also seek to build robust cartilage ECM through collagen types IX, XI, and XIV, which are needed for forming mature collagen type II-based fibers. Modulation, expression, or deposition of these collagen types can conceivably be manipulated to build new cartilage ECM in people who have cartilage degeneration due to injury or disease. Before this is possible, proteomic characterization of human cartilage at different developmental and aging time points is crucial. This work indicates that bottom-up proteomics will continue to be a powerful tool in the fields of tissue characterization, tissue degeneration, and tissue engineering in cartilage and a multitude of other tissues in the body.

References

- 1 Hu, J. C. & Athanasiou, K. A. A Self-Assembling Process in Articular Cartilage Tissue Engineering. *Tissue Engineering* **12**, 969-979, doi:10.1089/ten.2006.12.969 (2006).
- 2 Ofek, G. *et al.* Matrix development in self-assembly of articular cartilage. *PLoS One* **3**, e2795, doi:10.1371/journal.pone.0002795 (2008).
- 3 Athanasiou, K. A., Darling, E. M., Hu, J. C., DuRaine, G. D. & Hari Reddi, A. Articular Cartilage. doi:10.1201/b14183 (2017).
- 4 Pacifici, M., Koyama, E., Iwamoto, M. & Gentili, C. Development of articular cartilage: what do we know about it and how may it occur? *Connect. Tissue Res.* **41**, 175-184, doi:10.3109/030082000009005288 (2000).
- 5 Morrison, E. H., Ferguson, M. W., Bayliss, M. T. & Archer, C. W. The development of articular cartilage: I. The spatial and temporal patterns of collagen types. *J. Anat.* **189 (Pt 1)**, 9-22 (1996).
- 6 Archer, C. W., Morrison, E. H., Bayliss, M. T. & Ferguson, M. W. The development of articular cartilage: II. The spatial and temporal patterns of glycosaminoglycans and small leucine-rich proteoglycans. *J. Anat.* **189 (Pt 1)**, 23-35 (1996).
- 7 Kempson, G. E. Relationship between the tensile properties of articular cartilage from the human knee and age. *Annals of the Rheumatic Diseases* **41**, 508-511, doi:10.1136/ard.41.5.508 (1982).
- 8 Williamson, A. K., Chen, A. C. & Sah, R. L. Compressive properties and function-composition relationships of developing bovine articular cartilage. *J. Orthop. Res.* **19**, 1113-1121, doi:10.1016/S0736-0266(01)00052-3 (2001).
- 9 Williamson, A. K., Chen, A. C., Masuda, K., Thonar, E. J. M. A. & Sah, R. L. Tensile mechanical properties of bovine articular cartilage: variations with growth and relationships to collagen network components. *J. Orthop. Res.* **21**, 872-880, doi:10.1016/S0736-0266(03)00030-5 (2003).

- 10 Ding, M., Dalstra, M., Linde, F. & Hvid, I. Mechanical properties of the normal human tibial cartilage-bone complex in relation to age. *Clin. Biomech.* **13**, 351-358, doi:10.1016/s0268-0033(98)00067-9 (1998).
- 11 Lotz, M. & Loeser, R. F. Effects of aging on articular cartilage homeostasis. *Bone* **51**, 241-248, doi:10.1016/j.bone.2012.03.023 (2012).
- 12 Peters, A. E., Akhtar, R., Comerford, E. J. & Bates, K. T. The effect of ageing and osteoarthritis on the mechanical properties of cartilage and bone in the human knee joint. *Sci. Rep.* **8**, 5931, doi:10.1038/s41598-018-24258-6 (2018).
- 13 Barbour, K. E., Helmick, C. G., Boring, M. & Brady, T. J. Vital Signs: Prevalence of Doctor-Diagnosed Arthritis and Arthritis-Attributable Activity Limitation - United States, 2013-2015. *MMWR Morb Mortal Wkly Rep* **66**, 246-253, doi:10.15585/mmwr.mm6609e1 (2017).
- 14 Center for Biologics, E. & Research. IDEs & INDs for Products to Repair or Place Knee Cartilage. (2019).
- 15 Book, S. A. & Bustad, L. K. The Fetal and Neonatal Pig in Biomedical Research. *Journal of Animal Science* **38**, 997-1002, doi:10.2527/jas1974.385997x (1974).
- 16 Cone, S. G., Warren, P. B. & Fisher, M. B. Rise of the Pigs: Utilization of the Porcine Model to Study Musculoskeletal Biomechanics and Tissue Engineering During Skeletal Growth. *Tissue Eng. Part C Methods* **23**, 763-780, doi:10.1089/ten.TEC.2017.0227 (2017).
- 17 Vapniarsky, N. *et al.* The Yucatan Minipig Temporomandibular Joint Disc Structure–Function Relationships Support Its Suitability for Human Comparative Studies. *Tissue Engineering Part C: Methods* **23**, 700-709, doi:10.1089/ten.tec.2017.0149 (2017).
- 18 Kwon, H., O'Leary, S. A., Hu, J. C. & Athanasiou, K. A. Translating the application of transforming growth factor- β 1, chondroitinase-ABC, and lysyl oxidase-like 2 for mechanically robust tissue-engineered human neocartilage. *J. Tissue Eng. Regen. Med.* **13**, 283-294, doi:10.1002/term.2791 (2019).
- 19 Gonzalez-Leon, E. A., Bielajew, B. J., Hu, J. C. & Athanasiou, K. A. Engineering self-assembled neomenisci through combination of matrix augmentation and directional remodeling. *Acta Biomater.* **109**, 73-81, doi:10.1016/j.actbio.2020.04.019 (2020).
- 20 Cissell, D. D., Link, J. M., Hu, J. C. & Athanasiou, K. A. A Modified Hydroxyproline Assay Based on Hydrochloric Acid in Ehrlich's Solution Accurately Measures Tissue Collagen Content. *Tissue Eng. Part C Methods* **23**, 243-250, doi:10.1089/ten.tec.2017.0018 (2017).
- 21 Calabro, A. *et al.* Fluorophore-assisted carbohydrate electrophoresis (FACE) of glycosaminoglycans. *Osteoarthritis Cartilage* **9 Suppl A**, S16-22, doi:10.1053/joca.2001.0439 (2001).
- 22 Bielajew, B. J., Hu, J. C. & Athanasiou, K. A. Methodology to Quantify Collagen Subtypes and Crosslinks: Application in Minipig Cartilages. *Cartilage*, 19476035211060508, doi:10.1177/19476035211060508 (2021).
- 23 Cox, J. & Mann, M. MaxQuant enables high peptide identification rates, individualized p.p.b.-range mass accuracies and proteome-wide protein quantification. *Nature Biotechnology* **26**, 1367-1372, doi:10.1038/nbt.1511 (2008).
- 24 Pomin, V. H. & Mulloy, B. Glycosaminoglycans and Proteoglycans. *Pharmaceuticals* **11**, doi:10.3390/ph11010027 (2018).
- 25 Sanchez-Adams, J., Leddy, H. A., McNulty, A. L., O'Connor, C. J. & Guilak, F. The mechanobiology of articular cartilage: bearing the burden of osteoarthritis. *Curr. Rheumatol. Rep.* **16**, 451, doi:10.1007/s11926-014-0451-6 (2014).
- 26 Tsukazaki, T. *et al.* Growth hormone directly and indirectly stimulates articular chondrocyte cell growth. *Osteoarthritis Cartilage* **2**, 259-267, doi:10.1016/s1063-4584(05)80078-0 (1994).

- 27 Althen, T. G. & Gerrits, R. J. Pituitary and serum growth hormone levels in Duroc and Yorkshire swine genetically selected for high and low backfat. *J. Anim. Sci.* **42**, 1490-1497, doi:10.2527/jas1976.4261490x (1976).
- 28 Macfadyen, M. A. *et al.* The commercial pig as a model of spontaneously-occurring osteoarthritis. *BMC Musculoskelet. Disord.* **20**, 70, doi:10.1186/s12891-019-2452-0 (2019).
- 29 Reiland, S. The effect of decreased growth rate on frequency and severity of osteochondrosis in pigs. *Acta Radiol. Suppl.* **358**, 107-122 (1978).
- 30 Proffen, B. L., McElfresh, M., Fleming, B. C. & Murray, M. M. A comparative anatomical study of the human knee and six animal species. *Knee* **19**, 493-499, doi:10.1016/j.knee.2011.07.005 (2012).
- 31 Takroni, T., Laouar, L., Adesida, A., Elliott, J. A. & Jomha, N. M. Anatomical study: comparing the human, sheep and pig knee meniscus. *J Exp Orthop* **3**, 35, doi:10.1186/s40634-016-0071-3 (2016).
- 32 López-Álvarez, M. *et al.* Quantitative evaluation of sulfation position prevalence in chondroitin sulphate by Raman spectroscopy. *Journal of Raman Spectroscopy* **50**, 656-664, doi:10.1002/jrs.5563 (2019).
- 33 Volpi, N. Disaccharide mapping of chondroitin sulfate of different origins by high-performance capillary electrophoresis and high-performance liquid chromatography. *Carbohydrate Polymers* **55**, 273-281, doi:10.1016/j.carbpol.2003.09.010 (2004).
- 34 Kulkarni, P. *et al.* Glycosaminoglycan measured from synovial fluid serves as a useful indicator for progression of Osteoarthritis and complements Kellgren–Lawrence Score. *BBA Clinical* **6**, 1-4, doi:10.1016/j.bbacli.2016.05.002 (2016).
- 35 Bielajew, B. J., Hu, J. C. & Athanasiou, K. A. Collagen: quantification, biomechanics, and role of minor subtypes in cartilage. *Nat Rev Mater* **5**, 730-747, doi:10.1038/s41578-020-0213-1 (2020).
- 36 Lei, J. *et al.* Proteomic analysis of knee cartilage reveals potential signaling pathways in pathological mechanism of Kashin-Beck disease compared with osteoarthritis. *Sci. Rep.* **10**, 6824, doi:10.1038/s41598-020-63932-6 (2020).
- 37 Önnérjörd, P., Khabut, A., Reinholt, F. P., Svensson, O. & Heinegård, D. Quantitative proteomic analysis of eight cartilaginous tissues reveals characteristic differences as well as similarities between subgroups. *J. Biol. Chem.* **287**, 18913-18924, doi:10.1074/jbc.M111.298968 (2012).
- 38 Donahue, R. P., Nordberg, R. C., Bielajew, B. J., Hu, J. C. & Athanasiou, K. A. The effect of neonatal, juvenile, and adult donors on rejuvenated neocartilage functional properties. *Tissue Eng Part A*, doi:10.1089/ten.TEA.2021.0167 (2021).
- 39 Wilson, R. *et al.* Changes in the chondrocyte and extracellular matrix proteome during post-natal mouse cartilage development. *Mol Cell Proteomics* **11**, M111 014159, doi:10.1074/mcp.M111.014159 (2012).
- 40 Eyre, D. Collagen of articular cartilage. *Arthritis Res.* **4**, 30-35, doi:10.1186/ar380 (2002).
- 41 Ansorge, H. L. *et al.* Type XIV Collagen Regulates Fibrillogenesis: PREMATURE COLLAGEN FIBRIL GROWTH AND TISSUE DYSFUNCTION IN NULL MICE. *J. Biol. Chem.* **284**, 8427-8438, doi:10.1074/jbc.M805582200 (2009).
- 42 Heinemeier, K. M. *et al.* Radiocarbon dating reveals minimal collagen turnover in both healthy and osteoarthritic human cartilage. *Sci. Transl. Med.* **8**, 346ra390, doi:10.1126/scitranslmed.aad8335 (2016).
- 43 Roughley, P. J. & Mort, J. S. The role of aggrecan in normal and osteoarthritic cartilage. *J Exp Orthop* **1**, 8, doi:10.1186/s40634-014-0008-7 (2014).
- 44 Hernandez, P. A. *et al.* Early-Onset Osteoarthritis originates at the chondrocyte level in Hip Dysplasia. *Scientific Reports* **10**, doi:10.1038/s41598-020-57431-x (2020).

- 45 Goetz, J. E. *et al.* A clinically realistic large animal model of intra-articular fracture that progresses to post-traumatic osteoarthritis. *Osteoarthritis Cartilage* **23**, 1797-1805, doi:10.1016/j.joca.2015.05.022 (2015).
- 46 Frisbie, D. D., Cross, M. W. & McIlwraith, C. W. A comparative study of articular cartilage thickness in the stifle of animal species used in human pre-clinical studies compared to articular cartilage thickness in the human knee. *Vet. Comp. Orthop. Traumatol.* **19**, 142-146 (2006).

Supplementary materials

Supplementary Table 1. Bottom-up proteomics results on porcine knee cartilage. All analytes are reported as protein percentage per total protein (PROT). Over 400 individual proteins were quantified through the bottom-up proteomics approach, and 42 proteins that had an intensity of >0.1% per protein in at least one sample are shown here.

Protein	Protein / Total Protein (%)			
	Fetal	Neonatal	Juvenile	Mature
Actin, cytoplasmic 1	0.41%	0.31%	0.06%	0.04%
Aggrecan core protein	0.23%	0.22%	0.12%	0.09%
Biglycan	0.34%	0.29%	0.19%	0.14%
Collagen type I alpha 1	1.50%	0.88%	1.06%	1.44%
Collagen type I alpha 2	0.52%	0.16%	0.30%	0.44%
Collagen type II alpha 1	65.13%	76.02%	86.92%	85.51%
Collagen type III alpha 1	0.59%	0.48%	1.67%	2.86%
Collagen type IV alpha 2	0.08%	0.04%	0.28%	0.15%
Collagen type IV alpha 5	0.03%	0.00%	0.06%	0.11%
Collagen type V alpha 1	0.12%	0.06%	0.08%	0.14%
Collagen type V alpha 2	0.13%	0.08%	0.12%	0.37%
Collagen type V alpha 3	0.02%	0.02%	0.08%	<0.01%
Collagen type VI alpha 1	0.04%	0.02%	0.02%	0.02%
Collagen type VI alpha 2	0.16%	0.12%	0.10%	0.13%
Collagen type VI alpha 3	0.78%	0.43%	0.32%	0.34%
Collagen type IX alpha 1	5.33%	3.83%	0.75%	0.48%
Collagen type IX alpha 2	2.10%	2.10%	0.40%	0.32%
Collagen type X alpha 1	0.01%	0.07%	<0.01%	0.01%
Collagen type XI alpha 1	3.81%	2.92%	1.11%	0.71%
Collagen type XI alpha 2	5.11%	4.52%	1.27%	1.04%
Collagen type XII alpha 1	0.35%	0.24%	0.33%	0.15%
Collagen type XIV alpha 1	0.95%	0.41%	0.07%	<0.01%
Collagen type XVI alpha 1	0.07%	0.09%	0.04%	0.05%
Collagen type XXVIII alpha 1	0.36%	0.47%	1.19%	1.28%
Cytochrome P450 2E1	0.15%	0.06%	0.00%	0.00%
Decorin	0.03%	0.09%	0.04%	0.08%
Glyceraldehyde-3-phosphate dehydrogenase	0.13%	0.20%	0.03%	0.02%
Hemoglobin subunit alpha	0.16%	0.28%	0.01%	0.02%
Hemoglobin subunit beta	0.20%	0.30%	0.01%	0.01%

Histone H1t	0.56%	0.18%	0.01%	0.01%
Histone H3.3	1.62%	0.48%	0.03%	0.02%
Histone H4	3.25%	1.35%	0.16%	0.06%
Hyaluronan and proteoglycan link protein 1	1.44%	0.81%	0.35%	0.29%
Lactadherin	<0.01%	0.01%	0.04%	0.12%
Phosphoglycerate kinase 1	0.11%	0.05%	0.02%	<0.01%
Prelamin-A/C	0.17%	0.10%	<0.01%	<0.01%
Ryanodine receptor 1	0.12%	0.08%	0.26%	0.07%
Tenascin	1.02%	0.76%	0.34%	0.24%
Transforming growth factor-beta-induced protein ig-h3	0.12%	0.11%	0.10%	0.10%
Tubulin beta chain	0.11%	0.05%	<0.01%	<0.01%
Tubulin alpha-1B chain	0.13%	0.05%	<0.01%	<0.01%
Vimentin	0.28%	0.09%	0.02%	0.03%

CHAPTER 5 | Proteomic, mechanical, and biochemical development of tissue-engineered neocartilage*

Abstract

The self-assembling process of cartilage tissue engineering is a promising technique to heal cartilage defects, preventing osteoarthritic changes. Given that chondrocytes dedifferentiate when expanded, it is not known if cellular expansion affects the development of self-assembled neocartilage. The objective of this study is to use proteomic, mechanical, and biochemical analyses to quantitatively investigate the development of self-assembled neocartilage derived from passaged, rejuvenated costal chondrocytes. It was found that temporal trends in neocartilage formation are similar to those seen in native hyaline articular cartilage development. For example, between days 7 and 84 of culture, tensile Young's modulus increases 4.4-times, total collagen increases 2.7-times, DNA content decreases 69.3%, collagen type II increases 1.5-times, and aggrecan drops 55.3% mirroring trends shown in native knee cartilage. Importantly, collagen type X, which is associated with cartilage calcification, remains at low levels ($\leq 0.05\%$) at all neocartilage developmental time points, similar to knee cartilage ($< 0.01\%$) and unlike donor rib cartilage (0.98%). In this work, bottom-up proteomics, a powerful tool to interrogate tissue composition, is used to quantify the proteome of maturing neocartilage vis-à-vis native hyaline cartilages. Furthermore, it is shown that self-assembled, costal chondrocyte-derived neocartilage is suitable for a non-homologous approach in the knee.

Introduction

Focal cartilage defects occur in 12% of the population¹ and 36% of athletes², and cartilage defects are well-known not to heal. Existing surgical procedures to address focal cartilage defects, such as microfracture or matrix-assisted autologous chondrocyte implantation, only provide short-term

* Authors: Bielajew BJ[†], Donahue RP[†], Lamkin EK, Hu JC, Hascall VC, Athanasiou KA. [†]equal contribution

relief^{3,4}. Focal cartilage defects can eventually degenerate to osteoarthritis (OA)⁵, which affects over 32.5 million adults in the US⁶. Tissue engineering holds promise for regenerating cartilage defects by alleviating pain, restoring function, and preventing the onset of OA^{3,7,8}. For successful translation of tissue-engineered cartilages from the laboratory to human usage, neocartilages must be well-characterized for quality control with appropriate release criteria for preclinical and clinical trials. The quality and safety profile of any implant will benefit greatly from the ability to quantitatively define the implant's composition.

Toward the precise determination of tissue composition for quality control and release criteria of tissue-engineered implants, it is desirable to quantify many analytes in a single sample with low sample volume. The advent of powerful quantitative bottom-up proteomics techniques⁹ enables the simultaneous quantification of hundreds of proteins in biological samples, for example, in cartilage extracellular matrix (ECM). This engenders tissue engineers to establish new quality control protocols, where bottom-up proteomics can be used as a basis for a multitude of release criteria. Applications of bottom-up proteomics to investigate tissue composition is applicable to any neotissue that has ECM-dependent functionality (e.g., cartilage, skin, tendon/ligament, heart valve). Moreover, quantitative bottom-up proteomics can be used as a tool to interrogate developmental changes in neotissues, such as in tissue-engineering approaches for hyaline articular cartilage.

Self-assembled neocartilage derived from primary articular chondrocytes matures similarly to the way that native cartilage develops (i.e., it mimics aspects of mesenchymal condensation)¹⁰. Additionally, self-assembled neocartilages have been produced with native-like mechanical properties, such as a tensile modulus of 8.4 MPa¹¹ and an aggregate modulus of 400 kPa¹²; these robust mechanical properties are crucial for implant survival and functionality¹³. However, harvesting primary articular chondrocytes, which were used in these neocartilages, can lead to donor site morbidity or yield cells with an osteoarthritic phenotype¹⁴. Thus, recent tissue-engineering efforts have focused on alternative cell sources such as costal chondrocytes from

the rib¹⁵. For example, self-assembled neocartilages have recently been made from expanded, rejuvenated costal chondrocytes¹⁶, which allows for thousands of robust neocartilage implants to be made from one biopsy¹⁷. However, it is unknown whether neocartilage produced from expanded chondrocytes develops similarly to native cartilage, given that chondrocyte expansion results in dedifferentiation¹⁸⁻²². Furthermore, it is not known whether neocartilage made with costal chondrocytes is suitable for non-homologous implantation into the knee.

The objective of this study is to determine, through mechanical, biochemical, and proteomic analyses, whether neotissues formed from passaged, rejuvenated, and self-assembled costal chondrocytes display features of the native hyaline cartilage developmental process. The study design compares multiple protein analytes throughout maturation of self-assembled neocartilage, thereby informing how ECM components form mechanically robust tissue. The hypothesis of this work is that self-assembled neocartilage derived from passaged, rejuvenated costal chondrocytes will follow temporal trends in mechanical, biochemical, and proteomic properties that have previously been characterized in native hyaline cartilage development²³. Specifically, as the self-assembled neocartilage develops from nascent tissue to mature neocartilage, it is expected that, 1) in mechanics, tensile and compressive properties will increase, 2) in biochemical composition, collagen content will increase, and glycosaminoglycan (GAG) and DNA content will decrease, and 3) in proteomics, collagen type II will increase, aggrecan and link protein will decrease, and, unlike in native costal cartilage, collagen type X will only be deposited at low levels (<0.1%). This work will further the understanding of how the self-assembling process mimics native cartilage development and will determine the suitability of costal chondrocyte-derived neocartilage for non-homologous implantation into the knee.

Methods

Costal cartilage harvest and isolation

Costal chondrocytes were harvested from the rib cartilage of three juvenile (aged 5-8 months) Yucatan minipig donors that were culled for reasons unrelated to this study (Figure 1A). Briefly, using sterile tools in a biosafety cabinet, costal cartilage was exposed, and the perichondrium was removed. Then, costal cartilage was minced to approximately 1 mm³ pieces and digested at 37°C in 0.4% w/v pronase for 1 hour followed by 0.2% w/v collagenase for 18 hours. Both enzymes were dissolved in Dulbecco's modified Eagle's medium (DMEM, high glucose, GlutaMAX supplement) supplemented with 3% fetal bovine serum (FBS) and 1% penicillin-streptomycin-fungizone (PSF). The resulting cell suspension was filtered through a 70 µm cell strainer and treated with ammonium-chloride-potassium lysis buffer, as previously described²⁴.

Costal chondrocyte expansion and aggregate rejuvenation

After isolation, costal chondrocytes were plated at 2.5M cells per T225 flask (~11,111 cells/cm²) in chemically defined chondrogenic (CHG) medium (Figure 1A), which consisted of DMEM, 1% PSF, 1% nonessential amino acids, 1% insulin-transferrin-selenous acid+, 100 nM dexamethasone, 50 µg/mL ascorbate-2-phosphate, 40 µg/mL L-proline, and 100 µg/mL sodium pyruvate. CHG medium was further supplemented with 2% FBS, 1 ng/mL transforming growth factor beta 1 (TGF-β1), 5 ng/mL basic fibroblast growth factor (bFGF), and 10 ng/mL platelet-derived growth factor (PDGF) during monolayer expansion to retain post-expansion chondrogenic potential²⁵. Medium was changed every 3-4 days during expansion. After one passage, chondrocytes were frozen in FBS containing 10% dimethyl sulfoxide (DMSO) for downstream use. Cells were thawed and plated in CHG medium containing FBS and growth factors, as described above. Between passages, cells were lifted using 0.05% trypsin-EDTA solution for 9 minutes, and the cell sheet was digested using 0.2% w/v collagenase in DMEM containing 3% FBS and 1% PSF for approximately 30 minutes with agitation every 10 minutes. After six

passages, the expanded cells underwent aggregate rejuvenation for 14 days to return them to a chondrogenic phenotype (Figure 1A), as previously described²⁶. Medium was changed every 3-4 days during aggregate rejuvenation. Cells were cultured in CHG medium supplemented with 10 ng/mL TGF- β 1, 100 ng/mL growth differentiation factor 5 (GDF-5), and 100 ng/mL bone morphogenetic protein 2 (BMP-2). Aggregates were then digested after culture in 0.05% trypsin-EDTA solution for 45 minutes followed by 0.2% w/v collagenase solution in DMEM supplemented with 3% FBS and 1% PSF for 90 minutes with agitation every 10 minutes. The resulting cell suspension was filtered through a 70 μ m cell strainer prior to the self-assembling process.

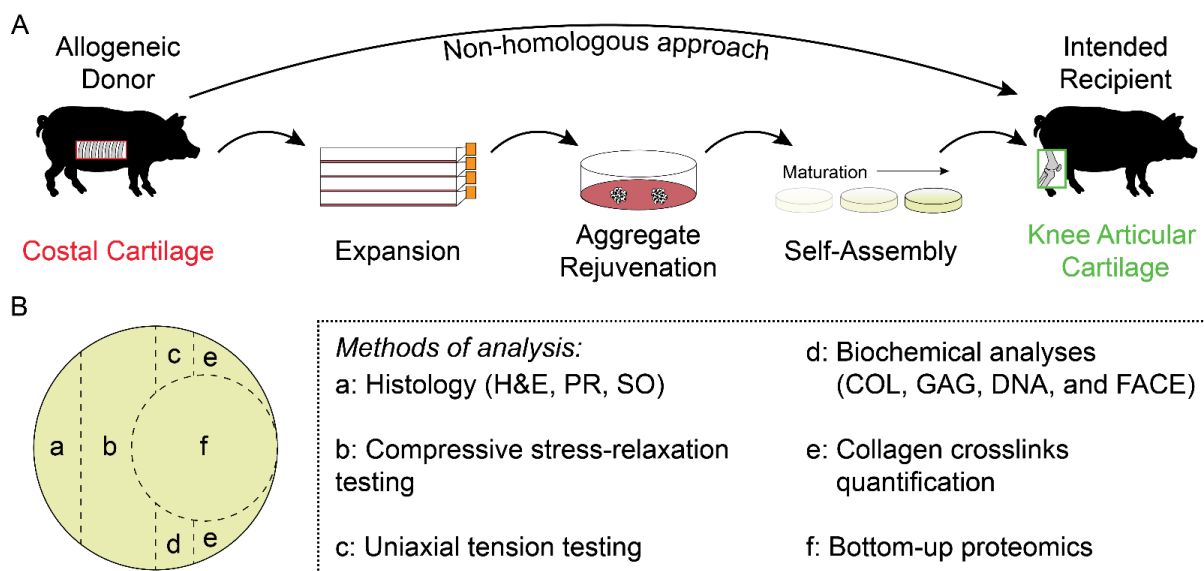


Figure 1. The tissue-engineering process using costal chondrocytes and neocartilage sample preparation. (A) Self-assembled constructs are envisioned to be used in the knee through an allogeneic, non-homologous approach. Donor costal chondrocytes were expanded, rejuvenated, and self-assembled for eventual implantation into the knee. (B) At specific maturation time points (i.e., days of culture), the neocartilage constructs were divided and assayed by various methods. Histological analysis included staining with hematoxylin and eosin (H&E), picrosirius red (PR), and safranin O with fast green counterstains (SO). Mechanical analysis included uniaxial tensile testing and compressive stress-relaxation testing. Biochemical analyses for total collagen (COL), glycosaminoglycan (GAG), and DNA content and fluorophore assisted carbohydrate electrophoresis (FACE) were performed from a papain digest.

Neocartilage self-assembly and bioactive factor treatment

As previously described¹⁷, scaffold-free neocartilage self-assembly was carried out for a total of 84 days (Figure 1A). Briefly, nonadherent wells of 5 mm diameter in size were made using molten 2% agarose and negative molds. The wells were hydrated with CHG medium, and the medium was changed at least three times prior to cell seeding. As previously optimized²⁷, 2M cells per

well were seeded in 100 μ L CHG medium. After 4 hours, medium was topped off with an additional 400 μ L CHG medium, and, subsequently, medium was exchanged every day until day 3 when constructs were unconfined from agarose wells. From day 3 onward, neocartilage constructs were fed 2 mL CHG medium every 2 days. Constructs were treated with bioactive factors, as previously described¹⁷. Briefly, TGF- β 1 (10 ng/mL) was supplemented continuously in CHG medium. Chondroitinase ABC (c-ABC) was applied to constructs at 2 U/mL in 0.4 mL of CHG for 4 hours on day 7 of self-assembly. C-ABC was activated with 50 mM of sodium acetate and quenched with 1 mM zinc sulfate. Lysyl oxidase-like 2 was added to the medium 0.15 μ g/mL with 0.146 mg/mL hydroxylysine and 1.6 μ g/mL copper sulfate from day 7 until the end of self-assembly.

Sample preparation

Self-assembled neocartilage constructs (n=7-9 per time point) were removed from culture after 1, 4, 7, 14, 28, 56, or 84 days of culture and photographed. Constructs at days 1 and 4 of culture disintegrated upon handling, and, thus, were not able to be photographed. Constructs were cut with a biopsy punch and scalpel for histological, mechanical, biochemical, and proteomic analyses as depicted in Figure 1B. Samples for photometric biochemical assays and crosslinks mass spectrometry were weighed to obtain the wet weights (WWs). WWs were not able to be taken on day 1 constructs because they disintegrated upon contact with the weigh boat. After at least 72 hours of lyophilization, samples were reweighed to obtain dry weights (DWs). Hydration was calculated based on the ratio of sample DW to WW.

Histology

As previously described²⁸, samples were fixed in 10% neutral buffered formalin for at least 72 hours, processed, embedded in paraffin, sectioned to 5 μ m thickness, and mounted on microscopy slides. Samples were then stained with hematoxylin and eosin (H&E), safranin O with fast green counterstain, or picosirius red. Representative images were taken at 20x magnification using a brightfield microscope.

Mechanical testing

Mechanical properties of constructs were quantified with compressive stress-relaxation and uniaxial tension tests. Punches of 3 mm diameter from neocartilage constructs were subjected to compressive stress-relaxation testing. Because day 1 and day 4 constructs disintegrated upon handling, they were not included in the mechanical testing analysis. As previously described²⁹, the sample height was determined using a tare load of 0.1 N. Samples were subjected to 15 preloading cycles of 5% strain based on the determined sample height. Strains of 10% and 20% were applied to the punch and held for 600 and 900 seconds, respectively. The force-displacement curves were fit to a standard linear solid model using a custom MATLAB code to determine relaxation modulus, instantaneous modulus, and coefficient of viscosity for each strain level. For tensile testing, samples were trimmed into dog bone shapes (approximately 0.75 mm by 0.45 mm) and glued to paper tabs of a predefined gauge length (1.55 mm), as previously described²⁸. Samples were pulled until failure at 1% strain per second. Force-displacement curves were analyzed using a custom MATLAB code to extract Young's modulus and ultimate tensile strength (UTS).

Collagen, GAG, and DNA assays

Construct pieces were subjected to overnight digestion with papain, followed by biochemical assays for quantification of total collagen (COL), GAG, and DNA contents, as previously described³⁰. Briefly, COL was quantified using a modified hydroxyproline assay³¹, GAG was quantified using a dimethylmethylene blue assay kit, and DNA was quantified using a PicoGreen assay kit. The COL, GAG, and DNA measurements were normalized to WW and DW.

Fluorophore assisted carbohydrate electrophoresis (FACE)

Papain digest aliquots (50 μ L) from each sample were lyophilized, and GAGs were precipitated with alcohol and digested with c-ABC. Chondroitin-6-sulfate (CS6) and chondroitin-4-sulfate (CS4) were derivatized using 2-aminoacridone, and CS6 was separated from CS4 using FACE,

as previously described³². CS6 and CS4 were quantified by integrating the optical density of CS6 and CS4 bands in ImageJ, then comparing the resulting integrated optical density in samples and standards. CS6 was divided by CS4 to obtain the chondroitin sulfate ratio.

Collagen crosslink quantification

Quantification of collagen crosslinks was performed, as previously described³³. Briefly, construct pieces approximately 1 mg in WW were lyophilized, weighed, reduced in NaBH₄, washed on a rocker plate overnight in ultrapure water, and hydrolyzed overnight in HCl. HCl was evaporated, hydrolysates were resuspended and filtered, and then hydrolysates were subjected to liquid chromatography-mass spectrometry with a Waters ACQUITY QDa quadrupole mass spectrometer to quantify mature pyridinoline (PYR), immature dihydroxylysinonorleucine (DHLNL), hydroxyproline (OHP), and internal standard pyridoxine. Because day 1 constructs disintegrated during the washing process, they were not included in the crosslinks analysis.

Bottom-up proteomics

Bottom-up proteomics was performed, as previously described³³. Three samples per group, chosen at random, were used for bottom-up proteomics. Briefly, construct pieces approximately 1 mg in WW were lyophilized, weighed, washed by vortexing twice in 10 mM ammonium citrate and twice in 50 mM ammonium bicarbonate, digested overnight in trypsin, and subjected to liquid chromatography-tandem mass spectrometry on a Thermo Fisher Scientific Orbitrap Fusion Lumos mass spectrometer. MaxQuant was used for label-free quantification³⁴, yielding a list of proteins normalized to total protein content (PROT). PROT/DW was quantified by dividing COL/DW from the hydroxyproline assay by COL/PROT from bottom-up proteomics (sum of all collagen proteins per PROT). Because day 1 and day 4 constructs disintegrated during the washing process, they were not included in the bottom-up proteomics analysis.

Statistical analysis

Data from this study were analyzed using a one-way analysis of variance (ANOVA), with the only factor being culture time, followed by a *post hoc* Tukey's honestly significant difference test performed in JMP Pro 14. All bar graphs were created in GraphPad Prism 9. A connecting letters report is used to show statistical significance in all bar graphs; bars that do not share the same letter are significantly different from each other.

Results

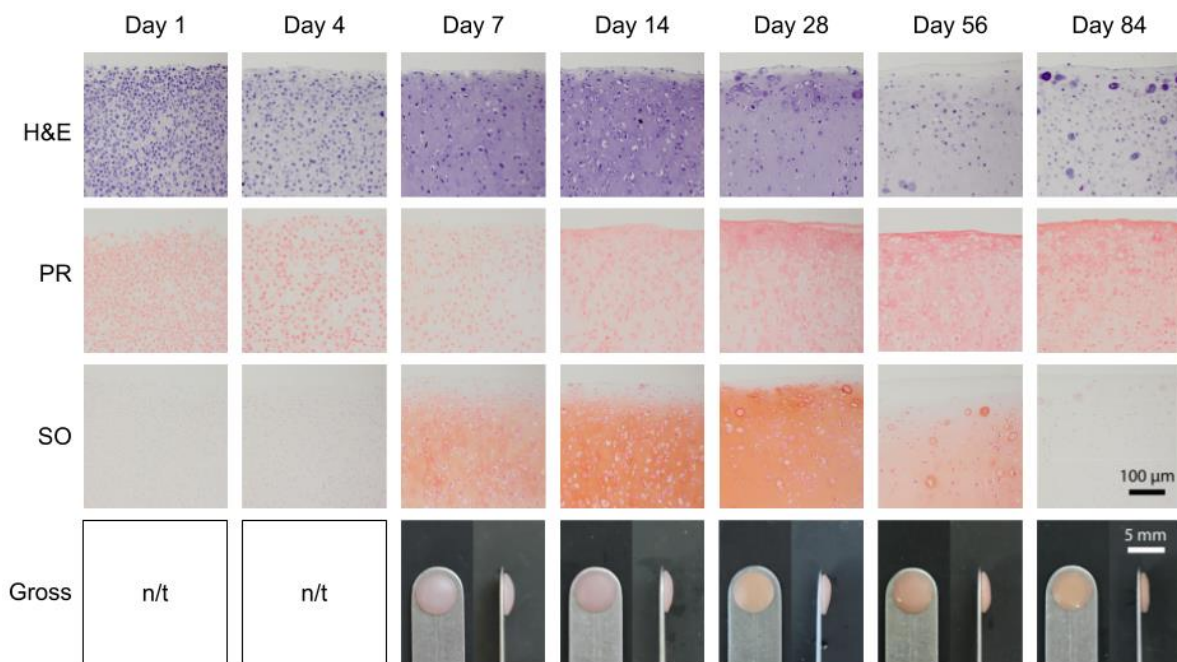


Figure 2. Histology and gross morphology of neocartilage constructs. Staining with hematoxylin and eosin (H&E), picosirius red (PR), and safranin O with fast green counterstain (SO) is shown in self-assembled neocartilage constructs at different time points in culture. Gross morphology is shown in front and side views. Gross morphology pictures for day 1 and day 4 of culture were not taken (n/t).

Neocartilage histology

Representative images for histology of H&E staining for cellular morphology, picosirius red staining for collagen, and safranin O staining for GAGs, as well as gross morphology, are reported in Figure 2. At earlier time points such as 1 and 4 days of culture, staining intensity is localized to the cells for both H&E and picosirius red stainings. As the tissue matures to 7-28 days of culture, the staining becomes more intense for hematoxylin in the ECM of the neocartilage, but rapidly

decreases after 56-84 days of culture, exhibiting almost no staining. However, the picosirius red staining becomes more intense over time. Safranin O staining follows a similar pattern to the H&E staining for 7-84 days of culture but yields minimal staining for the earlier 1- and 4-day time points. From 7 to 84 days of culture, constructs appear flat and robust.

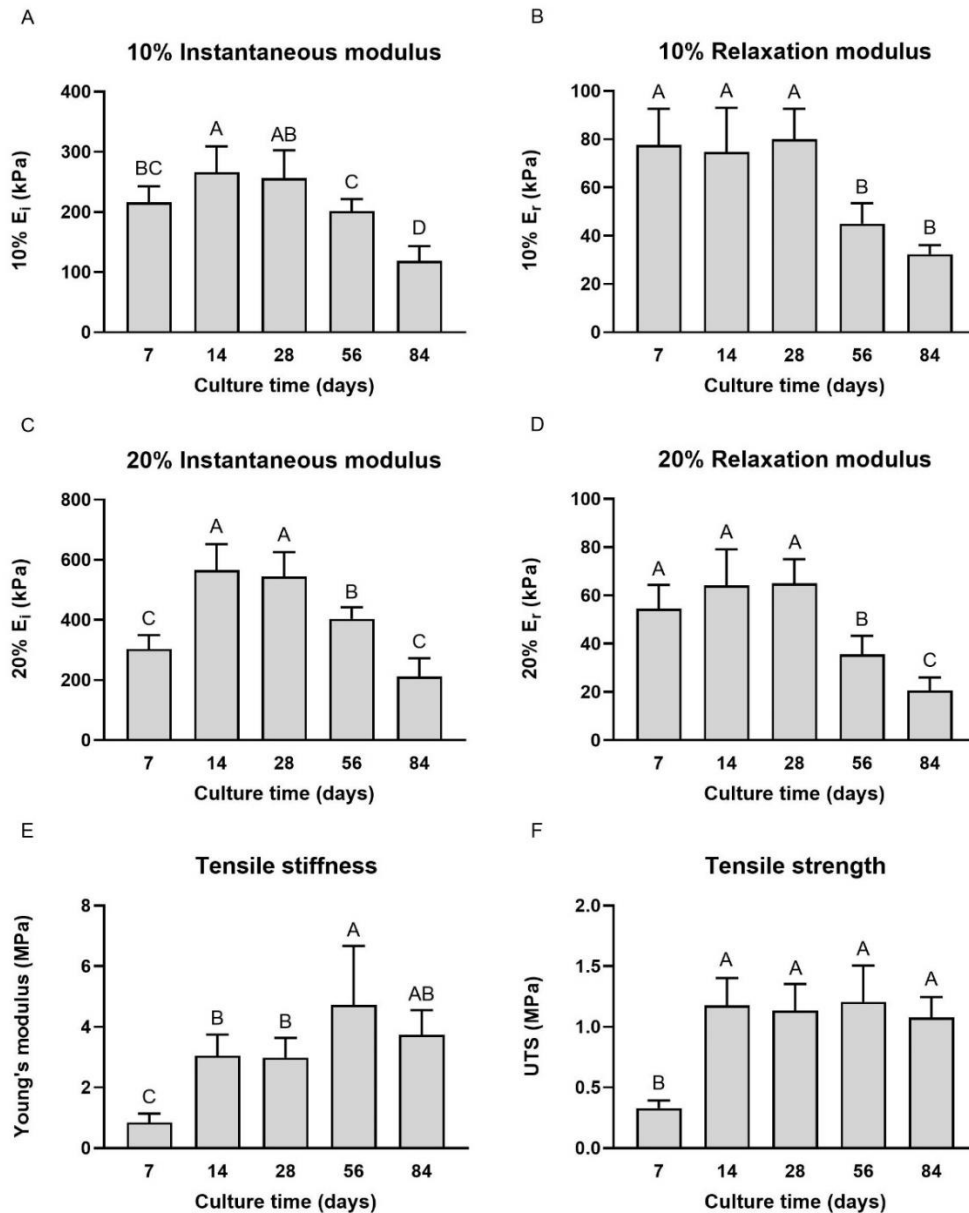


Figure 3. Mechanical properties of neocartilage constructs. At different time points throughout self-assembled neocartilage culture, compressive properties are shown in the 10% and 20% instantaneous modulus (E_i) (A, C) and relaxation modulus (E_r) (B, D) graphs. Tensile properties are shown in the Young's modulus (E) and ultimate tensile strength (UTS) graphs (F). Bars that do not share the same letter are significantly different from each other/

Mechanical properties

Mechanical properties from compressive stress-relaxation testing and uniaxial tension testing are reported in Figure 3. Across culture times, instantaneous modulus for both 10% and 20% strain levels peaked at 14 days of culture. The maximum values for 10% and 20% instantaneous modulus obtained at 14 days were 266 ± 43 kPa and 565 ± 87 kPa, respectively, significantly higher than the values at both 7 days (216 ± 27 kPa for 10%, 304 ± 46 kPa for 20%, $p<0.05$) and 56 days of culture (202 ± 20 kPa for 10% and 404 ± 39 kPa for 20%, $p<0.01$); however, they were not different from 28 days of culture (Figure 3A, C). For both 10% and 20% relaxation modulus, maximal points were observed at 28 days of culture, with significant decreases at 56 and 84 days ($p<0.0001$) (Figure 3B, D). Young's modulus (4.7 ± 1.9 MPa) and UTS (1.2 ± 0.3 MPa) peaked at 56 days, 5.9-times and 4.0-times higher than their respective values of 0.8 ± 0.3 MPa and 0.3 ± 0.1 MPa at 7 days (Figure 3E-F). Young's modulus slightly decreased to 3.7 ± 0.8 MPa at 84 days of culture, which was 4.6-times higher than day 7, but the difference between 56 and 84 days of culture was not significant (Figure 3E). UTS exhibited a significant increase from 7 to 14 days of culture ($p<0.0001$), at which point it plateaued without any significant changes at any later time points (Figure 3F). Additional outcomes including 10% and 20% coefficients of viscosity, strain at failure, and toughness are reported in Supplementary Table 1.

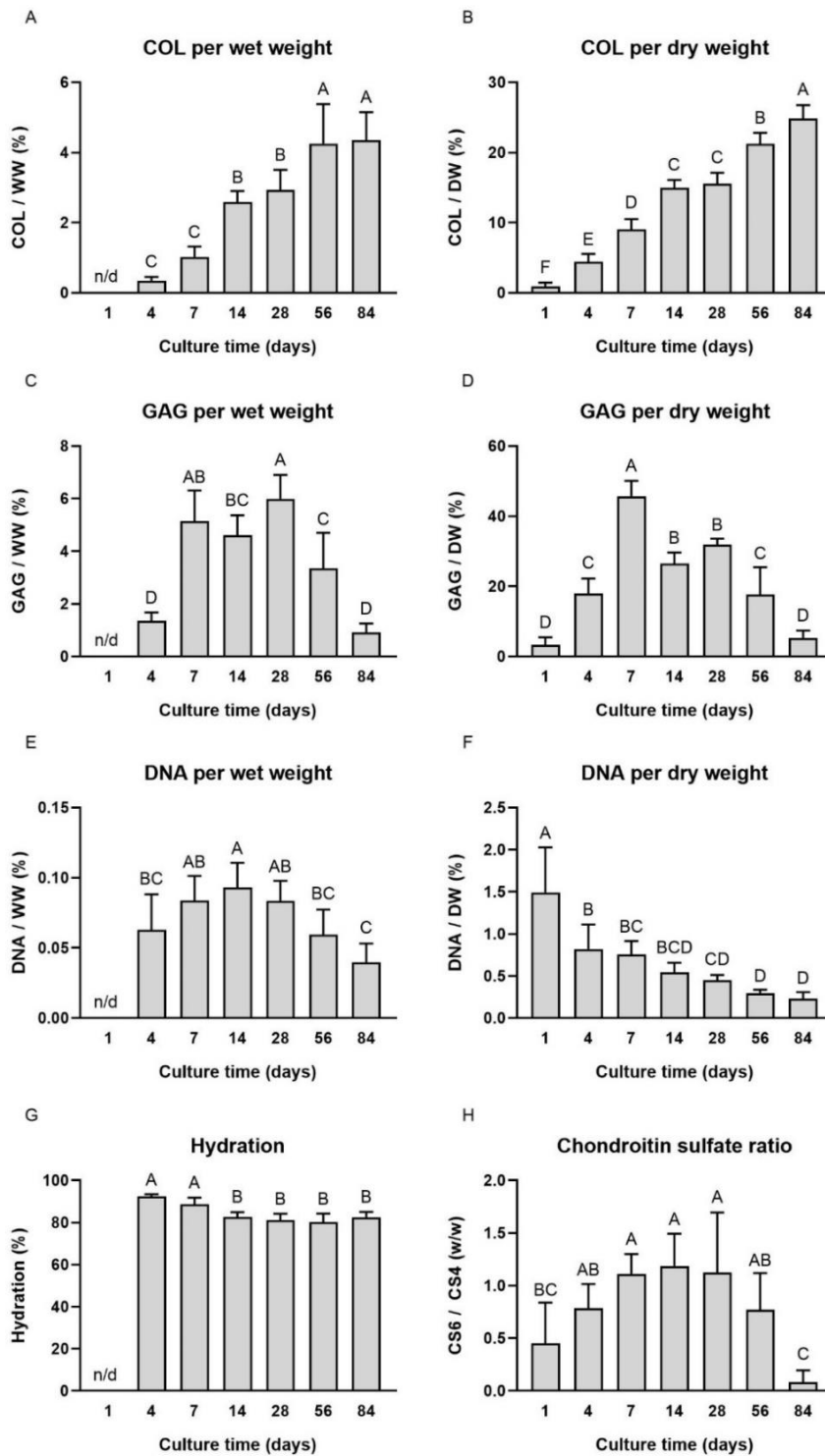


Figure 4. Biochemical composition of neocartilage constructs. At different time points throughout self-assembled neocartilage culture, the biochemical composition is shown. Total collagen (COL) content (A-B), glycosaminoglycan (GAG) content (C-D), and DNA content (E-F) are normalized to both wet weight (WW) and dry weight (DW). Hydration (G) is reported, along with the chondroitin-6-sulfate (CS6) to chondroitin-4-sulfate (CS4) ratio (H). Bars that do not share the same letter are significantly different from each other.

Biochemical properties

For biochemical analysis of ECM content, COL, GAG, and DNA content are reported in Figure 4. For COL/DW and COL/WW values, steady increases were observed over culture time, with the highest value seen at day 84 for both measurements ($24.8 \pm 1.9\%$ and $4.4 \pm 0.8\%$, respectively) (Figure 4A-B). The COL/DW increased 27.6-times from day 1 to day 84 and 2.7-times from day 7 to day 84 (Figure 4B). Interestingly, GAG/DW peaked at 7 days of culture ($45.7 \pm 4.4\%$), which was significantly higher than any other group ($p < 0.0001$) (Figure 4D), while GAG/WW peaked at 28 days of culture ($6.0 \pm 0.9\%$) but was not significantly different from 7 days of culture ($5.1 \pm 1.2\%$) (Figure 4C). By 84 days of culture, GAG content decreased toward those levels seen at 1-4 days of culture in both measures (Figure 4C-D). DNA/DW also trended down with time, exhibiting an 84.6% decrease from days 1 to 84 and a 69.3% decrease from days 7 to 84 (Figure 4F). Similarly, DNA/WW also significantly decreased between 14 days of culture to 84 days ($p < 0.0001$) (Figure 4E). Generally, hydration also decreased with time, exhibiting a 9.6% decrease from 7 days of culture to 56 days ($p < 0.0001$) (Figure 4G). The CS6:CS4 ratio rose until 14 days of culture (1.2 w/w) before exhibiting a stark and significant decrease between 56 and 84 days (0.8 ± 0.4 w/w to 0.1 ± 0.1 w/w, $p < 0.01$) (Figure 4H).

Crosslink quantification

Collagen crosslink analysis is reported in Figure 5. PYR/DW was at a maximum after 84 days of culture, measuring 1273 ± 51 ng/mg (Figure 5A). PYR/OHP significantly increased between 4 days (7.9 ± 1.7 mmol/mol) and 7 days (20.3 ± 6.9 mmol/mol) of culture ($p < 0.01$) but had no significant differences between days 7 and 84 (Figure 5B). For DHLNL/DW, the values significantly increased over time from 100 ± 79 ng/mg after 4 days of culture to a maximum of 708 ± 430 ng/mg at 56 days of culture ($p < 0.01$) (Figure 5C). The opposite trend was observed for DHLNL/OHP; between 4 days (14.4 ± 4.1 mmol/mol) and 28 days (7.3 ± 1.3 mmol/mol) of culture, there was a significant decrease in immature crosslinks ($p < 0.05$) (Figure 5D). Overall, the maturity of the

crosslinking within the constructs' ECM increased, as depicted by the PYR/DHLNL ratio (Figure 5E), significantly increasing 4.0-times from 4 days (0.6 ± 0.2 mol/mol) to 84 days of culture (2.4 ± 1.1 mol/mol, $p < 0.05$).

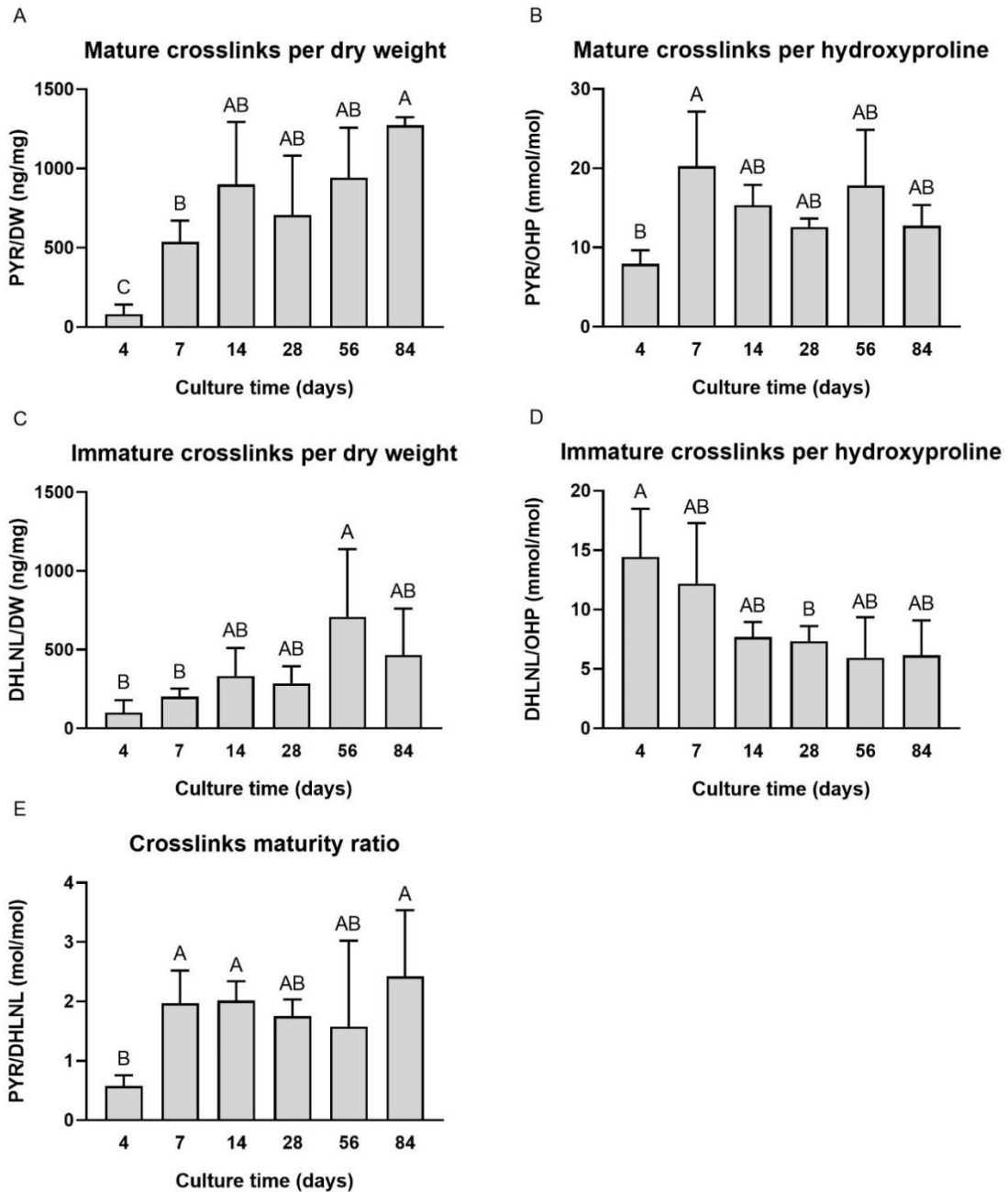


Figure 5. Collagen crosslink composition of neocartilage constructs. Throughout self-assembled neocartilage culture, mature pyridinoline crosslinks (PYR) and immature dihydroxylysinoxonorleucine crosslinks (DHLNL) are reported. PYR is normalized to dry weight (DW) (A) and hydroxyproline (OHP) (B). DHLNL is normalized to DW (C) and OHP (D). The maturity ratio is reported (E). Bars that do not share the same letter are significantly different from each other.

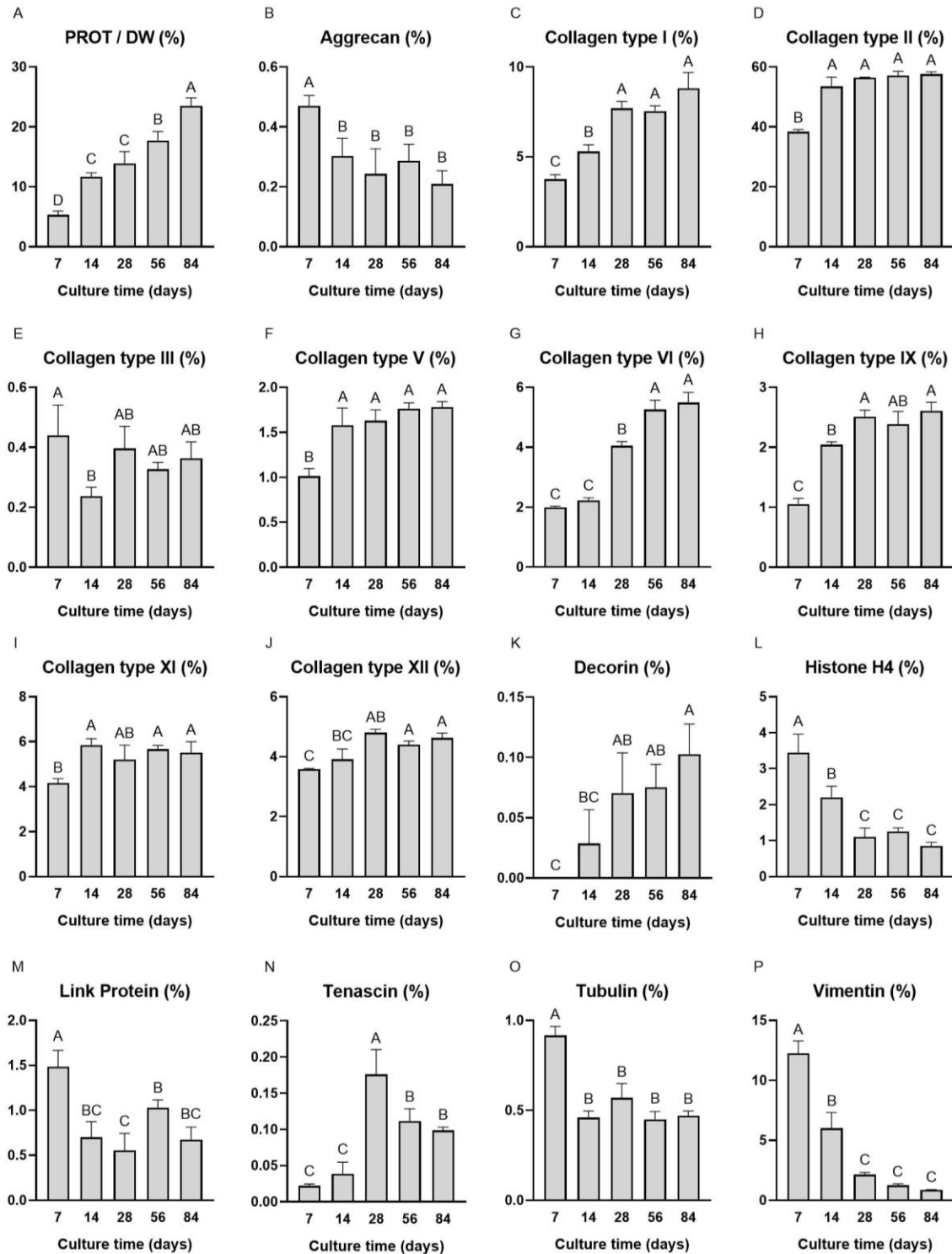


Figure 6. Bottom-up proteomics analysis of neocartilage constructs. Total protein (PROT) content (A) and 15 selected protein analytes of interest are reported. Graphs (B-P) are reported as percent protein per PROT. Bars that do not share the same letter are significantly different from each other.

Bottom-up proteomic analysis

Bottom-up proteomics analysis identified and quantified a total of 364 protein analytes. Those with an intensity greater than 0.1%/PROT in at least one sample and all collagen chains (86 analytes total) are reported as averages in Supplementary Table 2. For *post hoc* analysis, 15 proteins of interest were chosen, and these data are reported in Figure 6. Overall, PROT/DW significantly increased with culture time, rising 4.4-times from 7 days ($5.30 \pm 0.66\%$) to 84 days ($23.50 \pm 1.35\%$) of culture ($p < 0.0001$) (Figure 6A). Similar trends were seen in collagen types I, II, V, VI, IX, XI, and XII, and decorin (Figure 6C-D, F-K). For example, per PROT, collagen type II increased 1.5-times from 7 days ($38.40 \pm 0.74\%$) to 84 days ($57.58 \pm 0.81\%$) of culture (Figure 6D). Aggrecan per PROT decreased over time, exhibiting a significant drop of 55.3% between 7 days ($0.47 \pm 0.03\%$) and 84 days ($0.21 \pm 0.04\%$) of culture ($p < 0.01$) (Figure 6B). Link protein followed a similar trend (Figure 6M). Most cell-associated proteins such as histone H4, tubulin, and vimentin all also decreased over time (Figure 6L, O-P). Tenascin exhibited a parabolic-shaped trend, peaking after 28 days of culture (Figure 6N). Collagen type X remained at levels below or equal to 0.05%/PROT for all culture time points (Supplementary Table 2).

Discussion

The self-assembling process has recently emerged as a tissue engineering method that creates neocartilage constructs on par with native hyaline cartilage functional properties^{11,35}. The objective of this study was to characterize the self-assembling process via mechanical, biochemical, and proteomic assays and determine whether the process using expanded and rejuvenated costal chondrocytes mirrors aspects of the development of native hyaline cartilage tissue. The hypotheses of this study were confirmed; self-assembled neocartilage derived from passaged, rejuvenated costal chondrocytes exhibited certain temporal trends in mechanics, biochemistry, and proteomics that were reminiscent of native hyaline cartilage development²³. For example, our group has previously characterized increases in tensile properties, COL, and collagen type II, and

decreases in DNA, aggrecan, and link protein when comparing juvenile to fetal porcine knee cartilage²³. Throughout maturation of self-assembled neocartilage, these same trends were mirrored with tensile properties, COL, and collagen type II increasing and DNA, aggrecan, and link protein decreasing during culture. Ultimately, this study 1) elucidated similarities in the ECM maturation of self-assembled neocartilage and native hyaline cartilage, 2) identified specific ECM components with quantities parallel to those in native hyaline articular cartilage and costal cartilage, 3) explored the proteomics of self-assembled cartilage ECM, including structure-function relationships and protein targets for future tissue-engineering techniques, and 4) established optimal time points for future implantation of self-assembled cartilage. Combined, these findings allow tissue engineers to identify targets and measures for potential quality control and release criteria for mechanically robust cartilage therapeutics, required for future preclinical and clinical studies.

The maturation of self-assembled neocartilage derived from expanded and rejuvenated costal chondrocytes followed mechanical trends of native hyaline cartilage development. In native porcine knee articular cartilage, there was a 10.5-times increase in tensile Young's modulus properties from the fetal to juvenile stage, then a slight decrease to mature tissue²³. The neocartilage in this experiment exhibited a similar trend in tensile Young's modulus, increasing 5.9-times from 7 days to 56 days of culture, before a slight decrease at 84 days of culture. In compressive properties, similar trends applied to both native knee cartilage and self-assembled neocartilage. Native cartilage increased in compressive properties from the fetal to juvenile stages²³, and self-assembled neocartilage instantaneous moduli increased from 7 days to 28 days of culture. A subsequent drop in compressive properties was seen in both native articular cartilage and neocartilage; the 20% relaxation modulus of native knee articular cartilage dropped 1.8-times from juvenile to mature²³, and, in neocartilage, this same property dropped 3.2-times from 28 days to 84 days of culture. While mechanical properties are the primary design criteria for tissue-engineered cartilages, the biochemical and proteomic properties are also of crucial importance.

Biochemical and proteomic analysis of the neocartilage in this study also revealed many similarities to native articular cartilage development. COL content in both native articular cartilage²³ and self-assembled neocartilage increased throughout development. In terms of specific collagen subtypes, collagen type II increased over time in both native articular cartilage²³ and neocartilage. The collagen subtype profiles in native tissue and neocartilage had some developmental differences; in native articular cartilage, collagen types I, VI, and XII did not significantly change with tissue age, while collagen types IX and XI decreased²³, but in neocartilage, collagen types I, VI, IX, XI, and XII all increased throughout culture. The collagen crosslink maturity ratio, which did not change throughout tissue development in native knee cartilage²³, increased in neocartilage; this was likely due to medium supplementation of lysyl oxidase-like 2, an enzyme that catalyzes the production of mature collagen crosslinks^{17,36}. The GAG content of native tissue decreased from neonatal to juvenile articular cartilage²³, and this trend was seen in later time points of self-assembly (i.e., days 28 and beyond); however, in earlier timepoints of self-assembly (i.e., days 1-14), GAG rapidly accumulated in the ECM. Similar to native knee cartilage²³, aggrecan and link protein, parts of hyaline cartilage's proteoglycan structure, decreased in neocartilage throughout development. In agreement with a previous study on matrix maturation in self-assembled cartilage, the CS6:CS4 ratio decreases in later time points of self-assembly¹⁰. However, the decrease in the CS6:CS4 ratio is opposite to the trend previously shown in aging knee cartilage²³. DNA and cellularity (from H&E staining) also decreased over time in neocartilage constructs, similar to the trends found in native tissue²³. As expected due to their respective roles in chromatin and cytoskeletal structure, histone H4, tubulin, and vimentin decreased in parallel with cellularity, similar to native cartilage trends. Tenascin, previously associated with fetal articular cartilage development, decreases during later tissue maturation³⁷. Thus, the increases seen here in tenascin in early stages of self-assembly may be correlated with the deposition of more ECM by the chondrocytes, but the subsequent decrease may be due to maturation of the neocartilage. Altogether, there were many mechanical, biochemical, and

proteomic trends that are mirrored between native articular cartilage development and culture of self-assembled neocartilage made from expanded, rejuvenated costal chondrocytes.

In the allogeneic, non-homologous cartilage tissue engineering approach used in this study (Figure 1A), costal chondrocytes from the rib were intended for tissue-engineering of knee articular cartilage. In this study, there were specific analytes where the neocartilage is more reminiscent of donor costal cartilage than recipient knee cartilage. For example, collagen type I in neocartilage comprised 7.55-7.70%/PROT between days 28 and 56 of culture, which was similar to the collagen type I quantity in native porcine floating costal cartilage (6.69%/PROT) and is higher than in the femoral condyle (1.22%/PROT)³³. Collagen type V was found to be in the range of 1.63-1.76%/PROT in neocartilage between 28 and 56 days of culture, which was between the quantities reported for floating costal cartilage (3.13%/PROT) and femoral condyle articular cartilage (0.29%/PROT)³³. While these collagen subtype quantities showed aspects of donor tissue phenotype, importantly, collagen type X, associated with hypertrophic and calcified cartilage^{38,39}, remained at or below 0.05%/PROT in all neocartilage time points. The quantity of collagen type X in native floating costal cartilage was 0.98%/PROT, and, in native femoral condyle cartilage, it was less than 0.01%/PROT³³. If there were an abundant presence of collagen type X, self-assembled neocartilage implants could potentially calcify, rendering them unsuitable for use in the knee. However, the self-assembling process was shown to change the costal chondrocyte phenotype toward that of articular chondrocytes and away from calcification as found in native costal cartilage. This is significant because costal cartilage offers important advantages as a cell source, such as isolation from non-diseased tissues and use in either autologous or allogeneic approaches¹⁶. While future tissue engineering studies will need to address these differences of donor and recipient tissues, the self-assembling process using costal chondrocytes produced a neocartilage that is suitable for non-homologous use in the knee.

Bottom-up proteomics was used to quantify all proteins in developing neocartilages, giving insight to structure-function relationships and protein targets for future tissue-engineering studies.

Well-documented structure-function relationships in articular cartilage predict a direct relationship between tensile properties and COL content⁴⁰, but the UTS in neocartilages plateaued after 14 days of culture while COL continues to increase throughout the entire culture time. Bottom-up proteomics may hint as to why this contradiction arises; the overall collagen subtype profile became less abundant in collagen type II relative to the other collagens after day 14, where collagen type II plateaued and collagen types I, VI, IX, and XII continued to increase. Given the role of collagen types IX and XII in fibrillogenesis⁴¹, it is possible that these other collagen types inhibited maturation of the collagen type II fibrils, and, thus, why tensile properties did not continue to increase after day 14. Collagen type IX was abundant in fetal knee cartilage (7.43%/PROT) but dropped in mature cartilage (0.80%/PROT)²³. In neocartilage, collagen type IX started at 1.05%/PROT at day 7 of culture and increased to 2.61%/PROT at day 84; the drop seen in native tissue was not observed. Unlike in native knee cartilage development, collagen type IX in neocartilage was not replaced by more collagen type II. Interestingly, there was no detectable collagen type XIV in neocartilages, but there was a small amount present in native articular cartilages (0.95%/PROT in fetal cartilage, <0.01%/PROT in mature cartilage)²³. Contrastingly, collagen type XII was abundant in neocartilage constructs (3.59-4.80%/PROT) compared to native cartilages (0.15-0.35%/PROT), approximately a 10-times difference. Because both collagen type XII and XIV play similar roles in fibrillogenesis⁴¹, the neocartilage may have been producing excessive collagen type XII as compensation for the lack of collagen type XIV. It would be of great interest to cartilage tissue engineers to determine novel mechanical or biochemical stimuli leading to the deposition of collagen type XIV. The field of tissue engineering will continue to benefit from bottom-up proteomic studies through deeper understanding of structure-function relationships and development of novel tissue-engineering strategies to target specific protein analytes, improving the functionality of engineered neotissues.

It is crucial to create neocartilages that can withstand the joint loading environment; thus, it is important to select an appropriate time of culture which maximizes neocartilage mechanical

properties. For knee articular cartilage, the main form of loading is compression⁴⁰, and, thus, it is desired to implant neocartilage when it has maximal compressive properties. Here, we showed that both instantaneous and relaxation moduli reached their maximum around 28 days of culture and decreased at later time points, making 28 days the optimal time point for knee articular cartilage implantation. While articular cartilage functions under tensile stresses as well, the tensile magnitudes are not as large as those seen in fibrocartilages¹⁴. Tensile stiffness and strength increased beyond 28 days of culture, with 56 and 84 days of culture exhibiting the greatest tensile stiffness and strength. Thus, these later time points may also be considered for fibrocartilage therapeutics. In addition to tensile properties, collagen type I also increased significantly at 28-84 days of culture compared to earlier time points, further mimicking the biochemical makeup of fibrocartilages like the knee meniscus and temporomandibular joint disc. This study identified optimal culture times for neocartilage (i.e., 28 days for knee articular cartilage and 56-84 days for fibrocartilages) which will be important as this technology is translated toward preclinical and clinical studies.

Tissue-engineered cartilage products are proceeding through the regulatory pipeline, with matrix-assisted autologous chondrocyte implantation already approved for use in the U.S. and many more in development.³ Recent tissue engineering approaches, such as the developmentally inspired self-assembling process, have resulted in robust neocartilages that have functional properties similar to native cartilage. Through this study, we observed that neocartilage made from passaged, rejuvenated costal chondrocytes had many similarities in ECM development to native knee cartilage, as shown through mechanical, biochemical, and proteomic analyses. Optimal time points were identified to maximize compressive and tensile properties for eventual implantation into suitable large animal models for hyaline cartilage and fibrocartilage ailments. Through bottom-up proteomics it was shown that there were some similarities to donor costal cartilage, such as the presence of collagen type I, and some differences in ECM composition of native knee cartilage and tissue-engineered cartilage, such as the temporal trends of collagen

types IX, XI, and XII. Importantly, collagen type X in the neocartilage was approximately 20-times lower than in native floating rib cartilage, supporting the non-homologous approach of using costal chondrocytes to produce neocartilages for the knee. Toward translation of engineered cartilages and other tissues, bottom-up proteomics should be considered for the study of structure-function relationships, development of quality control protocols, and creation of a multitude of release criteria. Because the ultimate goal of tissue engineering is to reach native tissue mimicry, bottom-up proteomics is a demonstrably powerful tool for investigating differences in, for example, native and engineered tissues. A deeper understanding of ECM composition will enable new tissue engineering strategies to recapitulate the unique biochemical and mechanical properties of native tissue, improving clinical outcomes for patients as tissue-engineered products undergo preclinical studies, clinical trials, and eventual widespread usage in humans.

References

- 1 Basad, E., Ishaque, B., Bachmann, G., Stürz, H. & Steinmeyer, J. Matrix-induced autologous chondrocyte implantation versus microfracture in the treatment of cartilage defects of the knee: a 2-year randomised study. *Knee Surg. Sports Traumatol. Arthrosc.* **18**, 519-527, doi:10.1007/s00167-009-1028-1 (2010).
- 2 Flanigan, D. C., Harris, J. D., Trinh, T. Q., Siston, R. A. & Brophy, R. H. Prevalence of chondral defects in athletes' knees: a systematic review. *Med. Sci. Sports Exerc.* **42**, 1795-1801, doi:10.1249/MSS.0b013e3181d9eea0 (2010).
- 3 Kwon, H. *et al.* Surgical and tissue engineering strategies for articular cartilage and meniscus repair. *Nat. Rev. Rheumatol.* **15**, 550-570, doi:10.1038/s41584-019-0255-1 (2019).
- 4 Kreuz, P. C. *et al.* Results after microfracture of full-thickness chondral defects in different compartments in the knee. *Osteoarthritis Cartilage* **14**, 1119-1125, doi:10.1016/j.joca.2006.05.003 (2006).
- 5 Venäläinen, M. S. *et al.* Quantitative Evaluation of the Mechanical Risks Caused by Focal Cartilage Defects in the Knee. *Sci. Rep.* **6**, 37538, doi:10.1038/srep37538 (2016).
- 6 Centers for Disease Control and Prevention. *Osteoarthritis*, <<https://www.cdc.gov/arthritis/basics/osteoarthritis.htm>> (2020).
- 7 Makris, E. A., Gomoll, A. H., Malizos, K. N., Hu, J. C. & Athanasiou, K. A. Repair and tissue engineering techniques for articular cartilage. *Nature Reviews Rheumatology* **11**, 21-34, doi:10.1038/nrrheum.2014.157 (2015).
- 8 Armiento, A. R., Stoddart, M. J., Alini, M. & Eglin, D. Biomaterials for articular cartilage tissue engineering: Learning from biology. *Acta Biomater.* **65**, 1-20, doi:10.1016/j.actbio.2017.11.021 (2018).
- 9 Blein-Nicolas, M. & Zivy, M. Thousand and one ways to quantify and compare protein abundances in label-free bottom-up proteomics. *Biochim. Biophys. Acta* **1864**, 883-895, doi:10.1016/j.bbapap.2016.02.019 (2016).

- 10 Ofek, G. *et al.* Matrix development in self-assembly of articular cartilage. *PLoS One* **3**, e2795, doi:10.1371/journal.pone.0002795 (2008).
- 11 Lee, J. K. *et al.* Tension stimulation drives tissue formation in scaffold-free systems. *Nat. Mater.* **16**, 864-873, doi:10.1038/nmat4917 (2017).
- 12 Natoli, R. M. *et al.* Intracellular Na and Ca² modulation increases the tensile properties of developing engineered articular cartilage. *Arthritis & Rheumatism* **62**, 1097-1107, doi:10.1002/art.27313 (2010).
- 13 Little, C. J., Bawolin, N. K. & Chen, X. Mechanical properties of natural cartilage and tissue-engineered constructs. *Tissue Eng. Part B Rev.* **17**, 213-227, doi:10.1089/ten.TEB.2010.0572 (2011).
- 14 Donahue, R. P., Gonzalez-Leon, E. A., Hu, J. C. & Athanasiou, K. Considerations for translation of tissue engineered fibrocartilage from bench to bedside. *J. Biomech. Eng.*, doi:10.1115/1.4042201 (2018).
- 15 Yoon, K.-H. *et al.* Costal Chondrocyte-Derived Pellet-Type Autologous Chondrocyte Implantation for Treatment of Articular Cartilage Defect. *The American Journal of Sports Medicine* **48**, 1236-1245, doi:10.1177/0363546520905565 (2020).
- 16 Donahue, R. P., Nordberg, R. C., Bielajew, B. J., Hu, J. C. & Athanasiou, K. A. The Effect of Neonatal, Juvenile, and Adult Donors on Rejuvenated Neocartilage Functional Properties. *Tissue Engineering Part A*, doi:10.1089/ten.tea.2021.0167 (2022).
- 17 Kwon, H., Brown, W. E., O'Leary, S. A., Hu, J. C. & Athanasiou, K. A. Rejuvenation of extensively passaged human chondrocytes to engineer functional articular cartilage. *Biofabrication* **13**, doi:10.1088/1758-5090/abd9d9 (2021).
- 18 Mao, Y., Hoffman, T., Wu, A. & Kohn, J. An Innovative Laboratory Procedure to Expand Chondrocytes with Reduced Dedifferentiation. *Cartilage* **9**, 202-211, doi:10.1177/1947603517746724 (2018).
- 19 Lee, J. *et al.* Fully Dedifferentiated Chondrocytes Expanded in Specific Mesenchymal Stem Cell Growth Medium with FGF2 Obtains Mesenchymal Stem Cell Phenotype In Vitro but Retains Chondrocyte Phenotype In Vivo. *Cell Transplant.* **26**, 1673-1687, doi:10.1177/0963689717724794 (2017).
- 20 Mao, Y. *et al.* Extracellular matrix derived from chondrocytes promotes rapid expansion of human primary chondrocytes in vitro with reduced dedifferentiation. *Acta Biomater* **85**, 75-83, doi:10.1016/j.actbio.2018.12.006 (2019).
- 21 Hall, A. C. The Role of Chondrocyte Morphology and Volume in Controlling Phenotype-Implications for Osteoarthritis, Cartilage Repair, and Cartilage Engineering. *Curr Rheumatol Rep* **21**, 38, doi:10.1007/s11926-019-0837-6 (2019).
- 22 Darling, E. M. & Athanasiou, K. A. Rapid phenotypic changes in passaged articular chondrocyte subpopulations. *Journal of Orthopaedic Research* **23**, 425-432, doi:10.1016/j.orthres.2004.08.008 (2005).
- 23 Bielajew, B. J. *et al.* Proteomic, Mechanical, and Biochemical Characterization of Cartilage Development. *Acta Biomater.* (2022).
- 24 Brown, W. E., Hu, J. C. & Athanasiou, K. A. Ammonium-Chloride-Potassium Lysing Buffer Treatment of Fully Differentiated Cells Increases Cell Purity and Resulting Neotissue Functional Properties. *Tissue Engineering Part C: Methods* **22**, 895-903, doi:10.1089/ten.tec.2016.0184 (2016).
- 25 Murphy, M. K., Huey, D. J., Reimer, A. J., Hu, J. C. & Athanasiou, K. A. Enhancing post-expansion chondrogenic potential of costochondral cells in self-assembled neocartilage. *PLoS One* **8**, e56983, doi:10.1371/journal.pone.0056983 (2013).
- 26 Murphy, M. K., Huey, D. J., Hu, J. C. & Athanasiou, K. A. TGF- β 1, GDF-5, and BMP-2 Stimulation Induces Chondrogenesis in Expanded Human Articular Chondrocytes and Marrow-Derived Stromal Cells. *STEM CELLS* **33**, 762-773, doi:10.1002/stem.1890 (2015).

- 27 Huang, B. J., Huey, D. J., Hu, J. C. & Athanasiou, K. A. Engineering biomechanically functional neocartilage derived from expanded articular chondrocytes through the manipulation of cell-seeding density and dexamethasone concentration. *J. Tissue Eng. Regen. Med.* **11**, 2323-2332, doi:10.1002/term.2132 (2017).
- 28 Link, J. M., Hu, J. C. & Athanasiou, K. A. Chondroitinase ABC Enhances Integration of Self-Assembled Articular Cartilage, but Its Dosage Needs to Be Moderated Based on Neocartilage Maturity. *Cartilage*, 1947603520918653, doi:10.1177/1947603520918653 (2020).
- 29 Vapniarsky, N. *et al.* The Yucatan Minipig Temporomandibular Joint Disc Structure-Function Relationships Support Its Suitability for Human Comparative Studies. *Tissue Eng. Part C Methods* **23**, 700-709, doi:10.1089/ten.TEC.2017.0149 (2017).
- 30 Gonzalez-Leon, E. A., Bielajew, B. J., Hu, J. C. & Athanasiou, K. A. Engineering self-assembled neomenisci through combination of matrix augmentation and directional remodeling. *Acta Biomater.* **109**, 73-81, doi:10.1016/j.actbio.2020.04.019 (2020).
- 31 Cissell, D. D., Link, J. M., Hu, J. C. & Athanasiou, K. A. A Modified Hydroxyproline Assay Based on Hydrochloric Acid in Ehrlich's Solution Accurately Measures Tissue Collagen Content. *Tissue Eng. Part C Methods* **23**, 243-250, doi:10.1089/ten.tec.2017.0018 (2017).
- 32 Calabro, A. *et al.* Fluorophore-assisted carbohydrate electrophoresis (FACE) of glycosaminoglycans. *Osteoarthritis Cartilage* **9 Suppl A**, S16-22, doi:10.1053/joca.2001.0439 (2001).
- 33 Bielajew, B. J., Hu, J. C. & Athanasiou, K. A. Methodology to Quantify Collagen Subtypes and Crosslinks: Application in Minipig Cartilages. *Cartilage*, 19476035211060508, doi:10.1177/19476035211060508 (2021).
- 34 Cox, J. & Mann, M. MaxQuant enables high peptide identification rates, individualized p.p.b.-range mass accuracies and proteome-wide protein quantification. *Nature Biotechnology* **26**, 1367-1372, doi:10.1038/nbt.1511 (2008).
- 35 Vapniarsky, N. *et al.* Tissue engineering toward temporomandibular joint disc regeneration. *Sci. Transl. Med.* **10**, doi:10.1126/scitranslmed.aag1802 (2018).
- 36 Kagan, H. M. & Li, W. Lysyl oxidase: properties, specificity, and biological roles inside and outside of the cell. *J Cell Biochem* **88**, 660-672, doi:10.1002/jcb.10413 (2003).
- 37 Hasegawa, M., Yoshida, T. & Sudo, A. Role of tenascin-C in articular cartilage. *Modern Rheumatology* **28**, 215-220, doi:10.1080/14397595.2017.1349560 (2018).
- 38 Schmid, T. M. & Linsenmayer, T. F. Immunohistochemical localization of short chain cartilage collagen (type X) in avian tissues. *J Cell Biol* **100**, 598-605, doi:10.1083/jcb.100.2.598 (1985).
- 39 Shen, G. The role of type X collagen in facilitating and regulating endochondral ossification of articular cartilage. *Orthod Craniofac Res* **8**, 11-17, doi:10.1111/j.1601-6343.2004.00308.x (2005).
- 40 Athanasiou, K. A., Darling, E. M., DuRaine, G. D., Hu, J. C. & Reddi, A. H. *Articular Cartilage*. 2 edn, (CRC Press, 2017).
- 41 Bielajew, B. J., Hu, J. C. & Athanasiou, K. A. Collagen: quantification, biomechanics, and role of minor subtypes in cartilage. *Nat Rev Mater* **5**, 730-747, doi:10.1038/s41578-020-0213-1 (2020).

Supplementary materials

Supplementary Table 1. Additional mechanical outcomes of neocartilage constructs. Additional outcomes for compressive stress-relaxation and uniaxial tension tests are reported as mean \pm standard deviation. Cells that do not share the same letter are significantly different from each other.

Outcome	Culture time (days)				
	7	14	28	56	84
Compressive stress-relaxation					
10% Coefficient of viscosity (MPa s)	11.6 \pm 2.5 ^A	2.1 \pm 0.7 ^B	1.4 \pm 0.6 ^B	1.1 \pm 0.2 ^B	1.4 \pm 1.2 ^B
20% Coefficient of viscosity (MPa s)	30.7 \pm 7.8 ^A	15.0 \pm 4.9 ^B	6.2 \pm 2.0 ^C	4.0 \pm 1.0 ^C	2.9 \pm 1.6 ^C
Uniaxial tension					
Strain at failure (mm/mm)	0.52 \pm 0.13	0.59 \pm 0.15	0.57 \pm 0.11	0.43 \pm 0.09	0.46 \pm 0.11
Toughness (Mpa m ⁻³)	0.13 \pm 0.05 ^B	0.38 \pm 0.16 ^A	0.34 \pm 0.15 ^A	0.30 \pm 0.10 ^A	0.27 \pm 0.08 ^{AB}

Supplementary Table 2. Bottom-up proteomics analytes of neocartilage constructs. All analytes are reported as a percentage per total protein (PROT) content. Of 364 identified analytes, those with an intensity greater than 0.1%/PROT in at least one sample and all collagen chains (86 proteins total) are reported.

Gene	Protein	Protein / Total Protein (%)				
		Culture time (days)				
		7	14	28	56	84
HMDH	3-hydroxy-3-methylglutaryl-coenzyme A reductase	0.03%	0.05%	0.03%	0.13%	0.04%
RS16	40S ribosomal protein S16	0.10%	0.07%	0.05%	0.04%	0.05%
RS20	40S ribosomal protein S20	0.08%	0.07%	0.03%	0.04%	0.02%
RS3	40S ribosomal protein S3	0.13%	0.10%	0.08%	0.07%	0.09%
RS9	40S ribosomal protein S9 (Fragment)	0.09%	0.04%	0.03%	0.04%	0.04%
RSSA	40S ribosomal protein SA	0.12%	0.10%	0.08%	0.06%	0.06%
RLA0	60S acidic ribosomal protein P0	0.06%	0.02%	0.03%	0.02%	0.03%
RL11	60S ribosomal protein L11	0.05%	0.10%	0.06%	0.05%	0.05%
RL14	60S ribosomal protein L14	0.07%	0.03%	0.05%	0.03%	0.04%
RL18	60S ribosomal protein L18	0.09%	0.07%	0.06%	0.04%	0.04%
RL6	60S ribosomal protein L6	0.15%	0.10%	0.05%	0.04%	0.02%
ACTS	Actin, alpha skeletal muscle	0.20%	0.10%	0.03%	0.05%	0.03%
ACTB	Actin, cytoplasmic 1	3.17%	1.96%	1.96%	1.53%	1.50%
PGCA	Aggrecan core protein	0.47%	0.30%	0.24%	0.28%	0.21%
ALBU	Albumin	0.35%	0.36%	0.09%	0.23%	0.27%
CRYAB	Alpha-crystallin B chain	0.03%	0.04%	0.09%	0.12%	0.07%
ANXA2	Annexin A2	1.14%	0.44%	0.37%	0.41%	0.38%
ARG11	Arginase-1	0.09%	0.09%	0.07%	0.06%	0.07%

ATPA	ATP synthase subunit alpha, mitochondrial	0.27%	0.18%	0.23%	0.19%	0.22%
ENOB	Beta-enolase	0.95%	0.78%	0.43%	0.14%	0.13%
PGS1	Biglycan	0.75%	0.69%	0.34%	0.95%	0.37%
CALR	Calreticulin	0.18%	0.09%	0.05%	0.06%	0.02%
COF1	Cofilin-1	0.17%	0.13%	0.07%	0.06%	0.04%
COL1A1	Collagen type I alpha 1	2.45%	3.24%	4.63%	4.77%	5.58%
COL1A2	Collagen type I alpha 2	1.31%	2.06%	3.07%	2.78%	3.23%
COL2A1	Collagen type II alpha 1	38.40%	53.49%	56.36%	57.20%	57.58%
COL3A1	Collagen type III alpha 1	0.44%	0.24%	0.40%	0.32%	0.36%
COL4A2	Collagen type IV alpha 2	<0.01%	0.04%	0.02%	0.05%	0.06%
COL4A4	Collagen type IV alpha 4	0.01%	0.03%	0.00%	0.00%	0.04%
COL4A5	Collagen type IV alpha 5	0.00%	0.03%	0.01%	0.01%	0.00%
COL5A1	Collagen type V alpha 1	0.33%	0.45%	0.38%	0.49%	0.42%
COL5A2	Collagen type V alpha 2	0.67%	1.12%	1.24%	1.26%	1.36%
COL5A3	Collagen type V alpha 3	0.01%	0.01%	0.01%	0.01%	0.00%
COL6A1	Collagen type VI alpha 1	0.12%	0.13%	0.15%	0.34%	0.25%
COL6A2	Collagen type VI alpha 2	0.51%	0.38%	0.72%	1.06%	1.03%
COL6A3	Collagen type VI alpha 3	1.46%	1.82%	3.26%	4.16%	4.44%
COL9A1	Collagen type IX alpha 1	0.63%	1.36%	1.75%	1.57%	1.82%
COL9A2	Collagen type IX alpha 2	0.42%	0.69%	0.77%	0.82%	0.79%
COL10A1	Collagen type X alpha 1	<0.01%	0.05%	0.02%	0.02%	0.03%
COL11A1	Collagen type XI alpha 1	2.11%	2.77%	2.33%	2.75%	2.46%
COL11A2	Collagen type XI alpha 2	2.05%	3.08%	2.88%	2.92%	3.06%
COL12A1	Collagen type XII alpha 1	3.59%	3.92%	4.80%	4.40%	4.62%
COL28A1	Collagen type XXVIII alpha 1	0.00%	0.03%	0.52%	0.05%	0.55%
PGS2	Decorin	0.00%	0.03%	0.07%	0.08%	0.10%
RPN1	Dolichyl-diphosphooligosaccharide-protein glycosyltransferase subunit 1	0.13%	0.09%	0.07%	0.08%	0.07%
EF1G	Elongation factor 1-gamma (Fragment)	0.17%	0.11%	0.05%	0.04%	0.05%
BIP	Endoplasmic reticulum chaperone BiP (Fragment)	0.18%	0.08%	0.06%	0.09%	0.07%
ENPL	Endoplasmin	0.33%	0.14%	0.09%	0.09%	0.09%
FMOD	Fibromodulin (Fragment)	0.09%	0.04%	0.03%	0.03%	0.01%
GELS	Gelsolin (Fragment)	0.19%	0.09%	0.07%	0.07%	0.08%
G6PI	Glucose-6-phosphate isomerase	0.14%	0.05%	0.01%	<0.01%	<0.01%
G3P	Glyceraldehyde-3-phosphate dehydrogenase	3.94%	1.58%	0.92%	0.49%	0.57%
HS71B	Heat shock 70 kDa protein 1B	0.66%	0.40%	0.42%	0.31%	0.24%

HSP76	Heat shock 70 kDa protein 6	0.12%	0.00%	0.02%	0.00%	<0.01%
HSPB1	Heat shock protein beta-1	0.49%	0.18%	0.18%	0.19%	0.13%
HS90A	Heat shock protein HSP 90-alpha	0.41%	0.19%	0.16%	0.13%	0.15%
H1T	Histone H1t	0.26%	0.20%	0.19%	0.10%	0.10%
H33	Histone H3.3	0.89%	0.48%	0.45%	0.39%	0.32%
H4	Histone H4	3.45%	2.21%	1.10%	1.25%	0.85%
HPLN1	Hyaluronan and proteoglycan link protein 1	1.49%	0.70%	0.55%	1.03%	0.67%
MX2	Interferon-induced GTP-binding protein Mx2	0.00%	0.02%	0.17%	0.02%	0.08%
MFGM	Lactadherin	0.18%	0.17%	0.30%	0.54%	0.46%
GGLO	L-gulonolactone oxidase	0.09%	0.08%	0.05%	0.00%	<0.01%
LDHA	L-lactate dehydrogenase A chain	0.41%	0.19%	0.08%	0.05%	0.04%
GANAB	Neutral alpha-glucosidase AB	0.11%	0.07%	0.04%	0.03%	0.03%
NDKB	Nucleoside diphosphate kinase B	0.15%	0.07%	0.02%	0.02%	0.01%
PPIA	Peptidyl-prolyl cis-trans isomerase A	0.22%	0.11%	0.07%	0.04%	0.03%
PRDX6	Peroxiredoxin-6	0.11%	0.05%	0.06%	0.03%	0.03%
PGK1	Phosphoglycerate kinase 1	0.91%	0.51%	0.32%	0.20%	0.13%
UBC	Polyubiquitin-C	0.18%	0.10%	0.16%	0.08%	0.12%
LMNA	Prelamin-A/C	1.66%	1.09%	0.63%	0.45%	0.37%
PPCE	Prolyl endopeptidase	0.36%	0.00%	0.00%	0.00%	0.00%
S10A6	Protein S100-A6	0.13%	0.18%	0.15%	0.11%	0.06%
RAB1B	Ras-related protein Rab-1B	0.13%	0.05%	0.05%	0.05%	0.06%
RYR1	Ryanodine receptor 1	0.00%	0.26%	0.00%	0.17%	0.16%
STAT1	Signal transducer and activator of transcription 1	0.23%	0.10%	0.44%	0.22%	0.09%
SPRC	SPARC	0.09%	0.02%	<0.01%	<0.01%	0.00%
TENA	Tenascin	0.02%	0.04%	0.18%	0.11%	0.10%
THIO	Thioredoxin	0.14%	0.01%	0.03%	<0.01%	0.00%
TPIS	Triosephosphate isomerase	0.86%	0.42%	0.14%	0.02%	0.02%
TPM4	Tropomyosin alpha-4 chain	0.11%	0.07%	0.01%	<0.01%	0.00%
TBA1B	Tubulin alpha-1B chain	0.55%	0.19%	0.33%	0.24%	0.27%
TBB5	Tubulin beta chain	0.37%	0.27%	0.24%	0.21%	0.20%
UGPA	UTP--glucose-1-phosphate uridylyltransferase	0.21%	0.04%	0.03%	0.03%	0.04%
VIME	Vimentin	12.25%	6.01%	2.14%	1.26%	0.87%
VDAC1	Voltage-dependent anion-selective channel protein 1	0.13%	0.06%	0.07%	0.06%	0.07%

CHAPTER 6 | Long-term safety and efficacy of temporomandibular joint disc regeneration in the Yucatan minipig*

Abstract

Up to 25% of the US population exhibits symptoms of temporomandibular joint (TMJ) disorders (TMDs). A subset of those include disc perforations, which can develop as a result of disc displacement. Toward addressing the disc perforation indication, the objective of this study was to examine the long-term safety and efficacy of tissue-engineered implants derived from allogeneic costal chondrocytes in the Yucatan minipig toward healing TMJ disc perforations of 3 mm in diameter. It was hypothesized that implants would not elicit a significant systemic or local immune response, and implant-treated discs would exhibit superior healing, with significantly higher functional properties compared to empty defect controls. After 24 weeks, implants were well-tolerated. Systemically, there was no response as evidenced by complete blood count and comprehensive metabolic panel parameters, and implant-treated discs exhibited a local immune response of T cells, B cells, and macrophages that dampened after 8 weeks. Implant-treated discs appeared to heal better than controls. When testing the repair tissue of implant-treated discs and the fill tissue of empty defects under uniaxial tension, repair tissue was 6.2-times tougher, 8.9-times more resilient, 3.4-times stronger, and had a 2.5-times higher strain at failure compared to fill tissue. Additionally, collagen type I and collagen type III were significantly higher and lower in repair tissue compared to fill tissue of controls. These values in implant-treated discs, 99.4% and 103.1% of native tissue values, respectively, indicated more native-like regeneration, unlike scar tissue in control discs. Overall, tissue-engineered implants proved to be safe and efficacious for healing TMJ disc perforations, establishing the translational potential of neocartilage implants for addressing discal TMD indications.

* Authors: Donahue RP, Bielajew BJ, Vapniarsky N, Heney CM, Arzi B, Hu JC, Athanasiou KA.

Introduction

The temporomandibular joint (TMJ) is a ginglymoarthrodial joint involved in speaking, chewing, and breathing¹. Temporomandibular disorders (TMDs), a group of ailments affecting the joint and surrounding structures, symptomatically affect between 5-25% of the US population²⁻⁶, are the second most common musculoskeletal condition in the US¹, and cost the US healthcare system up to \$4 billion per year⁷. Pathologies of the TMJ disc, a fibrocartilaginous structure between the temporal bone of the skull and mandible, are central to TMDs. These pathologies include disc displacement, which can lead to disc thinning developing into disc perforation. It has been reported that approximately 70% of all TMD cases involve disc displacement⁸, where the disc is mispositioned relative to its normal anatomic location. Concurrently with or independent of displacement, disc thinning and perforation can also occur. Up to 15% of displaced discs develop perforations, affecting up to 9 million people in the US alone⁹⁻¹¹; thus, disc perforations are a significant clinical indication. While not all discal TMDs require medical intervention, a large portion of them cause intractable day-to-day pain and dysfunction.

Unlike joints such as the knee where there are established algorithms for treatment of cartilage afflictions, current treatments for discal TMDs are not well-defined¹². Generally, treatment options depend on severity of the disc condition¹³. For example, analgesics, mechanical stabilizers, and some arthroscopic procedures may be suitable for early-stage cases¹², but open surgical procedures are reserved for the most severe cases, with only 5-10% of TMD patients being candidates for surgery^{14,15}. Discectomy and total joint replacements are plagued with the need for revision surgeries due to joint degradation after disc removal and young patient age coupled with average joint replacement lifetime¹. Currently, there is no suitable intermediate solution between noninvasive and late-stage surgical interventions for the TMJ disc that can significantly halt progression of TMJ disc pathologies or regenerate damaged tissues. Thus, the field would benefit from new interventions that would provide a long-term alternative to joint replacements.

Tissue engineering has gained traction as a long-term solution to discal TMDs. Tissue-engineered implants for TMJ disc regeneration must withstand joint loading, especially under high tensile strains¹⁶. Recently, several orthotopic preclinical studies examining safety and efficacy of tissue-engineered implants in large animal models have been performed. For example, a recent study investigated poly(glycerol sebacate) and gelatin scaffolds toward regeneration of osteochondral defects in the goat mandibular condyle¹⁷. Work in the TMJ discs of Yucatan minipigs also showed success in healing disc thinning defects using scaffold-free, self-assembled neocartilage¹⁸. For large animal models, the minipig has recently emerged as the gold-standard for preclinical studies in the TMJ¹⁹ due to its similarities in anatomy, biochemical and mechanical properties, diet, and joint loading²⁰.

A major challenge in cartilage tissue-engineering is cell sourcing. Numerous cell sources have been investigated as alternates to directly harvesting TMJ chondrocytes due to issues such as donor site morbidity and potential harvest of diseased cells from TMD-affected tissues unsuitable for tissue engineering²¹. For example, due to their vast availability and expansion capabilities, mesenchymal stem cells derived from bone marrow have been used with 3D-printed TMJ disc scaffolds as a potential replacement²². Previously, costal cartilage has been used for autologous replacement of the TMJ disc²³, motivating the use and investigation of costal chondrocytes as a cell source. Costal chondrocytes are more abundant and more easily harvested than other chondrocyte sources, including both TMJ chondrocytes and knee articular chondrocytes, and have been shown to create robust neocartilage implants^{1,24}. Additionally, previous work examined the feasibility of using an allogeneic approach with costal chondrocytes in the Yucatan minipig, resulting in healing of TMJ disc thinning defects¹⁸. Therefore, costal chondrocytes have been proven to be a suitable cell source for TMJ disc tissue engineering.

Our recent study showed short-term (i.e., 8-week) safety and efficacy of a nonhomologous, allogeneic approach using costal chondrocyte-derived implants in the Yucatan minipig TMJ disc¹⁸. Using self-assembled neocartilage implants, TMJ disc thinning (i.e., partial

thickness) defects successfully healed without a significant local or systemic immune response, indicating immunogenic tolerance to an allogeneic donor source. Additionally, there was 4.4-times greater defect closure in implant-treated groups compared to empty defect controls, and the osteoarthritis (OA) score was 3.0-times higher (indicative of a worse clinical outcome) in controls compared to implant-treated groups. Importantly, implants facilitated mechanically robust healing, resulting in 3.4-times stiffer repair tissue (tissue filling in the implant-treated defect) compared to empty defect fill tissue (tissue filling in the control defect). Additionally, intralaminar fusion (measuring the integration of the two laminae of the pocket) was 3.2-times stiffer when treated with an implant. Given these promising results, additional research into the capabilities of self-assembled implants to heal TMJ disc perforations (i.e., full thickness defects), further down the degenerative pathway compared to thinning defects, is essential given the widespread prevalence of TMJ disc perforations in human populations.

Driven by success in disc thinning models and the pervasiveness of disc perforations, the objective of this study was to validate the long-term (i.e., 24-week) safety and efficacy of self-assembled neocartilage implants derived from allogeneic costal chondrocytes in perforation defects of the Yucatan minipig TMJ disc. It was hypothesized that 1) compared to untreated empty defect controls, implant-treated discs would heal with repair tissues that have a collagen profile more consistent to native TMJ discs, and 2) repair tissues of implant-treated discs would exhibit superior mechanical properties compared to control fill tissue. Additionally, it was hypothesized that the extracellular matrix of the neocartilage implants would remodel toward that of native TMJ discs. Finally, it was expected that implants would not elicit a significant systemic or local immune response. Upon completion of this study, substantial preclinical data will be generated toward translation of self-assembled neocartilage implants for eventual human use.

Results

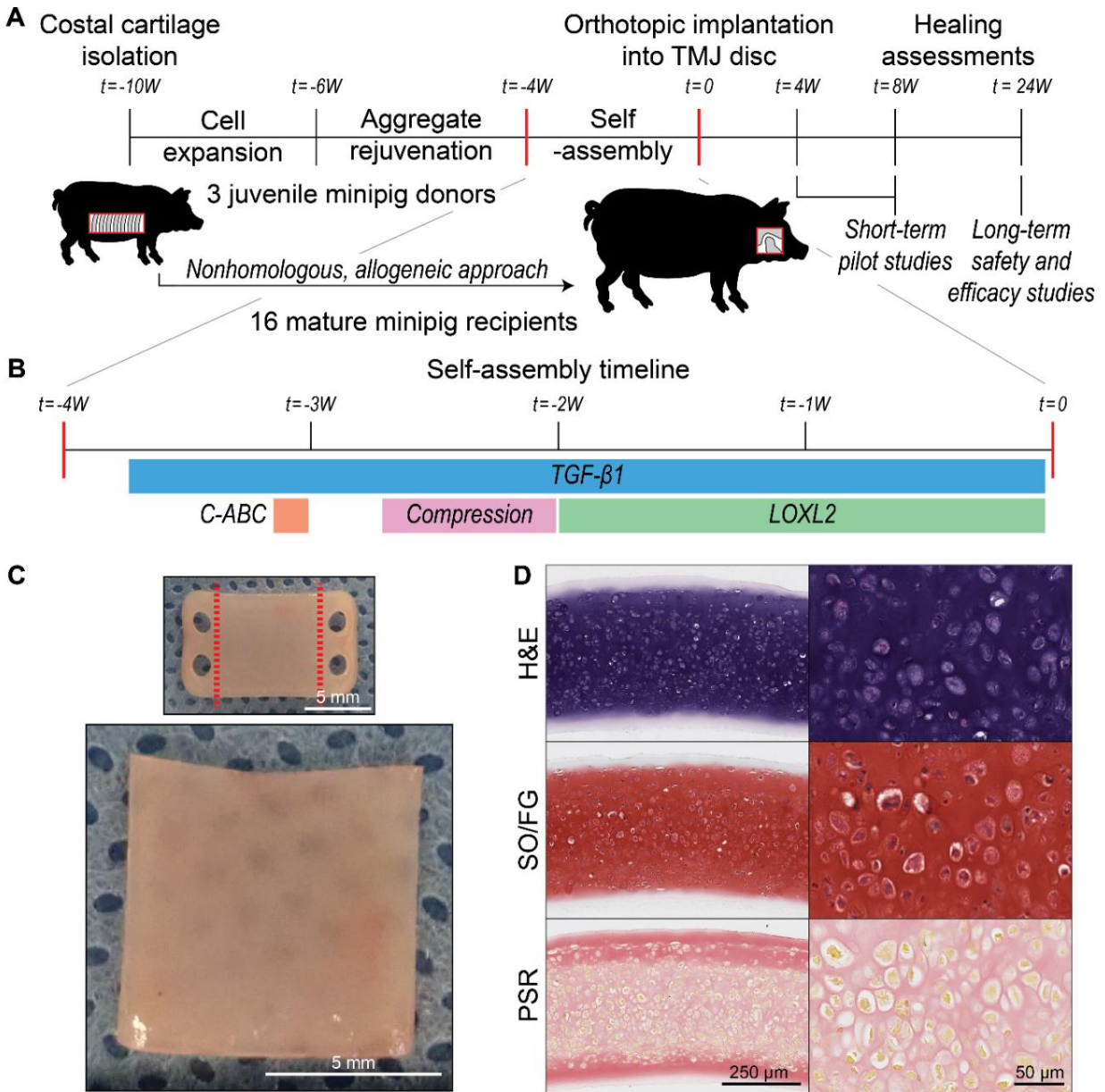


Figure 1. Neocartilages were fabricated using the self-assembling process and exhibited robust matrix content for implantation into the TMJ disc. (A) After costal cartilage isolation from three juvenile minipigs, chondrocytes underwent expansion, aggregate rejuvenation, and self-assembly prior to nonhomologous, allogeneic implantation into the TMJ disc. After implantation, minipigs were euthanized and assessed for healing in the short-term or long-term studies. (B) The self-assembling process included addition of bioactive factors, such as transforming growth factor beta 1 (TGF-β1), chondroitinase ABC (C-ABC), and lysyl oxidase-like 2 (LOXL2), and passive axial compressive to improve the functional properties of implants. (C) The original implant (8x13 mm) was trimmed to 8x8 mm for implantation. (D) The implant exhibited homogenous chondrocyte distribution in the matrix, seen in hematoxylin and eosin staining (H&E), and staining with safranin O staining with fast green counterstaining (SO/FG) and picosirius red staining (PSR) showed glycosaminoglycan and total collagen distribution, respectively.

Tissue-engineered implants approached native tissue values, and the intralaminar perforation surgical technique secured tissue-engineered implants in the Yucatan minipig TMJ disc

Implants were fabricated from donor costal cartilage for a nonhomologous, allogeneic approach in the Yucatan minipig TMJ disc (Figure 1A). Specifically, costal chondrocytes harvested from the minipig rib underwent three passages²⁵ to an expansion factor of 64 and were placed into aggregate rejuvenation for 11 days prior to self-assembly²⁶. During the self-assembling process (Figure 1B), chondrocytes were treated with bioactive factors and passive axial compression²⁷, previously shown to improve functional properties^{18,27}. Implants (originally 8x13 mm) were trimmed to approximately 8x8 mm (Figure 1C) for use in the intralaminar perforation surgical technique (Figure 2). Prior to implantation, implants exhibited matrix staining for glycosaminoglycans (GAGs) via safranin O staining with fast green counterstain (SO/FG) and collagen via picrosirius red staining (PSR) with cells being homogeneously distributed after 28 days of self-assembly as seen through hematoxylin and eosin staining (H&E) (Figure 1D), consistent with prior studies²⁸. Prior to surgery, the implants' mechanical properties were as follows: tensile Young's modulus of 7.05 ± 1.39 MPa, ultimate tensile strength (UTS) of 2.28 ± 0.45 MPa, compressive 20% relaxation modulus of 177 ± 55 kPa, and compressive 20% instantaneous modulus of 777 ± 115 kPa, similar to the mechanical properties of the native minipig TMJ disc²⁰. Thus, these implants were considered suitable for implantation into perforation defects in the Yucatan minipig in both short-term pilot studies and long-term safety and efficacy studies (Figure 1A).

The intralaminar perforation surgical technique has been previously described and used to secure implants in the TMJ disc (Figure 2)¹⁸. Here, the surgical approach was altered from a disc thinning (i.e., one-sided or partial thickness) defect model to a perforation (i.e., two-sided or full thickness) defect model. Using a preauricular approach, the TMJ disc was identified, and a horizontal incision in the disc was created (Figure 2A-D). A perforation defect was then made in the centrolateral region of the disc with a 3 mm diameter disposable biopsy punch, and the implant

was placed in the horizontal pocket (Figure 2E-F, Supplementary Figure 1). The incision was sutured shut on the lateral edge of the disc, avoiding placement of sutures on the disc articulating surface, and the lateral aspect of the disc was attached to the condylar process using a Mitek bone anchor (Figure 2G-H). This surgical technique effectively secured the implant in place without the need for sutures on the articulating surfaces of the TMJ disc, avoiding stress concentrations which have been shown to cause degradation of the articular surfaces²⁹.

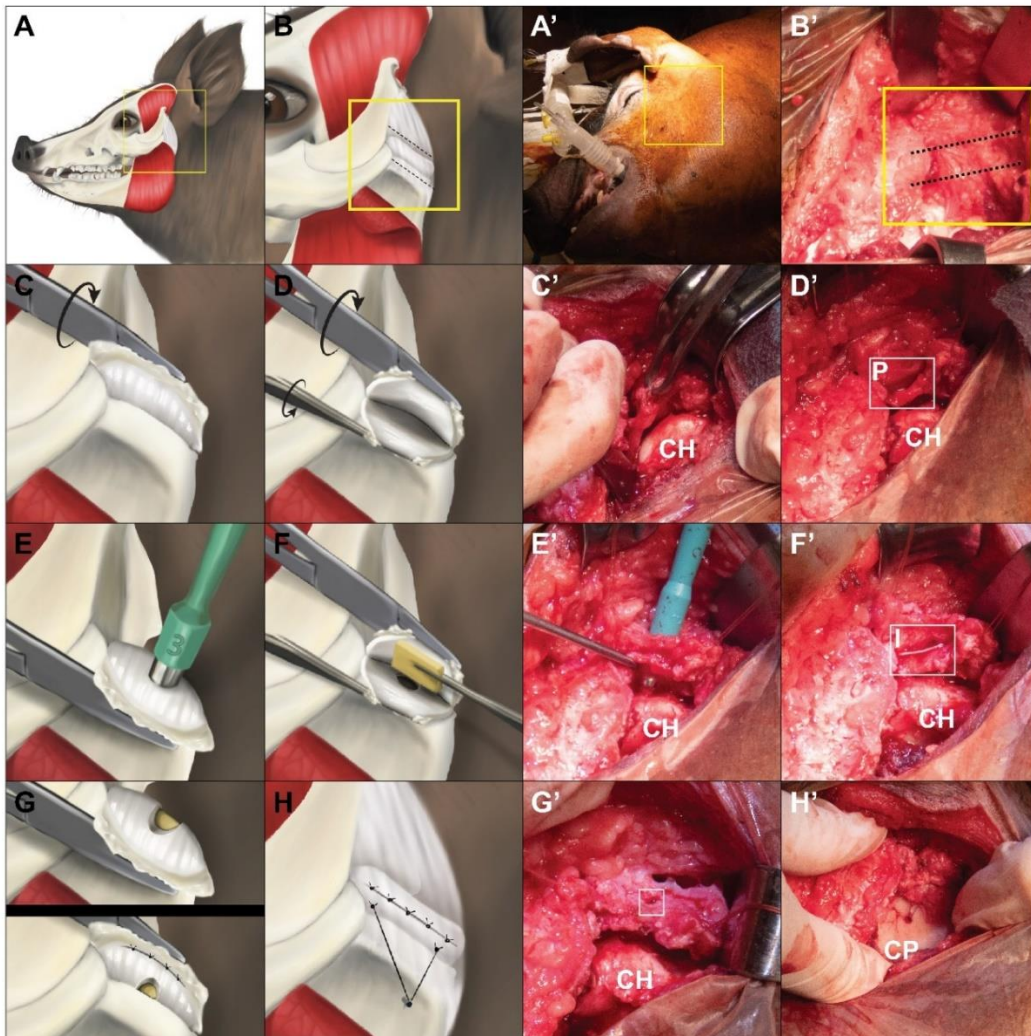


Figure 2. The intralaminar perforation surgical technique secured tissue-engineered implants in perforation defects. (A) The animal was prepared for surgical intervention, and (B) the TMJ was identified (dashed lines). (C) Upon freeing the TMJ disc, the condylar head (labeled as “CH”) was identified, and the superior and inferior joint spaces were clearly visible. (D) The incision was created, and the pouch (“P”) was deepened, where the implant was placed. (E) The 3 mm diameter perforation defect was created with a disposable biopsy punch. (F) The implant (“I”) was placed in the pocket, and (G) the pocket was sutured shut along the lateral edge. Upon rotation, the defect (white box) was present on the superior surface of the disc. (H) The lateral portion of the disc was attached back to the condylar process (“CP”) with a double-armed Mitek bone anchor.

Perforation defects in the TMJ disc healed with tissue-engineered implants

Initial pilot studies at 4 and 8 weeks demonstrated efficacy of healing perforation defects with tissue-engineered implants. All four minipigs (n=2 animals/timepoint) exhibited complete defect closure (Supplementary Figure 2). Moving forward, a statistically driven safety and efficacy study examining the long-term healing of perforation defects in the TMJ disc consisting of 12 animals (n=6/group, with implant-treated and empty defect control groups) was performed. After 24 weeks, all six implant-treated discs exhibited complete repair tissue fill (Figure 3A, Supplementary Figure 3). In comparison, control discs also had some degree of tissue fill, as seen in images depicting their gross morphologies; one of the six discs still had defects present on the superior and inferior surfaces of the disc (Figure 3A, Supplementary Figure 3). Control discs appeared worse in gross morphology images than implant-treated discs, exhibiting surface abrasions on the superior surfaces of the discs (Figure 3A). This same morphology was found only in the worst-cases of the implant-treated group (Figure 3A, Supplementary Figure 3). Opposing condylar surfaces also presented a heterogeneous response to surgical intervention (Supplementary Figure 4). When quantifying the osteoarthritic changes on the articulating surface of the condyle via a modified ICRS score, there was no significant difference between the two groups (Supplementary Table 1). Although there were some condylar changes, this was most likely due to the suture rubbing on the condyle over the study length.

When assessing anteroposterior cross sections of the discs, controls did not completely heal along the entire incision (Figure 3B). In contrast, a majority of implant-treated discs exhibited complete healing in the central biconcave portion of the disc (Figure 3B). When testing the intralaminar fusion between the two laminae under tension in the superoinferior direction, it was noted that there were no significant differences between the groups (Supplementary Table 2). When examining implant location via histology, all discs that received tissue-engineered implants had posterior migration of the implant (Figure 3B) compared to the original centrolateral implantation site and defect location (Supplementary Figure 1). This is most likely due to the

biomechanical loading of the joint during articulation, which applies compressive loads to the disc transmitted through the condyle. When these compressive forces are applied in the center of the TMJ disc, it develops high tensile strains in the periphery of the disc, causing the implant to migrate into the thicker portion of the posterior band. The H&E staining of the areas surrounding implants revealed a cellular response after 24 weeks; the implant was surrounded by cells from the host response, compared to the control which remained open and lacked any cellular response (Figure 3B). Despite the varied healing responses in the two groups, implant-treated discs exhibited more robust gross morphologic healing.

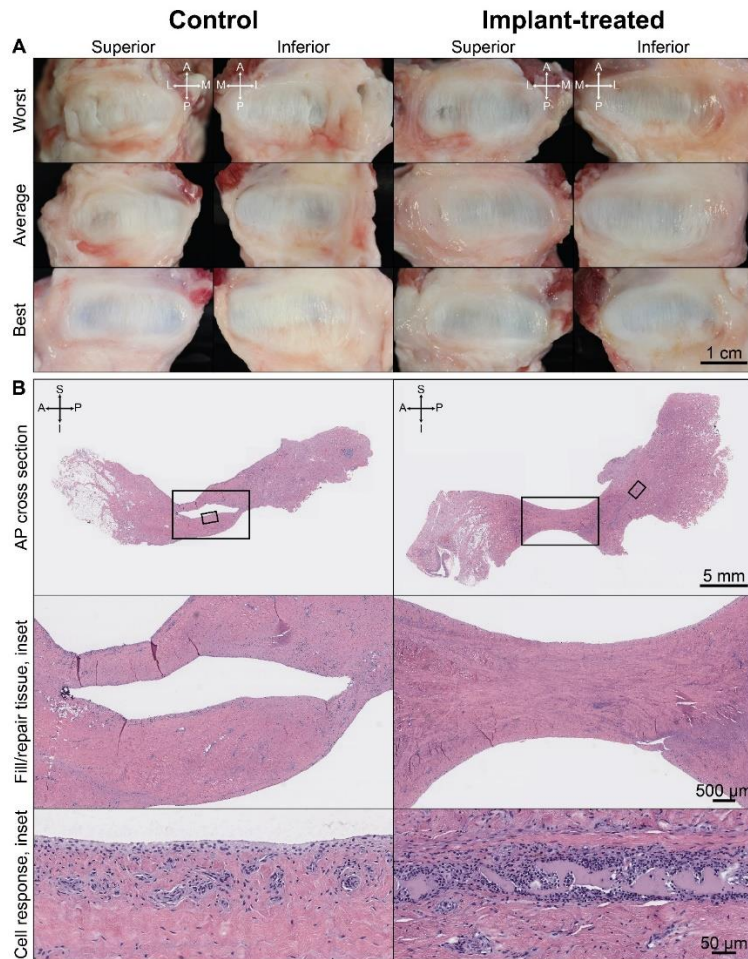


Figure 3. Gross morphology and histological cross sections of TMJ discs showed lack of complete healing in controls and repair tissue in implant-treated groups. (A) All six implant-treated discs appeared better than controls. (B) When examining anteroposterior (AP) cross sections of the TMJ discs, the incision did not completely heal in controls. In implant-treated discs, which did completely heal with repair tissue, there was a cellular host response to the implant, while control discs remained open and lacked a cellular response. A, anterior, I, inferior, L, lateral, M, medial, P, posterior, S, superior.

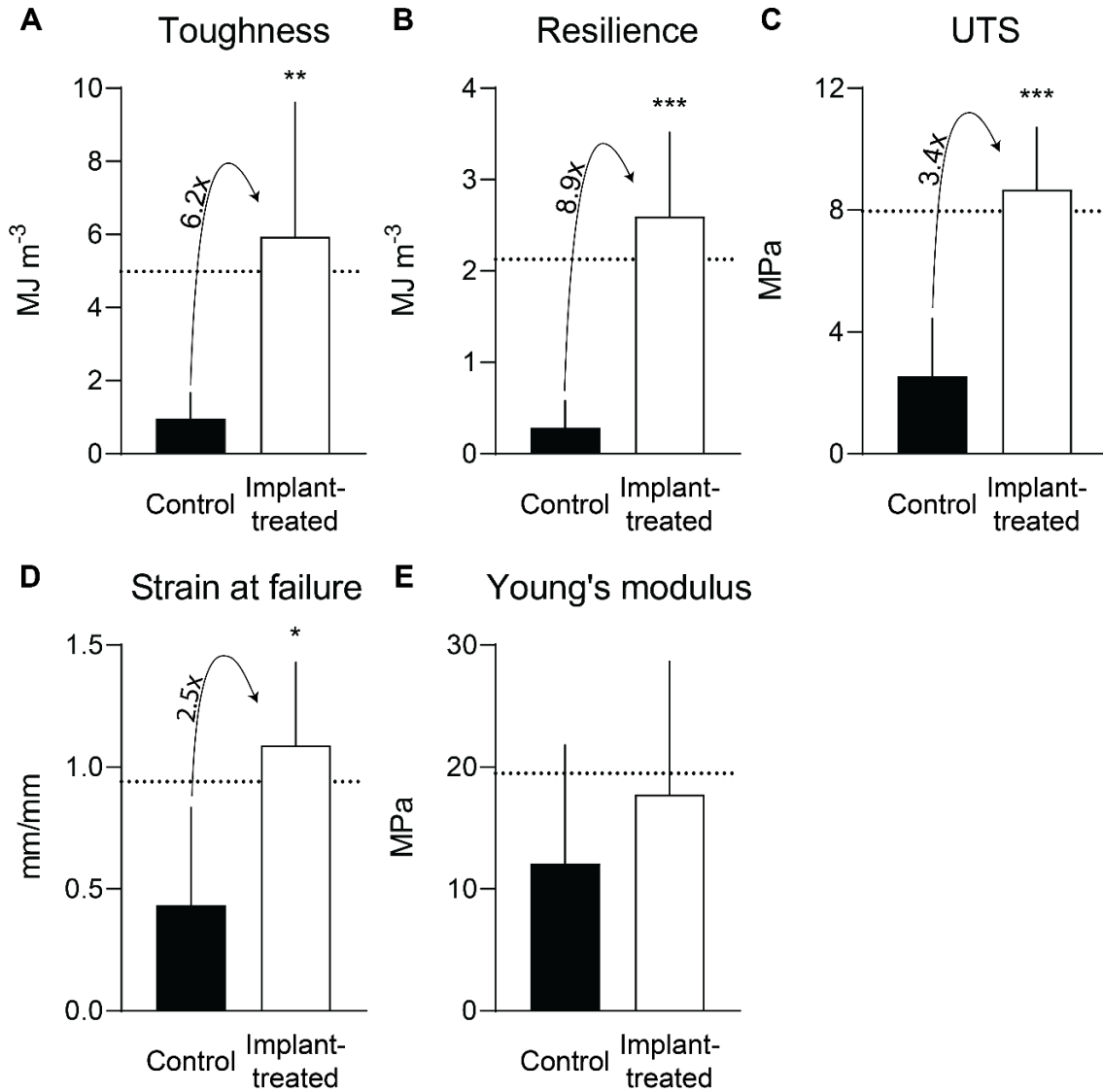


Figure 4. Tensile properties of repair tissue of implant-treated discs were higher compared to fill tissue of controls. When compared to fill tissue of control discs, repair tissue had a (A) 6.2-times higher toughness, (B) 8.9-times higher resilience, (C) 3.4-times higher ultimate tensile strength (UTS), and (D) 2.5-times higher strain at failure. (E) Young's modulus of repair tissue trended up with implant treatment but was not significantly different to control fill tissue. Dashed lines represent native TMJ disc values.

Tissue-engineered implants facilitated regeneration of mechanically robust repair tissue that reached native TMJ disc tensile properties

Despite a heterogeneous gross morphological healing response, tissue-engineered implants facilitated robust healing when compared to controls, as indicated by multiple statistically significant outcome measures on disc function. The tissues that filled in the defects in the centrolateral portion of the disc were tested under uniaxial tension to determine toughness,

resilience, UTS, strain at failure, and tensile Young's modulus (Figure 4). Implant-treated discs exhibited repair tissue values above 90% of contralateral control disc values (dashed lines), while fill tissue values in controls were under 50% of native tissue values for every measure except tensile Young's modulus (Figure 4). Importantly, repair tissue of implant-treated discs was 6.2-times tougher, 8.9-times more resilient, 3.4-times stronger, and had a 2.5-times higher strain at failure than control fill tissue, all of which were statistically significant (Figure 4A-D). While Young's modulus trended upwards with implant treatment, this difference was not significant (Figure 4E). Ultimately, tissue-engineered implants resulted in more robust repair tissue compared to the fill tissue found in control discs.

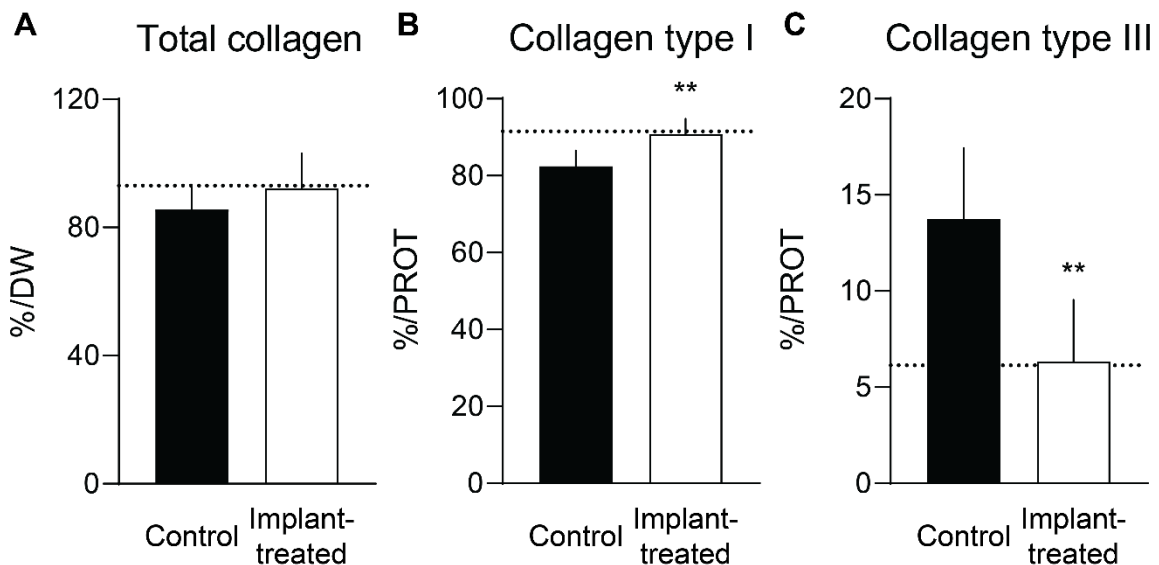


Figure 5. Collagens in the matrix of repair tissue was reminiscent of native TMJ disc content. (A) Total collagen per dry weight (DW) was not significantly different between the two groups but trended upwards in implant-treated discs. In the control group, (B) there was less collagen type I per total protein (PROT) and (C) more collagen type III per PROT, indicative of a scar-like tissue. In contrast, implant-treated discs exhibited native-like regeneration of collagen type I in their repair tissue. Dashed lines represent native TMJ disc values.

Repair tissue of implant-treated discs mimicked the native TMJ disc biochemical content

Mechanical properties develop from structure-function relationships with the extracellular matrix of TMJ discs. Collagen is the major component of the TMJ disc, encompassing more than 90% of the dry weight (DW) of the disc (dashed line, Figure 5A). When comparing to fill tissue of controls, the total collagen content of repair tissues of implant-treated discs trended upwards

toward native TMJ disc values (Figure 5A), but this trend was not significant. However, significant differences emerge among the tissues when analyzing individual collagen subtypes. Collagen type I, the main collagen type found in the TMJ disc, was significantly lower per total protein (PROT) content in fill tissue of controls compared to repair tissue (Figure 5B). The repair tissue contained 99.4% of native tissue collagen type I, indicating the regenerative capacity of the tissue-engineered implants. Additionally, mature pyridinoline (PYR) and immature dihydroxylysinoxorleucine (DHLNL) crosslinks in the repair tissue of the implant-treated group also were on par with native tissue crosslink content (Supplementary Table 3). In contrast, collagen type III was 53.9% lower in repair tissue of implant-treated discs than in fill tissue of controls, which contained 2.2-times more collagen type III than native TMJ disc (Figure 5C). Because collagen type III is associated with scarring³⁰, it is possible that the lower mechanical properties of the control fill tissue resulted from scar tissue formation; scar tissues have previously been shown to have inferior mechanics compared to healthy tissues³¹. The full bottom-up proteomics results for fill and repair tissues are reported in Supplementary Table 4. Overall, repair tissue from implant-treated discs displayed a matrix composition biomimetic to native TMJ discs, unlike the inferior scar-like tissue of control discs.

Implantation of tissue-engineered neocartilages resulted in no abnormal systemic effects

Following surgery, animals were returned to their pens and examined daily for behavior and food intake. Within 2 hours of surgery, animals were alert and ambulating. In the days following surgery, animals were provided a soft diet and water bowls as opposed to spigots to minimize joint loading. Throughout the study, jaw function continued, and minipigs maintained or gained weight. Animals were then euthanized at the predetermined timepoint (i.e., 4, 8, or 24 weeks). Full body necropsy was then performed to examine signs of toxicity due to the implant. All organ systems including the integumentary, cardiovascular, respiratory, musculoskeletal (other than the

TMJ), digestive, urogenital, endocrine, and nervous systems displayed normal morphology and exhibited no signs of cellular damage, inflammation, or neoplastic growth.

To examine the systemic response to tissue-engineered implants, a complete blood count and comprehensive metabolic panel were performed (Figure 6, Supplementary Table 5). Implants were well-tolerated with little to no differences in white blood cell counts from baseline values (WBC column, Figure 6A). A few animals exhibited large increases in eosinophils in the implant-treated group (Figure 6A), indicating eosinophilia, but the direct cause could not be directly attributed to implant treatment. Specifically, it was noted that little to no eosinophils were found in histological sections of implant-treated animals (Figure 3, Figure 7), suggesting a cause other than implant treatment. Otherwise, all blood count parameters were within normal ranges (Supplementary Table 5). In the comprehensive metabolic panel, all values were within normal limits, and little to no differences were observed for all analytes (Figure 6B). Overall, tissue-engineered implantation did not result in any adverse systemic effects.

Tissue-engineered implants were well-tolerated immunologically

After surgery, acute joint swelling occurred for every animal, consistent with surgical intervention of the TMJ. After 2 weeks, joint swelling subsided in both groups, and all incisions were completely healed upon suture removal. The incision site had minimal scarring present at animal euthanasia. After euthanasia, TMJs were excised *en bloc* for examination and analysis, and there was no sign of inflammation or neoplastic growth. In all animals, the joint capsule was intact and appeared morphologically normal. The synovium appeared normal, and synovial fluid volume was minimal and clear in color, similar to a healthy joint. Histologically, the synovium showed no abnormal cellular response and was nonreactive in both control and implant-treated joints (Supplementary Figure 5).

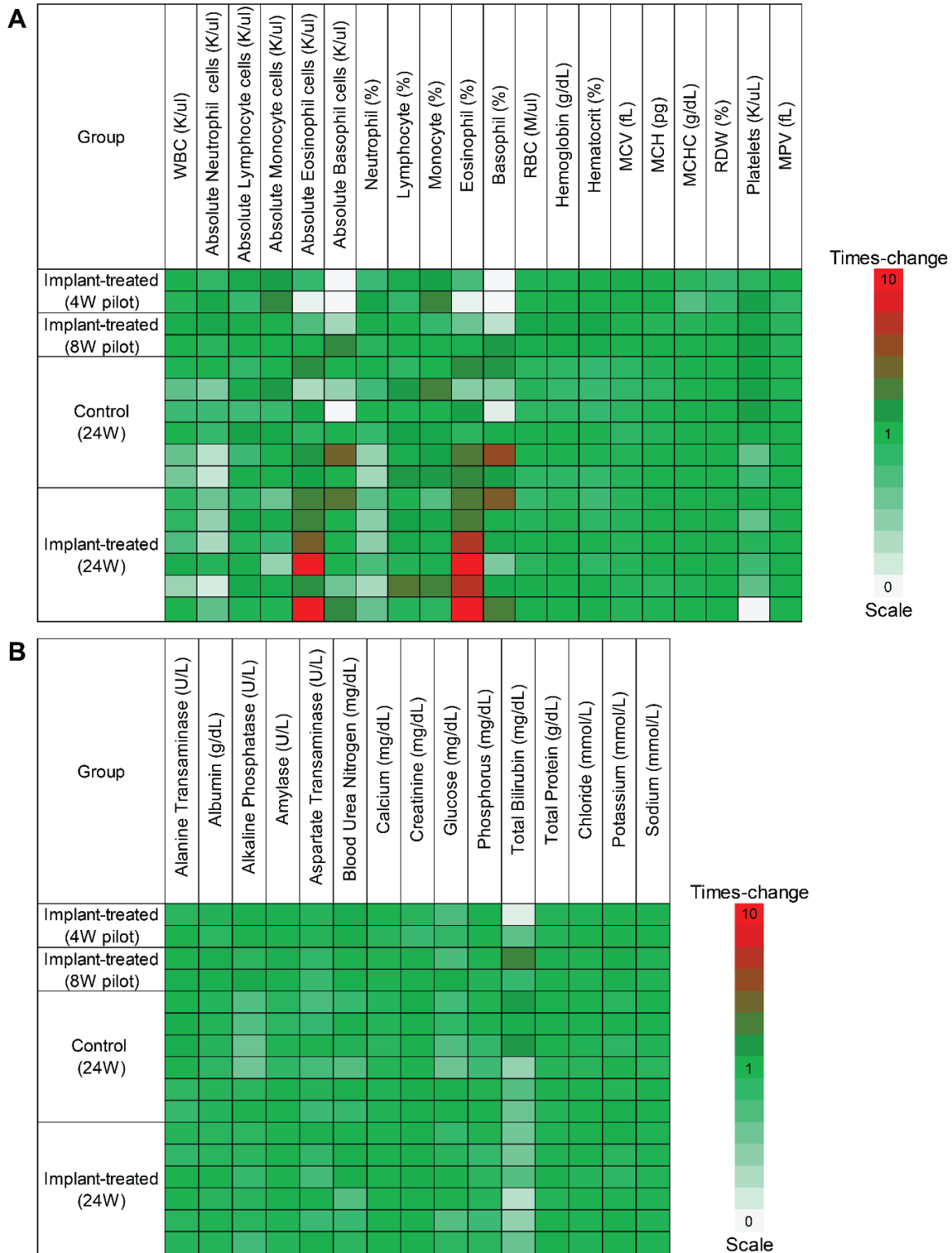


Figure 6. Heatmap of normalized complete blood count and comprehensive metabolic panel parameters show no abnormal systemic effects. (A) The complete blood count and (B) comprehensive metabolic panel parameters were normalized to the pre-operative values. Each row represents a different animal. Eosinophils and basophils showed some large changes from pre-operative values but could not be attributed to implant treatment.

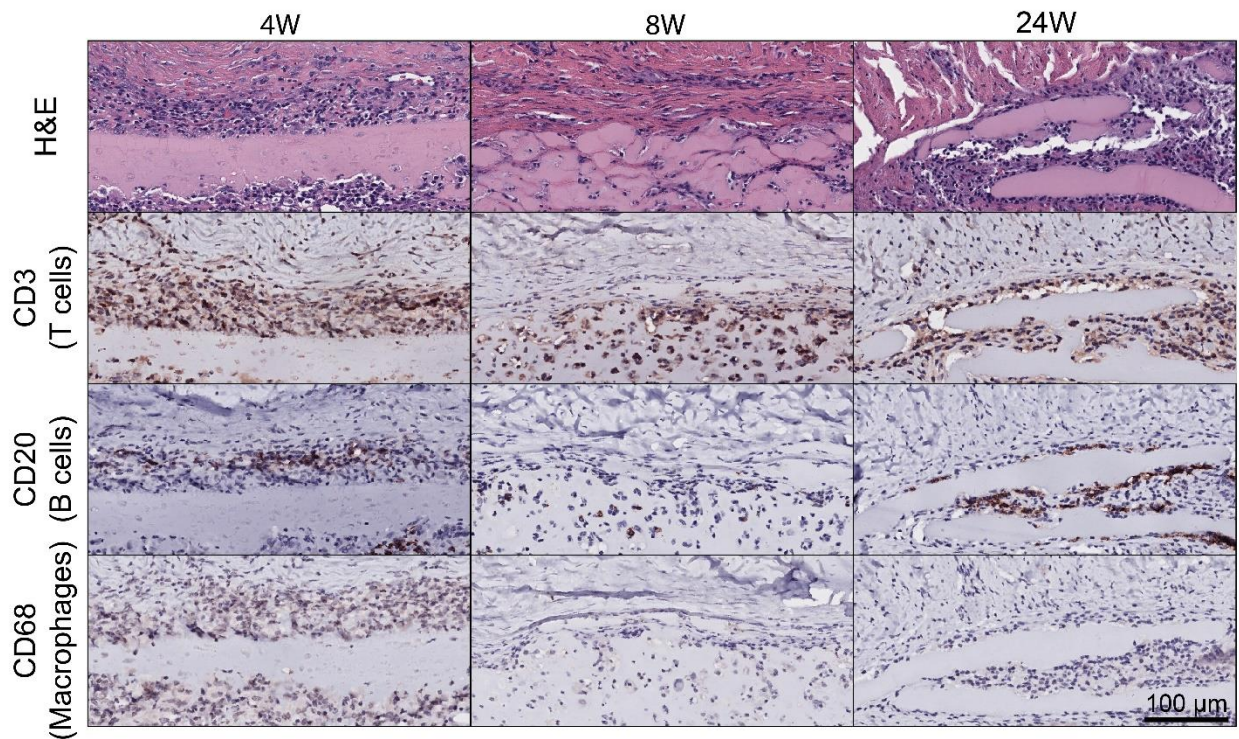


Figure 7. Immunohistochemical staining for T cells, B cells, and macrophages showed immunogenic tolerance to tissue-engineered implants. Over time, cellularity decreased as seen in H&E, while T cell (CD3) and B cell (CD20) staining remained relatively consistent. CD68 staining for macrophages decreased.

When examining the local immune response to tissue-engineered implants in the TMJ disc, cellularity around the implant generally decreased over time between 4 and 8 weeks, while animals at 24 weeks exhibited similar overall cellularity compared to animals after 8 weeks (Figure 7), indicating that the animals were reaching a steady state in terms of the immune response to the implant. Specifically, when considering immunohistochemical staining for CD3 (T cells), CD20 (B cells), and CD68 (macrophages) (Figure 7) with the appropriate positive and negative controls (Supplementary Figure 6), it became apparent that immune cells were mounting a response to the implant. Specifically, T cells and B cells were sustained throughout all timepoints, being located around the periphery of the implant (Figure 7). However, macrophage numbers generally decreased over time (Figure 7). Additionally, through H&E staining, no multinucleated giant cells,

polymorphonuclear cells, or capsule formation were noted (Figure 7). Thus, implants were well-tolerated immunogenically over time.

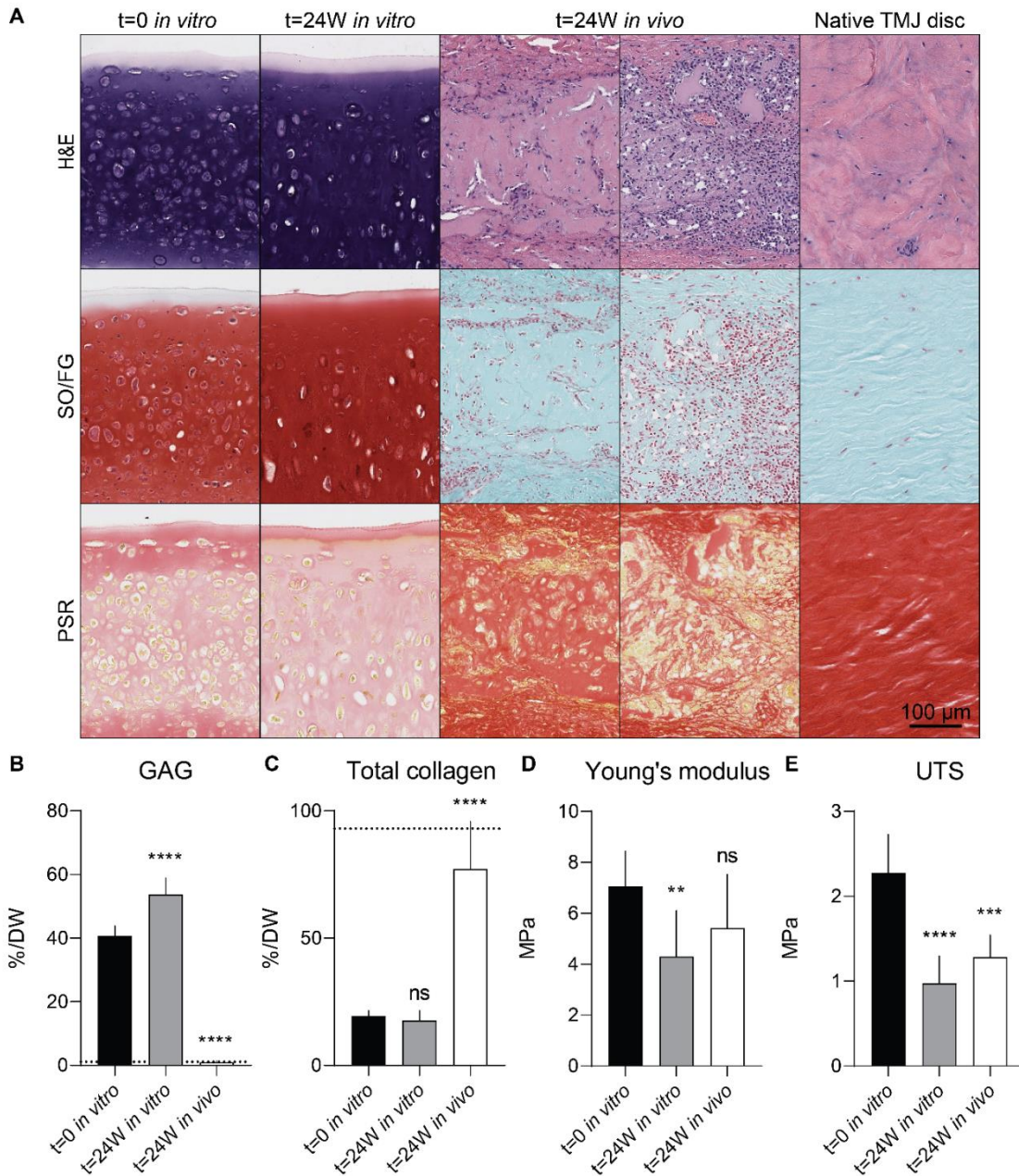


Figure 8. Histological and biochemical properties of neocartilages after implantation showed remodeling toward native TMJ discs. (A) In terms of matrix content, safranin O staining with fast green counterstaining (SO/FG) and picrosirius red staining (PSR) followed quantitative trends of (B) glycosaminoglycan (GAG) content and (C) total collagen content. (D) Young's modulus and (E) ultimate tensile strength (UTS) also decreased across extended culture. Dashed lines represent native TMJ disc values. ns, not significant.

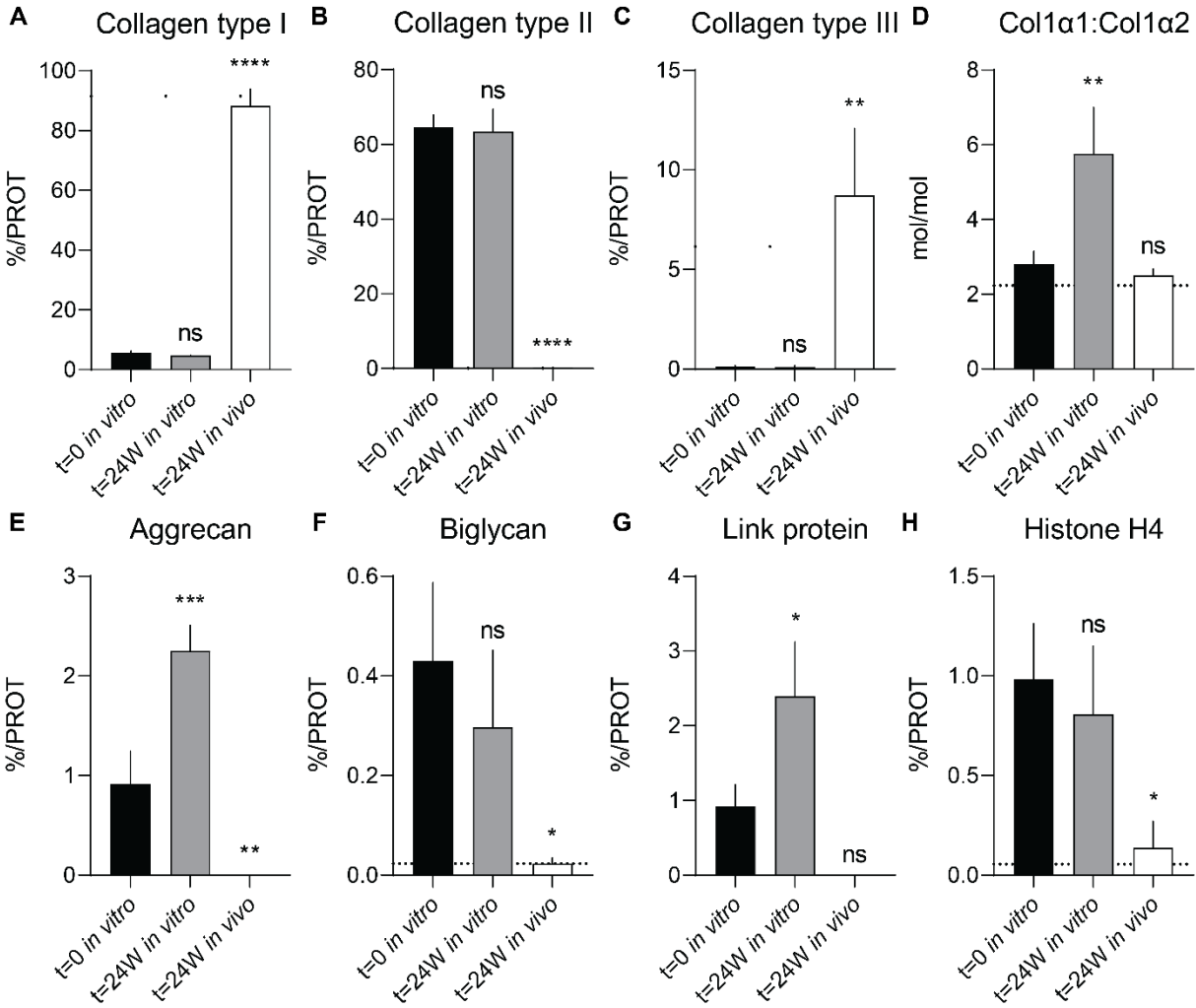


Figure 9. Bottom-up proteomic analysis of neocartilages after implantation also showed remodeling toward native TMJ disc content. Bottom-up proteomics data are presented per total protein (PROT) as a percentage. (A) Collagen type I increased toward native TMJ disc values, while (B) collagen type II decreased. (C) Collagen type III and (D) the ratio between the two collagen type I alpha chains are presented. (E) Aggrecan, (F) biglycan, and (G) link protein all decreased after implantation, and (H) histone H4 followed the trends in cellularity as seen in histology. Dashed lines represent native TMJ disc values. ns, not significant.

Tissue-engineered implants remodeled to a native-like tissue

Tissue-engineered implants remodeled after 24 weeks to a native-like tissue. Compared to *in vitro* controls cultured alongside the study, the *in vivo* implants after 24 weeks exhibited matrix components reminiscent of a native TMJ disc; GAG content (stained by SO/FG) drastically decreased while collagen content (stained by PSR) increased (Figure 8A). GAG and collagen content of *in vivo* implants after 24 weeks were 87.1% and 82.8% of native tissue values (indicated by dashed lines), significantly lower and higher, respectively, when compared to t=0 *in vitro*

controls (Figure 8B-C). *In vitro* implants cultured for another 24 weeks after implantation were not significantly different in collagen content compared to values at implantation (Figure 8C). Remodeling toward a native-like tissue is further corroborated when examining analytes from bottom-up proteomics (Figure 9, Supplementary Table 4). For example, the implant was initially high in collagen type II ($64.54 \pm 3.36\%$ /PROT), which was remodeled toward the native TMJ disc content, having $88.29 \pm 5.55\%$ /PROT collagen type I and $0.21 \pm 0.13\%$ /PROT collagen type II after 24 weeks of implantation (Figure 9A-B). Collagen type III, which is present in low levels in the native TMJ discs due to colocalization with collagen type I, also rose to $8.73 \pm 3.36\%$ in implants after 24 weeks *in vivo* (Figure 9C). Aggrecan, biglycan, and link protein all were drastically lower in *in vivo* implants compared to *in vitro* controls, similar to native TMJ discs (Figure 9E-G). Histone H4, involved with chromatin structure, decreased by 86.7% after implantation *in vivo* (Figure 9H), which was consistent with the decrease in cellularity of the implant observed in H&E staining (Figure 8A).

For mechanical properties, Young's modulus and UTS significantly dropped 39.0% and 57.2% after 24 weeks of *in vitro* culture, but *in vivo* implants only dropped significantly by 43.6% in UTS dropped after 24 weeks (Figure 8D-E). Concurrently, as was seen through H&E staining (Figure 8A), the implant was broken down by the immune cells surrounding the implant *in vivo*, which was likely weakening its structure as repair tissue was regenerated. This reduction in tensile properties was also reflected in PYR content, commonly associated with tensile properties³², which was only 46.5% of native tissue levels by DW after 24 weeks of implantation (Supplementary Table 6). Despite this, the ratio of mature to immature crosslinks (PYR:DHLNL) in implants significantly rose after 24 weeks toward levels of native tissue (Supplementary Table 6). Additionally, despite similar collagen quantities between $t=0$ and $t=24W$ *in vitro* controls (Figure 8C), tensile properties of the implants cultured *in vitro* also dropped between these two points. When examining the ratio of Col1 α 1 and Col1 α 2 as quantified by bottom-up proteomics, the native tissue had a ratio of approximately two (Figure 9D), as would be expected in native tissues

composed of collagen type I³³. Previous studies which examined the mechanical properties of homotrimeric forms of collagen type I, where collagen type I molecules form from three Col1 α 1 chains rather than the typical two Col1 α 1 chains and one Col1 α 2 chain, noted weakening of the tissue in disease-states where this occurred³³. The same weakening may be occurring in the extended *in vitro* culture as the ratio between the two alpha chains increased over 2-times that of the ratio at implantation (i.e., t=0 *in vitro*) and of native TMJ disc (Figure 9D). Compressive properties, which increased with GAG content *in vitro* but were not measured in *in vivo* implants due to tissue availability, are reported in Supplementary Table 7. Despite these temporal drops in tensile properties of excised implants, their biochemical components remodeled toward native tissue values of TMJ discs.

Discussion

The objective of this study was to investigate the safety and efficacy of long-term implantation of costal chondrocyte-derived, self-assembled neocartilage implants in TMJ disc perforations. The hypothesis that repair tissue would have a collagen profile similar to native tissue with superior mechanical properties compared to control fill tissue was supported by the *in vivo* data. Implant-treated discs exhibited mechanically robust healing of perforation defects with repair tissue that mimicked the native TMJ disc biochemically. In contrast, control fill tissue consisted of a biochemical make-up consistent with scar tissue formation, which led to inferior functional properties. Compared to the control fill tissue, the repair tissue of implant-treated discs was 615.4% tougher, 894.5% more resilient, and 340.8% stronger. Additionally, implants underwent significant remodeling; both total collagen and GAG content converged toward native TMJ disc biochemical values. Systemic safety of tissue-engineered implants, as analyzed through necropsy, complete blood counts, and comprehensive metabolic panels, was confirmed. As examined by staining for general cellularity via H&E and immunohistochemical staining for immune cells, the implants were immunogenically well-tolerated over time. This study supports

the safety and efficacy of self-assembled TMJ disc implants for long-term healing of disc perforation defects. The data presented here are significant in demonstrating the feasibility of using TMJ disc implants in future clinical studies examining TMJ disc healing in humans.

This study showed that self-assembled implants that underwent expansion, rejuvenation, and self-assembly were suitable for allogeneic, nonhomologous implantation. Previously, our group showed that self-assembled, allogeneic implants derived from expanded and rejuvenated costal chondrocytes were suitable for nonhomologous use in the TMJ disc¹⁸. Despite being only within the lower range of reported tensile properties in native tissue²⁰, the TMJ disc implants used here, with an average tensile Young's modulus of 7.05 MPa and UTS of 2.28 MPa, survived the joint loading environment after implantation. As a result, implants surgically placed into discs remodeled over 24 weeks. After 24 weeks, implants still retained more than 50% of their original tensile values. Because the implants survived, their regenerative capacity was activated which allowed for native-like recapitulation of functional properties in the repair tissue and remodeling of the implant over time. Over the 24 weeks examined here, the neocartilage implants proved to be crucial in regenerating the minipig TMJ disc, because controls treated without an implant had inferior mechanical, biochemical, and proteomic properties of their fill tissue.

All implant-treated TMJ discs exhibited healing as indicated by gross morphology, but control discs also exhibited a degree of tissue fill. The gross healing response of both groups exhibited a wide range of morphologies, but implant-treated discs appeared better than those of controls. Furthermore, the repair tissue of implant-treated discs had significantly improved mechanical outcomes compared to fill tissue of controls. Thus, gross morphology may not be the best indicator of a robust healing outcome. Since control fill tissue did not exhibit mechanical robustness, one can expect that the untreated discs may further degenerate with time. This may be due to stress concentrations that develop at the interface between the softer control fill tissue and the stiffer healthy native tissue. This is well documented in knee articular cartilage. For example, when a focal defect develops in articular cartilage, stress concentrations develop in

adjacent native cartilage which can induce cell death and, eventually, degeneration³⁴. In the TMJ disc, an analogous process would occur at the interface between fill tissue and native fibrocartilage, causing accelerated degeneration which may necessitate future disc removal or total joint replacement in the analogous human TMDs¹. Thus, use of a tissue-engineered implant to achieve native-like properties of the TMJ disc has potential to halt the degenerative processes in the joint since the TMJ disc is central to TMDs^{1,12}.

Similar to the TMJ disc, the condyles showed heterogeneity in osteoarthritic changes as a result of implantation of a tissue-engineered therapeutic into the TMJ disc. There was no significant difference in OA scoring of joints which received an implant compared to those that did not, indicating that the changes in condylar degenerative status are most likely a direct result of surgical intervention in the TMJ disc. For example, in the approach described here, the Mitek anchor sutures pass over the condylar process and small portions of the condyle's articulating surface depending on the individual animal anatomy. This may have caused some degeneration in the areas where the suture contacts the articular cartilage; this phenomenon has been previously reported in the knee²⁹. However, a vast majority of the articulating surface in the condylar head was spared of abrasions, with most degenerative changes only appearing on the condylar process where the suture was placed and a small portion of the articulating surface. Given the double-armed nature of these bone anchor sutures, future studies using the surgical techniques described here may consider only using one arm of the suture to secure the disc or alternative methods to preserving the lateral attachment. Despite the minor degenerative changes seen on the adjacent articulating surface, the use of the intralaminar perforation surgical technique was crucial toward achieving TMJ disc regeneration using a tissue-engineered implant.

It was shown that the tissue-engineering approach in this perforation defect model resulted in robust repair tissue that was similar to the native TMJ disc. Specifically, the repair tissue of implant-treated discs was similar to native tissue in terms of toughness, resilience, UTS, and strain at failure. Additionally, repair tissues were significantly tougher, more resilient, and stronger

than the fill tissue of empty defects. Given the structure-function relationships of the matrix content and tissue mechanical properties, the composition of the repair tissue compared to the fill tissue was investigated. Repair tissue in the implant-treated group had significantly more collagen type I, the main collagen type found in the TMJ disc. Collagen type III, which is also present in the TMJ disc at low levels³⁵, was found to be significantly greater by more than 2-times in fill tissue of empty defects compared to native or repair tissue. This is consistent with scar tissue, where collagen type III is elevated over normal levels and mechanical properties decrease³⁶. Given the TMJ disc's mechanical loading under large tensile strains, this is a significant finding which explains the inferior mechanical properties of empty defect fill tissue. The tissue-engineered implant placed in the TMJ disc facilitated more collagen type I deposition which improved repair tissue mechanics toward that of native tissue, in direct opposition to what was seen in controls.

TMJ disc implants demonstrated exceptional systemic safety in the Yucatan minipig model in this study. As examined during necropsy, organ systems displayed no neoplastic growth or abnormalities, demonstrating that the implants do not exhibit systemic tumorigenicity. This finding was further corroborated by the complete blood count and comprehensive metabolic panel outcomes; there was minimal reaction to the tissue-engineered implant as indicated by the bloodwork. Within the joint space, after 4, 8, or 24 weeks, there was no synovium reaction and no neoplastic growth, indicating that chondrocytes within the implant do not have any effects outside of the TMJ disc. Ultimately, the long-term *in vivo* data show that self-assembled neocartilages were systemically safe for implantation into the TMJ disc, which is a promising step toward seeking future regulatory approval for use in humans.

After implantation *in vivo*, there was a cellular response surrounding and infiltrating the neocartilage as shown through H&E staining. Through immunohistochemical staining for CD3, CD20, and CD68 for T cells, B cells, and macrophages, respectively, it was apparent that the cells surrounding the implant were immune cells. T cells and B cells were present throughout the three timepoints examined, indicating that there was a steady state immune response after

implantation; however, CD68 staining decreased over time. While CD68 is typically associated as a pan-macrophage marker, recent studies have shown that it may be a marker of an inflammatory macrophage phenotype^{37,38}. Given the decrease in CD68 staining between 4 and 24 weeks, the acute inflammatory immune response was shown to resolve. In agreement with previous studies examining macrophage response in natural healing cascades³⁹, over time, it was expected that macrophages polarized toward a pro-healing response. Additional work is necessary to confirm macrophage polarization, such as staining discal sections for pro-healing macrophage markers like CD163⁴⁰. Additionally, this phenomenon might be examined by looking at *in vitro* cocultures of implants with macrophages polarized toward different states⁴¹. Ultimately, implants facilitated a long-term healing response toward TMJ disc regeneration as evidenced by not only immunohistochemistry but the long-term mechanical healing of implant-treated discs.

Implants undergo progressive remodeling throughout the long-term healing response. As evidenced by histological and biochemical data, the implant is being remodeled to resemble native tissue. For example, the implant increased in collagen and decreased in GAG content toward levels of native TMJ discs, reaching 82.8% and 87.1% of native tissue values, respectively. This was further corroborated by the bottom-up proteomics analysis, which showed that GAG-associated proteins, such as aggrecan and link protein, likewise converged toward native TMJ disc levels. Moreover, the collagen type II-rich neocartilage (64.54%/PROT) remodeled to a collagen type I-rich tissue (88.29%/PROT) after implantation, and collagen type III increased to native tissue levels. Importantly, collagen type III in implants (8.73%/PROT) after 24 weeks was lower than that found in fill tissue of control discs (13.74%/PROT), indicating that the remodeling was toward native tissue-like regeneration and not scar tissue. Given these biochemical changes, it would be expected that mechanical properties would increase as well, but the opposite was shown; UTS significantly decreased by 43.5% over 24 weeks of implantation. For the *in vitro* controls cultured under a static environment, Col1 α 1:Col1 α 2 ratio increased over 24 weeks of culture, reminiscent of diseased tissues³³. In contrast, excised *in vivo* implant maintained a similar

Col1 α 1:Col1 α 2 ratio to native tissue indicating that the orthotopic location is a more appropriate environment for TMJ disc implant remodeling. Most importantly, the remodeled implant activated the regenerative capacity of the TMJ discs and produced repair tissue that was more mechanically robust and biomimetic than fill tissue of controls.

This study generated significant preclinical data toward demonstration of safety and efficacy of TMJ disc implants in healing perforation defects. For safety, both the systemic and local responses showed that implants were well-tolerated. Although there was a local immune response at 4 weeks, it resolved toward a steady state response, indicating that implants were immunogenically well-tolerated. Additionally, implants remodeled toward the native TMJ disc biochemical makeup. Ultimately, neocartilage implants resulted in the regeneration of fibrocartilaginous repair tissue in implant-treated discs. In terms of efficacy, repair tissue exhibited more collagen type I, indicative of TMJ disc regeneration, and less collagen type III, indicative of scar tissue formation, compared to fill tissue in the control group. The repair tissues of implant-treated discs had robust mechanical properties, which all reached native TMJ disc values, and were many times higher in toughness, resilience, strength, and strain at failure than control fill tissues. Given the regenerative capacity of tissue-engineered implants in the TMJ disc, future interventions may be able to halt the degenerative processes, thus avoiding the need for discectomy or total joint replacement. However, there are many hurdles that need to be overcome prior to translation of TMJ disc implants to widespread human use, including both scientific and regulatory hurdles¹. This study paves the path toward eventual widespread use of tissue-engineered TMJ disc implants in the millions of people experiencing intractable pain and dysfunction as a result of TMDs.

Materials and methods

Tissue engineering of implants

Three juvenile Yucatan minipig donors (males, 5-8 months), culled for reasons unrelated to this study, were used for costal chondrocyte sourcing, as previously described²⁴. Briefly, costal cartilage was exposed using sterile tools in a biosafety cabinet, perichondrium was removed, and costal cartilage was minced to approximately 1 mm³ sized pieces. Costal cartilage pieces were digested in 0.4% (w/v) pronase for 1 hour at 37°C and then in 0.2% (w/v) collagenase for 18 hours at 37°C. Enzymes were resuspended in Dulbecco's modified Eagle's medium (DMEM, high glucose, GlutaMAX supplement) with 3% fetal bovine serum (FBS) and 1% penicillin-streptomycin-fungizone (PSF). After collagenase treatment, single-cell suspensions were filtered using 70 µm cell strainers and treated with ammonium-chloride-potassium lysis buffer, as previously described⁴².

After lysis buffer treatment, chondrocytes were plated in T225 flasks at 2.5M cells per flask (~11,111 cells/cm²) in chondrogenic (CHG) medium (DMEM, 1% PSF, 1% nonessential amino acids, 1% insulin-transferrin-selenous acid+, 100 nM dexamethasone, 50 µg/mL ascorbate-2-phosphate, 40 µg/mL L-proline, 100 µg/mL sodium pyruvate). Expansion medium consisted of CHG medium supplemented with 2% FBS, 1 ng/mL TGF-β1, 5 ng/mL basic fibroblast growth factor (bFGF), and 10 ng/mL platelet-derived growth factor (PDGF)²⁵. During expansion, medium was changed every 3-4 days. Chondrocytes were frozen in FBS containing 10% dimethyl sulfoxide (DMSO) after one passage, then thawed for continued downstream expansion. Passaging consisted of lifting cells with 0.05% trypsin-EDTA treatment for 9 minutes, followed by digestion of the lifted cells with 0.2% (w/v) collagenase in DMEM with 3% FBS and 1% PSF for 30 minutes (37°C, agitation every 10 minutes). After three passages, cells underwent aggregate rejuvenation, as previously described²⁶. Aggregate rejuvenation medium consisted of CHG medium supplemented with 10 ng/mL TGF-β1, 100 ng/mL growth differentiation factor 5 (GDF-5), and 100 ng/mL bone morphogenetic protein 2 (BMP-2). During aggregate rejuvenation,

medium was changed every 3-4 days. After 11 days, aggregates were digested in 0.05% trypsin-EDTA for 45 minutes and 0.2% (w/v) collagenase in DMEM with 3% FBS and 1% PSF for 90 minutes (37°C, agitation every 10 minutes). After collagenase treatment, the solution was filtered with 70 µm cell strainers to yield a single-cell suspension.

After aggregate rejuvenation, self-assembly of neocartilage was performed, as previously described⁴³. Briefly, nonadherent wells of 8x13 mm were made using molten 2% agarose and negative molds. Wells were hydrated with CHG medium, which was changed three times prior to cell seeding. Cells (7M/implant) were seeded into each well with 300 µL of CHG medium. After 4 hours, 2 mL of CHG medium was added, and medium was exchanged every day up until day 2, at which point implant were unconfined by releasing them from the wells. From unconfining to end of culture at day 28, neocartilage implants were fed with 7 mL of CHG medium every other day. After day 2 of self-assembly, CHG medium was supplemented with TGF-β1 (10 ng/mL). At day 7 of self-assembly, C-ABC was applied for 4 hours at 1.5 U/mL in CHG medium²⁷. C-ABC was activated using 50 mM sodium acetate and quenched using 1 mM zinc sulfate. Passive axial compression was applied from days 10-14 as a mechanical stimulus and to keep implants flat²⁷. From day 14 of self-assembly onward, LOXL2 was added to the CHG medium at 0.15 µg/mL, along with 0.146 mg/mL hydroxylysine and 1.6 µg/mL copper sulfate.

The day prior to surgery, implants for *in vivo* use were placed on ice (4°C) in a 50 mL conical tube with HEPES-buffered CHG medium supplemented with TGF-β1 and LOXL2 for transportation to the veterinary operating room (7 hours). Upon arrival, implants were placed in an incubator at 37°C for equilibrium prior to surgery the following day. The remaining implants (n=9) were split in half under sterile conditions. Half of the implant was used to establish baseline properties prior to implantation as a control (t=0 *in vitro*). The other half remained in culture until animal sacrifice to serve as a measure of *in vitro* remodeling (t=24W *in vitro*).

In vivo experiments

All animal work was approved by the UC Irvine (#AUP-21-033) and UC Davis (#21430) Institutional Animal Care and Use Committees (IACUCs). This study consisted of 16 Yucatan minipigs (n=4 males, n=12 females). For initial pilot studies, two male animals at both 4 and 8 weeks (n=4 total) were used for initial feasibility studies prior to initiating long-term studies (i.e., 24 weeks). For 24-week timepoints, female minipigs (n=12 total) were used; six minipigs were designated as empty defect controls, while the remaining six minipigs received a tissue-engineered implant.

Presurgical medication and anesthesia

Yucatan minipigs were fasted for 24 hours prior to surgery. Animals were pretreated with Telazol (tiletamine/zolazepam) at 3-6mg/kg via intramuscular (IM) administration. An intravenous (IV) catheter was used in the auricular vein for administration of lactated Ringer's solution at 5-10 mL/kg/hr and other medications. Anesthesia was induced using ketamine at 5 mg/kg and diazepam at 0.2-0.5 mg/kg, as well as isoflurane delivered via facemask. Minipig larynxes were treated with 2% lidocaine (1-2 mL) prior to intubation with a cuffed endotracheal tube (sized based on individual animal). Preemptive analgesia was provided with morphine at 0.5 mg/kg via IM delivery. Throughout surgery, anesthesia was maintained with 1-3% isoflurane in 100% oxygen. End-tidal carbon dioxide was maintained between 35-45 mmHg via positive ventilation. Monitoring via capnography, electrocardiography, thermometer, and blood pressure measurements was performed throughout surgery. Animal body temperature was maintained at physiological temperature (37-38°C) via a heating pad.

Surgical implantation and defect creation

As previously described¹⁸, prior to surgical intervention, the lateral side of the head was shaved and aseptically prepared for surgery using iodine-based solutions followed by alcohol (Figure 2A). Subsequently, an approximately 10cm curvilinear incision along the curvature of the ventral

aspect of the zygomatic arch and extended superiorly over the temporal process of the zygoma toward the ear was made with a #15 blade (Figure 2B) followed by blunt dissection through the subcutaneous adipose tissue and the periosteum. Using a periosteal elevator, the masseter muscle was reflected ventrally and posteriorly, and the tissues of the TMJ were identified, including the condylar process and the mandibular head, the masseter muscle that attaches to the condylar process, and the lateral TMJ disc attachments. Using sharp dissection, the tissue was thinned to further identify the lateral aspects of the joint. The condylar process was subsequently exposed using a combination of sharp and blunt dissections. Using a sharp elevation of the superior TMJ disc attachments of the joint capsule, the superior joint space was exposed. An incision through the inferior TMJ disc attachments of the joint capsule (below the disc) exposed the inferior joint space. The disc and articular cartilages were protected during all blunt and sharp dissections through the joint capsule.

At this juncture, the lateral, superior and inferior aspects of the disc were exposed (Figure 2C). Using 3.5x loupe magnification, the intralaminar incision was created in the lateral edge of the disc using a #15 scalpel blade, yielding an incision approximately 12 mm wide. This incision was deepened into the disc to create a pouch with an inferior and superior lamina measuring approximately 12 mm deep by 12 mm wide (Figure 2D). The lateral edges of the laminae were then grasped and held together while a 3 mm diameter disposable biopsy punch was pushed through both laminae, creating a full thickness perforation defect in the centrolateral region of the disc (Figure 2E, Supplementary Figure 1). Careful manipulation of the biopsy punch ensured that adjacent articulating surfaces were not damaged. A tissue-engineered implant measuring 8x8 mm (Figure 1C) was placed between the two laminae (Figure 2F), and the pouch was closed on the lateral margin using a 5-0 Monocryl suture in a simple interrupted fashion (Figure 2G). The suture was not passed through the implant. The TMJ disc was reattached to the lateral component of the condylar process using a Mitek bone anchor (QuickAnchor Plus, #0 suture)⁴⁴. A Jacob's chuck was used with the supplied 2.0x9.7 mm drill bit to pre-drill a hole prior to placement of the

bone anchor with self-expanding flanges. The suture was then used to secure the lateral edge of the TMJ disc to the condylar process (Figure 2H). The remaining layers of tissue, including the joint capsule and masseter muscle, were closed using 3-0 Monocryl suture.

Postoperative medication and animal care

For postoperative analgesia, minipigs were administered a mixture of meloxicam at 0.1-0.4 mg/kg via IV, IM, or oral delivery once daily for 3 days, fentanyl at 1-5 µg/kg/hr via patch for 3 days, and buprenorphine at 0.005-0.05mg/kg via a single IM dose. Minipigs also received a single dose of perioperative antibiotics. Until ambulation and mentation, minipigs were closely recovered and observed in narrow padded pens and monitored for postoperative complications. The animals were then returned to their normal housing pens. For diet, a soft diet (i.e., liquid yogurt, softened pellet food) was provided for 3 days after surgery. Additionally, water bowls were provided for animals instead of standard spigots to minimize postoperative joint loading. Sutures were removed 14 days after surgery.

Animal euthanasia

After 4 weeks, 8 weeks, or 24 weeks, minipigs were humanely euthanized with an IM injection of Telazol (3-6 mg/kg) followed by an IV injection of Euthazol (phenytoin/pentobarbital, 1 mL/4.5kg). Upon animal euthanasia, a veterinary pathologist carried out a full necropsy examining organ systems for any signs of toxicity or neoplastic growth. The TMJ discs and the mandibular heads on the condylar process were removed *en bloc* as one unit.

TMJ sample preparation

Prior to any dissections, TMJ tissue samples were documented photographically. Discs were subsequently removed from the condyle, and the condyle and disc were photographed from multiple angles and views. A small amount of synovium from the inner lateral wall of the inferior joint space was excised for histological analysis. Condyles were also kept for histological analysis.

Upon documentation, discs were sectioned anteroposteriorly to identify the implant location and/or the repair or fill tissue (Supplementary Figure 7). Careful dissection of the disc was guided by gross morphology images of the disc and observation of irregularities that indicated the location of fill/repair tissue. From these sections, the following samples were identified: implant histological section, implant tensile testing sample, fill/repair tissue tensile testing sample, intralaminar tensile testing sample, implant biochemistry sample, fill/repair tissue biochemistry sample, implant mass spectrometry sample, and fill/repair tissue mass spectrometry sample. Contralateral samples from the centrolateral region of the disc were also excised for use as native tissue controls.

In vitro sample preparation

At time of implantation ($t=0$) and at animal euthanasia ($t=24W$), halves of *in vitro* (non-implanted) implants were sectioned into samples for histological analyses, compressive stress-relaxation testing, uniaxial tensile testing, biochemical testing, and mass spectrometry analyses.

Histology and immunohistochemistry

Synovium, condyle, and disc samples were fixed in 10% neutral buffered formalin for at least 72 hours. After fixation, condyles underwent decalcification with 10% formic acid and were grossly cut to capture any osteoarthritic changes on the articulating surface of the condyle. Samples were subsequently processed, embedded in paraffin wax blocks, sectioned to 4 μm thickness for immunohistochemistry or 5 μm thickness for all other stains using a microtome, and mounted on microscopy slides. Samples were stained with H&E, SO/FG, and PSR, as previously described⁴⁵. Only H&E was performed for condyle and synovium sections. Immunohistochemistry was performed for CD3 (T cells), CD20 (B cells), and CD68 (macrophages) markers using the primary and secondary antibodies listed with the antigen retrieval method, blocking serums, and developments in Supplementary Table 8, as previously described¹⁸. Whole slide scans were then captured using a Roche VENTANA DP 200 slide scanner, and QuPath software was used to visualize the slides digitally⁴⁶.

Mechanical testing

Samples from *in vitro* controls were subjected to mechanical testing with compressive stress-relaxation tests and uniaxial tensile tests. Compressive stress-relaxation testing was performed on 3 mm diameter sample punches, taken with a disposable biopsy punch. Sample height was detected using a tare load of 0.1 N, and samples were subjected to 15 preloading cycles of 5% strain, as previously described²⁰. Strain of 20% was applied to the punch for 900 seconds until equilibrium. The relaxation modulus, instantaneous modulus, and coefficient of viscosity were determined by fitting the resulting force-displacement curves to a standard linear solid model with a custom MATLAB script. For tensile tests of *in vitro* controls, dog bone-shaped samples were glued to paper tabs of a predefined gauge length. Samples were tested at 1% strain per second until failure. Resulting force-displacement curves were analyzed with a custom MATLAB script to determine the tensile Young's modulus and UTS of samples.

Tissues excised from the TMJ disc underwent uniaxial tensile testing in the anteroposterior direction for the excised implants, fill/repair tissues, and contralateral native tissue samples. Uniaxial tensile tests for intralaminar fusion were performed in the superoinferior direction. Briefly, the samples were clamped using hemostats attached to a uniaxial testing machine (Instron model 5655). Prior to initiating the uniaxial tensile test, a 0.2 N tare load was applied to remove slack from samples. Images were then taken from the front and side of the sample to calculate the cross-sectional area, and the gauge length was measured using a caliper. The gauge length was defined as the pretest grip-to-grip clamping distance. Samples were then tested at 1% strain per second until failure. Resulting force-displacement curves were analyzed with a custom MATLAB script to determine the Young's modulus, UTS, strain at failure, toughness (entire area under the curve), and resilience (area under the curve of linear region only) of tissue samples.

Biochemical testing

Biochemical assays for total collagen and GAG content were performed on *in vitro* control implants, excised *in vivo* implants, excised fill/repair tissues, and excised contralateral TMJ discs. Prior to assays, hydrated samples were weighed to obtain a wet weight (WW) and then lyophilized for at least 72 hours. After lyophilization, samples were reweighed to obtain a DW. Briefly, a modified hydroxyproline assay was used to quantify total collagen⁴⁷ and a dimethylmethylene blue assay kit was used to quantify sulfated GAGs. The total collagen and GAG contents were normalized to DW.

Mass spectrometry analyses for crosslinks quantification and bottom-up proteomics

Pieces of tissue for crosslinks quantification and bottom-up proteomics were split from a singular piece of tissue for mass spectrometry analyses. Collagen crosslink quantification was performed, as previously described³⁵. Briefly, tissue pieces (~1 mg WW) were lyophilized for at least 72 hours, and DWs were measured. Samples were reduced for 1 hr in NaBH₄, washed overnight in ultrapure water, and hydrolyzed in HCl for 18 hours. Hydrolysates were evaporated, resuspended, filtered, and analyzed on a Waters ACQUITY QDa LC-MS system. PYR, DHLNL, hydroxyproline (OHP), and internal standard pyridoxine were quantified by taking the area under the curve of the extracted ion chromatograms of each analyte's mass.

Bottom-up proteomics analysis was performed, as previously described³⁵. Briefly, tissue pieces (~1 mg WW) were lyophilized for at least 72 hours, digested overnight in trypsin in a heat block at 65°C, desalted with Waters Sep-pak C18 cartridges, and analyzed with a Thermo Fisher Scientific Orbitrap Fusion Lumos mass spectrometer. Label-free quantification was performed with MaxQuant⁴⁸ to normalize all identified protein analytes to PROT content.

ICRS scoring

Evaluation of the degenerative, osteoarthritic changes on the condyles was carried out using the International Cartilage Repair Society (ICRS) scoring system⁴⁹. Briefly, H&E slides were analyzed

by a veterinary pathologist to perform histological grading on decalcified sections of condyles. If a sample required two mediolateral sections to be graded, the grades were averaged and reported. A gross stage was also determined by measuring the percentage of the articulating surface affected by osteoarthritic changes (i.e., osteophytes, chondral or osteochondral defects, fibrillation, etc.). The total OA score was calculated by multiplying the gross stage by the histologic grade.

Statistical analyses

Data were analyzed with a Student's t-test or one-way analysis of variance (ANOVA) followed by a *post hoc* Dunnett's test performed using *t=0 in vitro* samples as the control group. All tests were performed and graphs were generated using GraphPad Prism 9. The number of asterisks were representative of the degree of significance; (ns) represents $p > 0.05$, (*) represents $p \leq 0.05$, (**) represents $p \leq 0.01$, (***) represents $p \leq 0.001$, and (****) represents $p \leq 0.0001$.

References

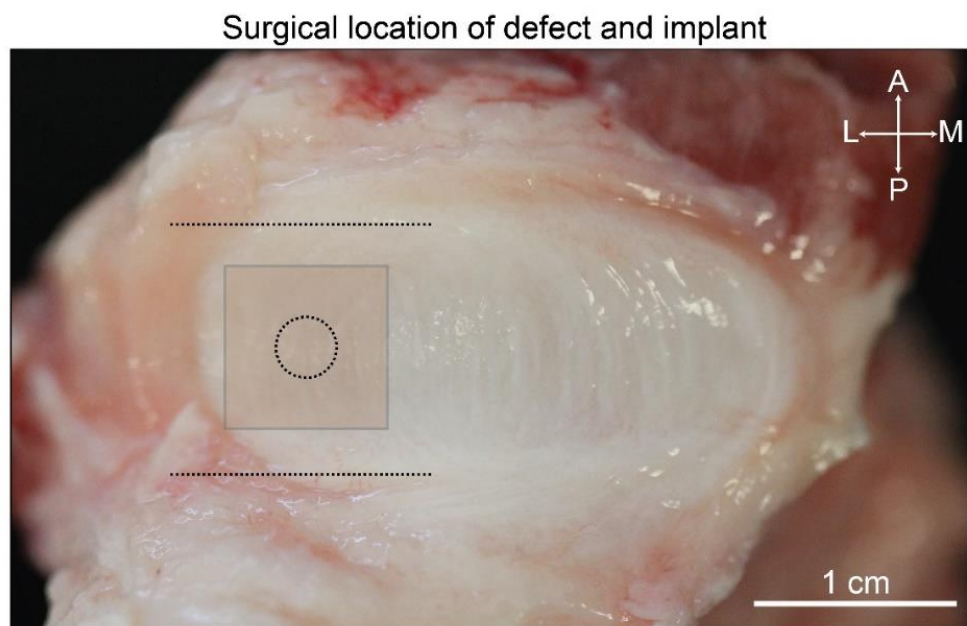
- 1 Donahue, R. P., Hu, J. C. & Athanasiou, K. A. Remaining Hurdles for Tissue-Engineering the Temporomandibular Joint Disc. *Trends Mol Med* **25**, 241-256, doi:10.1016/j.molmed.2018.12.007 (2019).
- 2 Johansson, A., Unell, L., Carlsson, G. E., Soderfeldt, B. & Halling, A. Gender difference in symptoms related to temporomandibular disorders in a population of 50-year-old subjects. *J Orofac Pain* **17**, 29-35 (2003).
- 3 Macfarlane, T. V., Blinkhorn, A. S., Davies, R. M., Kincey, J. & Worthington, H. V. Orofacial pain in the community: prevalence and associated impact. *Community Dent Oral Epidemiol* **30**, 52-60, doi:10.1034/j.1600-0528.2002.300108.x (2002).
- 4 Pow, E. H., Leung, K. C. & McMillan, A. S. Prevalence of symptoms associated with temporomandibular disorders in Hong Kong Chinese. *J Orofac Pain* **15**, 228-234 (2001).
- 5 Goulet, J. P., Lavigne, G. J. & Lund, J. P. Jaw pain prevalence among French-speaking Canadians in Quebec and related symptoms of temporomandibular disorders. *J Dent Res* **74**, 1738-1744, doi:10.1177/00220345950740110401 (1995).
- 6 Solberg, W. K., Woo, M. W. & Houston, J. B. Prevalence of mandibular dysfunction in young adults. *J Am Dent Assoc* **98**, 25-34, doi:10.14219/jada.archive.1979.0008 (1979).
- 7 Schiffman, E. *et al.* Diagnostic Criteria for Temporomandibular Disorders (DC/TMD) for Clinical and Research Applications: recommendations of the International RDC/TMD Consortium Network* and Orofacial Pain Special Interest Group dagger. *J Oral Facial Pain Headache* **28**, 6-27, doi:10.11607/jop.1151 (2014).
- 8 Farrar, W. B. & McCarty, W. L., Jr. The TMJ dilemma. *J Ala Dent Assoc* **63**, 19-26 (1979).
- 9 Katzberg, R. W. & Westesson, P.-L. *Diagnosis of the temporomandibular joint*. 1 edn, (W.B. Saunders, 1993).

- 10 Munoz-Guerra, M. F., Rodriguez-Campo, F. J., Escorial Hernandez, V., Sanchez-Acedo, C. & Gil-Diez Usandizaga, J. L. Temporomandibular joint disc perforation: long-term results after operative arthroscopy. *J Oral Maxillofac Surg* **71**, 667-676, doi:10.1016/j.joms.2012.12.013 (2013).
- 11 Kuribayashi, A., Okochi, K., Kobayashi, K. & Kurabayashi, T. MRI findings of temporomandibular joints with disk perforation. *Oral Surg Oral Med Oral Pathol Oral Radiol Endod* **106**, 419-425, doi:10.1016/j.tripleo.2007.11.020 (2008).
- 12 Bielajew, B. J. *et al.* Knee orthopedics as a template for the temporomandibular joint. *Cell Rep Med* **2**, 100241, doi:10.1016/j.xcrm.2021.100241 (2021).
- 13 Aryaei, A., Vapniarsky, N., Hu, J. C. & Athanasiou, K. A. Recent Tissue Engineering Advances for the Treatment of Temporomandibular Joint Disorders. *Curr Osteoporos Rep* **14**, 269-279, doi:10.1007/s11914-016-0327-y (2016).
- 14 Dolwick, M. F. & Dimitroulis, G. Is there a role for temporomandibular joint surgery? *British Journal of Oral and Maxillofacial Surgery* **32**, 307-313, doi:10.1016/0266-4356(94)90052-3 (1994).
- 15 Dimitroulis, G. Management of temporomandibular joint disorders: A surgeon's perspective. *Aust Dent J* **63 Suppl 1**, S79-S90, doi:10.1111/adj.12593 (2018).
- 16 Li, Q. *et al.* Effect of jaw opening on the stress pattern in a normal human articular disc: finite element analysis based on MRI images. *Head Face Med* **10**, 24, doi:10.1186/1746-160X-10-24 (2014).
- 17 Chin, A. R., Gao, J., Wang, Y., Taboas, J. M. & Almarza, A. J. Regenerative Potential of Various Soft Polymeric Scaffolds in the Temporomandibular Joint Condyle. *J Oral Maxillofac Surg* **76**, 2019-2026, doi:10.1016/j.joms.2018.02.012 (2018).
- 18 Vapniarsky, N. *et al.* Tissue engineering toward temporomandibular joint disc regeneration. *Sci Transl Med* **10**, 1-10, doi:10.1126/scitranslmed.aag1802 (2018).
- 19 Almarza, A. J. *et al.* Preclinical Animal Models for Temporomandibular Joint Tissue Engineering. *Tissue Eng Part B Rev* **24**, 171-178, doi:10.1089/ten.TEB.2017.0341 (2018).
- 20 Vapniarsky, N. *et al.* The Yucatan Minipig Temporomandibular Joint Disc Structure-Function Relationships Support Its Suitability for Human Comparative Studies. *Tissue Engineering Part C: Methods* **23**, 700-709, doi:10.1089/ten.tec.2017.0149 (2017).
- 21 Acri, T. M. *et al.* Tissue Engineering for the Temporomandibular Joint. *Adv Healthc Mater* **8**, e1801236, doi:10.1002/adhm.201801236 (2019).
- 22 Legemate, K., Tarafder, S., Jun, Y. & Lee, C. H. Engineering Human TMJ Discs with Protein-Releasing 3D-Printed Scaffolds. *J Dent Res* **95**, 800-807, doi:10.1177/0022034516642404 (2016).
- 23 Sharma, H., Chowdhury, S., Navaneetham, A., Upadhyay, S. & Alam, S. Costochondral Graft as Interpositional material for TMJ Ankylosis in Children: A Clinical Study. *J Maxillofac Oral Surg* **14**, 565-572, doi:10.1007/s12663-014-0686-9 (2015).
- 24 Donahue, R. P., Nordberg, R. C., Bielajew, B. J., Hu, J. C. & Athanasiou, K. A. The effect of neonatal, juvenile, and adult donors on rejuvenated neocartilage functional properties. *Tissue Eng Part A*, doi:10.1089/ten.TEA.2021.0167 (2021).
- 25 Murphy, M. K., Huey, D. J., Reimer, A. J., Hu, J. C. & Athanasiou, K. A. Enhancing post-expansion chondrogenic potential of costochondral cells in self-assembled neocartilage. *PLoS One* **8**, e56983, doi:10.1371/journal.pone.0056983 (2013).
- 26 Kwon, H., Brown, W. E., O'Leary, S. A., Hu, J. C. & Athanasiou, K. A. Rejuvenation of extensively passaged human chondrocytes to engineer functional articular cartilage. *Biofabrication* **13**, doi:10.1088/1758-5090/abd9d9 (2021).
- 27 Huwe, L. W., Sullan, G. K., Hu, J. C. & Athanasiou, K. A. Using Costal Chondrocytes to Engineer Articular Cartilage with Applications of Passive Axial Compression and Bioactive Stimuli. *Tissue Eng Part A* **24**, 516-526, doi:10.1089/ten.TEA.2017.0136 (2018).

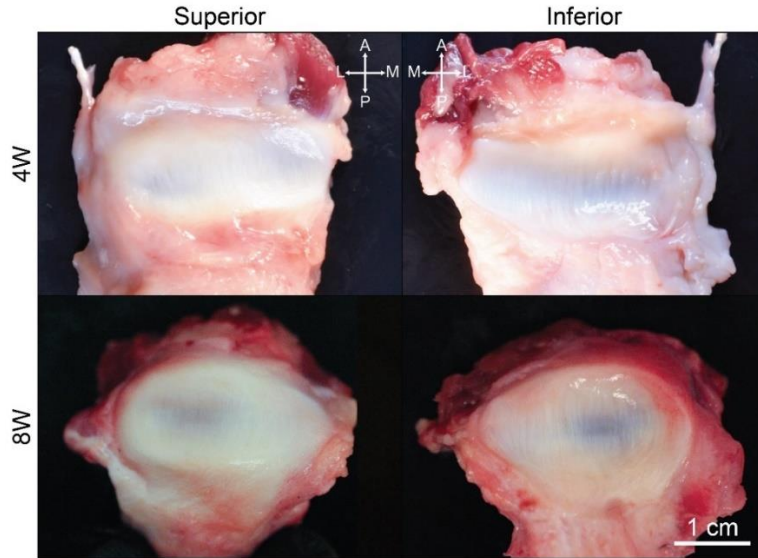
- 28 Kwon, H., O'Leary, S. A., Hu, J. C. & Athanasiou, K. A. Translating the application of transforming growth factor- β 1, chondroitinase-ABC, and lysyl oxidase-like 2 for mechanically robust tissue-engineered human neocartilage. *Journal of Tissue Engineering and Regenerative Medicine* **13**, 283-294, doi:10.1002/term.2791 (2019).
- 29 Hunziker, E. B. & Stahli, A. Surgical suturing of articular cartilage induces osteoarthritis-like changes. *Osteoarthritis Cartilage* **16**, 1067-1073, doi:10.1016/j.joca.2008.01.009 (2008).
- 30 Merkel, J. R., DiPaolo, B. R., Hallock, G. G. & Rice, D. C. Type I and type III collagen content of healing wounds in fetal and adult rats. *Proc Soc Exp Biol Med* **187**, 493-497, doi:10.3181/00379727-187-42694 (1988).
- 31 Corr, D. T. & Hart, D. A. Biomechanics of Scar Tissue and Uninjured Skin. *Adv Wound Care (New Rochelle)* **2**, 37-43, doi:10.1089/wound.2011.0321 (2013).
- 32 Makris, E. A., Hu, J. C. & Athanasiou, K. A. Hypoxia-induced collagen crosslinking as a mechanism for enhancing mechanical properties of engineered articular cartilage. *Osteoarthritis Cartilage* **21**, 634-641, doi:10.1016/j.joca.2013.01.007 (2013).
- 33 Chang, S. W., Shefelbine, S. J. & Buehler, M. J. Structural and mechanical differences between collagen homo- and heterotrimers: relevance for the molecular origin of brittle bone disease. *Biophys J* **102**, 640-648, doi:10.1016/j.bpj.2011.11.3999 (2012).
- 34 Wang, S. *et al.* Strain distribution of repaired articular cartilage defects by tissue engineering under compression loading. *J Orthop Surg Res* **13**, 19, doi:10.1186/s13018-018-0726-0 (2018).
- 35 Bielajew, B. J., Hu, J. C. & Athanasiou, K. A. Methodology to Quantify Collagen Subtypes and Crosslinks: Application in Minipig Cartilages. *Cartilage* **13**, 1742S-1754S, doi:10.1177/19476035211060508 (2021).
- 36 Hance, A. J. & Crystal, R. G. Rigid control of synthesis of collagen types I and III by cells in culture. *Nature* **268**, 152-154, doi:10.1038/268152a0 (1977).
- 37 Sisino, G. *et al.* Diabetes during pregnancy influences Hofbauer cells, a subtype of placental macrophages, to acquire a pro-inflammatory phenotype. *Biochim Biophys Acta* **1832**, 1959-1968, doi:10.1016/j.bbadis.2013.07.009 (2013).
- 38 Wijesundera, K. K. *et al.* M1- and M2-macrophage polarization in thioacetamide (TAA)-induced rat liver lesions; a possible analysis for hepato-pathology. *Histol Histopathol* **29**, 497-511, doi:10.14670/HH-29.10.497 (2014).
- 39 Krzyszczyk, P., Schloss, R., Palmer, A. & Berthiaume, F. The Role of Macrophages in Acute and Chronic Wound Healing and Interventions to Promote Pro-wound Healing Phenotypes. *Front Physiol* **9**, 419, doi:10.3389/fphys.2018.00419 (2018).
- 40 Hu, J. M. *et al.* CD163 as a marker of M2 macrophage, contribute to predicte aggressiveness and prognosis of Kazakh esophageal squamous cell carcinoma. *Oncotarget* **8**, 21526-21538, doi:10.18632/oncotarget.15630 (2017).
- 41 Donahue, R. P. *et al.* Stiffness- and bioactive factor-mediated protection of self-assembled cartilage against macrophage challenge in a novel co-culture system *In press. Cartilage* (2022).
- 42 Brown, W. E., Hu, J. C. & Athanasiou, K. A. Ammonium-Chloride-Potassium Lysing Buffer Treatment of Fully Differentiated Cells Increases Cell Purity and Resulting Neotissue Functional Properties. *Tissue Engineering Part C: Methods* **22**, 895-903 (2016).
- 43 Hu, J. C. & Athanasiou, K. A. A self-assembling process in articular cartilage tissue engineering. *Tissue Eng* **12**, 969-979, doi:10.1089/ten.2006.12.969 (2006).
- 44 Mehra, P. & Wolford, L. M. Use of the Mitek anchor in temporomandibular joint disc-repositioning surgery. *Proc (Bayl Univ Med Cent)* **14**, 22-26, doi:10.1080/08998280.2001.11927726 (2001).
- 45 Link, J. M., Hu, J. C. & Athanasiou, K. A. Chondroitinase ABC Enhances Integration of Self-Assembled Articular Cartilage, but Its Dosage Needs to Be Moderated Based on

- Neocartilage Maturity. *Cartilage*, 1947603520918653, doi:10.1177/1947603520918653 (2020).
- 46 Bankhead, P. *et al.* QuPath: Open source software for digital pathology image analysis. *Sci Rep* **7**, 16878, doi:10.1038/s41598-017-17204-5 (2017).
- 47 Cissell, D. D., Link, J. M., Hu, J. C. & Athanasiou, K. A. A Modified Hydroxyproline Assay Based on Hydrochloric Acid in Ehrlich's Solution Accurately Measures Tissue Collagen Content. *Tissue Eng Part C Methods* **23**, 243-250, doi:10.1089/ten.tec.2017.0018 (2017).
- 48 Cox, J. & Mann, M. MaxQuant enables high peptide identification rates, individualized p.p.b.-range mass accuracies and proteome-wide protein quantification. *Nat Biotechnol* **26**, 1367-1372, doi:10.1038/nbt.1511 (2008).
- 49 Pritzker, K. P. *et al.* Osteoarthritis cartilage histopathology: grading and staging. *Osteoarthritis Cartilage* **14**, 13-29, doi:10.1016/j.joca.2005.07.014 (2006).

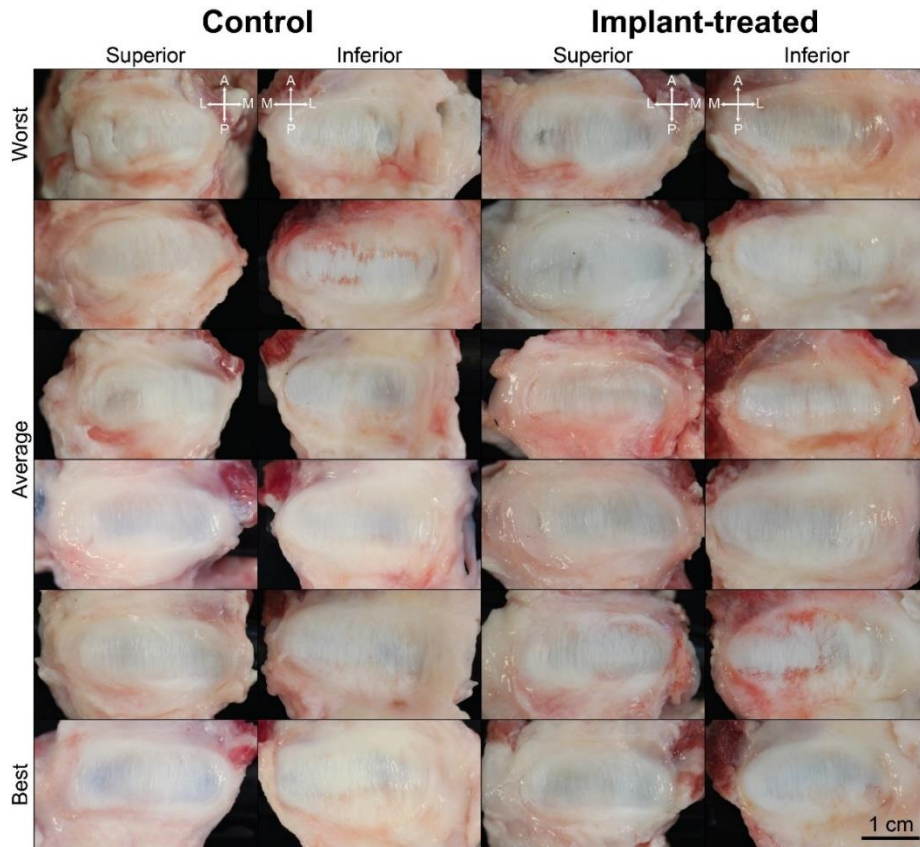
Supplementary materials



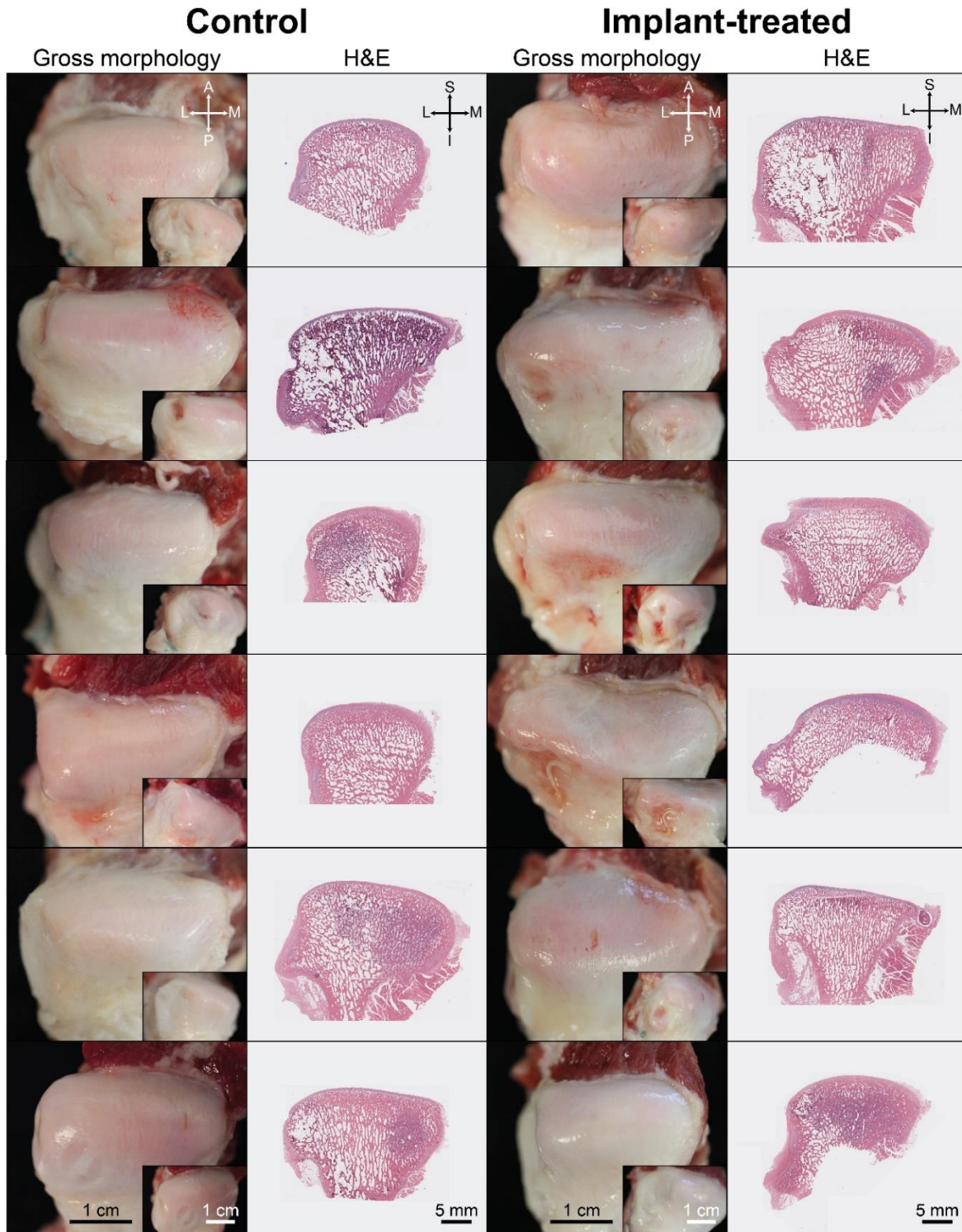
Supplementary Figure 1. Depiction of the surgical placement of the incision, defect, and implant. The defect (dashed circle) was placed in the centrolateral aspect of the disc in the center of the incision margins (dashed lines). The implant (solid square) was positioned within the incision margins. A, anterior, L, lateral, M, medial, P, posterior.



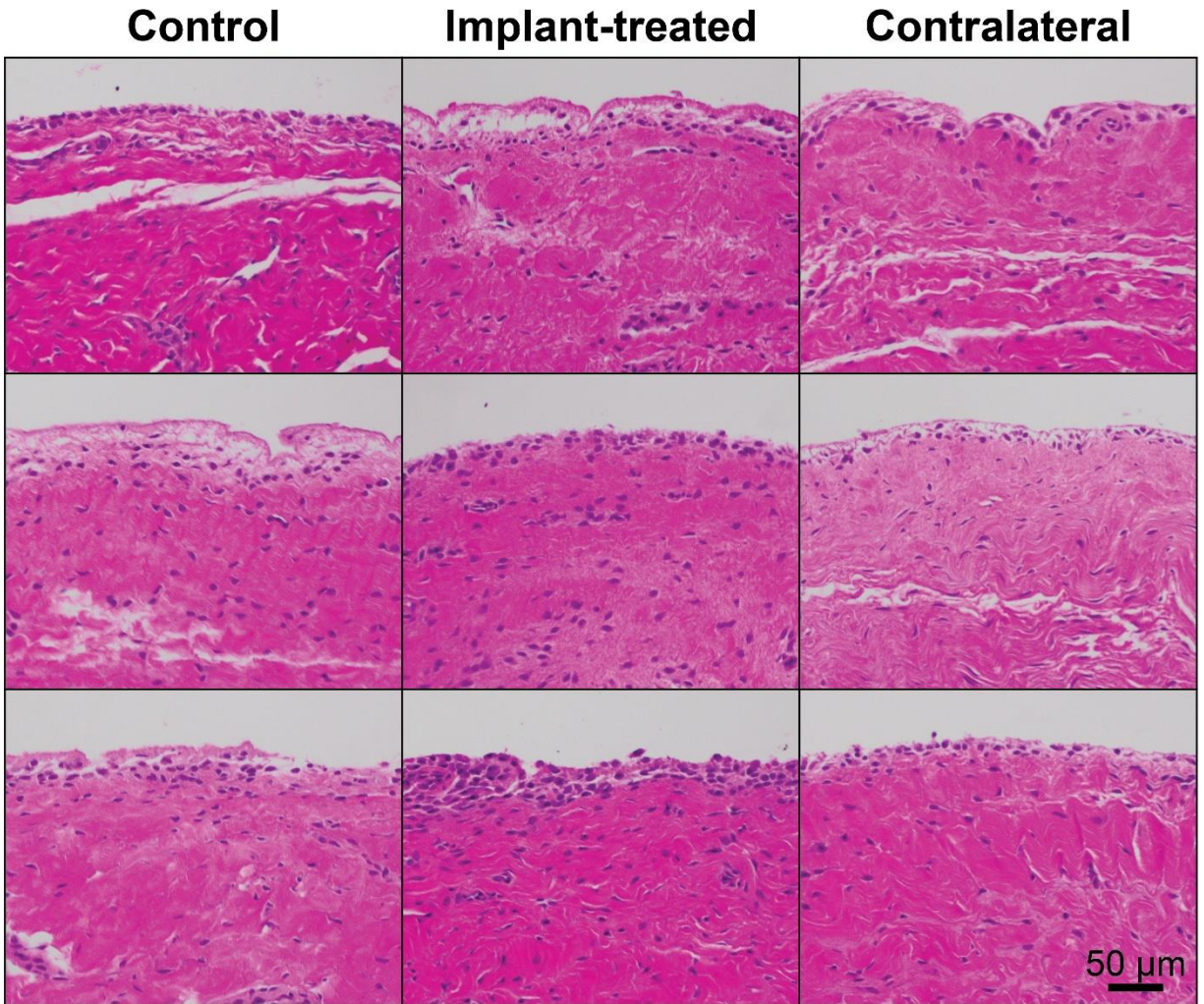
Supplementary Figure 2. Short-term gross morphology of implant-treated TMJ discs. After 4 or 8 weeks of healing, TMJ discs exhibited repair tissue in the defect placed in the centrolateral portion of the disc. A, anterior, L, lateral, M, medial, P, posterior.



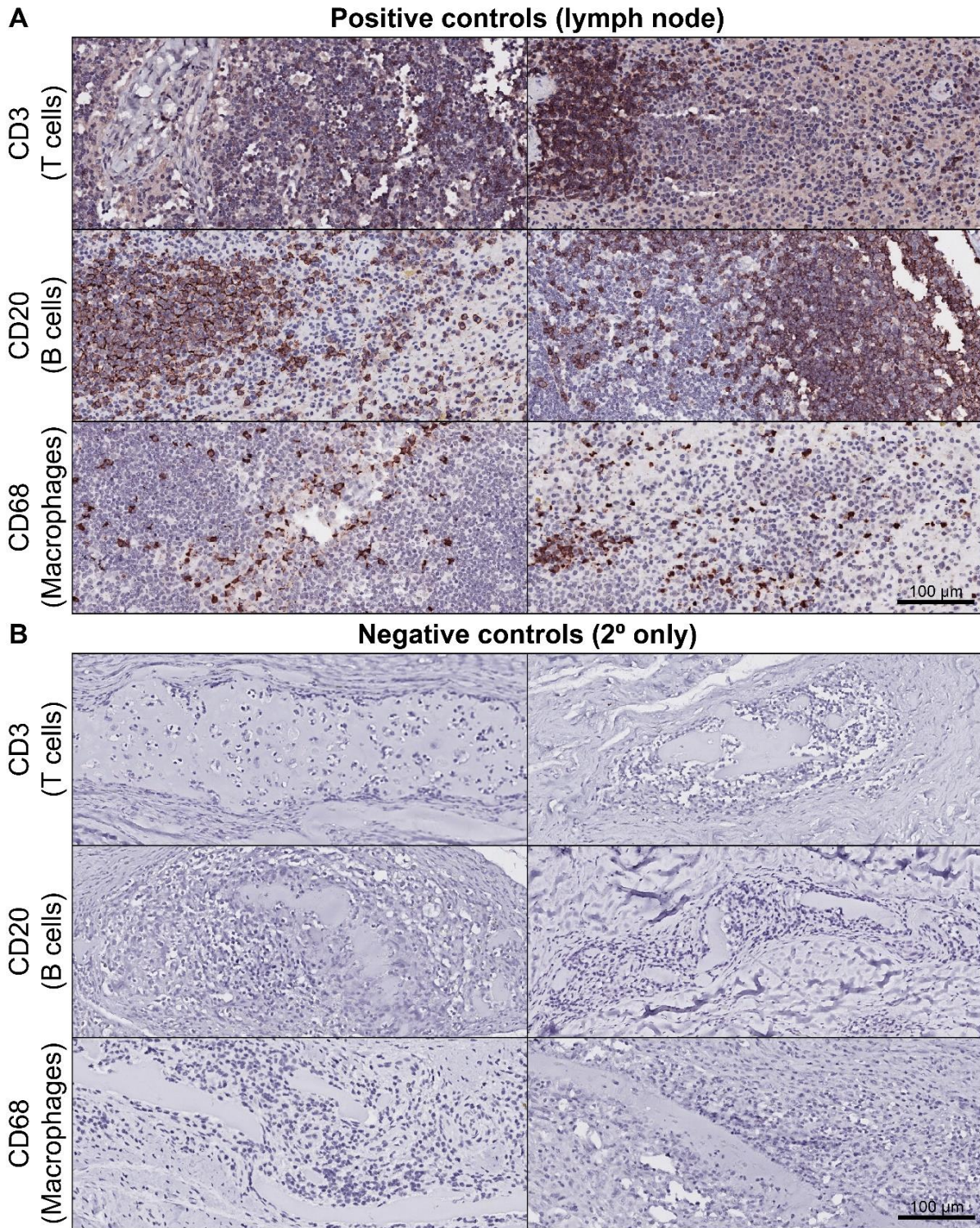
Supplementary Figure 3. Gross morphology of all discs in the long-term study. After 24 weeks, TMJ discs exhibited a heterogeneous healing response. A, anterior, L, lateral, M, medial, P, posterior.



Supplementary Figure 4. Gross morphology and mediolateral histological cross sections of condyles. After 24 weeks of implantation, the condyles had a heterogeneous response to the presence of a TMJ disc implant and suture anchor as shown by both gross morphology and hematoxylin and eosin (H&E) sections. Insets are rotated views of the lateral area (left) of the condyle. A, anterior, I, inferior, L, lateral, M, medial, P, posterior, S, superior.

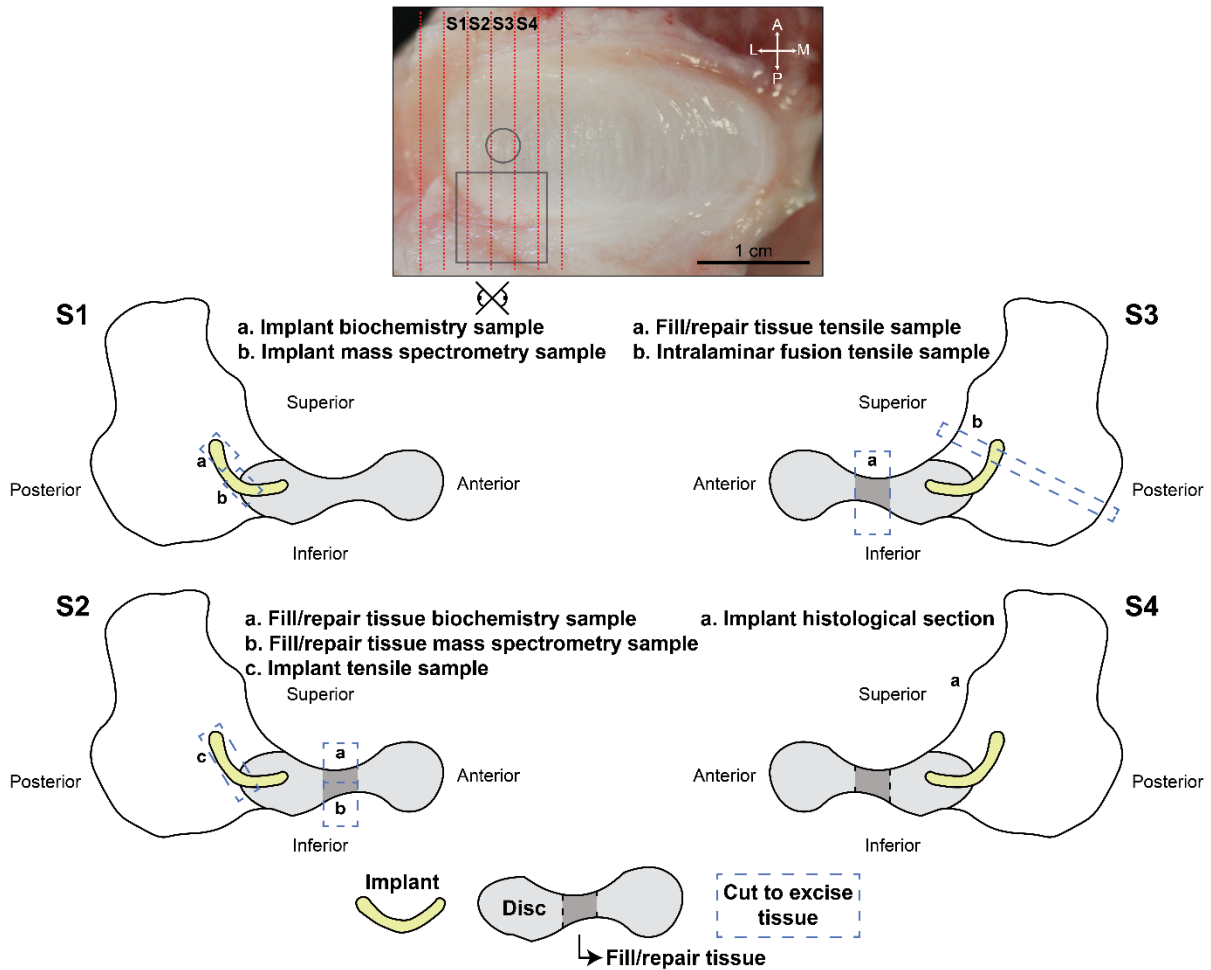


Supplementary Figure 5. The synovium of empty defect and implant-treated TMJs. Consistent with contralateral synovium, control and implant-treated synovium did not exhibit any abnormal cellular response in three different animals (rows) per group (columns).



Supplementary Figure 6. Controls for immunohistochemical staining. (A) Lymph node positive controls exhibited staining for T cell, B cells, and macrophages, while (B) negative secondary antibody-only controls lacked staining, as expected.

Serial sectioning in anteroposterior direction to identify implant and fill/repair tissue



Supplementary Figure 7. TMJ disc sample preparation and excision. From serial sectioning (red lines) of the TMJ disc, the implant (square) and fill/repair tissue (circle) were identified. Upon examining sections, the following samples were identified from approximately four serial sections (as depicted): S1) implant biochemistry sample, implant mass spectrometry sample, S2) fill/repair tissue biochemistry sample, fill/repair tissue mass spectrometry sample, implant tensile testing sample, S3) fill/repair tissue tensile testing sample, intralaminar tensile testing sample, and S4) implant histological section. A, anterior, L, lateral, M, medial, P, posterior.

Supplementary Table 1. Osteoarthritis scores of condyles. A histological score and gross stage were assigned to each animal and were multiplied to get the osteoarthritis (OA) score, according to the International Cartilage Repair Society scoring scheme⁴⁹. There was no difference between the groups.

Group	Animal	Histological Grade	Gross Stage	OA Score
Control	1	0.00	1	0.00
	2	6.00	2	12.00
	3	2.25	2	4.50
	4	3.50	2	7.00
	5	2.00	0	0.00
	6	4.50	2	9.00
	Final Score			
Implant-treated	1	5.50	1	5.50
	2	0.00	0	0.00
	3	1.25	2	2.50
	4	5.00	2	10.00
	5	4.75	1	4.75
	6	4.00	1	4.00
	Final Score			

Supplementary Table 2. Tensile properties of intralaminar fusion. When tested under uniaxial tension in the superoinferior direction, there was no difference in the intralaminar stiffness or strength between control and implant-treated groups.

Group	Young's modulus (MPa)	UTS (MPa)
Control	1.34±1.18	0.66±0.43
Implant-treated	1.40±0.94	0.68±0.46

Supplementary Table 3. Crosslinks in the fill and repair tissues. For implant-treated discs, mature pyridinoline (PYR) and immature dihydroxylysinoxorleucine (DHLNL) crosslinks normalized to dry weight (DW) and hydroxyproline (OHP) were near native TMJ disc levels but were not statistically different compared to controls.

Group	PYR/DW (ng/mg)	PYR/OHP (mmol/mol)	DHLNL/DW (ng/mg)	DHLNL/OHP (mmol/mol)	PYR/DHLNL (mol/mol)
Control	5633±672	42.55±9.33	1603±280	16.56±2.23	2.553±0.293
Implant-treated	4968±755	34.20±8.42	1467±446	14.04±4.47	2.578±0.646
Native TMJ disc	5518±1686	35.94±8.73	1367±500	12.32±3.48	2.968±0.138

Supplementary Table 4. Bottom-up proteomics data for all tissues. Bottom-up proteomics data are presented per total protein as a percentage.

Gene	Protein	t=0 <i>in vitro</i>	t=24W <i>in vitro</i>	t=24W <i>in vivo</i>	Control	Implant-treated	Native TMJ disc
ACTB	Actin, cytoplasmic 1	1.09%	0.75%	0.06%	0.09%	0.03%	0.05%
PGCA	Aggrecan core protein (Fragments)	0.92%	2.25%	0.00%	0.00%	0.00%	0.00%
ANXA2	Annexin A2	0.43%	0.27%	0.00%	0.03%	0.01%	0.03%
ATPA	ATP synthase subunit alpha, mitochondrial	0.13%	0.06%	0.00%	0.00%	0.00%	0.00%
ENOB	Beta-enolase	0.13%	0.13%	0.00%	0.00%	0.00%	0.00%
PGS1	Biglycan (Fragments)	0.43%	0.29%	0.02%	0.03%	0.04%	0.02%
Col1a1	Collagen type I alpha 1	4.19%	4.03%	63.08%	56.65%	61.49%	63.09%
Col1a2	Collagen type I alpha 2	1.49%	0.72%	25.21%	25.78%	29.43%	28.42%
Col2a1	Collagen type II alpha 1	64.54%	63.48%	0.21%	0.24%	0.21%	0.09%
Col3a1	Collagen type III alpha 1	0.15%	0.11%	8.73%	13.74%	6.34%	6.15%
Col4a2	Collagen type IV alpha 2	0.00%	0.00%	0.07%	0.02%	0.03%	0.04%
Col5a1	Collagen type V alpha 1	0.36%	0.26%	0.11%	0.20%	0.13%	0.09%
Col5a2	Collagen type V alpha 2	1.07%	0.83%	0.16%	0.21%	0.14%	0.14%
Col5a3	Collagen type V alpha 3	0.00%	0.00%	0.14%	0.23%	0.13%	0.11%
Col6a1	Collagen type VI alpha 1	0.17%	0.13%	0.06%	0.08%	0.06%	0.05%
Col6a2	Collagen type VI alpha 2	0.77%	0.63%	0.32%	0.35%	0.34%	0.25%
Col6a3	Collagen type VI alpha 3	2.71%	2.22%	1.01%	0.83%	0.68%	0.68%
Col9a1	Collagen type IX alpha 1	1.65%	1.88%	0.00%	0.00%	0.00%	0.00%
Col9a2	Collagen type IX alpha 2	0.73%	0.94%	0.00%	0.06%	0.01%	0.00%
Col11a1	Collagen type XI alpha 1	3.12%	3.69%	0.01%	0.01%	0.02%	0.02%
Col11a2	Collagen type XI alpha 2	3.86%	4.41%	0.06%	0.05%	0.04%	0.03%
Col12a1	Collagen type XII alpha 1	3.66%	3.75%	0.01%	0.11%	0.14%	0.02%
Col14a1	Collagen type XIV alpha 1	0.00%	0.00%	0.19%	0.17%	0.02%	0.05%
Col27a1	Collagen type XXVII alpha 1	0.00%	0.00%	0.00%	0.03%	0.00%	0.02%
Col28a1	Collagen type XXVIII alpha 1	0.00%	0.07%	0.00%	0.00%	0.00%	0.00%

CSN4	COP9 signalosome complex subunit 4	0.12%	0.05%	0.00%	0.00%	0.00%	0.01%
CSN6	COP9 signalosome complex subunit 6	0.05%	0.04%	0.00%	0.00%	0.00%	0.03%
PGS2	Decorin	0.02%	0.00%	0.03%	0.08%	0.06%	0.04%
FRIL	Ferritin light chain (Fragment)	0.03%	0.06%	0.00%	0.00%	0.00%	0.00%
FMOD	Fibromodulin (Fragment)	0.07%	0.04%	0.00%	0.01%	0.00%	0.01%
G3P	Glyceraldehyde-3-phosphate dehydrogenase	0.51%	0.25%	0.00%	0.01%	0.01%	0.00%
HSPB1	Heat shock protein beta-1	0.30%	0.17%	0.00%	0.00%	0.00%	0.00%
H33	Histone H3.3	0.27%	0.33%	0.03%	0.09%	0.02%	0.02%
H4	Histone H4	0.98%	0.81%	0.14%	0.21%	0.09%	0.05%
HPLN1	Hyaluronan and proteoglycan link protein 1	0.92%	2.39%	0.00%	0.00%	0.00%	0.00%
MFGM	Lactadherin	0.25%	0.58%	0.00%	0.00%	0.00%	0.00%
LDHA	L-lactate dehydrogenase A chain	0.09%	0.06%	0.00%	0.00%	0.00%	0.00%
PGK1	Phosphoglycerate kinase 1	0.32%	0.24%	0.00%	0.00%	0.00%	0.00%
LMNA	Prelamin-A/C	0.43%	0.22%	0.06%	0.08%	0.04%	0.05%
SMPX	Small muscular protein	0.00%	0.01%	0.00%	0.01%	0.01%	0.04%
TENA	Tenascin	0.04%	0.03%	0.00%	0.03%	0.15%	0.05%
TBA1B	Tubulin alpha-1B chain	0.11%	0.09%	0.01%	0.02%	0.01%	0.02%
TBB5	Tubulin beta chain	0.12%	0.08%	0.02%	0.03%	0.01%	0.01%
UGPA	UTP--glucose-1-phosphate uridylyltransferase	0.05%	0.08%	0.00%	0.00%	0.00%	0.00%
VIME	Vimentin	2.11%	2.38%	0.20%	0.29%	0.17%	0.20%

Supplementary Table 5. Raw values for the complete blood count and comprehensive metabolic panel parameters. The parameters were assayed at implantation (t=0) and animal euthanasia (t=4W, t=8W, or t=24W).

Group	ID # and Assay Point	WBC (K/uI)	Absolute Neutrophil cells (K/uI)	Absolute Lymphocyte cells (K/uI)	Absolute Monocyte cells (K/uI)	Absolute Eosinophil cells (K/uI)	Absolute Basophil cells (K/uI)	Neutrophil (%)	Lymphocyte (%)	Monocyte (%)	Eosinophil (%)	Basophil (%)	RBC (M/uI)	Hemoglobin (g/dL)	Hematocrit (%)	MCV (fL)	MCH (pg)	MCHC (g/dL)	RDW (%)	Platelets (K/uL)	MPV (fL)
Implant treated (4W pilot)	1680 t=0	8.18	4.58	3.05	0.31	0.22	0.02	55.93	37.26	3.83	2.73	0.25	7.25	12.5	34.9	48.2	17.2	35.8	20.4	450	9.3
	1680 t=4W	8.90	3.91	4.18	0.62	0.18	n/a	43.97	46.97	6.99	2.00	n/a	7.09	12.3	41.5	59	19	32.0	16.2	407	9.2
	7852 t=0	10.02	3.47	4.24	0.25	2.03	0.02	34.63	42.35	2.51	20.28	0.23	6.92	11.7	35.2	50.8	16.9	33.2	19.6	210	13.0
	7852 t=4W	9.52	5.24	3.43	0.76	0.10	n/a	55.00	36.00	8.00	1.00	n/a	7.13	14.1	41.7	59	20	23	15.9	383	11
Implant treated	3550 t=0	6.54	2.29	3.00	0.20	1.00	0.03	35.01	45.90	3.36	15.26	0.48	5.59	8.8	28.3	50.6	15.7	31.1	18.4	212	11.3

(8W pilot)	3550 t=8W	8.02	3.42	3.66	0.22	0.71	0.01	42.62	45.64	2.73	8.91	0.11	8.48	12.6	43.2	51.0	14.9	29.2	18.1	324	10.4
	3556 t=0	10.82	6.64	3.29	0.34	0.53	0.01	61.37	30.44	3.13	4.93	0.12	5.67	8.5	29.7	52.3	15.0	28.6	16.9	170	13.0
	3556 t=8W	10.82	6.11	3.71	0.38	0.59	0.03	56.48	34.28	3.53	5.44	0.26	7.30	11.5	38.4	52.6	15.8	29.9	17.5	311	12.4
Control (24W)	6586 t=0	11.28	7.24	3.80	0.19	0.05	0.01	64.18	33.68	1.66	0.43	0.05	6.64	11.9	41.3	62.2	17.9	28.8	16.3	243	11.4
	6586 t=24W	10.98	7.41	3.23	0.19	0.14	0.01	67.53	29.42	1.69	1.24	0.12	6.06	10.5	33.2	54.8	17.3	31.6	17.4	399	11.2
	6593 t=0	17.04	12.97	2.96	0.10	0.95	0.05	76.10	17.39	0.59	5.60	0.31	5.93	10.6	35.1	59.2	17.9	30.2	16.2	319	10.4
	6593 t=24W	11.02	6.39	4.10	0.22	0.29	0.02	58.03	37.18	2.04	2.60	0.15	5.53	8.8	27.9	50.4	15.9	31.5	18.8	571	10.2
	6613 t=0	8.56	3.18	4.98	0.20	0.15	0.06	37.15	58.12	2.31	1.74	0.67	6.41	12.0	39.3	61.3	18.7	30.5	16.3	160	10.8
	6613 t=24W	6.64	2.45	3.80	0.16	0.22	0.00	36.95	57.30	2.40	3.30	0.05	5.71	10.4	31.6	55.4	18.2	32.9	18.6	313	11.9
	6615 t=0	12.28	9.33	2.12	0.15	0.66	0.02	75.94	17.30	1.25	5.36	0.16	5.09	9.8	32.6	64.1	19.3	30.1	16.5	378	9.4
	6615 t=24W	12.32	7.71	3.76	0.23	0.59	0.02	62.55	30.56	1.89	4.80	0.20	5.79	10.7	32.4	56.0	18.5	33.0	17.8	486	11.2
6657 t=0	11.02	5.41	4.73	0.26	0.61	0.01	49.07	42.93	2.32	5.56	0.12	6.25	11.2	36.0	57.6	17.9	31.1	16.8	441	10.0	

	6657 t=24W	6.78	1.31	3.70	0.28	1.44	0.05	19.32	54.61	4.07	21.26	0.74	6.37	11.6	35.2	55.2	18.2	33.0	18.1	271	10.6
	6668 t=0	9.46	6.40	2.53	0.16	0.35	0.02	67.69	26.75	1.67	3.73	0.16	5.37	9.8	31.0	57.7	18.2	31.6	17.5	523	9.3
	6668 t=24W	5.10	1.20	3.12	0.19	0.58	0.02	23.49	61.12	3.63	11.45	0.30	4.68	8.5	25.7	54.9	18.2	33.1	17.7	409	9.9
Implant treated (24W)	6633 t=0	11.34	5.61	4.69	0.31	0.72	0.01	49.48	41.35	2.69	6.39	0.08	6.49	10.6	37.8	58.2	16.3	28.0	16.1	188	10.5
	6633 t=24W	10.02	3.26	4.10	0.18	2.43	0.04	32.53	40.93	1.83	24.28	0.43	5.40	9.7	29.4	54.4	18.0	33.0	17.9	234	11.7
	6639 t=0	6.98	4.37	2.19	0.12	0.28	0.01	62.64	31.36	1.77	4.07	0.16	6.43	10.8	38.3	59.5	16.8	28.2	16.7	351	12.0
	6639 t=24W	6.14	1.74	3.32	0.16	0.91	0.01	28.34	54.08	2.62	14.78	0.19	6.01	10.6	33.3	55.4	17.6	31.8	18.4	218	13.0
	6641 t=0	9.90	5.12	4.22	0.29	0.21	0.05	51.73	42.63	2.95	2.14	0.54	5.94	10.1	34.8	58.6	17.0	29.0	16.0	341	9.0
	6641 t=24W	6.98	1.58	4.04	0.23	1.08	0.05	22.63	57.93	3.26	15.45	0.74	6.43	11.3	35.4	55.0	17.6	31.9	18.0	319	9.3
	6643 t=0	7.26	3.44	3.43	0.28	0.11	0.00	47.39	47.27	3.83	1.45	0.06	6.00	10.3	38.1	63.5	17.2	27.0	16.3	417	8.5
	6643 t=24W	9.26	3.19	4.22	0.11	1.73	0.00	34.45	45.58	4.23	18.70	0.03	5.42	10.5	32.8	60.6	19.4	32.0	17.4	322	9.7
	6652 t=0	24.92	21.20	2.23	0.19	1.13	0.16	85.09	8.95	0.76	4.55	0.65	5.63	11.4	35.3	62.7	20.2	32.3	16.0	449	10.0

6652 t=24W	9.26	2.50	3.32	0.24	3.12	0.09	26.95	35.82	2.56	33.72	0.94	6.79	12.4	39.8	58.6	18.3	31.2	18.3	289	11.3
6655 t=0	9.36	4.90	3.91	0.31	0.22	0.02	52.33	41.79	3.35	2.37	0.17	5.18	9.2	30.7	59.3	17.8	30.0	16.3	263	12.0
6655 t=24W	9.80	3.16	3.81	0.30	2.48	0.06	32.23	38.84	3.04	25.29	0.61	5.78	10.0	32.3	55.8	17.3	31.0	18.7	1.6	12.5

Group	ID # and Assay Point	Alanine Transaminase (U/L)	Albumin (g/dL)	Alkaline Phosphatase (U/L)	Amylase (U/L)	Aspartate Transaminase (U/L)	Blood Urea Nitrogen (mg/dL)	Calcium (mg/dL)	Creatinine (mg/dL)	Glucose (mg/dL)	Phosphorus (mg/dL)	Total Bilirubin (mg/dL)	Total Protein (g/dL)	Chloride (mmol/L)	Potassium (mmol/L)	Sodium (mmol/L)
Implant treated (4W pilot)	1680 t=0	39.8	4.13	51.7	2102.7	30.5	12.5	9.51	0.982	71.0	5.65	0.258	6.30	101.3	3.86	138
	1680 t=4W	36.6	3.99	61.4	2224.4	28.3	16.0	9.80	0.907	51.2	6.09	0.021	6.02	99.2	3.83	137
	7852 t=0	45.7	4.43	31.5	1601.2	32.0	16.4	10.36	1.146	70.6	4.68	0.138	6.52	101.7	4.37	139

	7852 t=4W	47.9	3.94	31.9	1632.9	30.7	20.4	9.57	0.903	60.3	4.73	0.090	6.17	101.6	4.32	142
Implant treated (8W pilot)	3550 t=0	26.2	3.96	69.3	2459.7	41.6	13.7	10.26	0.932	110.2	5.64	0.034	6.20	103.8	3.89	140
	3550 t=8W	26.8	4.40	63.3	2711.9	35.6	13.8	10.09	1.015	80.4	5.59	0.112	6.84	102.8	4.77	137
	3556 t=0	30.5	4.54	38.1	1876.2	23.6	14.2	10.55	0.950	88.4	6.12	0.089	6.38	102.7	3.70	141
	3556 t=8W	33.8	4.78	52.1	2171.1	18.8	16.2	10.47	1.014	119.9	5.92	0.072	6.51	99.7	4.05	138
Control (24W)	6586 t=0	39.4	4.84	55.6	1778.1	46.5	14.9	10.42	0.832	77.9	5.15	0.148	7.13	99.8	4.48	136
	6586 t=24W	40.7	4.53	38.3	1616.4	33.5	11.9	9.77	1.027	58.8	5.06	0.304	7.36	102.5	4.08	139
	6593 t=0	33.4	4.18	63.4	2143.6	35.7	11.8	10.30	0.737	85.9	5.54	0.077	6.93	100.6	4.00	138
	6596 t=24W	41.2	4.01	43.4	1888.0	28.7	13.4	9.81	0.836	73.9	5.49	0.094	7.62	102.4	4.20	138
	6613 t=0	33.8	4.58	66.1	2295.3	29.1	12.3	10.91	0.946	93.3	5.83	0.088	7.12	103.0	4.30	142
	6613 t=24W	42.7	4.29	38.5	2237.0	29.5	11.9	9.94	1.126	65.2	4.93	0.199	7.15	101.4	3.82	137

	6615 t=0	42.6	4.81	60.5	1991.2	36.1	22.5	10.51	1.066	122.3	6.17	0.133	7.88	106.9	4.03	145
	6615 t=24W	43.4	4.24	34.5	1723.5	26.9	15.6	10.08	1.065	71.4	4.80	0.052	7.46	98.7	4.07	133
	6657 t=0	38.5	4.80	138.5	2171.6	38.1	13.2	10.42	0.836	76.5	5.44	0.025	7.30	98.5	4.45	135
	6657 t=24W	34.0	4.57	126.2	2392.6	36.8	15.0	10.25	1.008	86.4	5.34	0.017	7.49	99.7	4.22	136
	6668 t=0	42.0	4.28	68.9	1201.8	39.9	13.6	10.07	0.872	73.2	4.87	0.185	7.21	98.6	3.72	135
	6668 t=24W	34.9	3.97	70.4	1234.3	31.0	11.1	9.75	0.981	74.4	5.03	0.107	6.84	101.2	4.31	136
Implant- treated (24W)	6633 t=0	35.7	4.56	50.7	1123.0	25.6	12.9	10.10	0.818	101.9	5.16	0.064	7.43	99.6	3.34	136
	6633 t=24W	33.7	4.19	45.1	1121.6	27.4	13.3	10.03	0.947	84.4	5.07	0.035	7.26	100.6	3.77	134
	6639 t=0	44.6	4.36	52.9	2128.6	33.2	11.9	10.08	0.923	91.7	5.35	0.123	7.06	99.3	4.03	136
	6639 t=24W	37.8	4.00	47.8	2178.0	28.1	13.5	10.12	1.083	84.5	4.34	0.067	6.95	99.4	3.67	134
	6641 t=0	34.1	4.28	57.4	2052.6	27.8	10.7	9.98	0.728	102.3	5.53	0.114	7.08	105.7	4.41	140

6641 t=24W	35.2	4.29	47.1	2130.8	21.0	12.9	10.26	0.880	110.7	5.05	0.078	7.51	97.9	3.91	134
6643 t=0	31.8	4.64	86.3	2014.2	30.4	16.0	10.21	0.862	80.2	5.08	0.315	7.66	103.2	3.68	139
6643 t=24W	31.5	4.28	79.6	2119.3	32.3	11.1	10.21	0.910	82.7	4.76	0.079	7.24	102.7	3.60	137
6652 t=0	39.0	4.52	52.7	2787.5	48.0	16.6	10.03	1.054	108.9	5.34	0.180	7.21	104.2	4.04	139
6652 t=24W	35.8	4.41	48.1	2721.9	37.7	13.2	10.38	1.139	74.1	4.11	0.073	7.51	102.1	4.73	134
6655 t=0	45.9	4.23	88.5	2961.7	33.5	13.5	9.92	0.756	87.4	5.55	0.074	6.99	101.8	4.73	135
6655 t=24W	43.0	4.06	66.9	2792.6	37.5	12.1	10.32	0.802	77.7	5.07	0.044	7.96	98.1	4.80	132

Supplementary Table 6. Crosslinks in the implants after extended culture or implantation. After 24 weeks of implantation, mature pyridinoline (PYR) and immature dihydroxylysinonorleucine (DHLNL) crosslinks normalized to dry weight (DW) significantly increase compared to pre-implantation values (i.e., t=0 *in vitro*). Those values normalized to hydroxyproline (OHP) approached native TMJ disc values but were not significantly different between groups.

Group	PYR/DW (ng/mg)	PYR/OHP (mmol/mol)	DHLNL/DW (ng/mg)	DHLNL/OHP (mmol/mol)	PYR/DHLNL (mol/mol)
t=0 <i>in vitro</i>	490±51	14.68±1.43	250±42	10.60±2.58	1.437±0.262
t=24W <i>in vitro</i>	424±37	18.14±2.59	187±58	11.45±4.46	1.732±0.470
t=24W <i>in vivo</i>	2570±583****	15.23±3.41	855±186****	7.08±1.73	2.194±0.437**
Native TMJ disc	5518±1686	35.94±8.73	1367±500	12.32±3.48	2.968±0.138

Supplementary Table 7. Compressive properties of neocartilage. Relaxation and instantaneous moduli values increased after 24 weeks of extended culture. Implants after 24 weeks *in vivo* were not tested (nt).

Group	20% Relaxation modulus (kPa)	20% Instantaneous modulus (kPa)	20% Coefficient of viscosity (MPa s)
t=0 <i>in vitro</i>	177±55	777±115	55.9±18.8
t=24W <i>in vitro</i>	435±151***	1214±465*	59.9±34.0
t=24W <i>in vivo</i>	nt	nt	nt

Supplementary Table 8. Immunohistochemistry parameters. For CD3, CD20, and CD68 staining, the brands of primary antibody, dilution ratios, antigen retrieval methods, blocking serums, secondary antibodies, and development methods are listed.

Primary antibody	Brand	Dilution ratio	Antigen retrieval	Blocking serum	Secondary antibody	Development
Rat anti-CD3	Dr. Moore's Leukocyte Antigen Biology Lab clone 3-12	1:10	Dako antigen retrieval solution, 30 min at 95°C	10% horse serum in PBS, 20 min at room temperature	Biocare Medical's 4+ detection systems anti-rat	Streptavidin horseradish peroxidase (HRP) GR608
Rabbit anti-CD20	NeoMarker RB-9013-P1	1:4	Dako antigen retrieval solution, 30 min at 95°C	10% horse serum in PBS, 20 min at room temperature	Biocare Medical's 4+ detection systems anti-rabbit	Streptavidin HPR HP604
Mouse anti-CD68	ThermoFisher Mac387	1:9	EDTA buffer, 30 min at 95°C	10% horse serum in PBS, 20 min at room temperature	Biocare Medical's 4+ detection systems anti-mouse	Streptavidin HPR HP604

CHAPTER 7 | Tissue-engineered implants regenerate large perforations in the Yucatan minipig temporomandibular joint disc*

Abstract

The temporomandibular joint (TMJ) disc in the jaw is frequently perforated in people with temporomandibular disorders (TMDs). Current surgical procedures for TMDs ameliorate pain temporarily but are ineffectual in the long-term. Arthroscopy studies have shown that most perforations consist of more than one third of the TMJ disc area, signifying the need to develop novel treatments for large defects. In this study, the objective was to validate the safety and efficacy of tissue-engineered neocartilage implants to regenerate large (6 mm diameter) perforations in the TMJ disc of the Yucatan minipig. It was hypothesized that large TMJ disc perforations treated with self-assembled neocartilage would result in mechanically robust, regenerated tissue. Furthermore, it was predicted that empty defect controls would remain perforated. All implant-treated perforations fully closed while all control discs remained perforated, with a defect perimeter of 14.6 ± 5.8 mm. Regenerated tissue was mechanically robust, with Young's modulus and ultimate tensile strength values that were 81.2% and 79.2% of native TMJ disc values, respectively. The biochemical and proteomic composition of regenerated tissue was shown to be similar to that of the native TMJ disc. For example, collagen types I and III were within native TMJ disc ranges. In the control TMJs, mandibular condyle cartilage showed degenerative changes, and tissue adjacent to the disc perforations showed significant decreases in collagen type I and significant increases in collagen type III, which may be indicative of degeneration. After 8 weeks, self-assembled neocartilage implants were shown to be safe via necropsy, complete blood count, and comprehensive metabolic panel, and, as predicted, there was a mild cellular response to the implant. With safety and efficacy shown in large perforation

* Authors: Donahue RP[†], Bielajew BJ[†], Vapniarsky N, Heney CM, Arzi B, Hu JC, Athanasiou KA. [†]equal contribution

defects, self-assembled neocartilage implants are primed for translation to clinical trials and human usage, where they are envisioned to improve clinical outcomes for millions of TMD patients.

Introduction

The temporomandibular joint (TMJ) is crucial for everyday functions including eating, talking, and breathing. Temporomandibular disorders (TMDs), which can result in debilitating pain and loss of function of the TMJ, symptomatically affect up to 83 million people in the U.S.¹⁻⁵. Most TMD cases involve anterior displacement of the TMJ disc⁶, and up to 15% of these cases also involve perforation of the disc⁷⁻⁹; however, perforation can also occur independently of disc displacement⁷. While many of these TMD patients seek medical treatment to decrease pain and improve function, long-term outcomes of most treatments are ineffectual¹⁰. Despite the high prevalence, the critical need for TMD treatments, including those for TMJ disc perforation, remains a largely unresolved clinical problem.

Current clinical treatments for TMDs are lacking. Even though osteoarthritis incidence in the TMJ is similar to that in the knee, the TMJ has only a fraction of current procedural terminology (CPT) codes for joint arthroplasty and approximately a 2000-fold fewer projected total joint procedure frequency when compared to the knee¹¹. While there exist non-invasive, early-stage therapies such as physical therapy, analgesics, and splints for TMDs¹², most non-surgical approaches are only palliative¹⁰, and surgery is not considered until pain becomes intolerable¹³. Moreover, due to the average implant lifetime coupled with the young age of patients, end-stage surgical treatments such as discectomy and total joint replacements often require revision¹¹. Thus, the TMJ surgical field would benefit immensely from an effective and lasting mid-stage intervention to avoid revision surgeries and to treat patients earlier in the disease timeline. A potential solution to address this unmet clinical need would be a safe and effective tissue engineering approach to treat mid-stage discal TMDs.

Tissue engineering has recently shown promise as a treatment for TMDs, with research focusing on regeneration of cartilage defects to replacing entire TMJ discs. For example, recent approaches include the use of 3D-printed gelatin-genipin scaffolds for TMJ cartilage regeneration¹⁴ and biodegradable polymeric TMJ disc implants¹⁵. However, despite the need for mid-stage treatments, there is only one cell-based therapeutic approach for TMDs in clinical trials worldwide¹⁶. To bring new tissue-engineered therapeutics to market, preclinical safety and efficacy must be validated in large animal models. The Yucatan minipig has recently been indicated as an exemplary large animal model for TMDs¹⁷, and it has recently been used in tissue-engineering experiments using self-assembled neocartilage implants in small disc thinning¹⁸ and small perforation¹⁹ indications. In the small (i.e., 3 mm diameter) perforation study, self-assembled neocartilage implants were shown to facilitate the deposition of a regenerated tissue with mechanical properties and extracellular matrix (ECM) components similar to native fibrocartilage, unlike the inferior fill tissue of empty defect controls¹⁹. With these advancements, tissue engineering is a promising solution to the unmet clinical needs, including disc perforation, of TMD patients.

It remains unknown whether self-assembled cartilage can regenerate larger perforations in the TMJ disc. According to one arthroscopic study, nearly 70% of TMJ disc perforations have an area larger than one third of the TMJ disc surface⁸, indicating a need to show efficacy in larger defect sizes. Thus, the present study scales up the defect size and uses self-assembled neocartilage implants to treat large (6 mm dia.) perforations in the TMJ disc. The objective of this study is to validate the safety and efficacy of self-assembled neocartilage implants for the regeneration of large TMJ disc perforations in the Yucatan minipig. Safety measures include blood analysis, complete necropsy, and histology for immune response. Efficacy validation includes mechanical testing, biochemical analysis, and bottom-up proteomics of implant-treated discal tissues compared to empty defect controls and native TMJ discs. The hypothesis is that large TMJ disc perforations treated with self-assembled neocartilage implants will produce regenerated

tissue that is mechanically robust and comprises an ECM similar to native TMJ disc in glycosaminoglycan (GAG), total collagen, and collagen subtype content. It is also predicted that control discs will not heal, resulting in no tissue fill. Additionally, it is predicted that implants will be well-tolerated, both systemically and locally, indicating a safe intervention for TMJ disc perforations. Because the clinical application of self-assembled neocartilage implants is dependent on validation of safety and efficacy in large animal models, this work represents a crucial step toward translating tissue-engineered TMJ disc implants to human clinical use.

Results

Tissue-engineered implants were suitable for implantation

Self-assembled neocartilage implants made from high-passage (passage 7) costal chondrocytes had a robust cartilaginous ECM. This study used a nonhomologous, allogeneic approach to engineer neocartilage implants for TMJ disc perforations in the Yucatan minipig (Figure 1A). After isolation of costal chondrocytes from three juvenile minipigs²⁰, implants were fabricated using the self-assembling process (Figure 1B), yielding an implant of approximately 11x17 mm in size that was trimmed to 11x11 mm for implantation into the TMJ disc (Figure 1C). After 6 weeks of self-assembly with bioactive factor application with transforming growth factor beta 1 (TGF- β 1), chondroitinase ABC (C-ABC), and lysyl oxidase-like 2 (LOXL2) (Figure 1B)²¹, the neocartilage implants stained intensely for GAGs and collagen (Figure 1D), consistent with previous histology of self-assembled neocartilages²². The mechanical properties of the implant prior to surgery were as follows: tensile Young's modulus of 6.15 ± 1.52 MPa, ultimate tensile strength (UTS) of 2.49 ± 0.85 MPa, 20% compressive relaxation modulus of 255 ± 85 kPa, and 20% compressive instantaneous modulus of 1061 ± 251 kPa. These implants, derived from highly passaged costal chondrocytes, were engineered to achieve functional properties approaching native TMJ disc values¹⁷ and were deemed sufficient to proceed with implantation in skeletally mature minipigs.

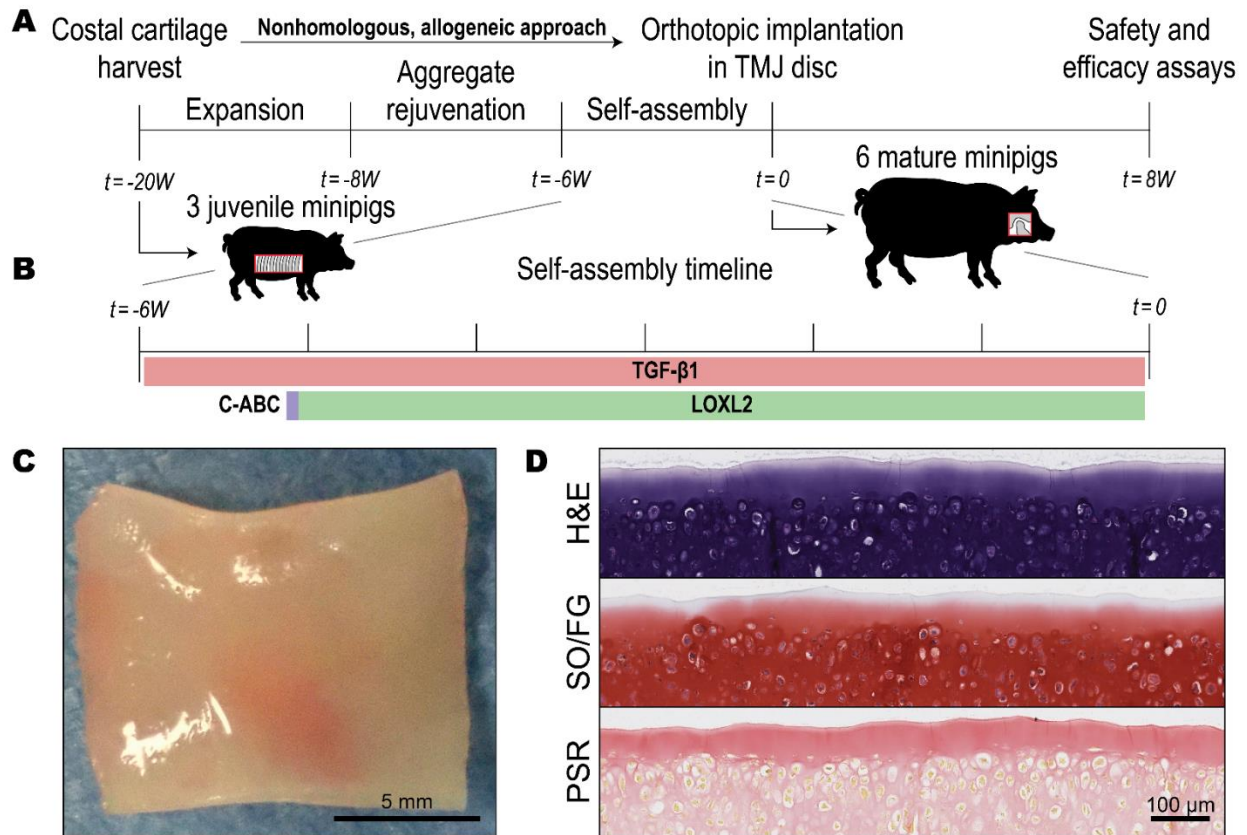


Figure 1. Tissue-engineered implants were suitable for nonhomologous usage in the TMJ disc. (A) Costal chondrocytes from the rib cartilage of juvenile minipigs were expanded, rejuvenated, and self-assembled prior to implantation into the minipig TMJ disc of mature animals. After 8 weeks in vivo, safety and efficacy assays were performed. (B) The self-assembly timeline is presented, including application of transforming growth factor beta 1 (TGF- β 1), chondroitinase ABC (C-ABC), and lysyl oxidase-like 2 (LOXL2) over the course of 6 weeks. (C) The implant measured approximately 11x11 mm after trimming and (D) showed intense staining with hematoxylin and eosin (H&E), safranin O with fast green counterstain (SO/FG) for glycosaminoglycan content, and picrosirius red (PSR) for total collagen content.

The intralaminar perforation surgical technique was successful in securing implants in large perforation defects

Modeled after previous surgical approaches for small TMJ disc defects^{18,19}, the intralaminar perforation technique was used to create and treat large perforation defects (6 mm diameter) in the Yucatan minipig TMJ disc (Figure 2). Previously, this technique was used in a small TMJ disc thinning (3 mm diameter, one-sided, partial thickness) defect model¹⁸, and, more recently, a small perforation (3 mm diameter, two-sided, full thickness) model¹⁹. After the TMJ disc was approached and identified, an incision was created along the lateral edge of the disc and deepened toward the medial aspect to create a pocket (Figure 2A), and, using a 6 mm biopsy punch, a large

perforation was created in the centrolateral region of the disc (Figure 2B). The neocartilage implant was placed inside the pocket (Figure 2C), the two laminae were sutured shut (Figure 2D), and the lateral edge of the disc was anchored to the condylar process using a bone anchor. This procedure allowed the implant to be secured without placing sutures in the disc articular surface, which has been previously reported to result in abrasion of the adjacent articular surfaces and dislodgement of the implant from the defect¹⁸. The application of the surgical technique to large defects was successful in securing and protecting the implant.

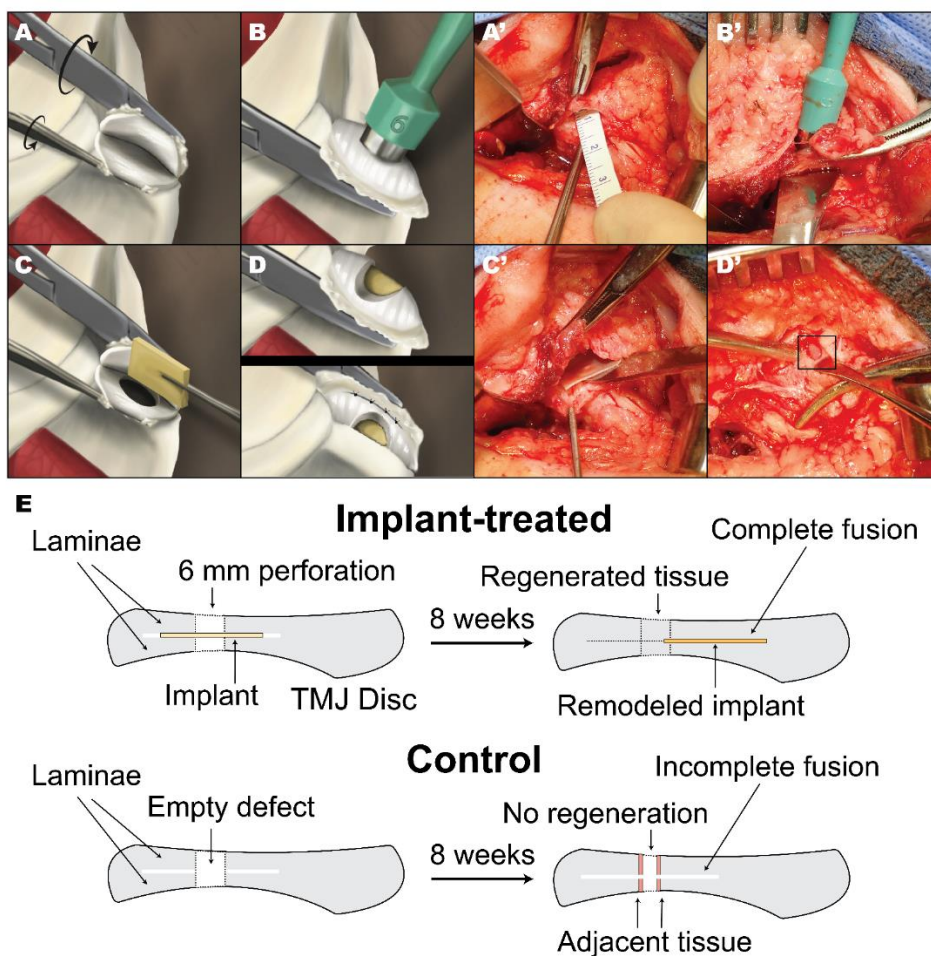


Figure 2. The intralaminar perforation technique secured implants in place toward regeneration of large perforation defects. After TMJ identification, (A) an incision was made into the lateral edge of the disc and deepened to accommodate the implant. (B) A 6 mm diameter disposable biopsy punch was used to create the perforation defect. (C) The 11x11 mm implant was placed into the lateral incision, and (D) it was viewable through the defect after implantation and suturing along the edge of the disc. After surgery, (E) implant-treated discs facilitated cartilage regeneration, resulting in intralaminar fusion and regenerated tissue deposition. Implants remodeled over 8 weeks and migrated in the posterior direction. Control discs did not regenerate, and tissue adjacent to the defect underwent biochemical changes.

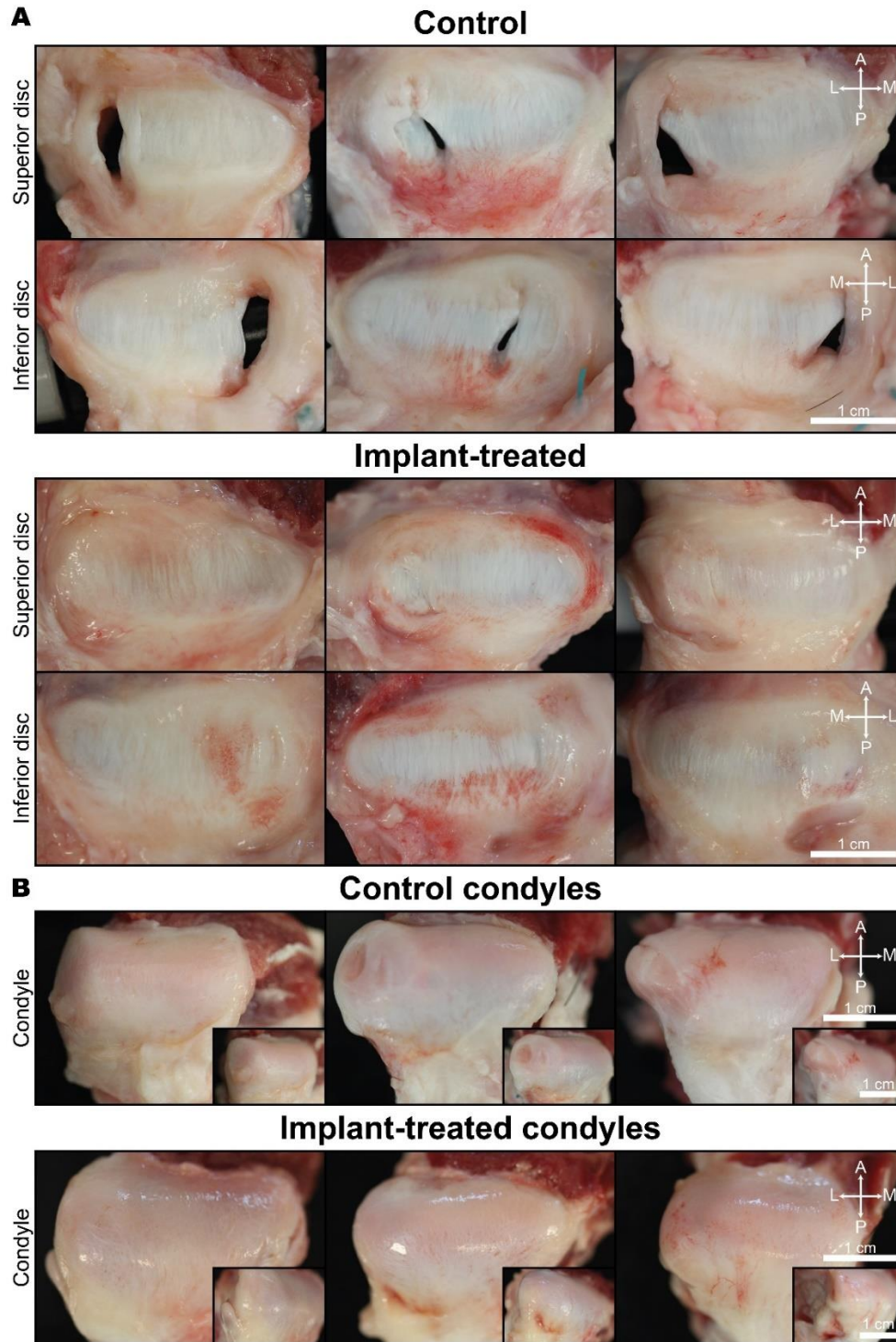


Figure 3. Control discs and condyles showed degenerative changes compared to implant-treated discs and condyles after 8 weeks. (A) In control discs, the created perforations were still present after 8 weeks, while implant-treated discs exhibited complete filling of defects with regenerated tissue. (B) Condyle articular cartilage defects were also present on two of the three articulating surfaces in the control group. In the implant-treated group, minor degenerative changes were shown on the condyles due to suture rubbing associated with surgical intervention. A, anterior, L, lateral, M, medial, P, posterior.

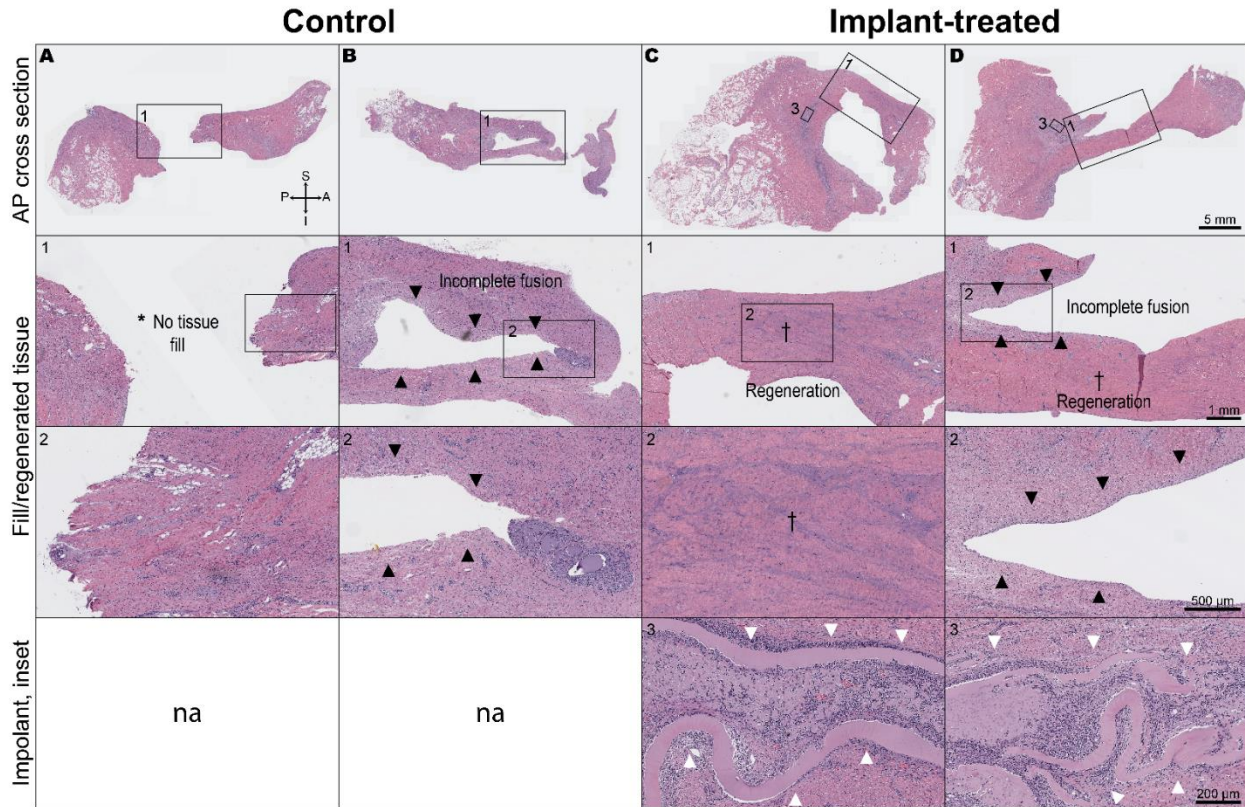


Figure 4. Implant-treated discs exhibited regeneration in the centrolateral region of the TMJ disc, and controls displayed lack of healing. When sectioned in an anteroposterior (AP) direction, four different samples between the two groups displayed various indications of healing and lack thereof. In column (A), a control disc did not exhibit tissue fill in the centrolateral portion (*) of the disc. In column (B), the pocket incision made during surgical implantation (black arrowheads) did not fuse in another control disc. In comparison, both implant-treated discs in columns (C) and (D) exhibited regenerated tissue (†) in the centrolateral portion of the disc, but column (D) did not exhibit complete fusion of the incision (black arrowheads). Both implant-treated discs also had implant remaining (white arrowheads) after 8 weeks of implantation. A, anterior, I, inferior, na, not available, P, posterior, S, superior.

Implants achieved tissue regeneration after 8 weeks; controls did not heal

Self-assembled neocartilage implants in the TMJ disc facilitated the deposition of regenerated tissue, while control discs remained empty and perforated after 8 weeks (Figure 2E). Here, the term “regenerated tissue” refers to the tissue that fills the perforations after 8 weeks in implant-treated TMJ discs. As seen in the gross morphological images of the excised TMJ discs, all three implant-treated animals exhibited remarkable healing of large perforations after 8 weeks, while the three control discs remained perforated (Figure 3A). Upon sectioning anteroposteriorly, implants were identified. Non-closure of the laminae and lack of tissue fill was observed in the controls (Figure 4A-B). Further examination of implant-treated discs showed incomplete

intralaminar fusion in one disc (Figure 4C). Regardless, regenerated tissues for the treated discs were present when examined under hematoxylin and eosin (H&E) staining (Figure 4C-D). The perimeter of the perforation after 8 weeks in controls was 14.6 ± 5.8 mm, significantly higher than implant-treated discs, which had a perimeter of zero (Figure 5A). Similarly, implant-treated discs exhibited no measurable defect area after 8 weeks of healing compared to control discs which had a defect area of 10.2 ± 7.8 mm² (Figure 5B). When examining the intralaminar fusion by mechanically testing the two laminae, Young's modulus and UTS values were 6.8-times and 3.0-times higher in implant-treated discs compared to controls, respectively, although these increases were not statistically significant (Supplementary Table 1). Both implant-treated and control condyles exhibited degenerative changes on the lateral condylar process due to suture anchor placement (Figure 3B), consistent with previous work¹⁹. However, control animals also had cartilage defects on two of three articulating surfaces, while implant-treated condyles did not exhibit cartilage defects (Figure 3B). Ultimately, when examining the gross morphology of the implant-treated discs and condyles, self-assembled neocartilage implants facilitated exceptional healing of discs, unlike the controls that all displayed disc perforations and condylar articular cartilage degeneration.

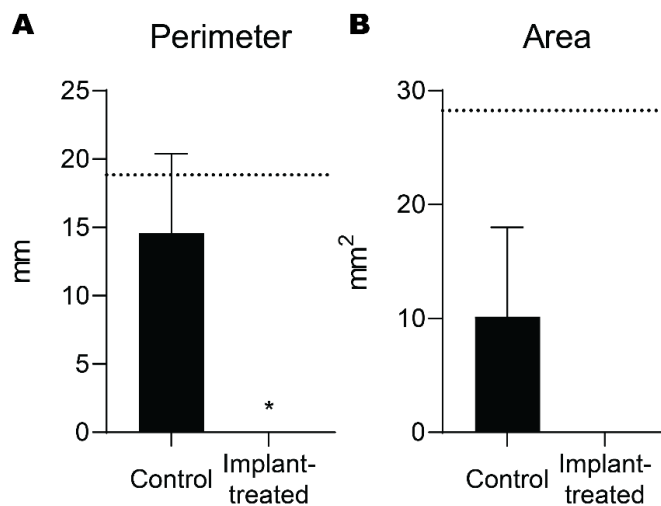


Figure 5. Defect perimeter and area after 8 weeks of implantation were higher in controls. Compared to implant-treated discs, empty defect controls still had measurable defects, which were significantly larger in perimeter. Dashed lines represent the original perforation defect perimeter and area.

Regenerated tissue, only present in implant-treated discs, displayed robust tensile properties

Regenerated tissue was mechanically robust, with mechanical properties approaching those of native TMJ disc fibrocartilage. The controls remained completely perforated; thus, with no tissue present, their mechanical properties were determined to be zero. Mechanical testing of regenerated tissue yielded a tensile Young's modulus of 18.09 ± 5.22 MPa and UTS of 4.77 ± 2.00 MPa, which were 81.2% and 79.2% of the values of the contralateral, native tissue controls, respectively (Figure 6A-B). Strain at failure, resilience, and toughness were 86.1%, 64.5%, and 64.4% of native tissue values, respectively (Figure 6C-E). All regenerated tissue mechanical outcomes were significantly higher than controls. Thus, after 8 weeks of *in vivo* implantation, exceptional healing was further evidenced by the robust mechanical properties of regenerated tissue in the implant-treated discs.

Regenerated tissue biochemical and proteomic composition was reminiscent of native TMJ discs

The biochemical and proteomic makeup of the regenerated tissue was similar to that of the native TMJ disc controls (tissue removed via biopsy punch during surgery). Due to lack of regenerated tissue in controls, biochemical measures for controls were all zero. In the regenerated tissue, total collagen content per dry weight (DW) was $72.8 \pm 20.9\%$, which was 85.9% of the value of the native TMJ disc (Figure 7A). Collagen types I and III were $92.25 \pm 2.99\%$ and $5.99 \pm 2.04\%$ per total protein (PROT), respectively, both within native TMJ disc ranges (Figure 7B-C). The collagen crosslink profile of regenerated tissue was also similar to native TMJ disc, with mature pyridinoline (PYR) crosslinks, immature dihydroxylysinoxidation (DHLNL) crosslinks, and crosslink maturity ratios all on par with native tissue values (Figure 7D-F). All biochemical and proteomic measurements were significantly higher in regenerated tissues than in controls (Figure 7). Other bottom-up proteomic analytes and crosslink measurements are reported in Supplementary Tables 2 and 3, respectively. Over the course of 8 weeks of healing, implant treatment facilitated

the regeneration of TMJ disc fibrocartilage, as shown through the native-like biochemical and proteomic contents in the regenerated tissue.

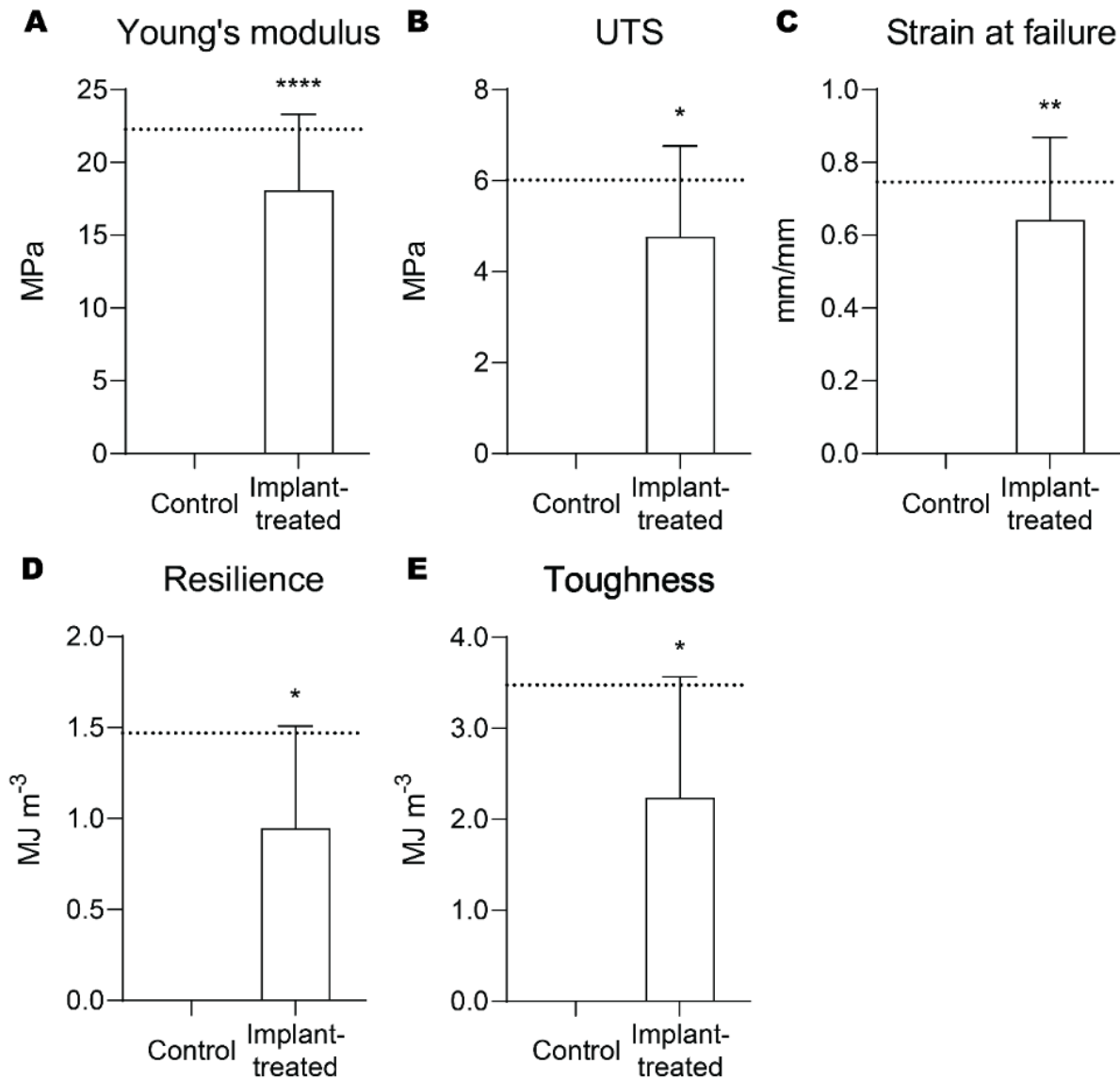


Figure 6. Regenerated tissue tensile properties approached native tissue values. In (A) Young's modulus, (B) ultimate tensile strength (UTS), (C) strain at failure, (D) resilience, and (E) toughness, regenerated tissue of implant-treated discs approached native tissue values (dashed lines), reaching an average of 75.1% of native tissue values across all outcomes.

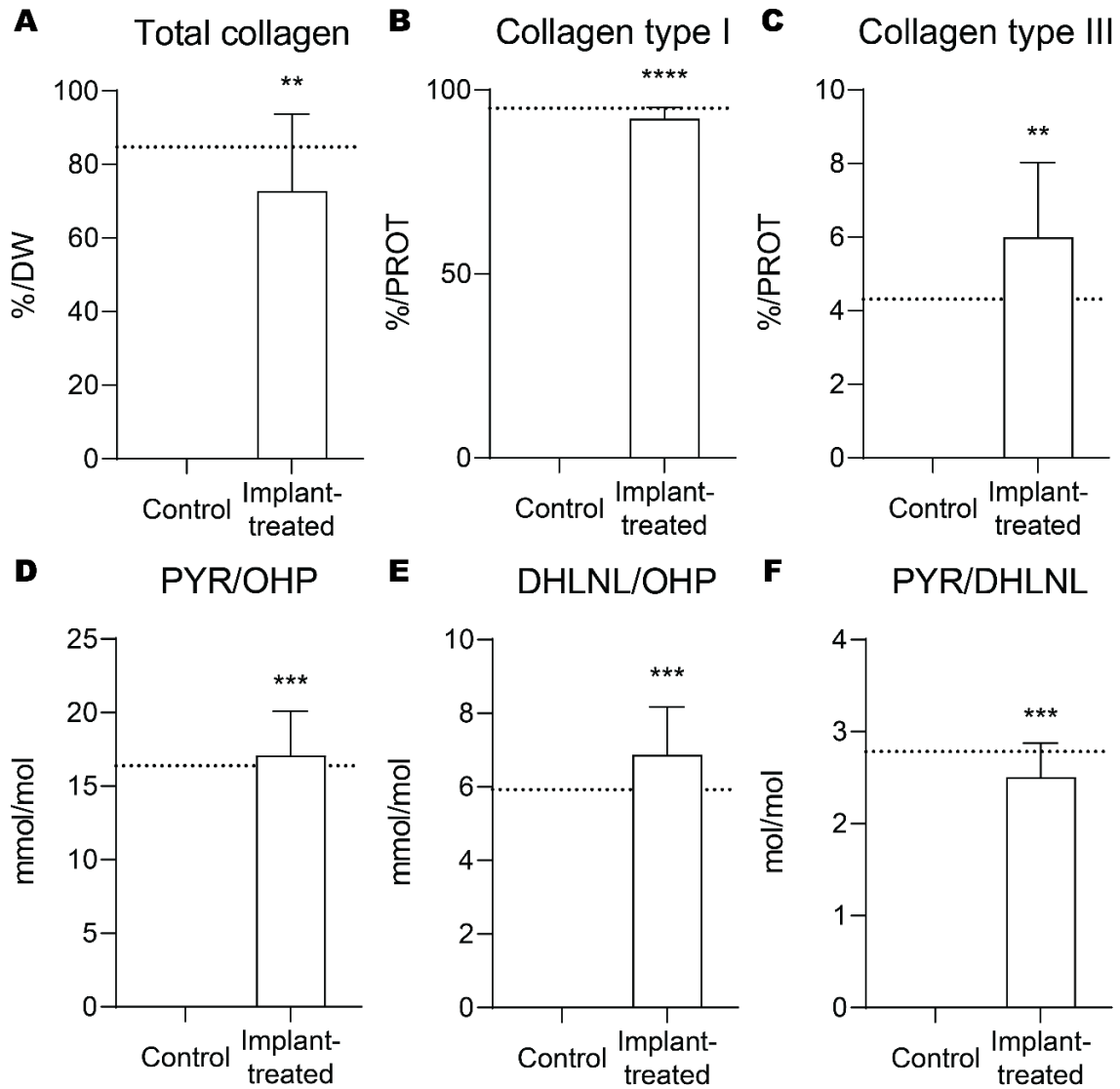


Figure 7. Biochemical and crosslink content of regenerated tissue recapitulated native TMJ disc content. After 8 weeks of healing, (A) total collagen, (B) collagen type I, and (C) collagen type III contents were on par with those of native TMJ discs (dashed lines). Collagen types I and III are reported per total protein (PROT). Similarly, (D) pyridinoline (PYR) and (E) dihydroxylysinoxonorleucine (DHLNL) content per hydroxyproline (OHP) and (F) their ratio were also near native tissue values.

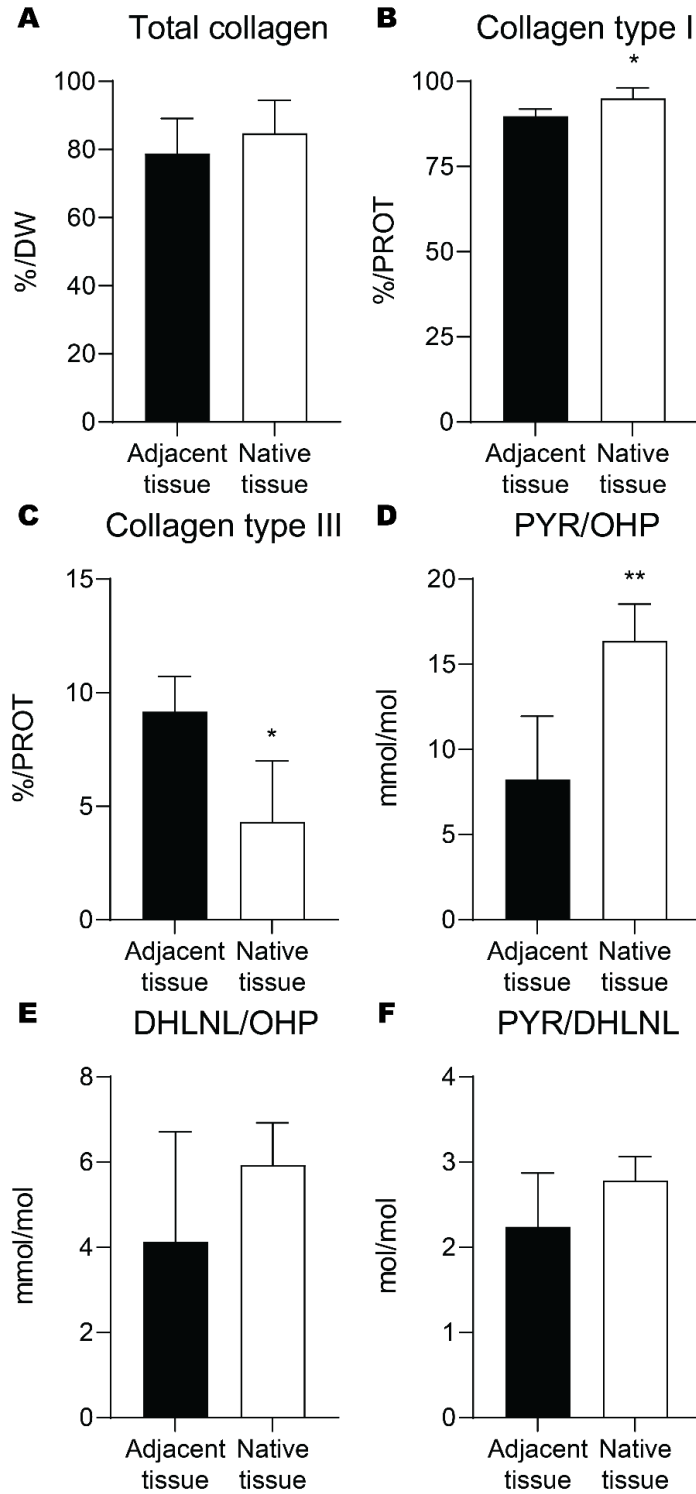


Figure 8. Adjacent tissue to control perforations deviated from native tissue in biochemical and crosslink content. (A) Total collagen, (B) collagen type I, and (C) collagen type III are reported for tissue adjacent to control defects and native TMJ discs. Collagen types I and III are reported per total protein (PROT). Crosslinks data including (D) pyridinoline (PYR) and (E) dihydroxylysinonorleucine (DHLNL) per hydroxyproline (OHP) and (F) their ratio are reported.

Tissue adjacent to perforations in controls deviated from native TMJ disc composition

The biochemical and proteomic properties of the tissue adjacent to the control perforations (referred to as “adjacent tissue”) were different than those of control TMJ disc tissue. Because the regenerated tissue was grossly indistinguishable from native TMJ disc, and because there was no discernible border between regenerated tissue and native tissue, the adjacent tissue was compared to native TMJ discs. Total collagen content per DW was not significantly different in adjacent tissue compared to native control TMJ discs (Figure 8A); however, collagen type I, the primary collagen subtype in the TMJ disc²³, was significantly lower in the adjacent tissue ($89.79 \pm 2.05\%/PROT$) than in native TMJ disc ($95.01 \pm 3.10\%/PROT$) (Figure 8B). Collagen type III, associated with scar tissue formation²⁴, was significantly higher in the adjacent tissue ($9.17 \pm 1.55\%/PROT$) than in native TMJ disc ($4.31 \pm 2.69\%/PROT$) (Figure 8C). Mature PYR crosslinks per hydroxyproline (OHP) were also lower in the adjacent tissue (8.2 ± 3.7 mol/mol) than in native TMJ disc (16.4 ± 2.2 mol/mol), indicating that the collagen of the adjacent tissue was less crosslinked (Figure 8D). Immature DHLNL crosslinks and the collagen crosslinks ratio were not significantly different, but the means were lower in adjacent tissue (Figure 8E-F). Additional proteomic and biochemical properties of adjacent tissue are reported in Supplementary Tables 2 and 4, respectively. The lower crosslink and collagen type I content and higher collagen type III content show that tissues adjacent to control perforations are undergoing postoperative biochemical changes, potentially indicating pathological progression of the control TMJ discs.

Implants remodeled, exhibiting biochemical and proteomic contents similar to native TMJ discs

The implants exhibited significant biochemical changes over the implantation period, where they remodeled toward the makeup of native TMJ disc (Figure 9). When compared to $t=0$ *in vitro* controls, $t=8W$ *in vivo* implants had many significant differences in biochemistry, mechanics, collagen crosslinks, and proteomics. Between the $t=0$ *in vitro* and $t=8W$ *in vivo* implants, total collagen significantly increased from $19.4 \pm 1.2\%/DW$ to $33.0 \pm 13.6\%/DW$, a 1.7-times increase,

although this value was still lower than native TMJ disc (84.8%/DW, dashed line) (Figure 10A). In contrast, implants cultured *in vitro* for 8 weeks did not have significantly different total collagen compared to the t=0 *in vitro* implants (Figure 10A). GAG content decreased from t=0 *in vitro* controls in both the t=8W *in vitro* and t=8W *in vivo* implants; however, only the GAG of the t=8W *in vivo* implants ($0.3 \pm 0.5\%/DW$) dropped to levels similar to native TMJ discs (1.2%/DW, dashed line) (Figure 10B). Some mechanical measurements of the implant significantly decreased after 8 weeks *in vivo*, with the UTS, resilience, and toughness dropping by 55.5%, 73.2%, and 58.9%, respectively (Figure 10C-F). Compressive properties of implants are reported in Supplementary Table 5, but t=8W *in vivo* implants were not tested due to lack of tissue availability. Despite these drops in tensile properties, biochemical content of implants remodeled toward native tissue levels of TMJ discs.

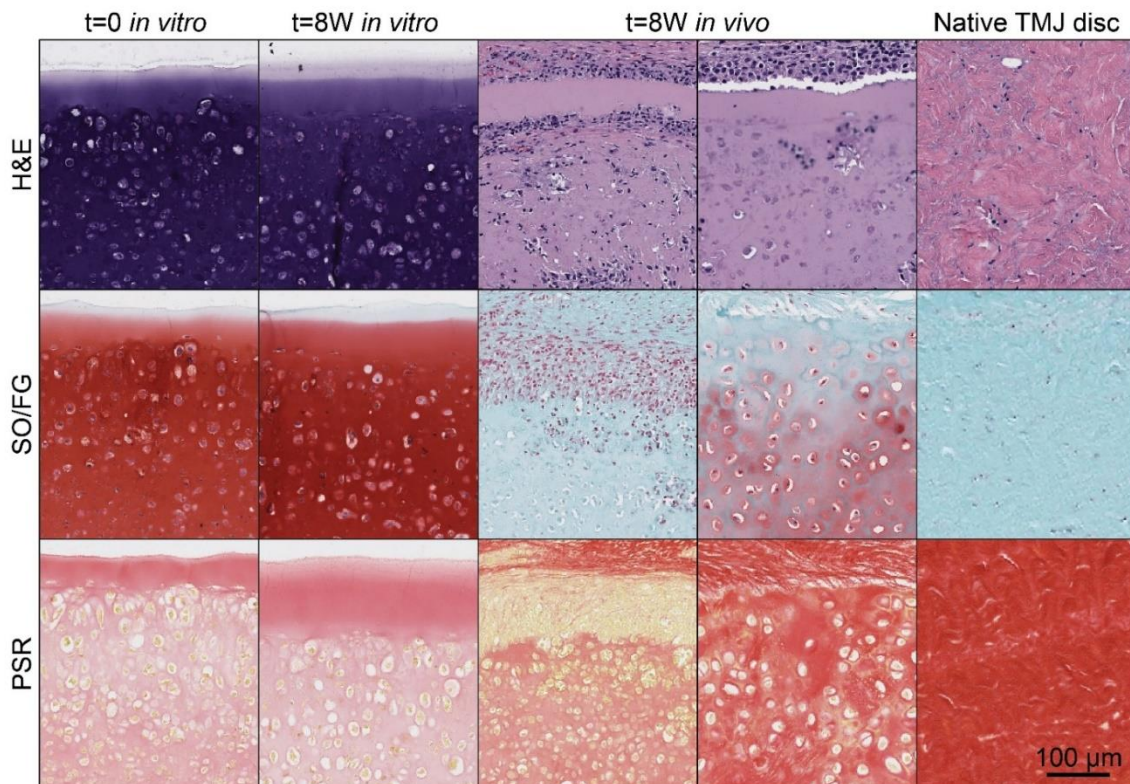


Figure 9. Histology of neocartilage implanted for 8 weeks displayed similarities to native TMJ discs. Hematoxylin and eosin (H&E) for general tissue and cellular morphology, safranin O with fast green counterstain (SO/FG) for glycosaminoglycans, and picosirius red (PSR) for total collagen are shown. Generally, there were few differences between t=8W *in vitro* implants t=0 *in vitro* implants, while implants placed *in vivo* for 8 weeks remodeled toward the native TMJ disc content in both animals presented (columns).

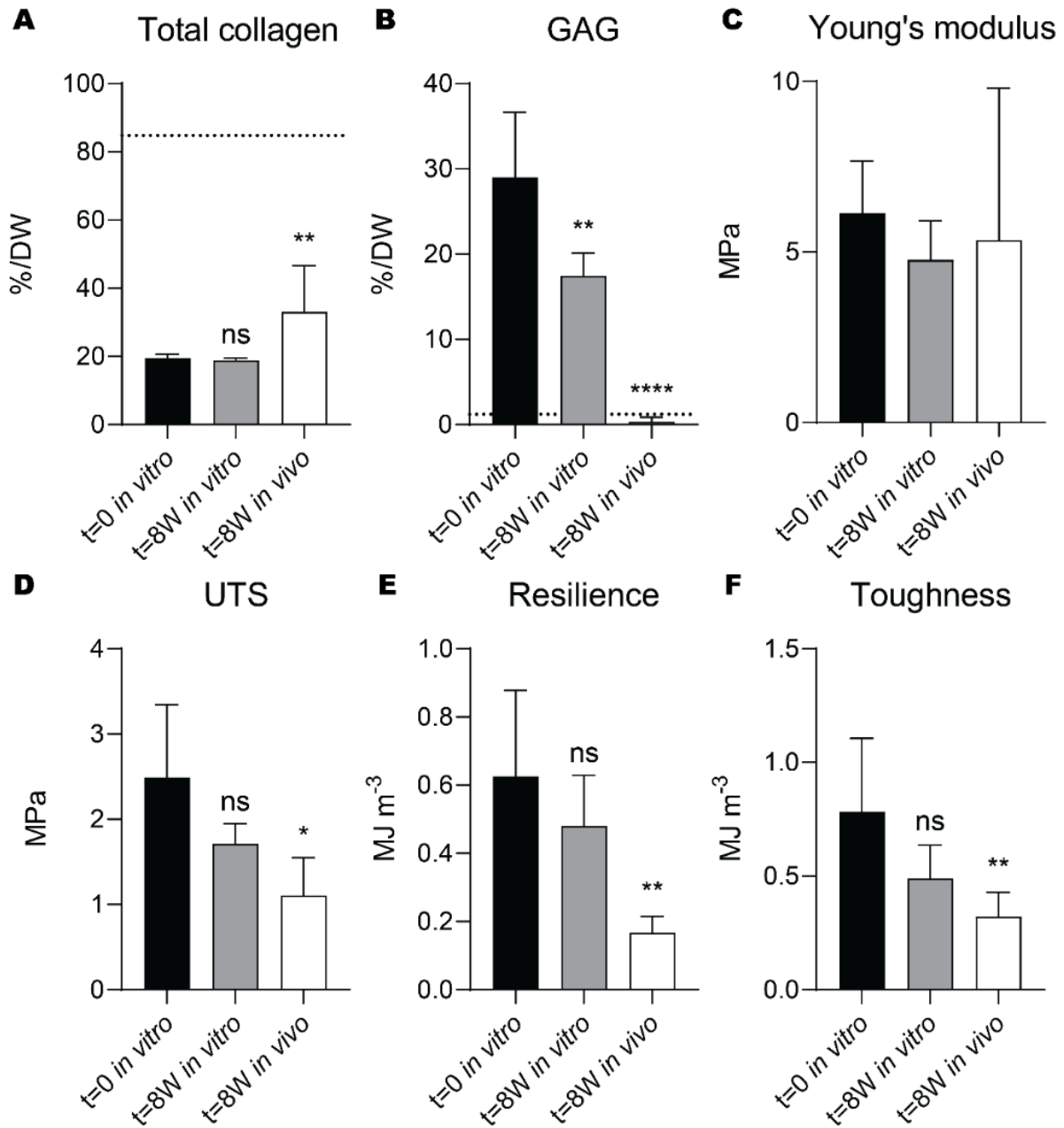


Figure 10. Biochemical properties of implants after 8 weeks remodeled toward native tissue values. Over 8 weeks, (A) total collagen and (B) glycosaminoglycan (GAG) contents trended toward native tissue values (dashed lines) in implants placed in vivo. (C) Young's modulus, (D) ultimate tensile strength (UTS), (E) resilience, and (F) toughness decreased after implantation.

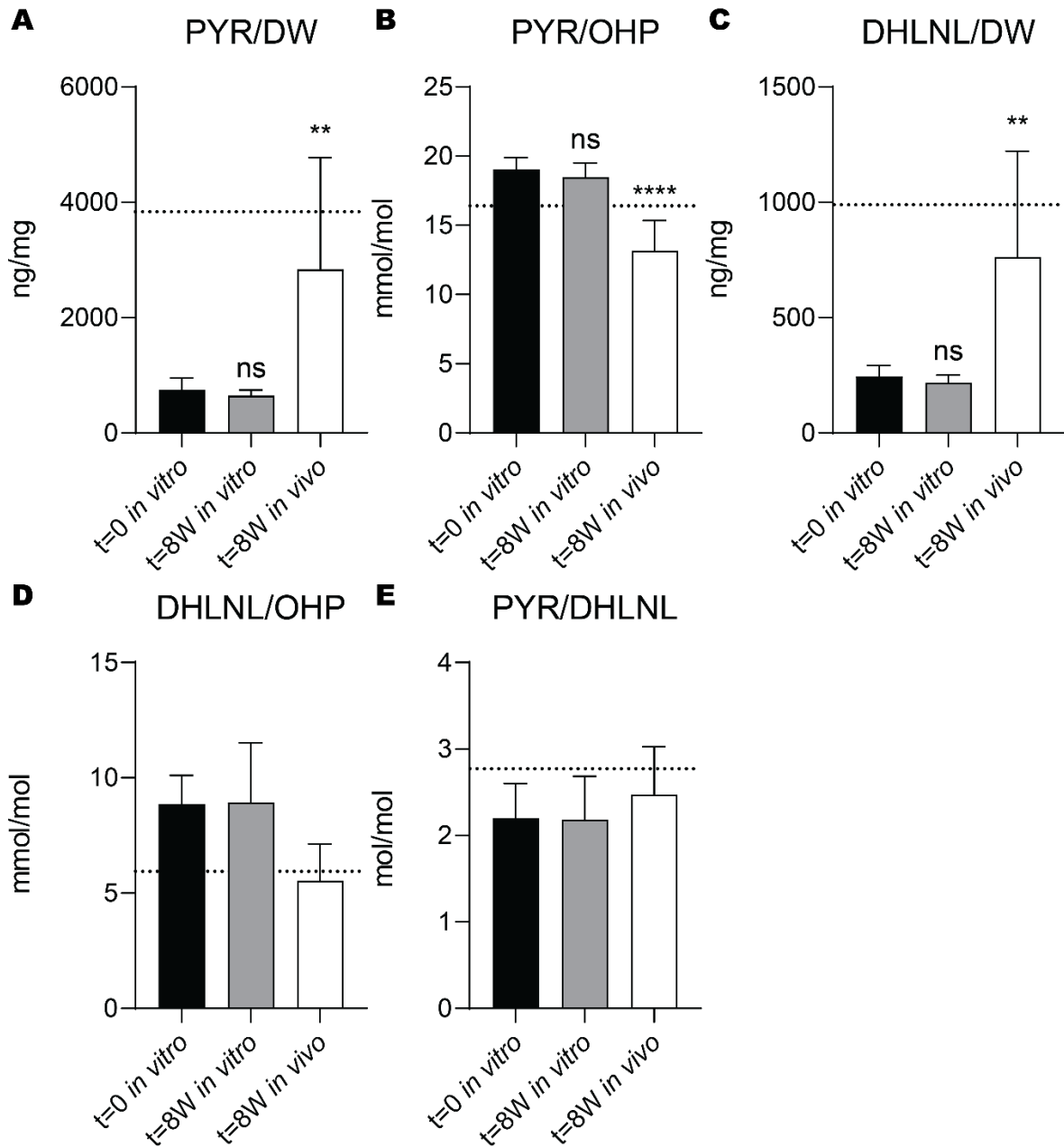


Figure 11. Crosslink content after 8 weeks remodeled toward native tissue values. (A) Pyridinoline (PYR) per dry weight (DW) and (B) per hydroxyproline (OHP), (C) dihydroxylysinoxidation (DHLNL) per DW and (D) per OHP, and (E) their ratios are reported.

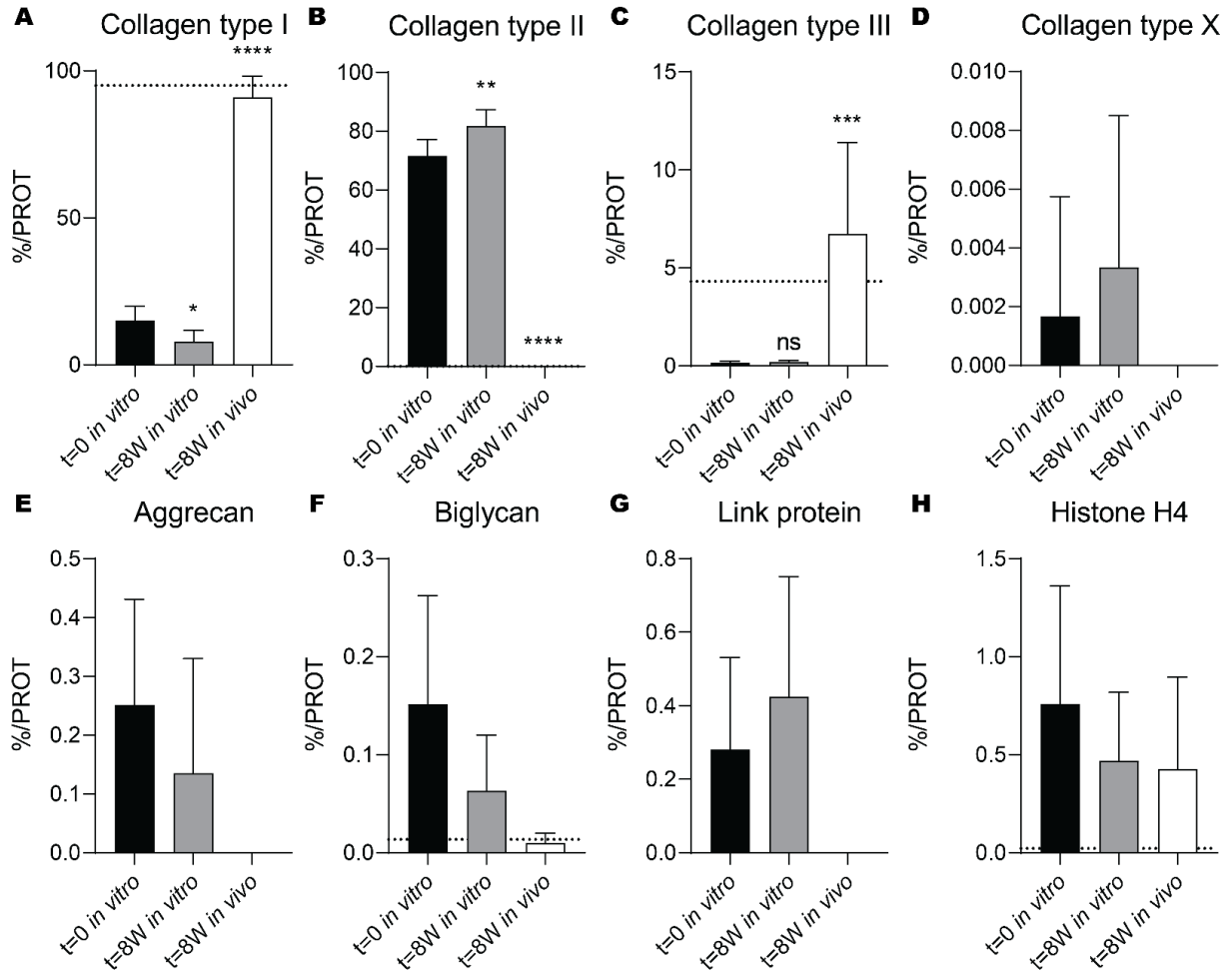


Figure 12. Proteomic analytes after 8 weeks of implantation further approached native tissue values. (A) Collagen type I, (B) collagen type II, (C) collagen type III, (D) collagen type X, (E) aggrecan, (F) biglycan, (G) link protein, and (H) histone H4 are presented per total protein (PROT) content as a percentage. Dashed lines represent native tissue values. Panels without dashed lines had no detectable protein in native tissue samples.

The collagen crosslink profile of the implants also underwent *in vivo* remodeling, with PYR/DW and DHLNL/DW both significantly increasing by 3.8-times and 3.1-times, respectively (Figure 11A, C). However, given the 1.7-times increase in total collagen in the t=8W *in vivo* implants compared to t=0 *in vitro* baseline values (Figure 10A), the increases in crosslinking per DW were likely conflated with increases in total collagen. The degree of collagen crosslinking (i.e., PYR/OHP) was significantly lower in t=8W *in vivo* implants (Figure 11B), which potentially led to inferior tensile properties (Figure 10C-F). However, most collagen crosslink measures of the t=8W *in vivo* implants were closer to native tissue values than t=0 *in vitro* implants (Figure 11). The

proteome of the neocartilage implants was also shown to remodel toward fibrocartilage over the 8-week implantation period. Collagen type I, the main collagen subtype of fibrocartilage²³, significantly increased 6.1-times over 8 weeks of implantation, while collagen type II, the main collagen subtype of hyaline cartilage²³, decreased by over 99.9% (Figure 12A-B). Collagen type III significantly increased 39.6-times toward levels of the native TMJ disc (Figure 12C). Importantly, collagen type X, associated with cartilage calcification²³, was minimal (<0.01%/PROT) in t=0 *in vitro* controls and was not found in t=8W *in vivo* implants, indicating that the costal chondrocyte-derived implants did not have a propensity to calcify. Other proteomic analytes, including aggrecan, biglycan, and link protein dropped to levels similar to native TMJ discs (Figure 12E-H). All bottom-up proteomic analytes are reported in Supplementary Table 2. Bottom-up proteomics further revealed that the ECM of the implants remodeled toward native tissue levels after 8 weeks, where they recapitulated the biochemical and proteomic profile of TMJ discs.

Implants exhibited safety, as shown by no adverse systemic response and minimal local response

Self-assembled neocartilage implants were immunogenically well-tolerated by the recipient minipigs. After surgery, animal jaw function was normal, and minipigs maintained or gained weight, as expected. After euthanasia, a full necropsy of the integumentary, cardiovascular, respiratory, musculoskeletal (non-TMJ), digestive, urogenital, endocrine, and nervous systems revealed normal morphology without cellular damage, inflammation, or neoplastic growth. The complete blood count and comprehensive metabolic panel (Figure 13, Supplementary Table 6) revealed few differences at 8 weeks from preoperative blood work. Two animals had moderate increases in eosinophil count (one in the control group at 4.46 K/ μ L, one in the implant-treated group at 2.62 K/ μ L, reference range 0.00-2.00 K/ μ L) (Figure 13A). Because the value observed in the implant-treated animal was closer to the reference value than the value observed in the control animal, the elevated eosinophil levels were considered to not be a result of the tissue-

engineered implants. The comprehensive metabolic panel showed that all measurements were within normal limits, with only minor differences from baseline values (Figure 13B).

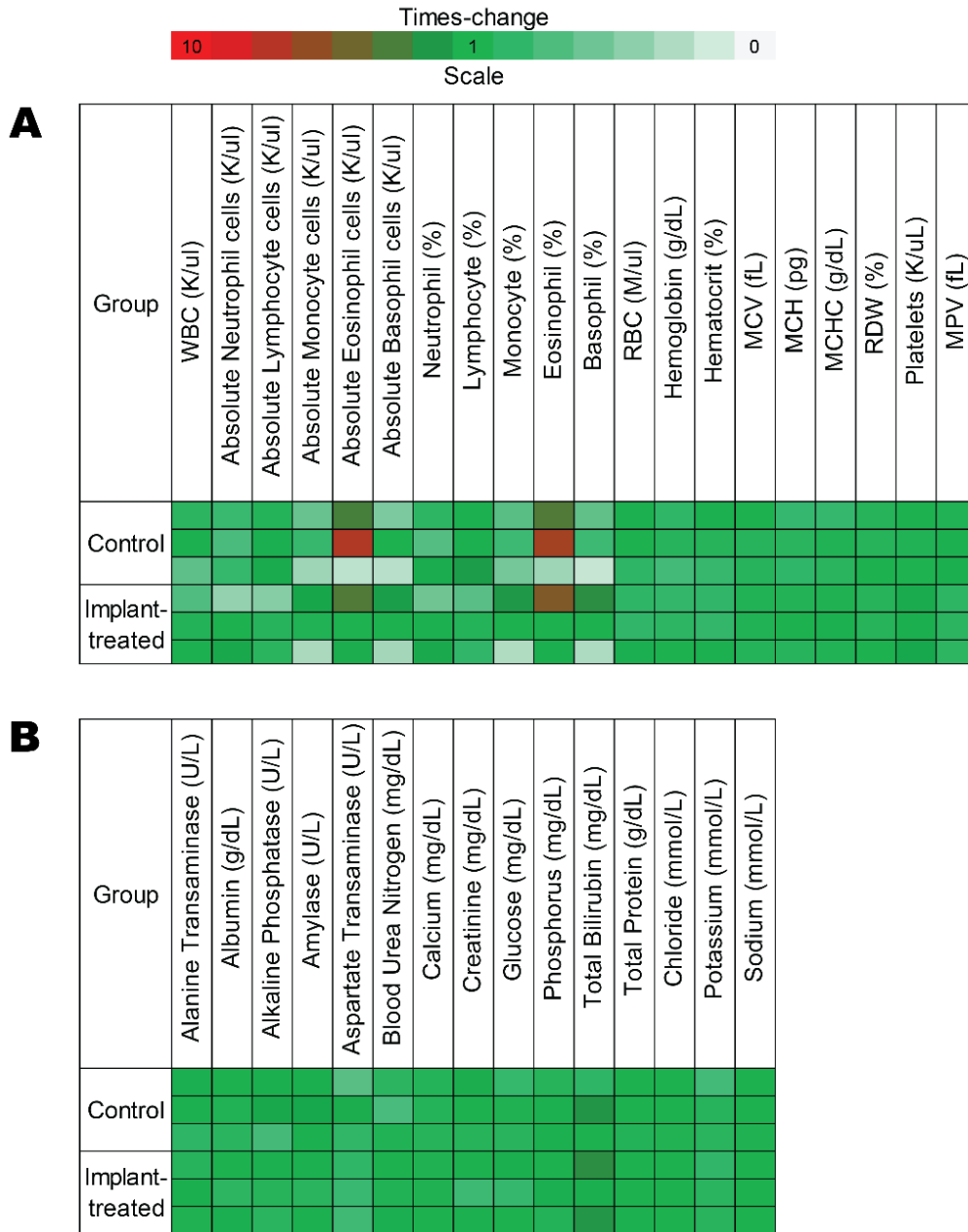


Figure 13. Heatmap of normalized complete blood count and comprehensive metabolic panel parameters showed no abnormal systemic effects due to implants. A majority of parameters after 8 weeks were within normal limits, despite some changes from t=0 baseline values. Each row represents a different animal. Moderate numbers of eosinophils were detected in one control and one implant-treated animal; this was determined to not be due to the implant treatment.

Locally, joints exhibited acute swelling and inflammation after surgical intervention which subsided within 2 weeks, as expected. Incisions healed and presented with minimal scarring at 8 weeks. Minipig TMJs exhibited no signs of inflammation or neoplastic growth as examined during *en bloc* excision. Additionally, the synovium appeared non-reactive through gross observation, the joint capsule was intact, and the synovial fluid was minimal and clear in color, indicative of a healthy joint. When further examining cross sections of implants surrounded by native TMJ disc through H&E, there was a moderate cellular immune response (Figure 14), consistent with previous 8-week studies^{18,19}. Through H&E, it was determined there were no multinucleated giant cells, polymorphonuclear cells, or capsule formation. Overall, through the examination of the systemic and local responses, safety of self-assembled neocartilage implants was shown.

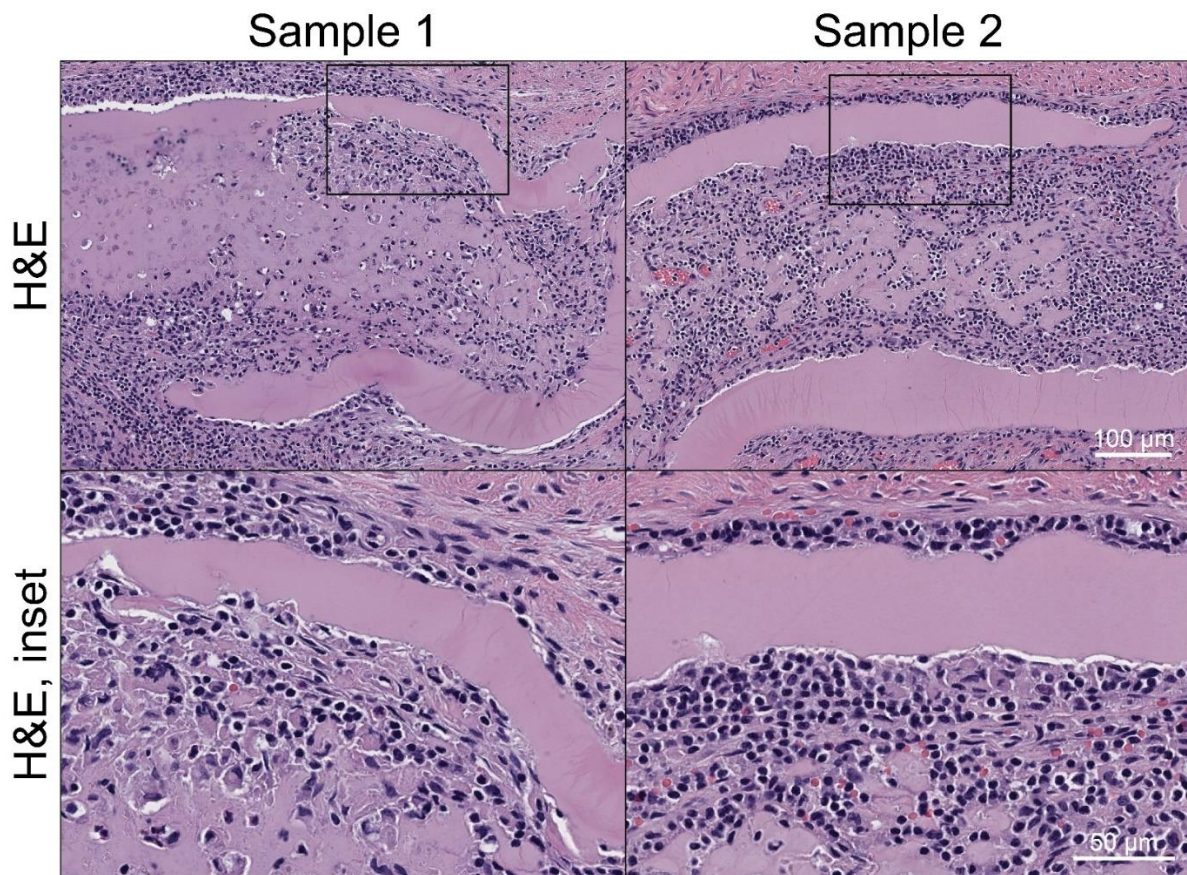


Figure 14. H&E revealed moderate cellular response to TMJ disc implants. After examination through hematoxylin and eosin (H&E), no multinucleated giant cells, polymorphonuclear cells, or capsule formation were observed.

Discussion

Cartilage tissue engineering has the potential to treat TMDs in millions of patients in the U.S. and worldwide, but safety and efficacy of the tissue-engineered implants must be validated through preclinical animal models and clinical trials before they can be widely used in humans. This work represents a significant step in showing safety and efficacy of self-assembled neocartilage implants for regenerating TMJ disc perforations in a clinically relevant, large animal model. Specifically, it was shown that 1) neocartilage implants safely resulted in regenerated TMJ disc fibrocartilage, 2) implanted neocartilages remodeled toward a TMJ disc fibrocartilaginous tissue, 3) TMJ disc fibrocartilage regeneration occurred within 8 weeks, and 4) perforations of 6 mm diameter were shown to be a critical defect size after 8 weeks. Through this work, the regeneration of fibrocartilage in large perforations of the TMJ disc using self-assembled neocartilage represents substantial progress for translation of tissue-engineered cartilage treatments for TMDs.

The present work represents a significant step forward in showing the safe and effective regenerative capability of self-assembled neocartilage. In this TMJ disc study, no neoplastic growth, cellular damage, or changes from preoperative values as a result of implant treatment were observed systemically. Locally, consistent with previous 8-week studies^{18,19}, a moderate cellular response with no signs of multinucleated giant cells, polymorphonuclear cells, or capsule formation was present, indicating neocartilage safety. The differences in the gross morphological appearances of the implant-treated TMJ discs and controls were stark; all control discs remained perforated after 8 weeks, while the implant-treated discs appeared similar in morphology to healthy TMJ discs. The regenerated tissue's tensile properties were, on average, 75.1% of native tissue values, with a biochemical makeup similar to native tissue. Shown through bottom-up proteomics, collagen type I and III quantities were 97.1% and 139.0% of native TMJ disc values, respectively, both within the range of native values. Altogether, the morphological, mechanical, biochemical, and proteomic results showed that neocartilage implants were effective for

regenerating TMJ disc fibrocartilage. Cartilage regeneration has remained elusive despite the longstanding effort to develop regenerative approaches²⁵. In this work, safe and efficacious fibrocartilage regeneration was achieved, representing a significant step forward in cartilage tissue engineering efforts.

Neocartilage implants were shown to remodel over time toward a fibrocartilaginous biochemical makeup. At t=8W *in vivo*, the implants increased in collagen content by 1.7-times and decreased in GAG by 98.9% compared to t=0 *in vitro* controls. Given the high amount of collagen and low GAG content of fibrocartilages¹⁷, these changes represent fibrocartilaginous remodeling in the neocartilage implant. This is further reinforced by the proteomics data; collagen type II was initially the primary collagen type upon implantation, accounting for 71.62% of protein, but this value drops to less than 0.05% after 8 weeks *in vivo*, the level of the native TMJ disc. Collagen types I and III, the main collagen subtypes of TMJ discs²³, increased 6.1-times and 39.6-times, respectively, also showing remodeling toward protein proportions of native TMJ disc controls. Other protein analytes, such as aggrecan, biglycan, link protein, and histone H4 also converge to levels similar to native TMJ discs. Given the hypocellularity of the implants at 8 weeks and the immune cells surrounding the implant, it was likely the remodeling seen here was driven by the host response to the implant. This can be verified in future *in vivo* work by implementation of cell tracking technology (e.g., GFP-transfected neocartilage or chromosomal *in situ* hybridization), which would show whether cells in the implant remain and deposit new ECM, or if they are cleared away over time. Though how the remodeling occurs remains to be fully understood, the results presented here are significant in showing that neocartilage implants remodeled toward the phenotype of native TMJ discs after an 8-week maturation time *in vivo*, further reinforcing the safety of the tissue-engineered implant.

In this work, regenerated tissue and implant analyses were performed 8 weeks after implantation. Comparisons to previous long-term studies (i.e., 24 weeks)¹⁹ may help predict how the implants in this study would continue to heal large perforations in the long term. For example,

it can be hypothesized that mechanical properties of the regenerated tissue would improve beyond 8 weeks. In the present study, the 8-week regenerated tissue had a UTS of 4.77 ± 2.00 MPa, which was 79.2% of the strength of native tissue. In a 24-week study on smaller perforations¹⁹, the regenerated tissue had a UTS of 8.67 ± 2.04 MPa, 1.8-times higher than this 8-week study. While the ~80% recovery of native UTS in 8 weeks is promising, the increase seen at 24 weeks indicates long-term survivability and functionality of the regenerated tissue. Differences in implant remodeling were also seen between the 24-week study¹⁹ and the present 8-week study. Proteomic analysis showed that the collagen subtypes of the implants remodeled toward fibrocartilage (i.e., more collagen types I and III, less collagen type II) in both studies; however, visualized with H&E staining, implant degradation appeared to begin between 8 and 24 weeks. The implant appeared hypocellular and intact after 8 weeks *in vivo* (Figure 9), but during the 24-week study¹⁹, neocartilage implants were infiltrated by immune cells and underwent additional remodeling. It can be hypothesized that longer term studies (i.e., one year long) would show the neocartilage implant completely remodel, leaving behind only regenerated TMJ disc. To completely assess the safety and efficacy of healing large perforations with self-assembled tissue-engineered implants, studies up to one year in length will be necessary to assess functionality and safety outcomes.

Defects of 6 mm diameter were considered to be a critical defect size after 8 weeks. In comparison to the 24-week study¹⁹, all but one of the 3 mm perforations in control discs closed. Here, all three 6 mm empty defects remained perforated after 8 weeks, and it was shown that tissue adjacent to these perforations had changes such as significantly lower collagen type I and mature crosslinking, and significantly higher collagen type III compared to native tissue. Given the cartilage degeneration on the mandibular condyle in the control group, it is possible that these changes are indicative of degeneration around the periphery of the perforation. However, longer term studies of large perforations will be crucial in determining whether these were degenerative changes (e.g., further decreases in collagen type I and crosslinks, further increases in collagen

type III) or reparative changes (e.g., closure of the perforation). While additional studies must be performed to determine whether untreated 6 mm perforations are capable of healing in the long-term, the 8-week time point was demonstrated to be an appropriate short-term endpoint for assessing regeneration of TMJ disc fibrocartilage in the Yucatan minipig model.

The intralaminar perforation technique has been used in three large animal models to date: a small disc-thinning model¹⁸, a small perforation model¹⁹, and, in the present study, a large perforation model. The 6 mm perforation (two-sided, full thickness) defect in this study represents an 8-times scale up in area from the initial 3 mm disc-thinning (one-sided, partial thickness) defect¹⁸. Through additional modifications to the technique, other TMD models, such as large disc-thinning (i.e., perforating one of the two laminae with a 6 mm biopsy punch) can be performed in the Yucatan minipig. Defects of the mandibular condyle are also common in TMDs and can occur in conjunction with discal TMDs²⁶. With the development of chondral or osteochondral tissue engineering strategies targeted toward the condylar cartilages, a broader array of pathologies could potentially be treated with a combination of the intralaminar perforation technique and an additional technique for the condyle. Arthroscopic implementation of the intralaminar perforation technique will also be beneficial, given improvements in recovery time for arthroscopies versus open surgeries^{27,28}. While the intralaminar perforation surgical approach was used in this study to regenerate disc perforations, extending the technique to address additional TMD indications will be beneficial to a wider patient population.

This work is impactful because it fulfills one of the most important translational objectives prior to clinical trials—showing safety and efficacy in a large animal model. The ultimate goal for TMJ cartilage tissue engineering is to create an effective human therapeutic, and large animal studies generate important preclinical data to begin translation of biomedical technologies to the clinic. With the safety and efficacy of neocartilage implants shown here, long-term, pivotal animal studies would be the next step toward beginning an investigational new drug (IND) and/or investigational device exemption (IDE) application to the US Food and Drug Administration (FDA).

The minipig has been established as an appropriate animal model for translation to human TMJ work^{17,19,29}, and robust neocartilage implants have been produced with human chondrocytes³⁰. Thus, with FDA approval, the tissue engineering process in this work can be applied in human clinical trials to advance the translation of neocartilage implants toward widespread human usage.

In 1983, the FDA approved the use of Vitek Inc.'s Proplast-Teflon implant for TMJ disc replacement. This implant was used in about 10,000 people, but, after surgery, the implant degraded and released Teflon into surrounding vasculature and tissue, causing catastrophic side effects including cranial breaching^{31,32}. Given the TMJ's close proximity to the brain and other sensory structures¹¹, safe, cell-based therapeutics made from materials recognized by the human body represents an exciting and hopeful prospect for people who suffer debilitating pain from TMDs. Despite the need to correct past mistakes of the TMJ field and provide modern solutions to TMDs, there are no FDA-approved, cell-based TMJ implants today^{10,11}. The regeneration of TMJ disc perforations in this study represents a critical step along the translational pathway, where, through the rigorous FDA-guided regulatory process, tissue-engineered TMJ cartilage therapeutics are envisioned to substantially improve TMD outcomes in millions of people.

Materials and methods

Tissue engineering of implants

Costal chondrocytes were sourced from three male juvenile (5-8 month) Yucatan minipigs, culled for purposes unrelated to this study, as previously described²⁰. Briefly, in a biosafety cabinet, ribcages were dissected using sterile tools to reveal costal cartilage, and, after perichondrium removal, cartilage was cut into small pieces, approximately 1 mm³ in size. Pronase and collagenase solutions were made by resuspending the enzymes at 0.4% (w/v) and 0.2% (w/v), respectively, in Dulbecco's modified Eagle's medium (DMEM, high glucose, GlutaMAX supplement) with 3% fetal bovine serum (FBS) and 1% penicillin-streptomycin-fungizone (PSF). Cartilage was digested in pronase solution for 1 hour followed by collagenase solution for 18

hours, both in a 37°C incubator. Digests were filtered through 70 µm cell strainers and treated with a lysis buffer³³. After this single-cell suspension was obtained, medium formulations were based on chondrogenic (CHG) medium, which contained DMEM, 1% PSF, 1% nonessential amino acids, 1% insulin-transferrin-selenous acid+, 100 nM dexamethasone, 50 µg/mL ascorbate-2-phosphate, 40 µg/mL L-proline, and 100 µg/mL sodium pyruvate.

For expansion, chondrocytes were seeded into T225 flasks at 2.5M cells per flask (~11,111 cells/cm²) in CHG medium supplemented with 2% FBS, 1 ng/mL TGF-β1, 5 ng/mL basic fibroblast growth factor (bFGF), and 10 ng/mL platelet-derived growth factor (PDGF), as previously described³⁴. Medium was changed every 3-4 days during expansion. To passage the cells, 0.05% trypsin-EDTA was added to flasks for 9 minutes, cell sheets were aspirated with a serological pipette and placed into 50 mL conical tubes, and cell sheets were digested in collagenase solution for 30 minutes at 37°C with agitation every 10 minutes. After one passage, chondrocytes were frozen for future usage in FBS with 10% dimethyl sulfoxide (DMSO). Thawed chondrocytes were plated for continued expansion. After seven passages, cells were transferred to aggregate rejuvenation culture³⁰. For aggregate rejuvenation, medium was comprised of CHG medium supplemented with 10 ng/mL TGF-β1, 100 ng/mL growth differentiation factor 5 (GDF-5), and 100 ng/mL bone morphogenetic protein 2 (BMP-2). During aggregate rejuvenation, medium was changed every 3-4 days. After 11 days of aggregate rejuvenation, 0.05% trypsin-EDTA was added to aggregates for 45 minutes at 37°C followed by collagenase solution for 90 minutes at 37°C with agitation every 10 minutes to digest aggregates into a single-cell suspension. Cells were then filtered through 70 µm cell strainers.

After aggregate rejuvenation, chondrocytes underwent self-assembly to form neocartilage³⁵. Briefly, 11x17 mm negative mold wells were made from 2% molten agarose. CHG medium was pipetted into the wells after they were solidified, and medium was changed three times. Cells (15M/well) were then seeded with 600 µL of CHG medium into each well. CHG medium (5 mL/well) was added 4 hours later, and medium was exchanged every day until implant

unconfinement on day 2, where implants were released from wells. After day 2 of self-assembly, CHG medium was supplemented with TGF- β 1 (10 ng/mL), and, every 2 days, neocartilage implants were fed with 10 mL of CHG medium until day 42. On day 7 of self-assembly, implants were treated with 1.5 U/mL C-ABC for 4 hours³⁶. After day 7, CHG medium was supplemented with 10 ng/mL TGF- β 1, 0.15 μ g/mL LOXL2, 0.146 mg/mL hydroxylysine, and 1.6 μ g/mL copper sulfate, as previously described²¹.

For transportation to the surgical suite, neocartilage implants for surgery were kept for 7 hours in a cooler with ice in 50 mL conical tubes with HEPES-buffered CHG medium supplemented with 10 ng/mL TGF- β 1, 0.15 μ g/mL LOXL2, 0.146 mg/mL hydroxylysine, and 1.6 μ g/mL copper sulfate. Implants were placed in an incubator at 37°C overnight for surgery the next day. Neocartilage implants that were not used for surgery were cut in half with a scalpel; one half was used as a t=0 control (t=0 *in vitro*), and the other half was cultured for an additional 8 weeks (t=8W *in vitro*).

In vivo experiments

All *in vivo* work was approved by the Institutional Animal Care and Use Committees (IACUCs) at University of California, Irvine (#AUP-21-033) and University of California, Davis (#21430). This study consisted of six Yucatan minipigs (n=6 females). Three minipigs were controls (empty defect), while the remaining three received tissue-engineered implants.

Presurgical medication and anesthesia

Minipigs were fasted for 24 hours before surgery. Prior to surgery, minipigs were pretreated with intramuscular (IM) Telazol (3-6mg/kg). Lactated Ringer's solution (5-10 mL/kg/hr) was administered via an intravenous (IV) catheter placed in the auricular vein. Ketamine (5 mg/kg), diazepam (0.2-0.5 mg/kg), and isoflurane via facemask were used to induce anesthesia. Prior to intubation, 2% lidocaine (1-2 mL) was used to treat larynxes, then minipigs were intubated with cuffed endotracheal tubes that were sized based on the individual animal. Morphine (0.5 mg/kg,

IM) was used for preemptive analgesia. During surgery, 1-3% isoflurane in 100% O₂ was used to maintain anesthesia. Positive ventilation was used to maintain end-tidal carbon dioxide between 35-45 mmHg. Throughout surgery, minipigs were monitored via capnography, electrocardiography, and thermometer and blood pressure measurements. A heating pad was used to maintain animal body temperatures at a physiological state (37-38°C).

Surgical implantation and defect creation

Prior to surgical intervention, skin by the operated joint was shaved and aseptically prepared for surgery with alcohol- and iodine-based solutions. As previously described¹⁸, a ~10cm curvilinear incision was made with a #15 scalpel blade following the curvature of the zygomatic arch. This incision was extended superiorly over the temporal process of the zygoma toward the ear, and then blunt dissection was used to continue the incision through the subcutaneous adipose tissue and the periosteum. Periosteum was reflected ventrally and posteriorly using a periosteal elevator, and the TMJ was identified, with the locations noted for the condylar process and mandibular head, the masseter muscle, and lateral TMJ disc attachments. The tissue was thinned out using sharp dissection to further identify the lateral aspects of the joint, and the condylar process was exposed by dissecting through the masseter muscle. The superior joint space was exposed by using a sharp elevation of the superior TMJ disc attachments. The inferior joint was exposed by incising the inferior TMJ disc attachments. The disc and articular cartilages were protected during all dissections.

After these dissections, the lateral, superior, and inferior aspects of the TMJ were accessible. Using a #15 scalpel blade, an incision (~12 mm wide) was created in the lateral edge of the disc. The incision was deepened into the disc (~12 mm deep) to create a pouch with inferior and superior laminae (Figure 2A). Holding the lateral edges of the laminae, a 6 mm diameter disposable biopsy punch was used to create a full thickness perforation through both laminae in the centrolateral region of the disc, avoiding adjacent articulating surfaces (Figure 2B). The

resulting TMJ disc punch was stored in phosphate-buffered saline. For the three minipigs that received tissue-engineered implants, implants were trimmed to 11x11 mm (Figure 1C) and inserted into the lateral incision (Figure 2C). Next, the incision was closed on the lateral edge (Figure 2D) using 5-0 Monocryl sutures, avoiding the implant. A Mitek bone anchor (QuickAnchor Plus, #0 suture) was used to reattach the TMJ disc to the condylar process³⁷. A hole in the condylar process was created using a Jacob's chuck with the supplied drill bit to place the bone anchor. The lateral aspect of the TMJ disc was attached to the double-armed suture to secure the disc to the condylar process, then the remaining layers of tissue were closed with 3-0 Monocryl suture.

Postoperative medication and animal care

Minipigs were given meloxicam (0.1-0.4 mg/kg via IV, IM, or oral delivery) once daily for 3 days, fentanyl (1-5 µg/kg/hr via patch) for 3 days, and buprenorphine (0.005-0.05mg/kg via IM dose) once for postoperative analgesia. Minipigs also received a single dose of perioperative antibiotics. Minipigs were closely observed in narrow pens lined with pads until ambulation and mentation were recovered, then minipigs were returned to housing pens. Minipigs were fed a soft diet for 3 days after surgery, and water bowls were provided rather than spigots. Sutures were removed 14 days after surgery.

Animal euthanasia

Minipigs were humanely euthanized 8 weeks after surgery with Telazol (3-6 mg/kg, IM) followed by Euthazol (phenytoin/pentobarbital, 1 mL/4.5kg, IV). After euthanasia, a full necropsy was performed by a veterinary pathologist to examine organ systems for signs of toxicity or neoplastic growth. TMJ discs and the mandibular heads on the condylar process were removed *en bloc*.

Sample preparation

TMJ tissue samples were photographed prior to dissections. Discs were removed, and the mandibular heads and discs were photographed. If defects were still present in the excised discs, the defect perimeter and area were measured using ImageJ on both the superior and inferior surfaces and averaged to obtain a final measurement. Discs were cut into sections in the anteroposterior direction. From these sections, the implant, regenerated tissue, and tissue adjacent to empty defects were identified. Implants, regenerated tissues, and adjacent tissues were divided into sections for histology, mechanics (tissue mechanics and intralaminar mechanics), biochemistry, and proteomics. The 6 mm punch taken during surgery was used as a native tissue control for collagen, GAG, crosslinks, and proteomics assays, and contralateral TMJ disc samples from the same region of the disc as the perforation were used for mechanical testing and histological controls. Halves of non-implanted neocartilages were divided into samples for histological, mechanical, biochemical, and proteomic analysis at time of implantation (t=0) and at animal euthanasia (t=8W).

Histology

Samples were fixed using 10% neutral buffered formalin for at least 72 hours. Next, samples were processed and embedded in paraffin blocks. Sections of 5 μm thickness were created using a microtome, and sections were mounted on microscopy slides. H&E, safranin O and fast green counterstain (SO/FG), and picosirius red (PSR) stains were performed on the sections, as previously described³⁸. Slides were scanned and digitally visualized using a Roche VENTANA DP 200 slide scanner and QuPath software³⁹.

Mechanical testing

For *in vitro* controls, dog bone-shaped samples were glued to paper tabs of a predefined gauge length for tensile testing. For TMJ disc samples (excised implants, regenerated tissues, contralateral native tissues, intralaminar fusion samples), hemostats were used to clamp samples,

a 0.2 N tare load was applied to remove slack, and calipers were used to measure the gauge length (pretest grip-to-grip clamping distance). Front and side views were photographed to calculate cross-sectional area. All samples underwent 1% strain per second until failure, and a custom MATLAB script was used to analyze the resulting force-displacement curves, determining the Young's modulus and UTS. Strain at failure, toughness (entire area under the curve), and resilience (area under the curve of linear region only) were also calculated. All TMJ disc tissues underwent uniaxial tensile testing in the anteroposterior direction, except for the intralaminar fusion tests, which were performed in the superoinferior direction.

Compressive stress-relaxation tests were performed on *in vitro* controls. Punches of 3 mm diameter for stress-relaxation were taken with a disposable biopsy punch. Using a tare load of 0.1 N, sample height was detected, then samples were preloaded with 15 cycles of 5% strain, as previously described¹⁷. The relaxation modulus, instantaneous modulus, and coefficient of viscosity were determined by applying 20% strain to the punch for 900 seconds, then fitting the resulting force-displacement curves to a standard linear solid model with a custom MATLAB script.

Biochemical testing

Biochemical assays for total collagen and GAG content were performed. Briefly, samples were weighed to obtain a wet weight (WW), they were lyophilized for at least 72 hours, and DWs were taken. Collagen was measured with a modified hydroxyproline assay⁴⁰, while sulfated GAG was measured with a dimethylmethylene blue assay kit.

Mass spectrometry analyses for crosslinks quantification and bottom-up proteomics

Mass spectrometry analyses for collagen crosslinks quantification and bottom-up proteomics were performed, as previously described⁴¹. Briefly, for collagen crosslinks, tissue pieces approximately 1 mg in WW were lyophilized for at least 72 hours, measured for DW, reduced in NaBH₄ for 1 hour, washed in mass spectrometry grade water overnight, and hydrolyzed in 6 N

HCl for 18 hours. Resulting hydrolysates were evaporated in a heat block, resuspended in 0.1% formic acid, filtered with centrifugal filters, and analyzed using a Waters ACQUITY QDa LC-MS system. Quantification of PYR, DHLNL, OHP, and internal standard pyridoxine was performed by taking the area under the curve of the extracted ion chromatograms of each analyte's mass in the TargetLynx module of MassLynx v4.1 software.

For bottom-up proteomics analysis, tissue pieces approximately 1 mg in WW were lyophilized for at least 72 hours, digested in mass spectrometry grade trypsin in a heat block at 65°C overnight, desalted with Waters Sep-pak C18 cartridges, and analyzed with a Thermo Fisher Scientific Orbitrap Fusion Lumos mass spectrometer. MaxQuant was used to perform label-free quantification⁴², reporting protein analytes normalized to PROT content.

Statistical analyses

A Student's t-test or a one-way analysis of variance (ANOVAs) with *post hoc* Dunnett's tests was performed on the data. For the Dunnett's tests, t=0 *in vitro* implants served as controls. Bar graphs were created using GraphPad Prism 9. The degree of significance was depicted by the symbols (ns), (*), (**), (***), and (****), to represent $p > 0.05$ (not significant), $p \leq 0.05$, $p \leq 0.01$, $p \leq 0.001$, and $p \leq 0.0001$, respectively.

References

- 1 Johansson, A., Unell, L., Carlsson, G. E., Soderfeldt, B. & Halling, A. Gender difference in symptoms related to temporomandibular disorders in a population of 50-year-old subjects. *J Orofac Pain* **17**, 29-35 (2003).
- 2 Macfarlane, T. V., Blinkhorn, A. S., Davies, R. M., Kincey, J. & Worthington, H. V. Orofacial pain in the community: prevalence and associated impact. *Community Dent Oral Epidemiol* **30**, 52-60, doi:10.1034/j.1600-0528.2002.300108.x (2002).
- 3 Pow, E. H., Leung, K. C. & McMillan, A. S. Prevalence of symptoms associated with temporomandibular disorders in Hong Kong Chinese. *J Orofac Pain* **15**, 228-234 (2001).
- 4 Goulet, J. P., Lavigne, G. J. & Lund, J. P. Jaw pain prevalence among French-speaking Canadians in Quebec and related symptoms of temporomandibular disorders. *J Dent Res* **74**, 1738-1744, doi:10.1177/00220345950740110401 (1995).
- 5 Solberg, W. K., Woo, M. W. & Houston, J. B. Prevalence of mandibular dysfunction in young adults. *J Am Dent Assoc* **98**, 25-34, doi:10.14219/jada.archive.1979.0008 (1979).
- 6 Farrar, W. B. & McCarty, W. L., Jr. The TMJ dilemma. *J Ala Dent Assoc* **63**, 19-26 (1979).

- 7 Katzberg, R. W. & Westesson, P.-L. *Diagnosis of the temporomandibular joint*. 1 edn, (W.B. Saunders, 1993).
- 8 Munoz-Guerra, M. F., Rodriguez-Campo, F. J., Escorial Hernandez, V., Sanchez-Acedo, C. & Gil-Diez Usandizaga, J. L. Temporomandibular joint disc perforation: long-term results after operative arthroscopy. *J Oral Maxillofac Surg* **71**, 667-676, doi:10.1016/j.joms.2012.12.013 (2013).
- 9 Kuribayashi, A., Okochi, K., Kobayashi, K. & Kurabayashi, T. MRI findings of temporomandibular joints with disk perforation. *Oral Surg Oral Med Oral Pathol Oral Radiol Endod* **106**, 419-425, doi:10.1016/j.tripleo.2007.11.020 (2008).
- 10 Donahue, R. P., Hu, J. C. & Athanasiou, K. A. Remaining Hurdles for Tissue-Engineering the Temporomandibular Joint Disc. *Trends Mol Med* **25**, 241-256, doi:10.1016/j.molmed.2018.12.007 (2019).
- 11 Bielajew, B. J. *et al.* Knee orthopedics as a template for the temporomandibular joint. *Cell Rep Med* **2**, 100241, doi:10.1016/j.xcrm.2021.100241 (2021).
- 12 Bouloux, G., Koslin, M. G., Ness, G. & Shafer, D. Temporomandibular Joint Surgery. *J Oral Maxillofac Surg* **75**, e195-e223, doi:10.1016/j.joms.2017.04.027 (2017).
- 13 Dimitroulis, G. Management of temporomandibular joint disorders: A surgeon's perspective. *Aust Dent J* **63 Suppl 1**, S79-S90, doi:10.1111/adj.12593 (2018).
- 14 Helgeland, E. *et al.* 3D printed gelatin-genipin scaffolds for temporomandibular joint cartilage regeneration. *Biomed Phys Eng Express* **7**, doi:10.1088/2057-1976/ac1e68 (2021).
- 15 Angelo, D. F. *et al.* A randomized controlled preclinical trial on 3 interpositional temporomandibular joint disc implants: TEMPOJIMS-Phase 2. *J. Tissue Eng. Regen. Med.* **15**, 852-868, doi:10.1002/term.3230 (2021).
- 16 Faculdade de Medicina de Petrópolis Faculdade Arthur Sá Earp Neto. *Nasal Septum Autologous Chondrocytes Transplantation for Condylar Resorption After Orthognathic Surgery*, <<https://clinicaltrials.gov/ct2/show/study/NCT03137914>> (2017).
- 17 Vapniarsky, N. *et al.* The Yucatan Minipig Temporomandibular Joint Disc Structure-Function Relationships Support Its Suitability for Human Comparative Studies. *Tissue Engineering Part C: Methods* **23**, 700-709, doi:10.1089/ten.tec.2017.0149 (2017).
- 18 Vapniarsky, N. *et al.* Tissue engineering toward temporomandibular joint disc regeneration. *Sci Transl Med* **10**, 1-10, doi:10.1126/scitranslmed.aaq1802 (2018).
- 19 Donahue, R. P. *et al.* Long-term safety and efficacy of temporomandibular joint disc repair in the Yucatan minipig. *In Preparation for Submission to Nature Biomedical Engineering*.
- 20 Donahue, R. P., Nordberg, R. C., Bielajew, B. J., Hu, J. C. & Athanasiou, K. A. The Effect of Neonatal, Juvenile, and Adult Donors on Rejuvenated Neocartilage Functional Properties. *Tissue Eng. Part A*, doi:10.1089/ten.TEA.2021.0167 (2022).
- 21 Makris, E. A., MacBarb, R. F., Paschos, N. K., Hu, J. C. & Athanasiou, K. A. Combined use of chondroitinase-ABC, TGF- β 1, and collagen crosslinking agent lysyl oxidase to engineer functional neotissues for fibrocartilage repair. *Biomaterials* **35**, 6787-6796, doi:10.1016/j.biomaterials.2014.04.083 (2014).
- 22 Link, J. M., Hu, J. C. & Athanasiou, K. A. Chondroitinase ABC Enhances Integration of Self-Assembled Articular Cartilage, but Its Dosage Needs to Be Moderated Based on Neocartilage Maturity. *Cartilage*, 1947603520918653, doi:10.1177/1947603520918653 (2020).
- 23 Bielajew, B. J., Hu, J. C. & Athanasiou, K. A. Collagen: quantification, biomechanics and role of minor subtypes in cartilage. *Nat Rev Mater* **5**, 730-747, doi:10.1038/s41578-020-0213-1 (2020).
- 24 Merkel, J. R., DiPaolo, B. R., Hallock, G. G. & Rice, D. C. Type I and type III collagen content of healing wounds in fetal and adult rats. *Proc Soc Exp Biol Med* **187**, 493-497, doi:10.3181/00379727-187-42694 (1988).

- 25 Huey, D. J., Hu, J. C. & Athanasiou, K. A. Unlike bone, cartilage regeneration remains elusive. *Science* **338**, 917-921, doi:10.1126/science.1222454 (2012).
- 26 Wilkes, C. H. Internal derangements of the temporomandibular joint. Pathological variations. *Arch Otolaryngol Head Neck Surg* **115**, 469-477, doi:10.1001/archotol.1989.01860280067019 (1989).
- 27 Barzegar, H., Mohseni, M., Sedighi, A., Shahsavari, A. & Mohammadpour, H. Arthroscopically-assisted vs. open surgery in repairing anterior cruciate ligament avulsion. *Pak J Biol Sci* **14**, 496-501, doi:10.3923/pjbs.2011.496.501 (2011).
- 28 Walton, J. R. & Murrell, G. A. A two-year clinical outcomes study of 400 patients, comparing open surgery and arthroscopy for rotator cuff repair. *Bone Joint Res* **1**, 210-217, doi:10.1302/2046-3758.19.2000072 (2012).
- 29 Almarza, A. J. *et al.* Preclinical Animal Models for Temporomandibular Joint Tissue Engineering. *Tissue Eng Part B Rev* **24**, 171-178, doi:10.1089/ten.TEB.2017.0341 (2018).
- 30 Kwon, H., Brown, W. E., O'Leary, S. A., Hu, J. C. & Athanasiou, K. A. Rejuvenation of extensively passaged human chondrocytes to engineer functional articular cartilage. *Biofabrication* **13**, doi:10.1088/1758-5090/abd9d9 (2021).
- 31 Kulber, D. A., Davos, I. & Aronowitz, J. A. Severe cutaneous foreign body giant cell reaction after temporomandibular joint reconstruction with Proplast-Teflon. *J Oral Maxillofac Surg* **53**, 719-722; discussion 722-713, doi:10.1016/0278-2391(95)90182-5 (1995).
- 32 Chuong, R. & Piper, M. A. Cerebrospinal fluid leak associated with proplast implant removal from the temporomandibular joint. *Oral Surg Oral Med Oral Pathol* **74**, 422-425, doi:10.1016/0030-4220(92)90286-y (1992).
- 33 Brown, W. E., Hu, J. C. & Athanasiou, K. A. Ammonium-Chloride-Potassium Lysing Buffer Treatment of Fully Differentiated Cells Increases Cell Purity and Resulting Neotissue Functional Properties. *Tissue Engineering Part C: Methods* **22**, 895-903 (2016).
- 34 Murphy, M. K., Huey, D. J., Reimer, A. J., Hu, J. C. & Athanasiou, K. A. Enhancing post-expansion chondrogenic potential of costochondral cells in self-assembled neocartilage. *PLoS One* **8**, e56983, doi:10.1371/journal.pone.0056983 (2013).
- 35 Hu, J. C. & Athanasiou, K. A. A self-assembling process in articular cartilage tissue engineering. *Tissue Eng* **12**, 969-979, doi:10.1089/ten.2006.12.969 (2006).
- 36 Huwe, L. W., Sullan, G. K., Hu, J. C. & Athanasiou, K. A. Using Costal Chondrocytes to Engineer Articular Cartilage with Applications of Passive Axial Compression and Bioactive Stimuli. *Tissue Eng Part A* **24**, 516-526, doi:10.1089/ten.TEA.2017.0136 (2018).
- 37 Mehra, P. & Wolford, L. M. Use of the Mitek anchor in temporomandibular joint disc-repositioning surgery. *Proc (Bayl Univ Med Cent)* **14**, 22-26, doi:10.1080/08998280.2001.11927726 (2001).
- 38 Kwon, H., O'Leary, S. A., Hu, J. C. & Athanasiou, K. A. Translating the application of transforming growth factor- β 1, chondroitinase-ABC, and lysyl oxidase-like 2 for mechanically robust tissue-engineered human neocartilage. *Journal of Tissue Engineering and Regenerative Medicine* **13**, 283-294, doi:10.1002/term.2791 (2019).
- 39 Bankhead, P. *et al.* QuPath: Open source software for digital pathology image analysis. *Sci Rep* **7**, 16878, doi:10.1038/s41598-017-17204-5 (2017).
- 40 Cissell, D. D., Link, J. M., Hu, J. C. & Athanasiou, K. A. A Modified Hydroxyproline Assay Based on Hydrochloric Acid in Ehrlich's Solution Accurately Measures Tissue Collagen Content. *Tissue Eng Part C Methods* **23**, 243-250, doi:10.1089/ten.tec.2017.0018 (2017).
- 41 Bielajew, B. J., Hu, J. C. & Athanasiou, K. A. Methodology to Quantify Collagen Subtypes and Crosslinks: Application in Minipig Cartilages. *Cartilage* **13**, 1742S-1754S, doi:10.1177/19476035211060508 (2021).

- 42 Cox, J. & Mann, M. MaxQuant enables high peptide identification rates, individualized p.p.b.-range mass accuracies and proteome-wide protein quantification. *Nat Biotechnol* **26**, 1367-1372, doi:10.1038/nbt.1511 (2008).

Supplementary materials

Supplementary Table 1. Intralaminar fusion metrics. When tested under uniaxial tension in the superoinferior direction, fusion between the two laminae and implant was higher in Young's modulus and ultimate tensile strength (UTS), but the difference was not significant.

Group	Young's modulus (MPa)	UTS (MPa)
Control	0.26±0.45	0.17±0.30
Implant-treated	1.78±1.16	0.51±0.15

Supplementary Table 2. Bottom-up proteomics raw data. All data for bottom-up proteomics analysis is reported per total protein content as a percentage with the mean and standard deviation (SD) for each group.

Gene	Protein	t=0 <i>in vitro</i>	t=8W <i>in vitro</i>	t=24W <i>in vivo</i>	Regenerated tissue	Adjacent tissue	Native TMJ disc
ACTB	Actin, cytoplasmic 1	0.36%	0.15%	0.39%	0.16%	0.03%	0.00%
PGCA	Aggrecan core protein (Fragments)	0.25%	0.14%	0.00%	0.00%	0.00%	0.00%
CRYAB	Alpha-crystallin B chain	0.03%	0.00%	0.00%	0.00%	0.00%	0.00%
ENOB	Beta-enolase	0.06%	0.02%	0.00%	0.00%	0.00%	0.00%
PGS1	Biglycan (Fragments)	0.15%	0.06%	0.01%	0.01%	0.00%	0.01%
COL1A1	Collagen type I alpha 1	11.61%	6.01%	63.03%	63.35%	64.02%	66.38%
COL1A2	Collagen type I alpha 2	3.54%	1.83%	27.94%	28.90%	25.77%	28.64%
COL2A1	Collagen type II alpha 1	71.62%	81.79%	0.03%	0.03%	0.07%	0.02%
COL3A1	Collagen type III alpha 1	0.17%	0.20%	6.73%	5.99%	9.17%	4.31%
COL5A1	Collagen type V alpha 1	0.35%	0.20%	0.07%	0.07%	0.07%	0.05%
COL5A2	Collagen type V alpha 2	1.16%	0.87%	0.13%	0.10%	0.15%	0.09%
COL5A3	Collagen type V alpha 3	0.00%	0.00%	0.00%	0.00%	0.25%	0.14%
COL6A2	Collagen type VI alpha 2	0.17%	0.10%	0.05%	0.11%	0.04%	0.03%

COL6A3	Collagen type VI alpha 3	0.73%	0.34%	0.20%	0.30%	0.13%	0.09%
COL9A1	Collagen type IX alpha 1	0.49%	0.41%	0.00%	0.00%	0.00%	0.00%
COL9A2	Collagen type IX alpha 2	0.29%	0.27%	0.00%	0.00%	0.00%	0.00%
COL10A1	Collagen type X alpha 1	0.00%	0.00%	0.00%	0.00%	0.00%	0.00%
COL11A1	Collagen type XI alpha 1	2.55%	2.59%	0.01%	0.01%	0.00%	0.01%
Col11A2	Collagen type XI alpha 2	2.10%	2.29%	0.00%	0.00%	0.00%	0.00%
COL12A1	Collagen type XII alpha 1	0.85%	0.45%	0.01%	0.02%	0.00%	0.01%
COL14A1	Collagen type XIV alpha 1	0.00%	0.00%	0.06%	0.02%	0.00%	0.01%
COL14A1	Collagen type XVI alpha 1	0.03%	0.02%	0.00%	0.00%	0.00%	0.00%
PGS2	Decorin	0.00%	0.00%	0.11%	0.05%	0.09%	0.07%
BIP	Endoplasmic reticulum chaperone BiP (Fragment)	0.11%	0.05%	0.01%	0.01%	0.00%	0.00%
FMOD	Fibromodulin (Fragment)	0.11%	0.05%	0.00%	0.01%	0.00%	0.00%
G3P	Glyceraldehyde-3-phosphate dehydrogenase	0.11%	0.03%	0.01%	0.01%	0.00%	0.00%
HS71B	Heat shock 70 kDa protein 1B	0.07%	0.04%	0.00%	0.00%	0.00%	0.00%
HBA	Hemoglobin subunit alpha	0.02%	0.00%	0.02%	0.01%	0.00%	0.06%
H4	Histone H4	0.76%	0.47%	0.43%	0.37%	0.04%	0.02%
HPLN1	Hyaluronan and proteoglycan link protein 1	0.28%	0.43%	0.00%	0.00%	0.00%	0.00%
MFGM	Lactadherin	0.35%	0.36%	0.00%	0.00%	0.00%	0.00%
NU2M	NADH-ubiquinone oxidoreductase chain 2	0.02%	0.00%	0.00%	0.00%	0.00%	0.00%
PGK1	Phosphoglycerate kinase 1	0.10%	0.05%	0.00%	0.00%	0.00%	0.00%
LMNA	Prelamin-A/C	0.08%	0.03%	0.11%	0.05%	0.01%	0.00%
TBB	Tubulin beta chain	0.04%	0.01%	0.02%	0.02%	0.00%	0.00%
VIME	Vimentin	0.75%	0.58%	0.49%	0.31%	0.10%	0.01%

Supplementary Table 3. Dry weight crosslink normalizations and biochemical data for regenerated tissue. Pyridinoline (PYR), dihydroxylysinoxaline (DHLNL), and glycosaminoglycan (GAG) content per dry weight (DW) are reported.

Group	PYR/DW (ng/mg)	DHLNL/DW (ng/mg)	GAG (%/DW)
Control	0±0	0±0	0±0
Implant-treated	3860±217****	1119±150***	0.352±0.347
Native TMJ disc	3802±920	995±289	1.200±0.492

Supplementary Table 4. Dry weight crosslink normalizations and biochemical data for adjacent tissue. Pyridinoline (PYR), dihydroxylysinoxaline (DHLNL), and glycosaminoglycan (GAG) content per dry weight (DW) are reported.

Group	PYR/DW (ng/mg)	DHLNL/DW (ng/mg)	GAG (%/DW)
Adjacent tissue	2954±1007	1046±549	0.886±0.177
Native TMJ disc	3802±920	995±289	1.200±0.492

Supplementary Table 5. Compressive properties of implants cultured in vitro. Since there was not enough tissue, t=24W in vivo samples were not tested (nt).

Group	20% Relaxation modulus (kPa)	20% Instantaneous modulus (kPa)	20% Coefficient of viscosity (MPa s)
t=0 <i>in vitro</i>	255±85	1061±251	52.2±35.0
t=8W <i>in vitro</i>	258±83	1004±258	37.9±37.3
t=8W <i>in vivo</i>	nt	nt	nt

Supplementary Table 6. Raw complete blood count and complete metabolic panel data. Parameters were assayed at implantation (t=0) and animal euthanasia (t=8W).

Group	ID # and Assay Point	WBC (K/uI)	Absolute Neutrophil cells (K/uI)	Absolute Lymphocyte cells (K/uI)	Absolute Monocyte cells (K/uI)	Absolute Eosinophil cells (K/uI)	Absolute Basophil cells (K/uI)	Neutrophil (%)	Lymphocyte (%)	Monocyte (%)	Eosinophil (%)	Basophil (%)	RBC (M/uI)	Hemoglobin (g/dL)	Hematocrit (%)	MCV (fL)	MCH (pg)	MCHC (g/dL)	RDW (%)	Platelets (K/uL)	MPV (fL)
Control	6819 t=0	12.56	5.86	6.20	0.35	0.13	0.02	46.63	49.39	2.79	1.06	0.14	4.94	10.8	28.0	56.7	21.9	38.6	17.9	396	10.6
	6819 t=8W	11.30	4.67	5.95	0.21	0.46	0.01	41.30	52.63	1.89	4.09	0.09	5.24	9.3	29.7	56.7	17.7	31.3	17.0	399	10.4
	1177 t=0	8.62	4.34	3.66	0.38	0.22	0.02	50.35	42.43	4.43	2.57	0.23	6.38	11.1	33.8	53.0	17.4	32.8	20.7	379	9.3
	1177 t=8W	9.10	3.13	4.06	0.31	1.58	0.02	34.39	44.65	3.45	17.32	0.18	6.43	10.3	31.9	49.6	16.0	32.3	19.5	368	10.1
	1329 t=0	11.10	3.29	2.35	0.96	4.46	0.04	29.61	21.21	8.68	40.14	0.37	8.04	15.1	44.0	54.7	18.8	34.3	19.2	334	9.4
	1329 t=8W	7.18	2.72	3.10	0.34	1.02	0.01	37.89	43.17	4.71	14.15	0.07	7.01	11.3	35.9	51.2	16.1	31.5	19.6	332	11.0
Implant-treated	2661 t=0	10.62	3.76	5.80	0.37	0.68	0.01	35.42	54.58	3.52	6.38	0.10	7.72	12.5	42.2	54.7	16.2	29.6	19.7	194	12.0
	2661 t=8W	7.46	1.52	2.71	0.59	2.62	0.02	20.34	36.33	7.95	35.10	0.28	6.68	10.5	35.8	53.6	15.7	29.3	18.7	258	10.6
	3774 t=0	9.80	2.39	4.77	0.64	1.98	0.02	24.34	48.72	6.48	20.24	0.22	6.78	10.6	36.3	53.6	15.6	29.0	20.3	329	10.8
	3774 t=8W	9.46	2.42	4.42	0.63	1.97	0.02	25.62	46.75	6.62	20.80	0.22	5.77	9.4	30.5	52.9	16.3	30.8	19.2	367	9.7
	4525 t=0	8.06	1.80	3.34	0.68	2.21	0.03	22.36	41.43	8.41	27.38	0.41	6.18	10.8	33.4	54.0	17.5	32.3	19.8	251	11.0
	4525 t=8W	8.68	2.69	3.06	0.21	2.72	0.01	30.95	35.21	2.39	31.34	0.12	6.83	11.1	35.2	51.6	16.3	31.5	19.8	389	9.8

Group	ID # and Assay Point	Alanine Transaminase (U/L)	Albumin (g/dL)	Alkaline Phosphatase (U/L)	Amylase (U/L)	Aspartate Transaminase (U/L)	Blood Urea Nitrogen (mg/dL)	Calcium (mg/dL)	Creatinine (mg/dL)	Glucose (mg/dL)	Phosphorus (mg/dL)	Total Bilirubin (mg/dL)	Total Protein (g/dL)	Chloride (mmol/L)	Potassium (mmol/L)	Sodium (mmol/L)
Control	6819 t=0	30.0	4.16	38.2	2252.9	36.7	16.4	10.71	0.903	117.8	5.66	0.038	6.76	99.6	4.37	138
	6819 t=8W	33.1	4.22	42.9	2561.3	24.5	14.7	10.26	1.089	97.1	5.35	0.033	6.86	101.2	3.28	138
	1177 t=0	27.0	4.33	29.8	2954.4	18.2	12.5	10.21	1.168	70.5	5.59	0.056	6.65	100.6	3.96	137
	1177 t=8W	28.6	4.27	44.7	4484.4	22.4	9.1	9.81	1.187	70.0	6.07	0.138	6.83	101.5	3.69	140
	1329 t=0	28.5	4.66	56.9	3600.6	29.1	13.3	10.31	1.136	89.7	5.59	0.216	6.67	102.8	3.82	138
	1329 t=8W	24.9	4.22	42.5	3917.0	24.8	12.9	9.79	1.073	82.9	5.90	0.222	6.46	100.9	3.51	137
Implant-treated	2661 t=0	33.9	4.53	67.6	2343.2	30.0	15.5	10.65	0.843	63.7	5.52	0.053	6.73	98.3	4.35	136
	2661 t=8W	31.4	4.7	72.1	2518.2	25.8	16.2	10.55	0.886	71.8	5.65	0.151	6.93	101.2	3.70	140
	3774 t=0	28.8	4.29	35.9	2101.3	25.0	12.1	10.29	0.982	89.8	5.10	0.025	6.10	102.7	4.43	136
	3774 t=8W	32.2	3.82	34.0	1914.4	19.9	11.9	10.21	0.768	73.1	5.63	0.030	6.19	103.1	4.02	137
	4525 t=0	21.3	4.72	66.0	2522.4	23.1	12.8	10.58	0.884	85.5	5.68	0.056	6.79	102.7	3.63	139
	4525 t=8W	21.1	5.22	59.7	2708.8	17.7	14.2	10.60	0.933	87.1	5.47	0.135	7.32	104.0	3.35	143

CONCLUSIONS AND FUTURE DIRECTIONS

Self-assembled neocartilages have the potential to treat TMDs that affect millions of people in the U.S. In this work, LC-MS methods were developed to quantify collagen subtypes and crosslinks and applied to the cartilages of the Yucatan minipig. Then, native cartilage development and self-assembled neocartilage maturation were characterized via quantitative collagenomic methods. It was shown that self-assembled neocartilage has similar temporal trends to native cartilage development. Finally, self-assembled constructs were used in small and large perforation defects *in vivo* to regenerate TMJ disc fibrocartilage in a clinically relevant, large animal model. Through quantitative collagenomics, it was shown that resulting regenerated cartilage has a similar collagenomic profile to native fibrocartilage. As a whole, this work contains the first studies that use collagenomics as a primary assessment tool throughout the tissue engineering process from *in vitro* tissue maturation to *in vivo* application of a tissue-engineered implant. This work represents significant progress toward translation of self-assembled neocartilage implants by applying novel quantitative collagenomic methods to neocartilage implants and regenerated cartilage tissues in the TMJ disc.

Prior to this work, collagen methods were underdeveloped, and all were lacking in cost effectiveness, specificity of collagen subtypes, or sensitivity. Through Specific Aim 1, LC-MS methods for high-throughput quantification of collagen types I and II, as well as mature and immature collagen crosslinks, were developed. As expected, fibrocartilages comprised mostly collagen type I (65-85% per dry weight in the TMJ disc, knee meniscus, and annulus fibrosus), while hyaline cartilages comprised mostly collagen type II (55-70% in the facet joint, femoral condyle, and femoral head). Through bottom-up proteomics, it was shown that fibrous and hyaline cartilages do not exist as independent groups of tissue, but, rather, a spectrum of cartilages as determined by the ratio of collagen types I and II. For example, in hyaline cartilages, the collagen type II to collagen type I ratio ranged from 74:1 in femoral condyle to 12:1 in floating rib costal

cartilage. In fibrocartilage, the ratio of collagen type I to collagen type II ranged from over 150:1 in the red-red meniscus to less than 10:1 in the annulus fibrosus. The quantitative collagenomic methods developed in Specific Aim 1 are low in cost and operator time and available to any researcher or scientist who has access to a facility with mass spectrometers (i.e., most research universities and hospitals). These LC-MS methods are widely applicable to biomedical fields including tissue characterization, disease states, and tissue engineering. Future considerations for LC-MS collagenomic methods include broadening the assays to account for more collagen subtypes and crosslinks. With the advantages of modern high sensitivity triple quadrupole mass spectrometers and sample preparation methods such as solid phase extraction or immunoprecipitation, other collagen subtypes (i.e., types III-XXVIII) and crosslinks (e.g., pentosidine, glucosepane, and arginoline) may be quantified in biological samples using modified versions of the methods developed in this work.

The quantitative collagenomic methods developed in Specific Aim 1 were applied in Specific Aim 2 to study the development of porcine knee cartilage from fetal to mature stages. Throughout cartilage development, well-known temporal changes such as an increase in collagen content and decreases in GAG and DNA were confirmed. Proteomic analysis showed that as cartilage developed, it increased in collagen types II and III by factors of 1.3 and 4.8, respectively, from fetal to mature. Other collagen types such as types IX and XI dropped by factors of 9.4 and 5.1, respectively, and XIV decreased from 0.95% per protein in fetal cartilage to <0.01% in mature cartilage. Because collagen subtypes IX, XI, and XIV have roles in collagen fibrillogenesis, where they associate with collagen type II as it matures from thin fibrils to thicker fibers, the decrease in these collagen types ties in to the permanent structure of cartilage ECM; cartilage loses the capability to repair itself as these minor collagens are degraded and replaced. Temporal decreases in aggrecan and link protein (2.6-times and 5.0-times, respectively, from fetal to mature) indicated that the known decrease in GAG with cartilage aging is non-enzymatic in nature, because enzymatic cleavage of aggrecan core protein leaves link protein intact. Increases

in cellular vimentin, an intermediate filament of the cytoskeleton, were also identified, shown by vimentin per DNA increasing 5.2-times from fetal to mature. Because vimentin has previously been shown to be deposited more in chondrocytes under mechanical stress, this increase likely resulted from cytoskeletal remodeling in response to increased loading with age as the pigs gained weight. While this native tissue characterization was important to define gold standards and understand how the proteome of cartilage changes with age, this study's purpose was also to define a baseline for comparing the maturation of self-assembled neocartilage.

The mechanics, biochemistry, and proteome of neocartilage matured over time, reflecting many qualities of native cartilage development. Like in native cartilage, total collagen increased over time while GAG and DNA decreased in later stages. From 7 days to 84 days of culture, collagen type II increased 1.5-times while aggrecan and link protein both decreased 2.2-times, similar to the developmental changes of native knee cartilage. Because collagen type X is associated with calcification of cartilage, its abundant presence would contraindicate neocartilage for use in diarthrodial joints; however, collagen type X was found to be minimal (<0.05% per protein) in neocartilage implants, similar to knee cartilage (<0.01% per protein) and TMJ disc (<0.01% per protein), and unlike floating rib cartilage (0.98% per protein). These results support the non-homologous approach of using costal cartilage for implantation into cartilage structures such as the knee or the TMJ disc. Interestingly, from day 7 to day 84 of culture, collagen types IX and XI increased 2.5-times and 1.3-times respectively, opposite of the trends seen in native knee cartilage. Unlike in native hyaline cartilage development, collagen types IX and XI were not replaced by collagen type II through maturation. Collagen type XIV, which was present in low amounts in porcine knee cartilage, was not present in neocartilage, while collagen type XII was approximately 10-times more abundant in neocartilage than in native cartilage. Because collagen types XII and XIV both play similar roles in fibrillogenesis, where they associate with collagen type II fibrils to regulate spacing and diameter, the overproduction of collagen type XII in neocartilage may be the result of a compensatory mechanism from a lack of collagen type XIV. Future tissue

engineering studies should aim to stimulate the production of collagen type XIV or determine how to induce turnover of collagen types IX and XI to more collagen type II to achieve a more biomimetic phenotype in engineered cartilage. These techniques will propel the maturation of thin collagen fibrils into thicker fibers, thus, improving the mechanical properties of neocartilage implants.

In Specific Aim 3, the methods developed in Specific Aim 1 and the non-homologous approach verified in Specific Aim 2 were applied to explore the collagenomics of cartilage regeneration in minipig TMJ disc perforations treated with self-assembled neocartilage. Small perforations exhibited healing at the 24-week time point in both implant-treated discs and control empty defects, but mechanical properties of implant-treated repair tissue were more robust, with 6.2-times higher toughness, 8.9-times higher resilience, and 3.4-times higher ultimate tensile strength. Neocartilage implants were well-tolerated immunogenically, with immune responses resolving over time, and no systemic abnormalities in complete blood count or comprehensive metabolic panel. Collagenomic techniques were used to show that implant-treated repair tissues consisted of regenerated fibrocartilage, with collagen type I and III values nearly indistinguishable from those of native TMJ disc (99.4% and 103.1%, respectively). Fill tissues in empty defect controls had 9.9% less collagen type I and 2.2-times more collagen type III than native TMJ disc, a phenotype more reminiscent of scar tissue, indicating inferior healing in the empty defect controls. Altogether, these data indicate that self-assembled neocartilage implants effectively treat small perforations of the TMJ disc in the minipig.

In the large perforation study of Specific Aim 3, at the 8-week time point, empty defect control discs remained perforated, with a defect perimeter of 14.6 ± 5.8 mm, while all implant-treated perforations fully closed (defect perimeter of 0 mm). Repair tissues in the implant-treated groups had tensile properties that were over 75% of the values of native TMJ disc on average, and, as in the small perforation study, safety of the self-assembled neocartilage was shown through immunostaining and bloodwork. Through collagenomic methods, it was revealed that the

regenerated tissue in the implant-treated TMJ discs had a similar collagen subtype profile of native TMJ disc, indicating that TMJ disc fibrocartilage is being regenerated through the implantation of self-assembled neocartilage. This impactful work is highly significant in that it shows successful regeneration of cartilage *in vivo*, with the regenerated tissues verified to be biomimetic fibrocartilage through collagenomics. The two *in vivo* studies in this work represent a significant intersection in the fields of proteomics and tissue engineering by using collagenomic techniques to gain a deep insight into the regenerative capabilities of tissue-engineered neocartilage implants in large animal models.

The long-term goal of this cartilage tissue engineering work is to create a widely available, marketed therapeutic for the millions of people who suffer from TMDs. Before this can happen, the Food and Drug Administration (FDA) requires significant evidence of safety and efficacy through preclinical and clinical trials. Given the promising results shown here in clinically relevant, large animal models for TMJ disc perforation, the next step along the translational pathway is the completion of a pivotal animal study. This study will be performed in a larger sample number of Yucatan minipigs and carried out for a longer time frame (i.e., one year). Additional safety assays including karyotyping and heterotopic implantation of neocartilage implants in nude mice will be performed; moreover, bottom-up proteomic techniques can be used to show safety by quantifying all components of neocartilage ECM, ensuring that there are not remnants of culture medium or deposition of non-cartilaginous proteins. Remaining safety and efficacy validation will be performed in a similar manner to the assays conducted in Specific Aim 3. With safety and efficacy shown in this orthotopic large animal model, an investigational new drug (IND) / investigational device exemption (IDE) application will be submitted to the FDA in pursuit of beginning clinical trials. Eventually, through three phases of clinical trials, premarket approval (PMA) and/or a biologics license application (BLA) for neocartilage implants can be obtained. This lengthy and demanding regulatory process, if completed, will result in the marketed usage of neocartilage implants in the U.S., allowing TMD patients to be treated with tissue-engineered cartilage.

Ultimately, this work 1) developed a novel, broadly applicable assay for collagen subtype and crosslink quantification, 2) investigated the collagenomics of native cartilage development and self-assembled neocartilage maturation, and 3) quantified the collagenomics of tissue-engineered cartilage regeneration in the Yucatan minipig TMJ disc. Through novel collagenomic analysis, it was shown that tissue-engineered cartilage therapeutics have great potential for treatment of TMDs by regenerating TMJ disc perforations in a clinically relevant, large animal model. Through the FDA regulatory process, including preclinical animal studies and clinical trials, tissue-engineered TMJ cartilage therapeutics are approaching human use, where they have the potential to substantially improve TMD outcomes in millions of people.

APPENDIX A | Engineering self-assembled neomenisci through combination of matrix augmentation and directional remodeling*

Abstract

Knee meniscus injury is frequent, resulting in over 1 million surgeries annually in the United States and Europe. Because of the near-avascularity of this fibrocartilaginous tissue and its intrinsic lack of healing, tissue engineering has been proposed as a solution for meniscus repair and replacement. This study describes an approach employing bioactive stimuli to enhance both extracellular matrix content and organization of neomenisci toward augmenting their mechanical properties. Self-assembled fibrocartilages were treated with TGF- β 1, chondroitinase ABC, and lysyl oxidase-like 2 (collectively termed TCL) in addition to lysophosphatidic acid (LPA). TCL+LPA treatment synergistically improved circumferential tensile stiffness and strength, significantly enhanced collagen and pyridinoline crosslink content per dry weight and achieved tensile anisotropy (circumferential/radial) values of neomenisci close to 4. This study utilizes a combination of bioactive stimuli for use in tissue engineering studies, providing a promising path toward deploying these neomenisci as functional repair and replacement tissues.

Introduction

Fibrocartilage is found in the knee meniscus, temporomandibular joint disc, pubic symphysis, annulus fibrosus of intervertebral discs, tendons, and ligaments. Damage to these tissues is common and can result in persistent pain while impeding daily activity. The knee meniscus is a wedge-shaped, semi-circular fibrocartilaginous tissue that is situated between the distal femur and tibial plateau; the meniscus protects articular cartilage via load distribution. Injury to the

* Published as: Gonzalez-Leon EA, Bielajew BJ, Hu JC, Athanasiou KA. Engineering self-assembled neomenisci through combination of matrix augmentation and directional remodeling. *Acta Biomaterialia* 2020; 109: 73-81.

meniscus is responsible for approximately 1 million surgeries annually in the U.S. and Europe, making it the most common orthopedic surgical procedure¹.

Meniscal function arises from collagen content, crosslinks, and organization. Under compressive load, menisci function by using their wedge shape to develop tension, which is resisted by circumferentially aligned collagen. The surface of the meniscus tissue exhibits random collagen alignment, while its middle depths show circumferentially aligned collagen fibers supported by tie fibers in the radial direction^{2,3}. Pyridinoline, a trivalent crosslink of collagen fibrils, contributes to mechanical properties of the knee meniscus⁴ and has been shown to strongly correlate with tensile properties of various collagenous tissues^{5,6}. Collagen content, crosslinking, and organization are, thus, critical to the tensile properties of menisci and their function.

The knee meniscus exhibits a gradient of healing capacity which decreases from its outer, fibrous portion toward the inner portion, which is more akin to hyaline articular cartilage and lacks vascularization⁷. Injuries may lead to surgery such as meniscectomy, i.e., tissue resection, especially if the injury is in the inner portion of the tissue, which can temporarily alleviate pain symptoms but is virtually guaranteed to result in osteoarthritis of the knee joint⁸. This lack of intrinsic healing properties makes the knee meniscus a prime candidate for repair or replacement via tissue engineering methods.

Both scaffold and scaffold-free strategies for tissue engineering the knee meniscus have been investigated. A scaffold-free method known as the self-assembling process has emerged for forming neotissue rings⁹⁻¹⁴ while resolving issues that may result from scaffold use such as stress shielding and scaffold degradation byproducts¹⁵. The self-assembling process depends on both integrin-matrix binding and cell-to-cell communication via cadherin binding¹⁶, resulting in a sequence of extracellular matrix (ECM) accumulation that is reminiscent to the sequence seen for native cartilage¹⁷. The neotissue rings are then cut into two meniscus-shaped constructs (termed “neomenisci”) that resemble the morphology of the native leporine knee meniscus. Mechanical properties are directly related to ECM content and organization and, as such, our

group has utilized bioactive agents during culture to enhance these biochemical features and create self-assembled fibrocartilage with compressive properties that reach levels seen in native tissue¹⁸. However, tensile mechanical properties of neomenisci are still lacking, especially in the circumferential direction. Tensile properties still require improvement before these engineered tissues can be deployed as functional repair or replacement alternatives; as such, this study aims to improve tensile properties of engineered neomenisci through the addition of bioactive stimuli during *in vitro* culture.

Bioactive stimuli have frequently been used to augment ECM content, leading to enhanced mechanical properties. Growth factors such as TGF- β 1^{14,18-20}, TGF- β 3²¹⁻²³, CTGF²³, PDGF²⁴⁻²⁶, bFGF^{24,27,28}, IGF-1^{24,25,27-30}, and EGF^{25,26} have shown efficacy toward enhancing tissue engineered fibrocartilage formation. In addition, our group has previously used anabolic growth factor TGF- β 1 to enhance ECM production, glycosaminoglycan (GAG)-cleaving enzyme chondroitinase ABC (C-ABC) to temporarily remove GAG, and collagen crosslinking enzyme lysyl oxidase-like 2 (LOXL2) to increase collagen crosslinking. These bioactive agents have been used alone or in combination to enhance mechanical properties of cartilaginous and fibrocartilaginous tissues^{13,18,19,31,32}. A treatment based on this cocktail of bioactive agents (collectively termed TCL) results in matrix augmentation contributing to more robust engineered tissues.

Less frequent than the use of bioactive stimuli are strategies to induce or to accentuate ECM organization of engineered neomenisci, resulting in anisotropy. An example is lysophosphatidic acid (LPA), a phospholipid mediator that induces contractions in fibroblasts³³, which has been used to induce contraction of collagen matrices seeded with fibroblasts or myofibroblasts³⁴⁻³⁶. In addition to inducing contraction in fibroblasts, LPA has also been shown to be an anti-apoptotic and pro-survival factor in both fibroblasts³⁷ and chondrocytes³⁸. Because we have observed that meniscal fibrochondrocytes seeded in a ring-shaped mold create circumferential hoop stress⁹, we have used LPA in the past to enhance this hoop stress and, thus,

circumferential ECM organization, by accentuating cellular traction forces that give rise to hoop stresses¹⁰. Thus, while self-assembled neomenisci already exhibit anisotropic tensile properties, indicating a certain degree of collagen alignment, cytoskeletal contraction induced by LPA enhances this anisotropy by increasing collagen organization.

Because TCL and LPA do not have overlapping functions, their use in combination may act synergistically toward bolstering tissue properties. Matrix augmentation has been observed in self-assembled cartilaginous tissues when applying TCL treatment, while LPA has induced directional remodeling in self-assembled neomenisci to enhance organization and anisotropy. The objective of this study was to increase the tensile properties of self-assembled neomeniscus constructs in an anisotropic fashion by combining TCL with LPA to increase and to remodel ECM content. Neomenisci were cultured for 5 weeks and treated with TCL and LPA alone or in combination. Unstimulated neomenisci served as controls. It was hypothesized that 1) treatment of constructs with TCL and LPA would lead to a synergistic increase in tensile properties, 2) an increase in tensile properties would be accompanied by an increase in the amount of pyridinoline collagen crosslinks, and 3) TCL+LPA treatment would produce neomenisci with anisotropic tensile mechanical properties.

Materials and methods

Chondrocyte and meniscus cell isolation

Primary bovine articular chondrocytes and meniscus cells were isolated from juvenile bovine knee joints (Research 87). Articular cartilage resected from the distal femur was minced and digested in 0.2% collagenase type II (Worthington) for 18 hours at 37°C. Meniscus tissue was isolated from the knee joint and digested as previously described¹⁰. Briefly, the outer rim was removed, and remaining meniscus tissue was minced and digested in 0.25% pronase (Sigma-Aldrich) for 2 hours followed by 0.2% collagenase type II for 18 hours. After isolation, cells were frozen at -80°C for 24 hours in Dulbecco's modified Eagle's medium (DMEM) supplemented with 20% fetal bovine

serum and 10% dimethyl sulfoxide medium at 30 million cells per milliliter and stored in liquid nitrogen until seeding.

Self-assembly and culture of constructs

Non-adherent agarose wells in the shape of the native leporine meniscus were prepared as previously described¹⁰⁻¹². Wells were saturated for five days prior to seeding with serum-free chondrogenic medium and throughout culture. Chondrogenic medium consists of: DMEM with GlutaMAX (Gibco, Grand Island, NY, USA); 1% nonessential amino acids (Gibco); 1% insulin, human transferrin, and selenous acid (ITS+; BD Biosciences, San Jose, CA, USA); 1% penicillin-streptomycin-fungizone (Lonza BioWhittaker, Walkersville, MD, USA); 3.5 nM dexamethasone (Sigma-Aldrich, St. Louis, MO, USA); 50 µg/mL ascorbate-2-phosphate (Sigma-Aldrich); 100 µg/mL sodium pyruvate (Sigma-Aldrich) and 40 µg/mL L-proline (Sigma-Aldrich). A 1:1 co-culture of primary articular chondrocytes and meniscal cells was seeded at a density of 20 million total cells per 180 µL as previously described⁹. An additional 2 mL of media was added 4 hours after construct seeding, and all medium was changed daily. Constructs were removed from the agarose wells after 7 days and kept in culture, during which medium was changed every other day (5 mL).

Treatments

Neomenisci treatment groups were as follows: 1) unstimulated controls, 2) LPA only, 3) TCL only, 4) TCL+LPA. TCL groups were treated with the combination of 1) TGF-β1 continuously throughout culture at 10 ng/mL, 2) a one-time C-ABC treatment, added to medium with a 0.05 M sodium acetate activator, at day 7 of culture at 2 U/mL for a duration of 4 hours, and 3) LOXL2 applied continuously from days 7-21 (weeks 2-3) at 0.15 ng/mL as previously described^{19,32,39}. Neomenisci that were treated with LPA (Enzo Life Sciences) were stimulated during days 21-28 (week 4) at a final concentration of 10 µM as previously described¹⁰. All constructs were cultured for 5 weeks at 37°C and 5% CO₂.

Tissue gross morphology, histology, and macroscopic characterization

At day 35, neomenisci were removed from culture, photographed, and measured using ImageJ (NIH). Wet weights were measured before resecting pieces for mechanical testing, biochemical analysis, and histology. For histology, construct samples were fixed in 10% neutral buffered formalin then embedded in paraffin and sectioned at 5 μm . Safranin O/Fast Green, Picrosirius Red, and hematoxylin and eosin (H&E) stains were conducted to visualize GAG, collagen, and cell distributions, respectively. Collagen fiber alignment of samples was examined using second-harmonic generation (SHG) imaging microscopy (Zeiss, Jena, Germany). The acquisition of SHG images was conducted using an excitation wavelength of 800 nm and a 20x objective.

Tensile and compressive testing

Tensile properties were assessed using uniaxial, strain-to-failure testing. Using custom-made jigs, samples were cut to a depth of 1.0 mm and gauge length of 0.95 mm and 0.40 mm for circumferential and radial tensile samples, respectively. Samples were then photographed, cut into dog-bone shapes, measured with ImageJ, and adhered to paper strips with cyanoacrylate glue at their ends to ensure that a glue bridge would not form across the gauge length. Samples were then clamped within a uniaxial testing machine (Instron model 5565) and subjected to a 1% s^{-1} strain rate until failure. Young's modulus (E_Y) was calculated from the linear portion of the stress-strain curve, and ultimate tensile strength (UTS) was calculated from the maximum stress.

Compressive properties were assessed using unconfined stress-relaxation testing, with a non-porous, stainless steel platen larger in diameter than the tissue sample. Punches measuring 2-3 mm in diameter were resected from neomenisci. Sample thickness was determined via a custom program on the testing machine (Instron model 5565). Samples were subjected to stress relaxation via a 20% step-strain while submerged in a PBS bath. Viscoelastic properties such as instantaneous modulus (E_I), relaxation modulus (E_R), and coefficient of viscosity (μ) were calculated by fitting data curves to a standard Kelvin solid model⁴⁰.

Analysis of tissue biochemical content

Biochemistry samples were weighed wet, then frozen and lyophilized to acquire dry weights. DNA content was calculated with the use of PicoGreen dsDNA reagent (Invitrogen), assuming a conversion factor of 7.7 pg DNA/cell. Collagen content was measured with the use of a Sircol standard (Biocolor) and a Chloramine-T colorimetric hydroxyproline assay⁴¹. GAG content was quantified using the Blyscan assay kit (Invitrogen). All quantification measurements for DNA, GAG, and collagen content were performed with a GENios spectrophotometer/spectrofluorometer (TECAN).

Quantification of pyridinoline crosslink content was performed via a liquid chromatography mass spectrometry (LC-MS) assay⁴². Lyophilized samples were hydrolyzed in 6N HCl at 105°C for 18 hours, then acid was evaporated by SpeedVac (Labconco). Dried hydrolysates were resuspended in 25% (v/v) acetonitrile and 0.1% (v/v) formic acid in water, centrifuged at 15,000g for 5 min, and the supernatant was transferred to a LCMS autosampler vial. Liquid chromatography was carried out on a Cogent Diamond Hydride HPLC Column (2.1 mm x 150 mm, particle size 2.2 µm, pore size 120 Å, MicroSolv). The elution gradient used 0.1% (v/v) formic acid in water as solvent A, and 100% acetonitrile as solvent B. The 5-minute elution gradient ran at 300 µL/min as follows: 0 min 25% B, 2 min 25% B, 2.2 min 5% B, 3 min 25% B. Mass spectrometry was performed on a Quadrupole Mass Detector (ACQUITY QDa, Waters) in ESI+ MS scan mode. The quadrupole range was set to 150 - 450 m/z with cone voltage 12.5 V. MassLynx software version 4.1 with TargetLynx was used to quantify pyridinoline in 10 µL injections of neomeniscus hydrolysate by integrating the extracted ion chromatogram of double-charged pyridinoline (m/z=215.1) into a standard curve of serially diluted pyridinoline standard (BOC Sciences). The standard curve contained 6 standards and was linear with $R^2 > 0.999$ on a range of 1,000 to 4.115 pg/µL pyridinoline.

Statistical analysis

For each biomechanical and biochemical test, n=6-7 samples were used. Results were analyzed with single-factor analysis of variance (ANOVA) followed by a Tukey's HSD post hoc test when merited ($p < 0.05$). TCL and LPA effect on anisotropy was analyzed with two-factor ANOVA followed by a Tukey's HSD post hoc test when merited ($p < 0.05$). All data are presented as means \pm standard deviations. For all figures, statistical significance is indicated by groups not sharing the same letters.

Results

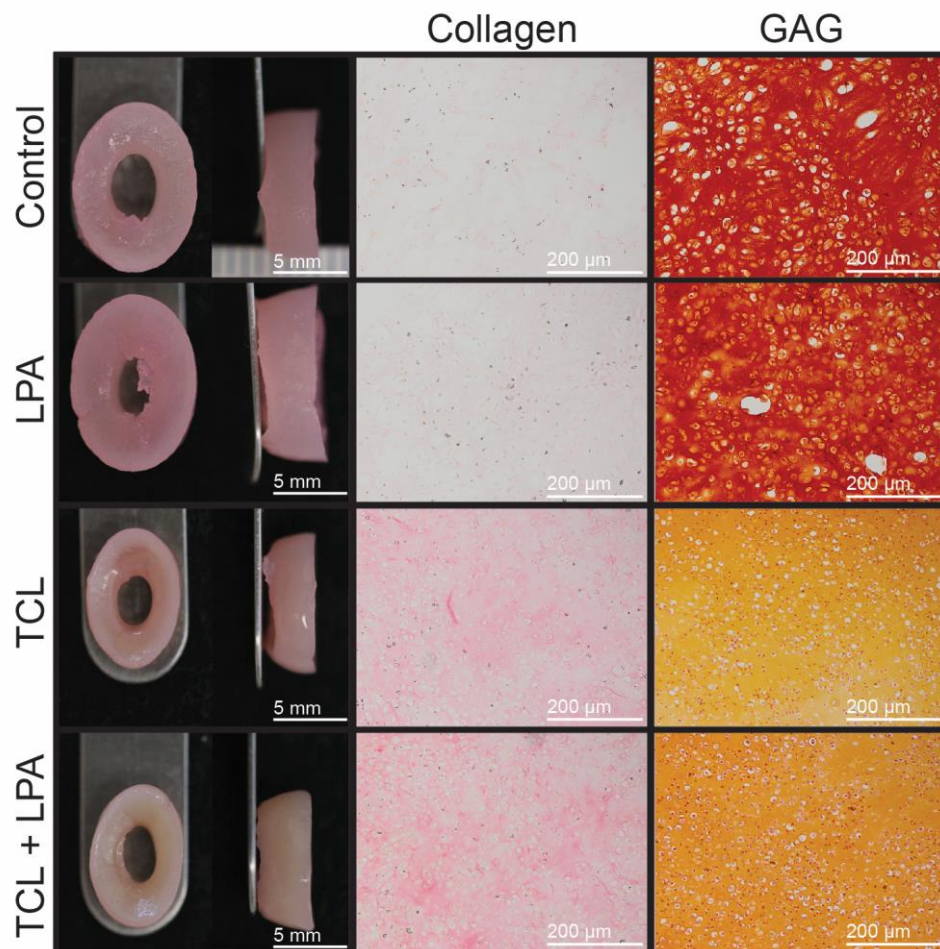


Figure 1. Gross morphology and histological staining of self-assembled neomenisci. Tissue engineered constructs retained the characteristic wedge-shape of the native knee meniscus during and after culture. Slight contraction occurred in TCL+LPA groups when compared to controls. Collagen staining of TCL+LPA treated constructs appeared more intense than that of control constructs, while GAG staining in the TCL and TCL+LPA groups was less intense than controls.

Gross morphology, histology, and immunohistochemistry

Neomenisci resembled native meniscus fibrocartilage^{43,44} in terms of gross appearance (Figure 1)⁴⁴⁻⁴⁶. The characteristic wedge-shaped profile was maintained after 5 weeks of culture. Morphologically, TCL and TCL+LPA treated groups were significantly smaller ($p<0.0005$) than controls and constructs treated with LPA alone in terms of outer major and minor diameters, inner minor diameter, and height (Table 1). TCL+LPA was significantly smaller in terms of inner major diameter when compared to all other groups ($p=0.03$). Both outer ($p=0.04$) and inner ($p=0.007$) aspect ratios (defined as major diameter/minor diameter) were also significantly higher in TCL+LPA treated neomenisci when compared to controls. Wet weights were significantly different among groups, with TCL and TCL+LPA groups both weighing significantly less ($p<0.0001$) than controls and LPA treated groups (Table 1). Hydration percentages were also significantly lower ($p<0.0001$) in TCL and TCL+LPA treated groups when compared to control and LPA-only groups (Table 1). Dry weights for TCL and TCL+LPA groups, in turn, were significantly lower than control and LPA-treated constructs.

Table 1. Morphological properties of neomenisci. Values marked with different letters within each category are significantly different ($p<0.05$), $n=7$ per group.

Group	Wet Weight (mg)	Dry Weight (mg)	Hydration (%)	Cells/construct (millions)	Outer Major Diameter (mm)	Outer Minor Diameter (mm)	Inner Major Diameter (mm)	Inner Minor Diameter (mm)	Outer Aspect Ratio	Inner Aspect Ratio	Height (mm)
Control	207 ± 8 ^C	25 ± 1 ^B	88 ± 0 ^B	13 ± 4	11 ± 0 ^B	8 ± 0 ^B	4 ± 0 ^B	3 ± 0 ^B	1 ± 0 ^B	1 ± 0 ^B	4 ± 0 ^B
LPA	224 ± 10 ^B	25 ± 2 ^B	89 ± 1 ^B	15 ± 4	11 ± 0 ^B	8 ± 0 ^B	4 ± 0 ^B	2 ± 0 ^B	1 ± 0 ^B	2 ± 0 ^{AB}	4 ± 0 ^B
TCL	89 ± 5 ^A	15 ± 1 ^A	83 ± 1 ^A	15 ± 1	9 ± 1 ^A	6 ± 0 ^A	3 ± 0 ^B	2 ± 0 ^A	1 ± 0 ^{AB}	2 ± 0 ^{AB}	3 ± 0 ^A
TCL + LPA	91 ± 5 ^A	15 ± 1 ^A	83 ± 1 ^A	16 ± 1	9 ± 0 ^A	6 ± 1 ^A	3 ± 0 ^A	2 ± 0 ^A	2 ± 0 ^A	2 ± 0 ^A	3 ± 0 ^A

Tissue biomechanics

Biomechanical data revealed a significant difference among control and treated constructs, especially those that were treated with TCL+LPA (Figure 2). Application of TCL+LPA resulted in increased tensile properties over both unstimulated control and LPA treatment groups. Circumferential Young's modulus and ultimate tensile strength (UTS) were highest ($p < 0.0001$) in TCL+LPA treated groups (Figure 2A, 2B). TCL+LPA treated constructs increased circumferential Young's modulus and UTS to 221% and 218% higher than control values, respectively. In addition, TCL+LPA treated constructs displayed increases to the radial Young's modulus ($p = 0.03$) and UTS ($p = 0.001$) of 152% and 239% over controls, respectively (Figure 2C, 2D).

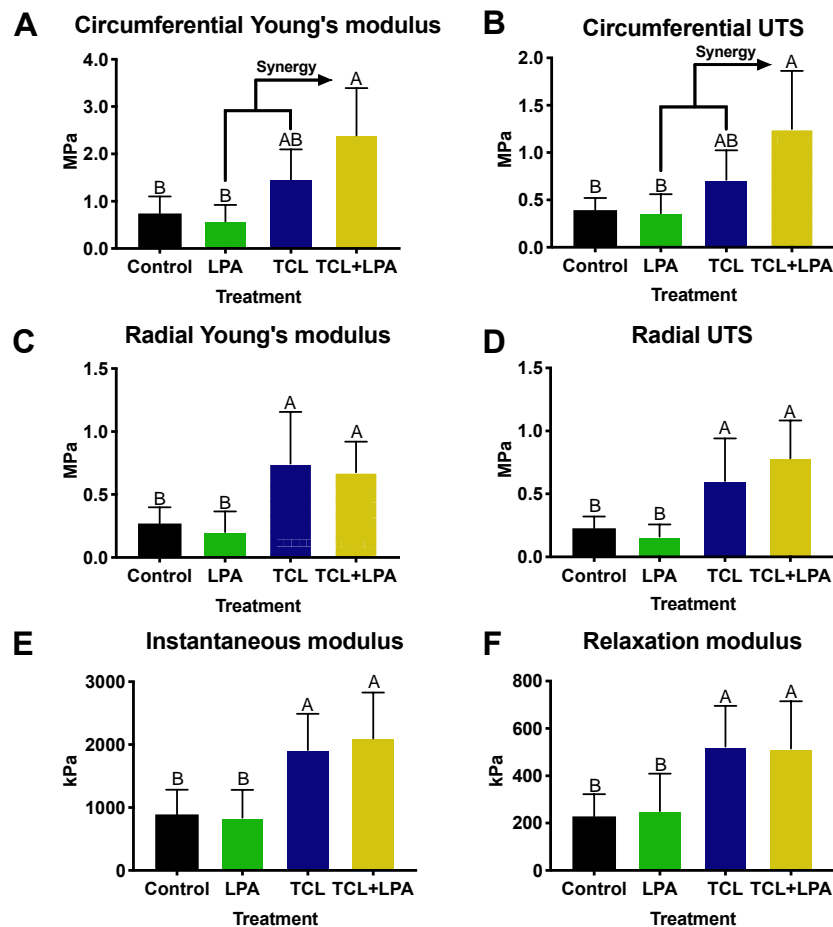


Figure 2. Mechanical properties of neomenisci. TCL+LPA synergistically increased circumferential tensile properties over controls. TCL+LPA and TCL treatments both increased radial tensile properties and compressive properties over controls and LPA only groups. All data are presented as means \pm standard deviations. For all figures, statistical significance is indicated by bars not sharing the same letters.

In addition to increases in tensile properties, compressive properties also were significantly higher in constructs treated with TCL+LPA when compared to non-treated controls. When quantifying compressive properties, TCL+LPA stimulated constructs yielded increases over controls in the instantaneous modulus ($p=0.003$) and relaxation modulus ($p=0.02$), by 135% and 125%, respectively (Figure 2E, 2F). TCL treatment also significantly increased ($p=0.01$) compressive properties over controls. No significant differences in coefficient of viscosity were seen among treatment groups.

Tissue biochemistry

Biochemical treatment led to significant increases in collagen content and pyridinoline crosslink content (Figure 3A, 3C). TCL+LPA treatment enhanced ($p<0.0001$) collagen and pyridinoline content per wet weight by 125% and 185% over control values, respectively. There were no significant differences in GAG content per wet weight among treatment groups. Collagen and pyridinoline content normalized by dry weight also showed increases ($p<0.003$) over controls when treating with TCL+LPA, by 61% and 81% of control values, respectively. However, there were no significant differences among groups in terms of pyridinoline normalized to collagen content (Figure 3D). GAG content normalized to dry weight was significantly lower ($p<0.0001$) for TCL+LPA treated constructs (by 39% of controls). TCL treatment also significantly decreased ($p<0.0001$) GAG content per dry weight when compared to control groups (Figure 3B). There were no significant differences in DNA content among groups (Table 1).

Tissue organization

Two-way ANOVA tests were conducted to examine the effect of TCL and LPA treatments on anisotropy of tensile properties, namely, tensile Young's modulus and UTS (Figure 4A, 4B). These tests showed that LPA treatment significantly increased ($p=0.02$) anisotropy, as indicated by differences of the Young's modulus values in the circumferential versus the radial directions, while TCL significantly decreased ($p=0.02$) UTS anisotropy. Anisotropy ratios of tensile properties

(circumferential/radial values) reached as high as 4-fold with TCL+LPA treatment. In addition, SHG signals in LPA and TCL+LPA treated groups appeared more intense than those of control and TCL treatment groups.

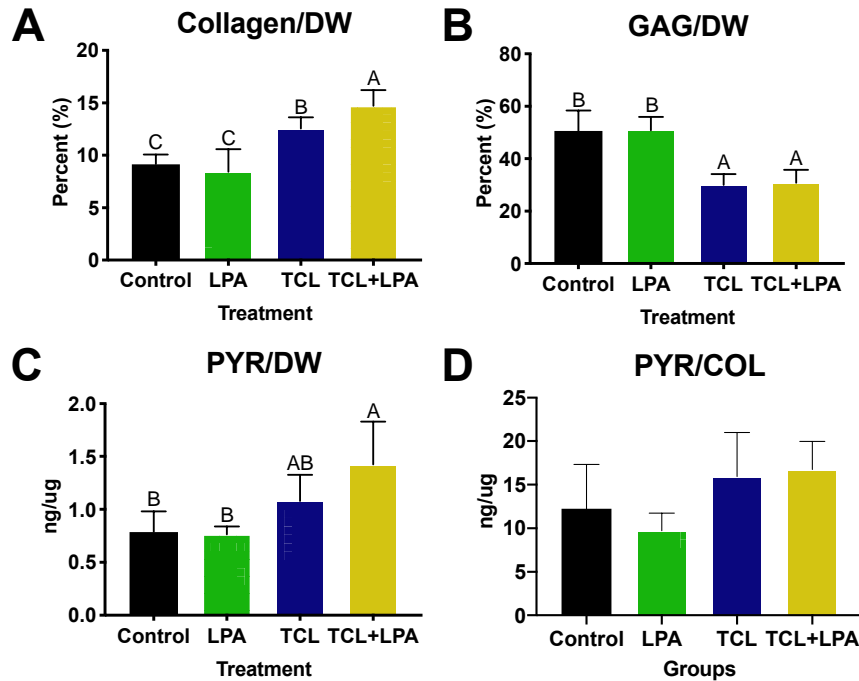


Figure 3. Biochemical properties of self-assembled neomenisci. TCL+LPA treatment enhanced collagen content over all other groups. GAG content was lowered closer to native tissue values in TCL+LPA and TCL groups. Pyridinoline crosslink content in TCL+LPA treated constructs increased over controls, while there were no differences among groups in pyridinoline crosslink content normalized to collagen content.

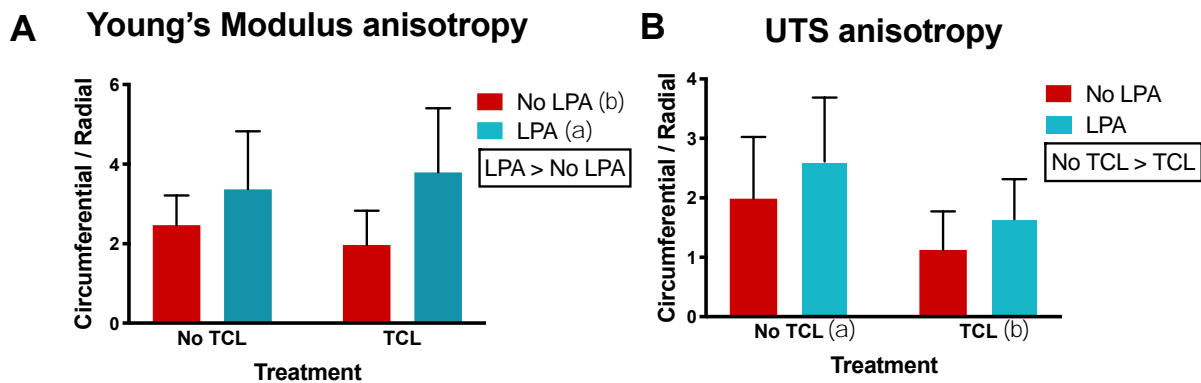


Figure 4. TCL+LPA treatment enhances anisotropy. Two-way analysis of variance shows LPA treatment significantly contributed to increases in Young's modulus anisotropy, while TCL significantly contributed to decreases in UTS anisotropy. Tukey's post hoc showed that none of the groups differed from one another (i.e., there were no statistical differences among the bars). Control groups are represented by the "No TCL" and "No LPA" bar. The alpha and beta represent statistical significance between treatment levels; treatments without these symbols indicate no significant differences between levels.

Discussion

Building upon prior work that showed increases in mechanical properties of self-assembled fibrocartilage treated with TCL¹⁸ and directionality imparted by LPA in neomenisci¹⁰, this study sought to promote matrix augmentation and directional remodeling in order to enhance tensile properties. Experimental results supported the three hypotheses underlying this study, namely: 1) TCL+LPA treatment would enhance the tensile properties of self-assembling neomenisci, 2) these increases in tensile properties would be accompanied by an increase in the amount of pyridinoline collagen crosslinks, and 3) TCL+LPA treatment would produce neomenisci with anisotropic tensile mechanical properties. To the best of our knowledge, this is the first study to use a treatment that both augments matrix content of engineered neomenisci and utilizes a soluble factor to enhance matrix organization and anisotropy. This study demonstrates the combination of matrix augmentation and directional remodeling as a beneficial strategy in tissue engineering of the knee meniscus.

The knee meniscus functions by developing tension when under compressive load, highlighting the importance of attaining tensile properties akin to native tissue in engineered neomenisci. It was found that TCL+LPA treatment resulted in synergistic enhancements to tensile properties of engineered neomenisci, increasing circumferential stiffness and strength by more than 2-fold. In addition, radial stiffness and strength were also increased by more than 1.5- and 2-fold, respectively. Values for tensile strength and stiffness in the circumferential direction were approximately 4-fold higher when compared to values from neomenisci in a study by our group that were treated with only LPA¹⁰. Also, tissue circumferential tensile properties were on par with those of self-assembled neomenisci that used both biochemical and mechanical stimulation to enhance matrix content organization¹³. However, circumferential tensile modulus values in neomenisci treated with TCL+LPA still fall short of native tissue values (100-300 MPa)⁴⁷, denoting the importance of research that aims to enhance this mechanical property that is crucial to meniscus function. In the radial direction, tensile strength and stiffness were approximately one-

tenth of values derived from native tissue (10-30 MPa)^{47,48}, respectively. Increasing tensile properties of engineered neomenisci is a critical step toward deploying them as functional tissues *in vivo*; ultimately, TCL+LPA treatment was effective in elevating tissue tensile properties, which results from its positive effects on matrix content and organization.

In addition to TCL+LPA treatment having beneficial increases to tensile properties, an accompanying increase in collagen content was also seen over all other groups (Figure 3). The significant difference in collagen content between TCL+LPA and TCL groups likely stems from the addition of LPA, which has been shown to increase collagen deposition in engineered tissue⁴⁹. Overall, collagen per dry weight in TCL+LPA groups reached values approximately 2-fold greater than those reported for self-assembled neomenisci treated with only LPA¹⁰. After being able to increase collagen content, it would be important to increase the degree of crosslinking and fiber organization to improve tensile properties. The TCL+LPA treatment used by this study provides a firm foundation for crosslinks by increasing collagen content closer to that of the native meniscus, in agreement with increases in tensile properties. The native meniscus contains mostly collagen types I and II, with some minor collagens such as types III, IV, VI, and XVIII⁴³. While the hydroxyproline assay only measures overall collagen, without discriminating individual collagen types, self-assembled neomenisci have been shown to contain both collagens I and II via IHC⁹. Other self-assembled fibrocartilages have also been shown to contain different ratios of collagen types I and II⁵⁰, and future work on self-assembled neomenisci may include methods to better determine the similarities and differences between different collagen types of native menisci and self-assembled neomenisci.

A significant increase to pyridinoline crosslink content over controls was seen in TCL+LPA treated constructs, which follows previous results seen when applying LOXL2 in self-assembled fibrocartilage¹⁸. This significant increase in crosslinking was observed in conjunction with significant increases in collagen content, indicating that collagen maturation and crosslinking are occurring at the same rate. The TCL+LPA group contained 1.42 ng/ μ g pyridinoline per dry weight

on average, which is on par with historical values for pyridinoline content of native fibrocartilages. For example, calculation using the pyridinoline per hydroxyproline and hydroxyproline per dry weight measurements of prior work⁵¹ shows that human menisci have 1.16 ng/ μ g pyridinoline per dry weight. Similarly, human intervertebral discs have been reported to contain 1.10 ng/ μ g pyridinoline per dry weight⁵². It is worth noting that these prior studies used an HPLC fluorescence detection assay for pyridinoline quantification as opposed to the LC-MS technique used in this paper. Because LC-MS methods have repeatedly been shown to be more precise and accurate than HPLC fluorescence detection methods^{53–55}, future characterization studies on native fibrocartilage crosslinks using LC-MS would yield more comparable data to those collected by our study. Overall, TCL+LPA treated neomenisci exhibited crosslink content that appears to meet or exceed values reported in the literature, though characterization of native tissue via LC-MS methods is warranted.

The anisotropic organization of ECM within the meniscus, with circumferential tensile stiffness being approximately 10-fold that of the radial direction⁴⁸, is crucial to the tissue's function. In this study, we showed that LPA was significant toward enhancing anisotropy, while TCL's robust matrix augmentation effect brought anisotropy ratios (circumferential/radial) closer to 1 (Figure 4). In addition, the SHG signal of TCL+LPA treated constructs appeared more intense than controls, indicating a higher degree of circumferentially aligned collagen fibers. While this study utilized soluble bioactive agents to induce or enhance anisotropy, other methods to induce or enhance anisotropy within engineered menisci include mechanical stimuli via a bioreactor¹³, scaffolds^{56,57}, or their use in combination⁵⁸. While these methods have proven to be effective toward inducing anisotropy, LPA can be seen as a chemical analogue to these techniques that simplifies the tissue engineering process. For example, bioreactor manufacturing can become expensive and time-consuming; in addition, the use of scaffolds can result in harmful effects such as degradation byproducts or stress shielding of cells, further highlighting the benefits of using chemical analogues to achieve proper matrix organization in engineered tissues. Despite financial

and temporal considerations, bioreactors that apply mechanical stimulation may further enhance matrix organization and have previously led to increased tensile properties of self-assembled cartilage³². Without proper collagen fiber alignment, augmenting ECM content would likely not improve mechanical properties substantially, rendering the tissue unable to behave as it would in its native environment. Tissue engineering of the meniscus should focus on enhancing both mechanical and anisotropic properties to levels of native tissue. Thus, future work may examine the use of TCL+LPA treatment, in conjunction with additional bioactive factors or mechanical stimuli to increase ECM alignment and, consequently, tensile properties.

Interestingly, while the combination of TCL+LPA induced improvements of neomenisci tensile properties, the LPA only group did not differ mechanically or morphologically from the control group. This contradicts previous results shown when using LPA in the tissue engineering of self-assembled neomenisci¹⁰. No increases in tensile properties over controls in the LPA treatment group may have resulted due to the higher amounts of GAG in non-TCL treated tissues, which may have induced more swelling pressure and caused resistance to contraction by the collagen network. The use of C-ABC, which temporarily depletes GAG within the ECM and allows for more dense organization of collagen fibers¹⁹, could have relieved this swelling pressure and allowed cell traction forces to align collagen fibers. In addition, this depletion of GAG due to C-ABC treatment likely contributed to lower wet weights and hydration percentages in TCL-treated groups, as negatively charged GAG attract water into the ECM¹⁴. Lower dry weights in groups treated with TCL may also likely stem from decreased GAG content as a result of C-ABC treatment. Also, despite morphological differences, a significant difference in circumferential tensile properties was not seen between TCL+LPA and TCL groups ($p=0.06$), although neomenisci treated with TCL+LPA trended higher. This trend may result from a significantly higher amount of collagen in the TCL+LPA group over TCL treated neomenisci, in addition to morphological differences that imply a degree of difference in organization.

Due to the prevalence and economic impact of meniscal injuries, creating engineered meniscal tissue that recapitulates native tissue properties is crucial for its successful translation from the benchtop to the clinic. Enhancements to mechanical, biochemical, and anisotropic tensile properties of neomenisci, induced by TCL+LPA treatment, narrow the gap between native and engineered tissue properties and provide a promising path toward translation. While this study utilized bioactive agents to induce anisotropic tensile properties in neomenisci, other groups have utilized techniques such as 3D-printed scaffolds to replicate this property with the consideration of translation as the end goal⁵⁸. In addition, as the native knee meniscus is zonally inhomogeneous, anisotropic engineered neomenisci with zonal variations have been created using the self-assembling process⁵⁹. Since an entire neomeniscus might not be required for a repair procedure, a portion may be cut out to interface with native tissue to achieve a healing response. Investigation for this sort of engineered-native tissue interaction would require visualization of cell migration, likely through fluorescent tagging of chondrocytes and meniscal cells used to engineer self-assembled neomenisci. A previous study in which our group implanted tissue engineered constructs into fibrocartilage of the temporomandibular joint (TMJ) disc showed host cells infiltrating the implant⁶⁰; due to the fibrocartilaginous nature and similarities between the knee meniscus and TMJ discs, we expect that a similar *in vivo* response may be seen when implanting neomenisci. Further *in vivo* work showing the safety and efficacy of engineered neomenisci toward repairing or replacing injured meniscal tissue, especially in large animal models, is required to navigate the Food and Drug Administration paradigm⁶¹ and translate these tissues to the clinic.

This work demonstrates that treatment with TCL+LPA can augment and align the mechanical properties of engineered fibrocartilaginous tissues. Higher collagen and pyridinoline crosslink content accompanied a synergistic increase in tensile properties, and anisotropic mechanical properties were observed in treated tissues. This work highlights the use of a combination of bioactive stimuli to achieve synergistic improvements in properties of engineered

knee meniscus tissue. Future studies combining TCL+LPA with mechanical stimuli or additional bioactive agents to further enhance tensile properties of neomenisci are warranted to ensure functionality of these tissues *in vivo*.

References

1. Salata, M. J., Gibbs, A. E. & Sekiya, J. K. A systematic review of clinical outcomes in patients undergoing meniscectomy. *Am. J. Sports Med.* **38**, 1907–1916 (2010).
2. Petersen, W. & Tillmann, B. Collagenous fibril texture of the human knee joint menisci. *Anat. Embryol. (Berl)*. **197**, 317–324 (1998).
3. Andrews, S. H. J. *et al.* Tie-fibre structure and organization in the knee menisci. *J. Anat.* **224**, 531–537 (2014).
4. Eleswarapu, S. V., Responde, D. J. & Athanasiou, K. A. Tensile properties, collagen content, and crosslinks in connective tissues of the immature knee joint. *PLoS One* **6**, e26178 (2011).
5. Williamson, A. K., Chen, A. C., Masuda, K., Thonar, E. J. M. A. & Sah, R. L. Tensile mechanical properties of bovine articular cartilage: Variations with growth and relationships to collagen network components. *J. Orthop. Res.* **21**, 872–880 (2003).
6. Chan, B. P., Fu, S. C., Qin, L., Rolf, C. & Chan, K. M. Pyridinoline in relation to ultimate stress of the patellar tendon during healing: an animal study. *J. Orthop. Res.* **16**, 597–603 (1998).
7. Arnoczky, S. P. & Warren, R. F. Microvasculature of the human meniscus. *Am. J. Sports Med.* **10**, 90–95 (1982).
8. Rangger, C., Kathrein, A., Klestil, T. & Glötzer, W. Partial meniscectomy and osteoarthritis. Implications for treatment of athletes. *Sports Med.* **23**, 61–68 (1997).
9. Aufderheide, A. C. & Athanasiou, K. A. Assessment of a bovine co-culture, scaffold-free method for growing meniscus-shaped constructs. *Tissue Eng.* **13**, 2195–2205 (2007).
10. Hadidi, P. & Athanasiou, K. A. Enhancing the mechanical properties of engineered tissue through matrix remodeling via the signaling phospholipid lysophosphatidic acid. *Biochem. Biophys. Res. Commun.* **433**, 133–138 (2013).
11. Hadidi, P., Yeh, T. C., Hu, J. C. & Athanasiou, K. A. Critical seeding density improves the properties and translatability of self-assembling anatomically shaped knee menisci. *Acta Biomater.* **11**, 173–182 (2015).
12. Hadidi, P. *et al.* Tendon and ligament as novel cell sources for engineering the knee meniscus. *Osteoarthr. Cartil.* **24**, 2126–2134 (2016).
13. Huey, D. J. & Athanasiou, K. A. Tension-compression loading with chemical stimulation results in additive increases to functional properties of anatomic meniscal constructs. *PLoS One* **6**, 1–9 (2011).
14. Huey, D. J. & Athanasiou, K. A. Maturation growth of self-assembled, functional menisci as a result of TGF- β 1 and enzymatic chondroitinase-ABC stimulation. *Biomaterials* **32**, 2052–2058 (2011).
15. Hu, J. C. & Athanasiou, K. A. A Self-Assembling Process in Articular Cartilage Tissue Engineering. *Tissue Eng.* **12**, 969–979 (2006).
16. Lee, J. K., Hu, J. C. Y., Yamada, S. & Athanasiou, K. A. Initiation of Chondrocyte Self-Assembly Requires an Intact Cytoskeletal Network. *Tissue Eng. Part A* **22**, 318–325 (2016).
17. Ofek, G. *et al.* Matrix development in self-assembly of articular cartilage. *PLoS One* **3**, (2008).

18. Makris, E. A., MacBarb, R. F., Paschos, N. K., Hu, J. C. & Athanasiou, K. A. Combined use of chondroitinase-ABC, TGF- β 1, and collagen crosslinking agent lysyl oxidase to engineer functional neotissues for fibrocartilage repair. *Biomaterials* **35**, 6787–6796 (2014).
19. MacBarb, R. F., Makris, E. A., Hu, J. C. & Athanasiou, K. A. A chondroitinase-ABC and TGF- β 1 treatment regimen for enhancing the mechanical properties of tissue-engineered fibrocartilage. *Acta Biomater.* **9**, 4626–4634 (2013).
20. Gunja, N. J., Uthamanthil, R. K. & Athanasiou, K. A. Effects of TGF- β 1 and hydrostatic pressure on meniscus cell-seeded scaffolds. *Biomaterials* **30**, 565–573 (2009).
21. Allen, K. D. & Athanasiou, K. A. Scaffold and growth factor selection in temporomandibular joint disc engineering. *J. Dent. Res.* **87**, 180–185 (2008).
22. Wang, C.-H. *et al.* Layering Poly (lactic-co-glycolic acid)-based electrospun membranes and co-culture cell sheets for engineering temporomandibular joint disc. *J. Biol. Regul. Homeost. Agents* **32**, 55–61 (2018).
23. Legemate, K., Tarafder, S., Jun, Y. & Lee, C. H. Engineering Human TMJ Discs with Protein-Releasing 3D-Printed Scaffolds. *J. Dent. Res.* **95**, 800–807 (2016).
24. Detamore, M. S. & Athanasiou, K. A. Effects of growth factors on temporomandibular joint disc cells. *Arch. Oral Biol.* **49**, 577–583 (2004).
25. Johns, D. E. & Athanasiou, K. A. Growth factor effects on costal chondrocytes for tissue engineering fibrocartilage. *Cell Tissue Res.* **333**, 439–447 (2008).
26. Kasemkijwattana, C. *et al.* The use of growth factors, gene therapy and tissue engineering to improve meniscal healing. *Mater. Sci. Eng. C* **13**, 19–28 (2000).
27. Detamore, M. S. & Athanasiou, K. A. Evaluation of three growth factors for TMJ disc tissue engineering. *Ann. Biomed. Eng.* **33**, 383–390 (2005).
28. Almarza, A. J. & Athanasiou, K. A. Evaluation of three growth factors in combinations of two for temporomandibular joint disc tissue engineering. *Arch. Oral Biol.* **51**, 215–221 (2006).
29. Kalpakci, K. N., Kim, E. J. & Athanasiou, K. A. Assessment of growth factor treatment on fibrochondrocyte and chondrocyte co-cultures for TMJ fibrocartilage engineering. *Acta Biomater.* **7**, 1710–1718 (2011).
30. Bhargava, M. M. *et al.* The Effect of Cytokines on the Proliferation and Migration of Bovine Meniscal Cells. *Am. J. Sports Med.* **27**, 636–643 (1999).
31. Makris, E. A., MacBarb, R. F., Responde, D. J., Hu, J. C. & Athanasiou, K. A. A copper sulfate and hydroxylysine treatment regimen for enhancing collagen cross-linking and biomechanical properties in engineered neocartilage. *FASEB J.* **27**, 2421–30 (2013).
32. Lee, J. K. *et al.* Tension stimulation drives tissue formation in scaffold-free systems. *Nat. Mater.* **16**, 864–873 (2017).
33. Grinnell, F. Fibroblast biology in three-dimensional collagen matrices. *Trends in Cell Biology* vol. 13 264–269 (2003).
34. Abe, M., Ho, C. H., Kamm, K. E. & Grinnell, F. Different Molecular Motors Mediate Platelet-derived Growth Factor and Lysophosphatidic Acid-stimulated Floating Collagen Matrix Contraction. *J. Biol. Chem.* **278**, 47707–47712 (2003).
35. Abe, M., Sogabe, Y., Syuto, T., Yokoyama, Y. & Ishikawa, O. Evidence that PI3K, Rac, Rho, and Rho kinase are involved in basic fibroblast growth factor-stimulated fibroblast–Collagen matrix contraction. *J. Cell. Biochem.* **102**, 1290–1299 (2007).
36. Parizi, M., Howard, E. W. & Tomasek, J. J. Regulation of LPA-Promoted Myofibroblast Contraction: Role of Rho, Myosin Light Chain Kinase, and Myosin Light Chain Phosphatase. *Exp. Cell Res.* **254**, 210–220 (2000).
37. Tigyi, G., Dyer, D. L. & Miledi, R. Lysophosphatidic acid possesses dual action in cell proliferation. *Proc. Natl. Acad. Sci.* **91**, 1908–1912 (1994).

38. Hurst-Kennedy, J., Boyan, B. D. & Schwartz, Z. Lysophosphatidic acid signaling promotes proliferation, differentiation, and cell survival in rat growth plate chondrocytes. *Biochim. Biophys. Acta - Mol. Cell Res.* **1793**, 836–846 (2009).
39. Makris, E. A., Responde, D. J., Paschos, N. K., Hu, J. C. & Athanasiou, K. A. Developing functional musculoskeletal tissues through hypoxia and lysyl oxidase-induced collagen cross-linking. *Proc. Natl. Acad. Sci.* **111**, E4832–E4841 (2014).
40. Allen, K. D. & Athanasiou, K. A. Viscoelastic characterization of the porcine temporomandibular joint disc under unconfined compression. *J. Biomech.* **39**, 312–322 (2006).
41. Cissell, D. D., Link, J. M., Hu, J. C. & Athanasiou, K. A. A Modified Hydroxyproline Assay Based on Hydrochloric Acid in Ehrlich's Solution Accurately Measures Tissue Collagen Content. *Tissue Eng. Part C Methods* **23**, 243–250 (2017).
42. Naffa, R. *et al.* Rapid analysis of pyridinoline and deoxypyridinoline in biological samples by liquid chromatography with mass spectrometry and a silica hydride column. *J. Sep. Sci.* **42**, 1482–1488 (2019).
43. Makris, E. A., Hadidi, P. & Athanasiou, K. A. The knee meniscus: Structure-function, pathophysiology, current repair techniques, and prospects for regeneration. *Biomaterials* **32**, 7411–7431 (2011).
44. Pauli, C. *et al.* Macroscopic And Histopathologic Analysis Of Human Knee Menisci In Aging And Osteoarthritis. *Osteoarthr. Cartil.* **19**, 1132–1141 (2011).
45. Ribitsch, I. *et al.* Structure-Function relationships of equine menisci. *PLoS One* **13**, 1–17 (2018).
46. Nakagawa, K. *et al.* Histological Analysis of the Wrapping Treatment for Meniscal Horizontal Tears in Rabbits. *Cartilage* (2019) doi:10.1177/1947603519870838.
47. Fithian, D. C., Kelly, M. A. & Mow, V. C. Material properties and structure-function relationships in the menisci. *Clin. Orthop. Relat. Res.* 19–31 (1990) doi:10.1097/00003086-199003000-00004.
48. Tissakht, M. & Ahmed, A. M. Tensile stress-strain characteristics of the human meniscal material. *J. Biomech.* **28**, 411–422 (1995).
49. Chabaud, S. *et al.* Lysophosphatidic acid enhances collagen deposition and matrix thickening in engineered tissue. *J. Tissue Eng. Regen. Med.* **9**, E65–E75 (2015).
50. Murphy, M. K., Masters, T. E., Hu, J. C. & Athanasiou, K. A. Engineering a fibrocartilage spectrum through modulation of aggregate redifferentiation. *Cell Transplant.* **24**, 235–245 (2015).
51. Takahashi, M., Suzuki, M., Kushida, K., Hoshino, H. & Inoue, T. The effect of aging and osteoarthritis on the mature and senescent cross-links of collagen in human meniscus. *Arthrosc. - J. Arthrosc. Relat. Surg.* **14**, 366–372 (1998).
52. Tan, C. I., Neil Kent, G., Randall, A. G., Edmondston, S. J. & Singer, K. P. Age-Related Changes in Collagen, Pyridinoline, and Deoxypyridinoline in Normal Human Thoracic Intervertebral Discs. *Journals Gerontol. Ser. A Biol. Sci. Med. Sci.* **58**, B387–B393 (2003).
53. Bandeira, R. D. da C. C. *et al.* Comparison of high performance liquid chromatography with fluorescence detector and with tandem mass spectrometry methods for detection and quantification of ochratoxin A in green and roasted coffee beans. *Brazilian Arch. Biol. Technol.* **56**, 911–920 (2013).
54. Wang, H., Walaszczyk, E. J., Li, K., Chung-Davidson, Y. W. & Li, W. High-performance liquid chromatography with fluorescence detection and ultra-performance liquid chromatography with electrospray tandem mass spectrometry method for the determination of indoleamine neurotransmitters and their metabolites in sea lamprey pl. *Anal. Chim. Acta* **721**, 147–153 (2012).

55. Milićević, D., Jurić, V., Stefanović, S., Baltić, T. & Janković, S. Evaluation and validation of two chromatographic methods (HPLC-Fluorescence and LC-MS/MS) for the determination and confirmation of ochratoxin A in pig tissues. *Arch. Environ. Contam. Toxicol.* **58**, 1074–1081 (2010).
56. Zhang, Z. Z. *et al.* Role of scaffold mean pore size in meniscus regeneration. *Acta Biomater.* **43**, 314–326 (2016).
57. Baek, J. *et al.* Repair of Avascular Meniscus Tears with Electrospun Collagen Scaffolds Seeded with Human Cells. *Tissue Eng. Part A* **22**, 436–448 (2016).
58. Zhang, Z. Z. *et al.* Orchestrated biomechanical, structural, and biochemical stimuli for engineering anisotropic meniscus. *Sci. Transl. Med.* **11**, (2019).
59. Higashioka, M. M., Chen, J. A., Hu, J. C. & Athanasiou, K. A. Building an Anisotropic Meniscus with Zonal Variations. *Tissue Eng. Part A* **20**, 294–302 (2014).
60. Vapniarsky, N. *et al.* Tissue engineering toward temporomandibular joint disc regeneration. *Sci. Transl. Med.* **10**, (2018).
61. Donahue, R. P., Gonzalez-Leon, E. A., Hu, J. C. & Athanasiou, K. A. Considerations for translation of tissue engineered fibrocartilage from bench to bedside. *Journal of Biomechanical Engineering* vol. 141 (2019).

APPENDIX B | The effect of neonatal, juvenile, and adult donors on rejuvenated neocartilage functional properties*

Abstract

Cartilage does not naturally heal, and cartilage lesions from trauma and wear-and-tear can lead to eventual osteoarthritis. To address long-term repair, tissue engineering of functional biologic implants to treat cartilage lesions is desirable, but the development of such implants is hindered by several limitations including 1) donor tissue scarcity due to the presence of diseased tissues in joints, 2) dedifferentiation of chondrocytes during expansion, and 3) differences in functional output of cells dependent on donor age. Toward overcoming these challenges, 1) costal cartilage has been explored as a donor tissue, and 2) methods have been developed to rejuvenate the chondrogenic phenotype of passaged chondrocytes for generating self-assembled neocartilage. However, it remains unclear how the rejuvenation processes are influenced by donor age, and, thus, how to develop strategies that specifically target age-related differences. Using histological, biochemical, proteomic, and mechanical assays, this study sought to determine the differences among neocartilage generated from neonatal, juvenile, and adult donors using the Yucatan minipig, a clinically relevant large animal model. Based on the literature, a relatively young adult population of animals was chosen due to a reduction in functional output of human articular chondrocytes after 40 years of age. After isolation, costal chondrocytes were expanded, rejuvenated, and self-assembled, and the neocartilages were assessed. The aggregate modulus values of neonatal constructs were at least 1.65-fold of those from the juvenile or adult constructs. Poisson's ratio also significantly differed among all groups, with neonatal constructs exhibiting values 49% higher than adult constructs. Surprisingly, other functional properties such as tensile

* Published as: Donahue RP[†], Nordberg RC[†], Bielajew BJ, Hu JC, Athanasiou KA. The effect of neonatal, juvenile, and adult donors on rejuvenated neocartilage functional properties. *Tissue Engineering Part A* 2022; online ahead of print. [†]equal contribution

modulus and glycosaminoglycan content did not significantly differ among groups. Total collagen content was slightly elevated in the adult constructs when compared to neonatal and juvenile constructs. A more nuanced view via bottom-up mass spectrometry showed that *Col2a1* protein was not significantly different among groups, but protein content of several other collagen subtypes (i.e., *Col1a1*, *Col9a1*, *Col11a2*, and *Col12a1*) was modulated by donor age. For example, *Col12a1* protein content in adult constructs was found to be 102.9% higher than neonatal-derived constructs. Despite these differences, this study shows that different aged donors can be used to generate neocartilages of similar functional properties.

Introduction

Hyaline articular cartilage does not naturally heal, and cartilage lesions from trauma or wear-and-tear can develop into osteoarthritis (OA). OA is associated with pain and loss of joint function^{1,2}. According to the Centers for Disease Control, OA affects over 32 million people in the U.S.³ and is projected to rise up to 60% in prevalence over the next two decades⁴. Tissue engineering is poised to provide a long-term, regenerative solution needed for cartilage defects, and the only currently approved cell-based therapy is matrix-assisted autologous chondrocyte implantation (MACI), which consists of expanding a patient's cells in the laboratory and re-implanting the cells on a collagen membrane⁵. For MACI and future cell-based therapies, such as tissue-engineered neocartilage, it is widely recognized that one of the biggest challenges to the field is cell sourcing, and the development of novel cell-based cartilage therapies is hindered by several limitations including 1) donor tissue scarcity due to the presence of diseased tissues in the joints, 2) dedifferentiation of cells during expansion, and 3) the differences in engineering potential of chondrocytes dependent on donor age⁶⁻⁸.

Donor tissue scarcity is a major challenge because cartilage tissue engineering techniques require high numbers of chondrocytes, especially when considering the development of large cartilage implants. For example, self-assembled cartilage constructs have been

generated up to 9.3 cm² but require 50 million chondrocytes⁹, which would require harvesting approximately half of the entirety of chondrocytes from one adult donor knee^{10,11}. This is an untenable proposition given that patients who require cartilage therapies have diseased tissues in their joints, further limiting the availability of healthy donor cartilage. Thus, one of the challenges for the translation of cartilage tissue engineering is selecting a cell source that is both functional and scalable. While fully differentiated, primary chondrocytes are a desirable cell source in that they are already primed to function as mature chondrocytes, practically, they are difficult to obtain in large numbers due to donor site morbidity in autologous cases, limited donor tissue supply in allogeneic cases, and prevalence of disease within the donor tissue.

Cell expansion can help address the issue of cell scarcity but is limited due to concerns of chondrocyte dedifferentiation. Passaging chondrocytes can allow for a cumulative expansion factor of 12.6X10⁶-fold¹², but passaging chondrocytes can lead to rapid dedifferentiation and loss of the chondrogenic phenotype¹³. To combat this, aggregate culture methods have been developed to rejuvenate cells to a chondrogenic phenotype and to restore the ability of passaged chondrocytes to generate functional self-assembled cartilage¹². Moreover, cartilage is considered relatively immuno-privileged¹⁴, and, therefore, passaged, allogeneic chondrocytes can be utilized to provide cells for a large number of patients. Specifically, at passage 11, it has been estimated that chondrocytes from a single 1 cm³ biopsy can generate cartilage implants for up to 10 million patients¹². At such a staggering expansion factor, selecting the appropriate donor source will be critical to the success of a tissue-engineered cartilage implant system.

Toward addressing the current bottleneck of cell sourcing, costal chondrocytes, in particular, are attractive due to their excellent expansion and redifferentiation capabilities^{15,16}. Additionally, previous use of costal cartilage in rhinoplasties¹⁷ and as an interpositional material for the temporomandibular joint (TMJ)¹⁸ make costal chondrocytes a logical cell source for tissue engineering of cartilages. It has been demonstrated that costal chondrocytes have a greater initial yield and capacity for expansion than articular chondrocytes and can redifferentiate without

ossification¹⁹. Harnessing these advantages, recent cartilage tissue engineering research has utilized costal chondrocytes for both scaffold-based^{20,21} and scaffold-free techniques²². Moreover, passaged costal chondrocytes can be used to repair fibrocartilage and have been demonstrated to repair defects in the TMJ disc²³. Therefore, costal chondrocytes can be further developed into a cell source to repair both articular cartilage and fibrocartilage.

When selecting a donor source, a factor that may play a role in the functional properties of a tissue-engineered cartilage construct is the age of the donor. Prior work has demonstrated that donor age can affect the functional output of chondrocytes. For example, it has been reported that the growth factor responsiveness of chondrocytes is modulated by donor age²⁴. Also, chondrocytes isolated from the knee of donors under the age of 13 produced significantly more proteoglycans and had greater proliferative capacity than older donors (i.e., up to 72 years old)⁶. In another study, increased levels of *Col II* and *Sox9* gene expression were reported in juvenile chondrocytes (i.e., 6-month-old donor) during monolayer expansion compared to adult chondrocytes (i.e., 34-year-old donor), and higher *Col II* and *Acan* gene expression were reported in juvenile chondrocyte-derived hydrogel neocartilages⁷. To combat the effect of aging chondrocytes, transforming growth factor beta 1 (TGF- β 1), basic fibroblast growth factor (bFGF), and platelet-derived growth factor (PDGF-BB) have been used to support post-expansion chondrogenic capacity for cells derived from older donors⁸. It was found that when these growth factors were applied, chondrocyte proliferation rate was significantly elevated from donors of all age groups (age 20-91 years), but chondrogenic capacity in neocartilage formation was elevated in donors only up to 40 years of age⁸. Additionally, this growth factor combination has been previously shown to increase neocartilage glycosaminoglycan (GAG) content, decrease the ratio of collagen types I to II, and enhance compressive properties¹⁶. Thus, even in experiments that aim to improve the utility of cells from older donors, it was shown that younger chondrocytes consistently have a higher functional output. Thus, autologous therapeutic strategies are hindered by the lack of methodologies that can enhance an older donor's cells to the levels of productivity

associated with cells from younger donors, and allogeneic approaches are limited to using scarcely available young donor sources. Based on the above literature examining articular chondrocytes, the work here focused on characterizing the age-related differences in costal cartilage-derived neotissues from a relatively young range of donors (i.e., neonatal, juvenile, young adult) due to the attractiveness of using these cells for potential therapies and the lack of such characterization in the literature.

Toward the translation of cartilage tissue-engineered products and toward addressing donor tissue scarcity, chondrocyte dedifferentiation, and different functional output of chondrocytes of various ages, the current study examined the effect of donor age on the functional properties of self-assembled neocartilage formed using expanded costal chondrocytes. Neocartilage constructs were generated from costal chondrocytes isolated from neonatal, juvenile (5-8 months), and skeletally mature adult (18-24 months) Yucatan minipigs. In terms of human age equivalencies, the neonatal minipigs correspond to several days old in the human, juvenile minipigs correspond to the start of sexual maturity at around 8-10 years old in the human^{25,26}, and adult minipigs correspond to the end of skeletal maturity at a maximum of 25 years old in the human^{27,28}. It is important to note that, in relation to human age, the adult group of minipigs here is relatively young (i.e., up to 25 years in humans) and were selected for this study as literature has shown a severe reduction in the capacity to create mechanically robust neotissue after 40 years of age in humans⁸. Thus, the objective of this study was to ultimately characterize the functional differences of neocartilage derived from these three minipig donor ages. As with cells derived from articular cartilage, it was hypothesized that donor age will have an effect on the biochemical and mechanical properties of neocartilage constructs derived from costal chondrocytes.

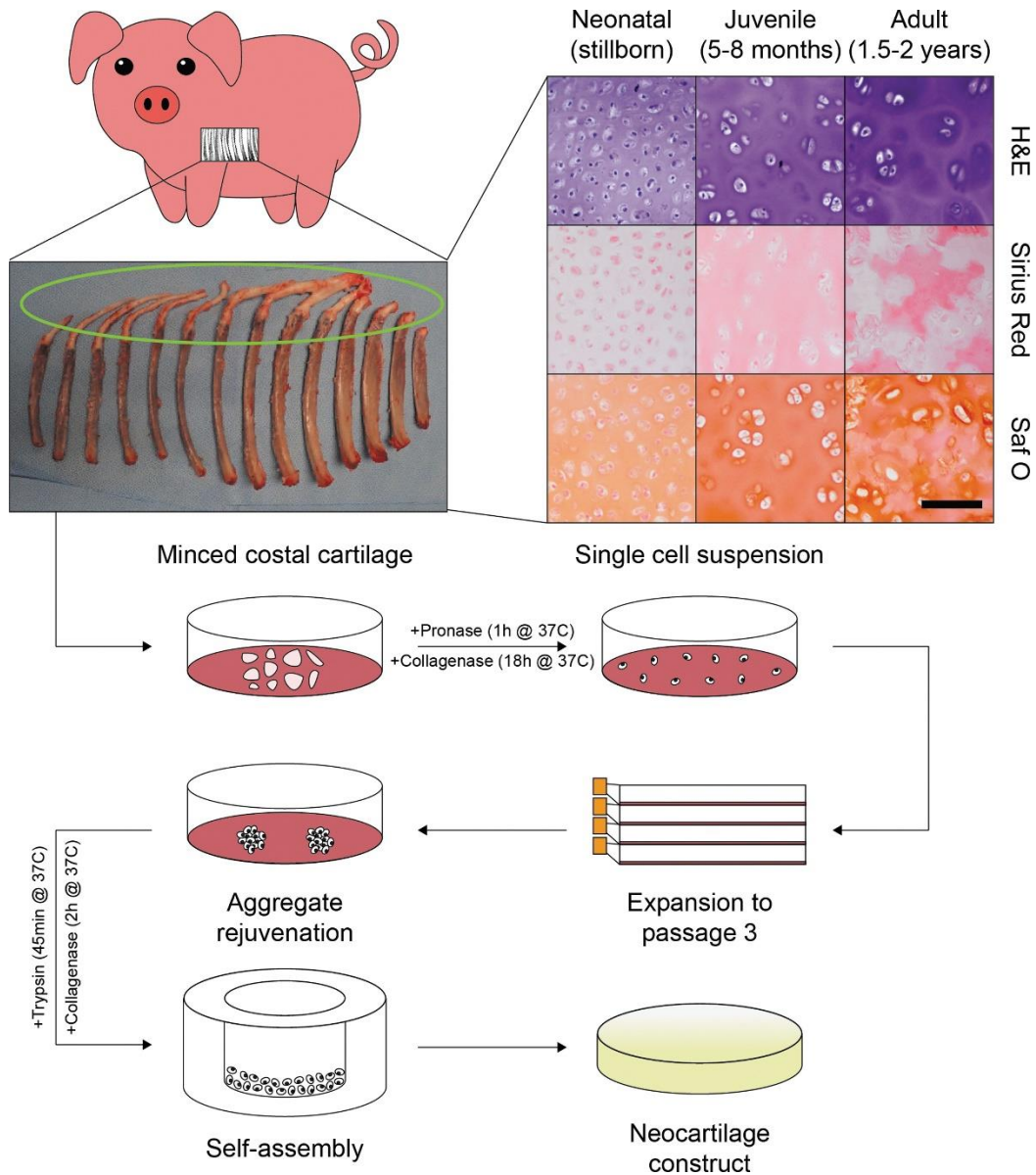


Figure 1. Costal cartilage harvest and isolation and the tissue engineering process. Costal cartilage (green oval) from the ribs of Yucatan minipigs of three different ages of animals was isolated from the surrounding soft tissue and separated from the bone, minced into small pieces, and enzymatically digested to obtain a single cell suspension. Histological staining showed differences in native costal cartilage among the three ages (neonatal, juvenile, and adult). Chondrocytes were then seeded into flasks for expansion to passage 3, then aggregate rejuvenated in nonadherent petri dishes. Subsequent seeding for self-assembly then occurred to obtain a neocartilage construct. Abbreviations: H&E, Hematoxylin and Eosin; Saf O, Safranin O; Sirius Red, Picrosirius Red. Scale bar = 200 μ m.

Materials and methods

Costal cartilage harvest and isolation

Tissues were obtained from Yucatan minipigs culled for reasons unrelated to this study. The ages of the minipigs donors were stillborn (neonatal); 5-8 months (juvenile), corresponding to start of

sexual maturity in humans (e.g., 10-12 years old)²⁵; and 1.5-2 years (skeletally mature adult), corresponding to completion of epiphyseal closure in humans (e.g., up to 25 years old)²⁷. Costal cartilage (green oval, Figure 1) was obtained from four minipigs (2 males, 2 females) for each age (12 total for the entire study) and separated from the bone. Soft tissues and perichondrium were removed from the costal cartilage before mincing into ~1 mm³ pieces. Costal cartilage was digested via agitation at 50 RPM using 0.4% w/v pronase for 1h at 37°C and then 0.2% w/v collagenase for 18h at 37°C. Both enzymes were supplemented with 3% fetal bovine serum (FBS) in Dulbecco's modified Eagle's Medium (DMEM) with 1% penicillin-streptomycin-fungizone (PSF). Following digestion, a single cell suspension was obtained by passing the cell suspension through a 70 µm strainer, and chondrocytes were rinsed using blank DMEM with 1% PSF in preparation for expansion and aggregate rejuvenation.

Chondrocyte expansion and aggregate rejuvenation

Immediately following isolation (Figure 1), chondrocytes were plated for expansion at 2.5 million per T225 flask (~11,111 cells/cm²) in chemically defined, chondrogenic (CHG) medium composed of DMEM supplemented with 1% PSF, 1% insulin-transferrin-selenous acid+ (ITS+), 1% nonessential amino acids (NEAA), 100 nM dexamethasone, 50 µg/mL ascorbate-2-phosphate, 40 µg/mL L-proline, and 100 µg/mL sodium pyruvate. CHG medium was further supplemented with 2% FBS, 1 ng/mL TGF-β1, 5 ng/mL bFGF, and 10 ng/mL PDGF-BB during expansion to passage 3¹⁶. Cells were frozen after one passage in FBS containing 10% dimethyl sulfoxide (DMSO) for downstream use in multiple experiments and thawed as needed for use at passage 3. Donors were cultured separately up until passage 2 and then subsequently combined based on donor age (i.e., two male and two female donors were combined for each age). Medium changes occurred every 3-4 days. Upon 90% confluence for each passage, cells were lifted using 0.05% Trypsin-EDTA for 9 minutes followed by 0.2% w/v collagenase supplemented with 3% FBS

in DMEM with 1% PSF for 40 minutes. After three passages, cells underwent aggregate rejuvenation.

For aggregate rejuvenation, cells were plated at 750,000 cells/mL in CHG medium containing 10 ng/mL TGF- β 1, 100 ng/mL growth differentiation factor 5 (GDF-5), and 100 ng/mL bone morphogenetic protein 2 (BMP-2) for 14 days²⁹. Petri dishes (25 x 100 mm) were covered with 1% agarose to make the surfaces nonadherent. Dishes were placed on an orbital shaker at 50 RPM for 24 hours after seeding, then switched to static culture for the remaining culture time. Medium changes occurred every 3-4 days. After 14 days, aggregates were digested using 0.05% Trypsin-EDTA for 45 minutes followed by 0.2% w/v collagenase supplemented with 3% FBS in DMEM with 1% PSF for 2 hours. Cells were passed through a 70 μ m cell strainer prior to the self-assembling process.

Neocartilage self-assembly

Two days before self-assembly, nonadherent cylindrical 5 mm diameter wells were made using 2% agarose and negative molds. CHG medium was exchanged at least three times prior to cell seeding. Based on prior work³⁰, 2 million cells per well was identified as the ideal seeding density, and cells were seeded at this density in 100 μ L of CHG. After 4 hours, medium was topped off in the well with another 400 μ L. CHG medium was then exchanged (450 μ L) every day until neocartilage was unconfined from the wells at day 5. From days 5-28, CHG medium was exchanged every other day (2 mL). After 28 days, cell culture was terminated, and samples were analyzed.

Sample processing and photometric biochemical analysis

After 28 days of self-assembly, each construct (n=7-8 per group) was photographed, measured for diameter and thickness (on the outside edge of the construct), and then split into samples for photometric biochemical analysis, pyridinoline (PYR) mass spectrometry analysis, bottom-up mass spectrometry proteomic analysis, mechanical testing, and histology. Pieces for biochemical

and PYR analysis were weighed to obtain a wet weight (WW) and frozen at -20 °C for further downstream processing. After lyophilization, a dry weight (DW) was taken for each sample, and biochemical samples were subsequently digested using papain for 18 hours at 60 °C. Total collagen content was quantified using a modified hydroxyproline assay, as previously described³¹. GAGs were also quantified through a dimethylmethylene blue assay (DMMB) per the manufacturer's protocol. Total collagen content and GAG content were normalized to DW. Hydration was calculated by subtracting the ratio of DW to WW from 1 and converted to a percentage by multiplying by 100.

Pyridinoline mass spectrometry analysis

As previously described³², liquid chromatography-mass spectrometry was performed to quantify PYR content. Briefly, neocartilage samples (~200-500 µg DW) were hydrolyzed in 6 N HCl at 105 °C for 24 hours, then acid was evaporated inside a chemical fume hood. Dried hydrolysates were resuspended in 400 µL of 25% v/v acetonitrile and 0.1% v/v formic acid in water and centrifuged at 15,000 g for 10 minutes through a 100 kDa molecular weight cut-off centrifugal filter, yielding a colorless, transparent, filtered hydrolysate. These filtered hydrolysates (5 µL) were analyzed on a Waters Quattro Premier XE triple quadrupole mass spectrometer with a Cogent Diamond Hydride 2.0 HPLC column on a Waters ACQUITY UPLC I-Class core system. Solvent A was 0.1% formic acid in water, and solvent B was 0.1% formic acid in acetonitrile. The gradient was as follows: initial 90% B, 1 minute 90% B, 2 minutes 20% B, 5 minutes 90% B, 10 minutes 90% B, flow rate 400 µL/min, and a total run time of 10 minutes. A standard curve of six serial dilutions of PYR standard was used to quantify the PYR in injected samples using area-under-curve measurements in the QuanLynx module of MassLynx v4.1. PYR samples were then normalized to collagen content.

Bottom-up mass spectrometry proteomic analysis

For bottom-up proteomics, three samples per group were washed twice in 10 mM ammonium citrate and twice in 50 mM ammonium bicarbonate, and mass spectrometry-grade trypsin was added in a 1:20 w/w ratio of trypsin to sample DW. Samples were digested overnight at 65 °C in 200 µL of 50 mM ammonium bicarbonate. Samples were filtered through 100 kDa molecular weight cut-off centrifugal filters and diluted 4:1 in 0.1% formic acid, yielding a colorless, transparent digest. The digests were analyzed using a Thermo Fisher Scientific UltiMate 3000 RSLC system with an Acclaim® PepMap RSLC column coupled to a Thermo Fisher Scientific Orbitrap Fusion Lumos mass spectrometer. Solvent A was 0.1% formic acid in water, and solvent B was 0.1% formic acid in acetonitrile. The gradient was as follows: 4% to 25% solvent B over 57 minutes, a flow rate of 300 nL/min, and a total run time of 60 minutes. Label-free quantitation was carried out using MaxQuant as previously described³³. Briefly, raw files were searched using MaxQuant (v. 1.6.0.16) against a FASTA containing the *Sus scrofa* proteome (SwissProt, version from May 2021) and *Sus scrofa* collagen proteins (TrEMBL). For quantification, intensities were determined as the full peak volume over the retention time profile.

Mechanical testing and analysis

For mechanical testing, creep indentation and uniaxial tensile tests were performed. For creep indentation testing, a 3 mm diameter punch of neocartilage was indented using a flat 1 mm diameter porous tip under a constant load, and force-displacement curves were fit to a linear biphasic model using finite element optimization and semi-analytical solutions to obtain aggregate modulus, Poisson's ratio, and permeability, as previously described³⁴. For uniaxial tensile tests, a dog bone-shaped piece of the neocartilage was glued to paper tabs, loaded into an Instron uniaxial tension machine, and pulled to failure at a rate of 1% strain per second. Force-displacement curves were used to calculate tensile Young's modulus and ultimate tensile strength (UTS) using a custom MathWorks' MATLAB code, as previously described³⁵.

Histological processing and staining

Immediately after culture, constructs were fixed in 10% neutral-buffered formalin for at least 72 hours. Constructs were then processed, embedded in paraffin, and sectioned at 6 μm thickness using a microtome. Sections were mounted on slides and stained with Safranin O (Saf O), Picrosirius Red (Sirius Red), and Hematoxylin and Eosin (H&E).

Statistical analyses

All statistical analysis was done with GraphPad's Prism 9. Quantitative gross morphological, biochemical, mechanical, and proteomic data was assessed using a one-way analysis of variance (ANOVA) with *post hoc* Tukey's honestly significant difference (HSD) test. Significance levels were set at $\alpha = 0.05$. A connecting letters report is used to show significant differences from the *post hoc* test, where groups that do not share the same letter are significantly different.

Results

Gross morphology and histology

Hydration for juvenile and adult constructs was $83.1 \pm 1.5\%$ and $83.3 \pm 1.5\%$ respectively (Table 1). Neonatal constructs exhibited a significantly lower hydration ($80.7 \pm 1.1\%$) when compared to juvenile ($p=0.001$) and adult ($p=0.005$) constructs, which were not significantly different from one another (Table 1). Neonatal constructs were significantly larger in diameter than juvenile and adult constructs (both $p < 0.0001$), while juvenile constructs were significantly thicker than neonatal and adult constructs (both $p < 0.0001$) (Figure 2A-C, Table 1). Adult constructs also appeared slightly more curved than neonatal and juvenile constructs (Figure 2A-C). Staining for general tissue and cellular morphology using H&E and total collagen content using Sirius Red appeared relatively consistent among constructs (Figure 2D-I). However, Saf O staining for GAG content appeared slightly more intense in neonatal constructs (Figure 2J) when compared to juvenile and adult constructs (Figure 2K-L).

Table 1. Morphological properties of neocartilage constructs. Juvenile and adult constructs exhibit significantly higher hydration, while neonatal constructs are significantly larger in diameter, and juvenile constructs are significantly thicker when compared to other groups.

Group	Hydration (%)	Diameter (mm)	Thickness (mm)
Neonatal	80.7±1.1 ^B	6.59±0.12 ^A	0.64±0.04 ^B
Juvenile	83.1±1.5 ^A	5.99±0.19 ^B	0.92±0.07 ^A
Adult	83.3±1.5 ^A	6.02±0.10 ^B	0.71±0.08 ^B

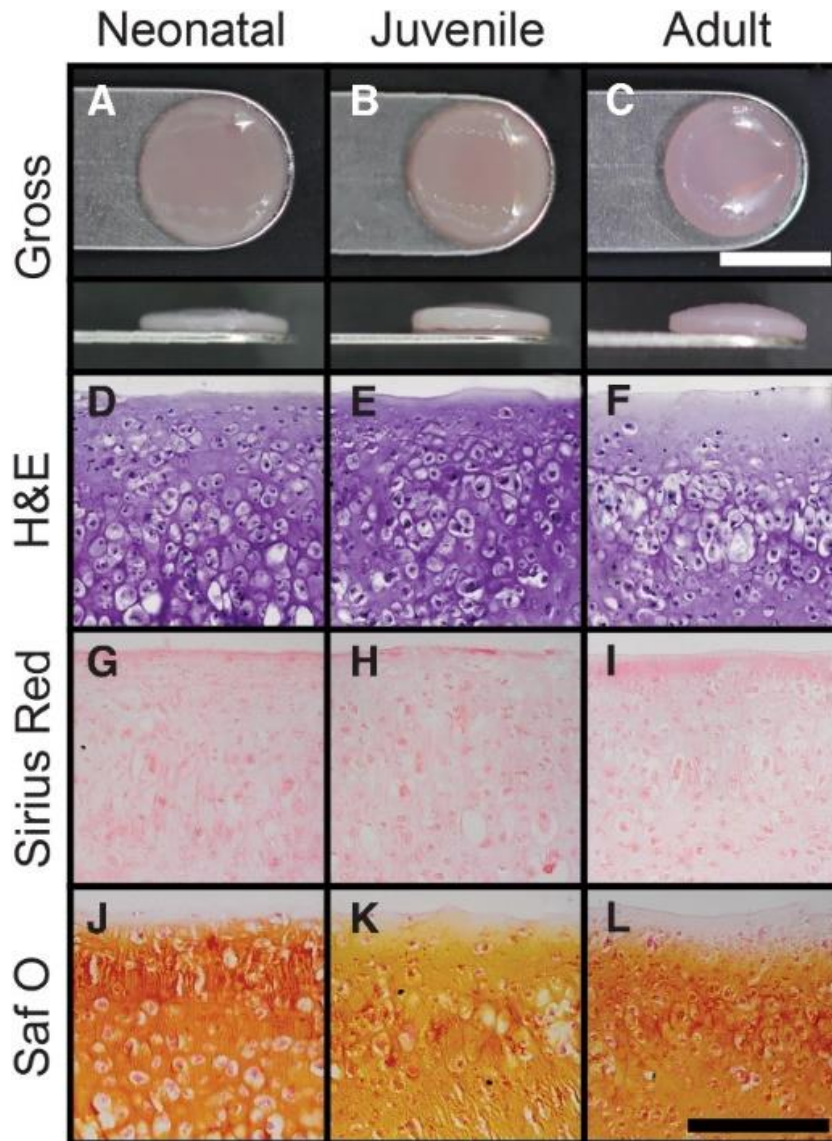


Figure 2. Gross morphology and histology of neocartilage constructs. Of the three groups examined, (A) neonatal, (B) juvenile, and (C) adult constructs, neonatal constructs appear to be the largest in diameter, and juvenile constructs appear thickest. Consistent staining by H&E (D–F) and by Sirius Red (G–I) for total collagen is observed. Slightly increased Saf O staining intensity was observed in (J) neonatal constructs compared to (K) juvenile and (L) adult constructs. White scale bar = 5 mm, black scale bar = 200 μ m.

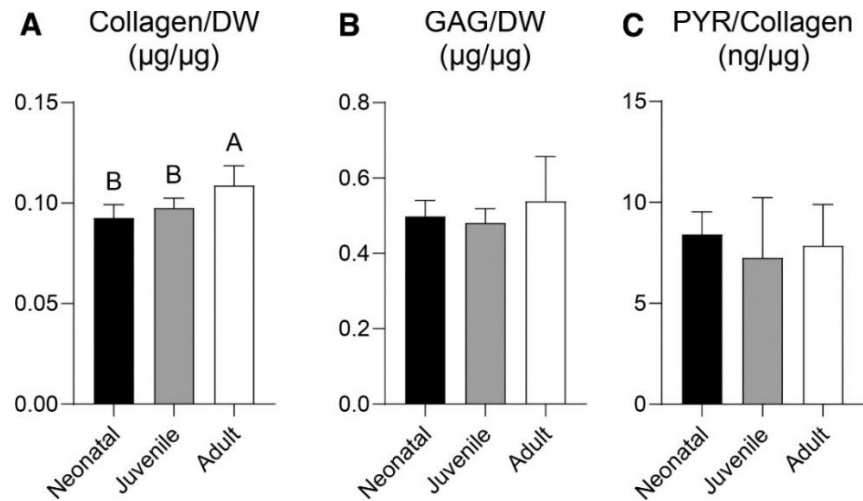


Figure 3. Biochemical properties of neocartilage constructs. (A) Collagen/DW increases with age of construct donors, while (B) GAG/DW and (C) PYR/Collagen did not exhibit any significant differences. DW, dry weight; GAG, glycosaminoglycan; HSD, honestly significant difference; PYR, pyridinoline.

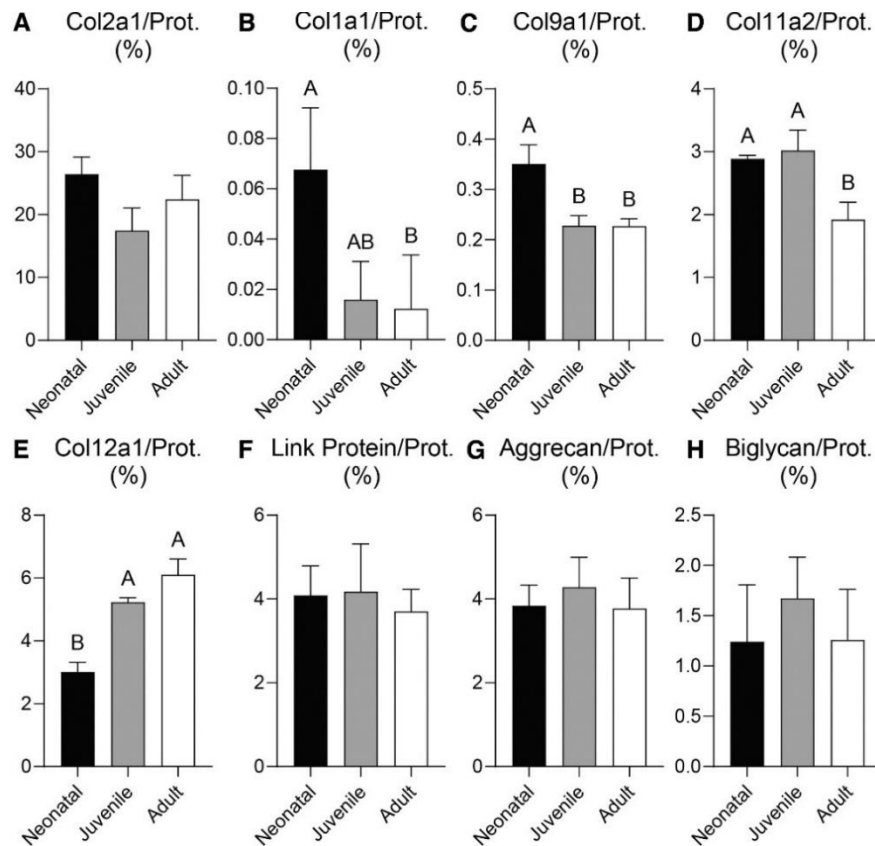


Figure 4. Proteomic analysis of neocartilage constructs. Interestingly, (A)Col2a1 protein did not significantly differ among groups, while (B)Col1a1, (C)Col9a1, and (D)Col11a2 proteins were significantly higher in neonatal constructs compared to adult constructs. Contrastingly, (E)Col12a1 protein content trends higher in adult-derived constructs, while there were no differences in (F) link protein, (G) aggrecan, and (H) biglycan, three crucial components of the matrix. Prot., protein.

Biochemical and proteomic properties

Collagen/DW for neonatal and juvenile constructs was 0.092 ± 0.006 $\mu\text{g}/\mu\text{g}$ and 0.098 ± 0.005 $\mu\text{g}/\mu\text{g}$, respectively, which was significantly less than the adult constructs (0.109 ± 0.010 $\mu\text{g}/\mu\text{g}$, $p=0.001$, $p=0.017$) (Figure 3A). GAG/DW for neonatal, juvenile, and adult constructs was 0.498 ± 0.042 $\mu\text{g}/\mu\text{g}$, 0.481 ± 0.037 $\mu\text{g}/\mu\text{g}$, and 0.539 ± 0.119 $\mu\text{g}/\mu\text{g}$, respectively; there was no statistical difference among the three groups (Figure 3B). There was also no statistical difference in PYR/Collagen (Figure 3C).

Eight proteins of interest were selected based on known roles in cartilage extracellular matrix. *Col2a1* protein content did not significantly differ among groups, but *Col1a1* ($p=0.039$), *Col9a1* ($p=0.003$), and *Col11a2* ($p=0.007$) protein content were all statistically higher in the neonatal group compared to adult-derived constructs (Figure 4A-D). The opposite was true for *Col12a1* protein content, statistically increasing in both juvenile ($p=0.001$) and adult ($p<0.0001$) construct groups compared to neonatal-derived constructs (Figure 4E). There were no statistical differences in link protein, aggrecan, and biglycan among the groups (Figure 4F-H).

Mechanical properties

Tensile properties remained unaffected as donor age was varied for constructs. When compared to neonatal constructs (1.91 ± 0.49 MPa), Young's modulus values of juvenile and adult constructs decreased by 23.9% and 24.5%, respectively; however, this trend was not significant (Figure 5A). UTS values varied from 0.37 ± 0.19 MPa for juvenile constructs to 0.52 ± 0.16 MPa for neonatal constructs (Figure 5B). Strain at failure increased with donor age, from 0.35 ± 0.06 mm/mm to 0.49 ± 0.15 mm/mm, although no groups were statistically different from one another (Figure 5C).

Compressive measurements include aggregate modulus, Poisson's ratio, and permeability from creep indentation testing. Aggregate modulus values significantly decreased between neonatal (409 ± 135 kPa) and juvenile (248 ± 104 kPa) constructs ($p=0.0199$) (Figure 5D). Additionally, the aggregate modulus of adult constructs significantly decreased by 39.8% from

neonatal constructs ($p=0.023$) (Figure 5D). The juvenile and adult groups did not differ in aggregate modulus values (Figure 5D). Poisson's ratio significantly changed among all groups; neonatal-derived constructs were significantly higher than both juvenile- ($p<0.0001$) and adult-derived ($p=0.041$) constructs (Figure 5E). For permeability, the values ranged from $56\pm37 \cdot 10^{-15} \text{ m}^4/\text{Ns}$ and $81\pm45 \cdot 10^{-15} \text{ m}^4/\text{Ns}$ (Figure 5F).

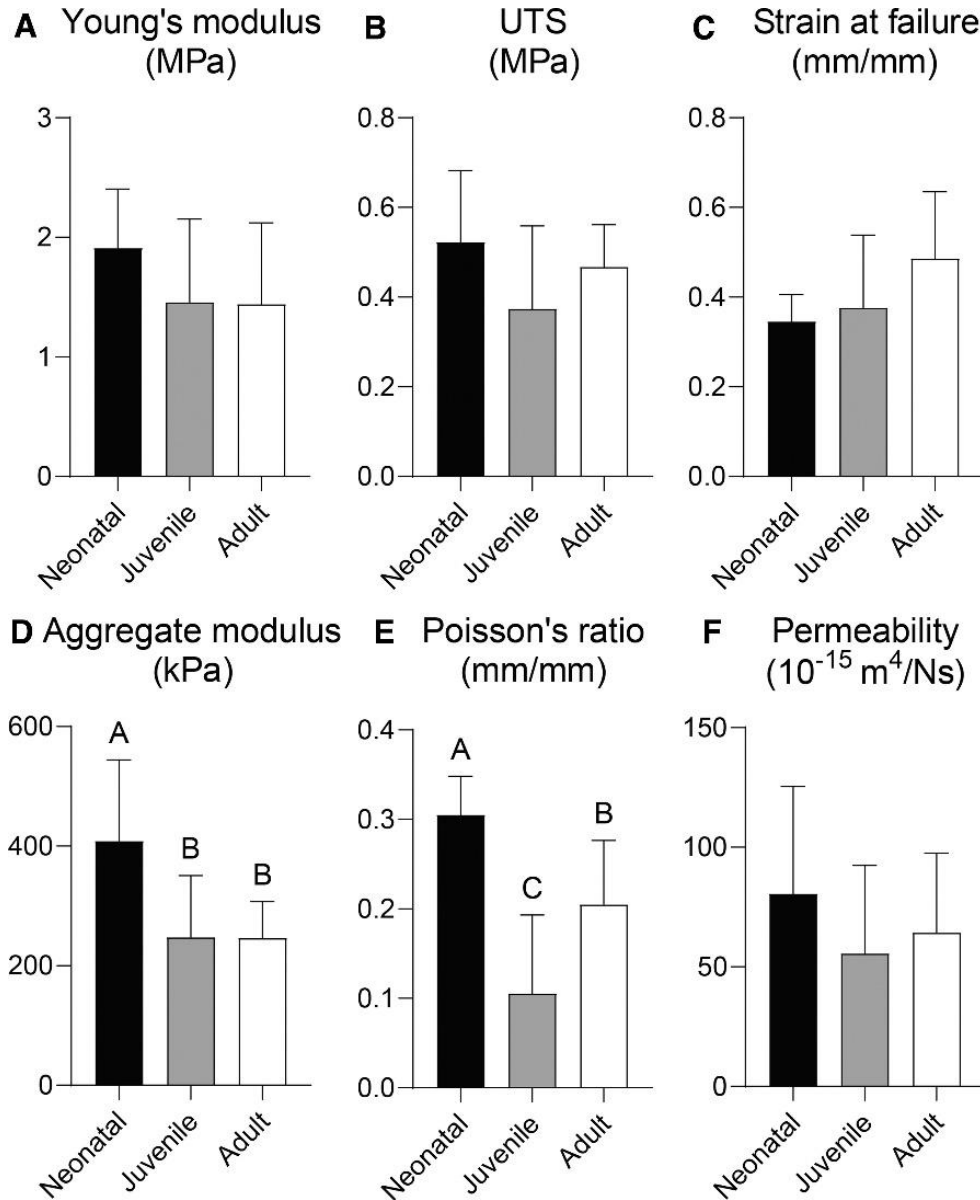


Figure 5. Mechanical properties of neocartilage constructs. Tensile properties, including (A) Young's modulus, (B) UTS, and (C) strain at failure, did not exhibit any significant differences. (D) Aggregate modulus significantly decreased with age of cell source from neonatal to juvenile and adult constructs, while (E) Poisson's ratio was significantly different among all groups. (F) Permeability remained unaffected by donor age. UTS, ultimate tensile strength.

Discussion

Tissue engineering of functional biologic implants is emerging as a potential solution for articular cartilage lesions, but neotissue development may be hindered by 1) donor tissue scarcity due to diseased tissue, 2) dedifferentiation of mature chondrocytes during expansion, and 3) varying functional output of chondrocytes due to differences in donor age. Toward overcoming two of three of these hurdles, costal cartilage, used here, has been explored as a donor tissue due to the cells' exceptional capability to expand and redifferentiate toward a chondrogenic phenotype. Toward addressing the last hurdle, this study's objective was to investigate the age-dependent, functional differences among neocartilage formed from neonatal, juvenile, and adult donors. It should be noted that the skeletally mature adult minipig donors used here would be equivalent to a young adult human, up to 25 years old²⁷. Generally, it was hypothesized that donor age will affect the biochemical and mechanical properties of neocartilage constructs. Surprisingly, despite age having been shown as a significant factor in the utility of articular chondrocytes⁶⁻⁸, for costal chondrocytes processed using the methods described here, such effects were generally not observed, most likely due to the rejuvenation process. Our results showed that age-related differences among constructs are minimal using costal chondrocytes from relatively young donors in conjunction with the tissue engineering processes described here and that differences in the production of minor collagens and compressive properties may be what differentiates younger and older donor neocartilages.

Gross morphological, biochemical, and mechanical analyses showed only minute differences in the measured outcomes. For gross measurements, neonatal-derived constructs were 9.5% larger in diameter, while juvenile-derived constructs were 29.5% thicker, than adult-derived constructs. The most drastic increase was in the aggregate modulus values of neonatal-derived constructs, with a significant 65% increase over adult constructs. Poisson's ratio also differed among constructs of different donor ages. However, the other measures including GAG content, PYR content, permeability, Young's modulus, UTS, and strain at failure were not

significantly different among groups. The tissue engineering process used here appears to modulate expanded then redifferentiated costal chondrocytes to a similar baseline of functional properties, showing few mechanical and biochemical differences among groups. Interestingly, the total collagen content was significantly higher in adult constructs, rising 11.5% over juvenile-derived constructs. In short, these results suggest that the use of costal cartilage in conjunction with aggregate rejuvenation may yield constructs with minimal functional differences due to age-related variability within younger donor populations.

To further investigate the differences in neocartilage matrix content, bottom-up proteomic analysis was used to highlight the differences in matrix proteins among constructs derived from neonates, juveniles, and young adults. The most abundant collagen subtype, collagen type II, did not exhibit significant differences among groups. Collagen type I was reduced with age, with the highest content in neonatal-derived constructs. Collagen types IX and XI also displayed this trend, which is expected, because their expression in native articular cartilage decreases with age^{36,37}. These collagen subtypes (IX and XI) are colocalized with collagen type II in articular cartilage^{38,39}. Interestingly, collagen type XII, a fibril-associated collagen that colocalizes with collagen type I fibrils in ligament, perichondrium, periosteum, dermis, and skeletal muscle⁴⁰⁻⁴³, increased with donor age. A study on collagen type XII spatial and temporal expression has shown that staining was present in the chondrocytes of the growth plate but was not associated at any developmental stage with the secondary ossification center⁴⁴. Postnatally, collagen type XII expression also increased in chondrocytes in the articular surface with age⁴⁴. This corroborates our finding that collagen type XII is present in higher amounts in the adult-derived constructs. Additionally, as is the case with a majority of biochemical and mechanical properties, other matrix content, including link protein, aggrecan, and biglycan, did not significantly differ among the three age groups. Although there are differences in the collagen subtype profile, it is not yet apparent how individual collagen subtypes might affect the mechanical properties of neocartilage; thus, future studies

should investigate the structure-function properties of these minor collagens and neocartilage mechanical properties.

The biochemical and mechanical values reported here are on par with those of previous studies that use various ages and species under control conditions (i.e., no supplementation of the self-assembling process with bioactive factors or mechanical stimulation) to engineer neocartilage constructs. For example, the Young's modulus and UTS reported here ranged from 1.44-1.91 MPa and 0.15-0.36 MPa, respectively. Previous studies utilizing porcine costal chondrocytes derived from 6-month-old animals (i.e., juvenile), then expanded three times and redifferentiated for 14 days, averaged approximately 1.35 MPa in Young's modulus⁴⁵. Similarly, constructs derived from the costal cartilage of 1-year-old sheep, expanded three passages then redifferentiated for 11 days, yielded Young's modulus of approximately 1.4 MPa and UTS of approximately 0.33 MPa⁴⁶, on par with the values reported here. Additionally, the GAG and total collagen contents (approximately 1.5-2% per WW and 7-8% per WW, respectively) are on par with the values here⁴⁶. Values of total collagen per WW in a separate study examining skeletally mature minipig costal chondrocytes expanded then redifferentiated are also on par with those presented here²³. Even across separate studies using expanded then redifferentiated costal chondrocytes in the self-assembling process, similar values of functional properties are found among a variety of species and ages, indicating that costal cartilage is a consistent cell source, further bolstering its use as a donor tissue source.

Despite the small differences in functional properties shown here, constructs isolated from different aged donors displayed unexpectedly similar properties after the same amount of expansion, aggregate rejuvenation, and self-assembly. A potential explanation of this result is that previous studies demonstrated that passage number, rather than donor age, may more greatly affect the functional properties of constructs derived from mesenchymal stem cells⁴⁷. Thus, at a standard passage number, donor age may be less of a factor than expected with the tissue engineering process being more influential on functional output. For example, the tissue

engineering process used here includes applying a cocktail of growth factors during expansion to passage 3, which has been shown to rescue cells from dedifferentiation, increasing post-expansion chondrogenic potential in subsequent 3D culture^{16,48-50}. Expansion of human articular chondrocytes, in the presence of TGF- β 1, PDGF-BB, and bFGF, was reported to be up to 3.7-fold more in all age groups and decreased only slightly with age when compared to cells cultured in control medium⁸. Additionally, TGF- β 1, GDF-5, and BMP-2 added during aggregate rejuvenation, have all been developmentally inspired, are implicated in chondrogenesis that occurs during mesenchymal condensation, and are shown to be effective in redifferentiation of articular chondrocytes²⁹. The data presented combined with the historical studies discussed here suggest that these growth factor cocktails, in conjunction with aggregate rejuvenation culture, at least partially ameliorate the age-dependent changes in costal chondrocyte function.

This study shows that the tissue engineering processes described here (i.e., expansion to passage 3, aggregate rejuvenation, and the self-assembling process) result in similarly robust constructs derived from neonates, juveniles, and skeletally mature adults. It is unclear whether this could be applied to older donors (i.e., 24+ month minipigs, corresponding to humans older than 25 years in age) or diseased chondrocytes. The adult minipigs of this study were 18-24 months old. Because Yucatan minipigs reach skeletal maturity at approximately 16-18 months²⁸ and can have a life span up to 15 years⁵¹, these are still relatively young adults, corresponding to a maximum of 25 years old in humans²⁷. Therefore, a limitation of this work is the exclusion of older donors from the study. However, based on literature from human articular chondrocytes⁸, it would be expected that functional properties would decrease in constructs derived from older donors (i.e., 40+ years of age in humans) compared to those examined here. Moreover, the chondrocytes were isolated from healthy cartilage tissue, and, thus, future studies should investigate whether these trends would apply to diseased chondrocytes. Lastly, future studies should focus on additional improvements in functional properties by use of additional stimuli such as bioactive factors³⁴ and mechanical bioreactors^{46,52} toward improving neocartilage properties to

native tissue values. Once design criteria are met, the *in vivo* performance of constructs in both healthy adults and diseased elderly patients should be examined in a clinically relevant defect model, establishing the potential reparative or regenerative effects of constructs derived from different donor ages. Despite the need for continued work in this area, the current study is significant in that it demonstrates that a range of relatively young donor ages may be used to generate mechanically robust, self-assembled neocartilage of similar functional properties.

This is the first study to investigate the effects of donor age on the self-assembling process. Using costal chondrocytes which were expanded and rejuvenated, it was demonstrated that, while neonatal chondrocytes yielded constructs with significantly higher aggregate modulus values and skeletally mature constructs had higher total collagen content, the majority of functional properties of the constructs were not significantly different among groups. This phenomenon is most likely due to the rejuvenation step used in the construct engineering process, which may have overcome any apparent age-related functional differences. Although functional properties were largely similar among donors of different ages, several minor collagens were modulated by donor age. These findings suggest that the tissue engineering processes used to fabricate self-assembled and mechanically robust neocartilage from passaged and rejuvenated chondrocytes are effective on chondrocytes isolated from young donors (i.e., 0-25 years in human age) of different developmental stages. Translationally, this is significant in that donors from a wide range of ages, from neonates to young adults, may be able to donate cells for expansion and the generation of allogeneic cartilage implants, which can help facilitate an efficient and comprehensive donor selection process.

References

- 1 Fernandes, T. L. *et al.* Macrophage: A Potential Target on Cartilage Regeneration. *Frontiers in immunology* **11**, 111-111, doi:10.3389/fimmu.2020.00111 (2020).
- 2 Camarero-Espinosa, S., Rothen-Rutishauser, B., Foster, E. J. & Weder, C. Articular cartilage: from formation to tissue engineering. *Biomater Sci* **4**, 734-767, doi:10.1039/c6bm00068a (2016).
- 3 Centers for Disease Control and Prevention. *Osteoarthritis*, <<https://www.cdc.gov/arthritis/basics/osteoarthritis.htm>> (2020).

- 4 Centers for Disease Control and Prevention. *Arthritis-Related Statistics*,
<https://www.cdc.gov/arthritis/data_statistics/arthritis-related-stats.htm> (2018).
- 5 Dunkin, B. S. & Lattermann, C. New and Emerging Techniques in Cartilage Repair: MACI.
Oper Tech Sports Med **21**, 100-107, doi:10.1053/j.otsm.2013.03.003 (2013).
- 6 Adkisson, H. D. t. *et al.* The potential of human allogeneic juvenile chondrocytes for
restoration of articular cartilage. *Am J Sports Med* **38**, 1324-1333,
doi:10.1177/0363546510361950 (2010).
- 7 Smeriglio, P. *et al.* Comparative potential of juvenile and adult human articular
chondrocytes for cartilage tissue formation in three-dimensional biomimetic hydrogels.
Tissue Eng Part A **21**, 147-155, doi:10.1089/ten.TEA.2014.0070 (2015).
- 8 Barbero, A. *et al.* Age related changes in human articular chondrocyte yield, proliferation
and post-expansion chondrogenic capacity. *Osteoarthritis Cartilage* **12**, 476-484,
doi:10.1016/j.joca.2004.02.010 (2004).
- 9 Huang, B. J., Brown, W. E., Keown, T., Hu, J. C. & Athanasiou, K. A. Overcoming
Challenges in Engineering Large, Scaffold-Free Neocartilage with Functional Properties.
Tissue Eng Part A **24**, 1652-1662, doi:10.1089/ten.TEA.2017.0495 (2018).
- 10 Eckstein, F., Winzheimer, M., Hohe, J., Englmeier, K. H. & Reiser, M. Interindividual
variability and correlation among morphological parameters of knee joint cartilage plates:
analysis with three-dimensional MR imaging. *Osteoarthritis Cartilage* **9**, 101-111,
doi:10.1053/joca.2000.0365 (2001).
- 11 Hunziker, E. B., Quinn, T. M. & Hauselmann, H. J. Quantitative structural organization of
normal adult human articular cartilage. *Osteoarthritis Cartilage* **10**, 564-572,
doi:10.1053/joca.2002.0814 (2002).
- 12 Kwon, H., Brown, W. E., O'Leary, S. A., Hu, J. C. & Athanasiou, K. A. Rejuvenation of
extensively passaged human chondrocytes to engineer functional articular cartilage.
Biofabrication, doi:10.1088/1758-5090/abd9d9 (2021).
- 13 Darling, E. M. & Athanasiou, K. A. Rapid phenotypic changes in passaged articular
chondrocyte subpopulations. *J Orthop Res* **23**, 425-432,
doi:10.1016/j.orthres.2004.08.008 (2005).
- 14 Arzi, B. *et al.* Cartilage immunoprivilege depends on donor source and lesion location.
Acta Biomater **23**, 72-81, doi:10.1016/j.actbio.2015.05.025 (2015).
- 15 Murphy, M. K., DuRaine, G. D., Reddi, A., Hu, J. C. & Athanasiou, K. A. Inducing articular
cartilage phenotype in costochondral cells. *Arthritis Res Ther* **15**, R214,
doi:10.1186/ar4409 (2013).
- 16 Murphy, M. K., Huey, D. J., Reimer, A. J., Hu, J. C. & Athanasiou, K. A. Enhancing post-
expansion chondrogenic potential of costochondral cells in self-assembled neocartilage.
PLoS One **8**, e56983, doi:10.1371/journal.pone.0056983 (2013).
- 17 Choi, W. R. & Jang, Y. J. Reconstruction of a Severely Damaged Cartilaginous Septum
with a Bypass L-Strut Graft using Costal Cartilage. *Facial Plast Surg* **37**, 92-97,
doi:10.1055/s-0041-1722957 (2021).
- 18 El-Sayed, K. M. Temporomandibular joint reconstruction with costochondral graft using
modified approach. *Int J Oral Maxillofac Surg* **37**, 897-902, doi:10.1016/j.ijom.2008.07.023
(2008).
- 19 Lee, J., Lee, E., Kim, H. Y. & Son, Y. Comparison of articular cartilage with costal cartilage
in initial cell yield, degree of dedifferentiation during expansion and redifferentiation
capacity. *Biotechnol Appl Biochem* **48**, 149-158, doi:10.1042/BA20060233 (2007).
- 20 Cho, S. A. *et al.* Effects of hesperidin loaded poly(lactic-co-glycolic acid) scaffolds on
growth behavior of costal cartilage cells in vitro and in vivo. *J Biomater Sci Polym Ed* **25**,
625-640, doi:10.1080/09205063.2014.888304 (2014).

- 21 O'Sullivan, N. A. *et al.* Adhesion and integration of tissue engineered cartilage to porous polyethylene for composite ear reconstruction. *J Biomed Mater Res B Appl Biomater* **103**, 983-991, doi:10.1002/jbm.b.33269 (2015).
- 22 Huwe, L. W., Brown, W. E., Hu, J. C. & Athanasiou, K. A. Characterization of costal cartilage and its suitability as a cell source for articular cartilage tissue engineering. *J Tissue Eng Regen Med* **12**, 1163-1176, doi:10.1002/term.2630 (2018).
- 23 Vapniarsky, N. *et al.* Tissue engineering toward temporomandibular joint disc regeneration. *Sci Transl Med* **10**, 1-10, doi:10.1126/scitranslmed.aag1802 (2018).
- 24 Guerne, P. A., Blanco, F., Kaelin, A., Desgeorges, A. & Lotz, M. Growth factor responsiveness of human articular chondrocytes in aging and development. *Arthritis Rheum* **38**, 960-968, doi:10.1002/art.1780380712 (1995).
- 25 National Institute of Child Health and Human Development. *Puberty and Precocious Puberty*, <<https://www.nichd.nih.gov/health/topics/puberty>> (2021).
- 26 Premier BioSource. *Swine Models*, <<http://www.premierbiosource.com/swine-models>>
- 27 Cech, D. J. & Martin, S. T. in *Functional Movement Development Across the Life Span (Third Edition)* (eds Donna J. Cech & Suzanne "Tink" Martin) 105-128 (W.B. Saunders, 2012).
- 28 Vapniarsky, N. *et al.* The Yucatan Minipig Temporomandibular Joint Disc Structure-Function Relationships Support Its Suitability for Human Comparative Studies. *Tissue Eng Part C Methods* **23**, 700-709, doi:10.1089/ten.TEC.2017.0149 (2017).
- 29 Murphy, M. K., Huey, D. J., Hu, J. C. & Athanasiou, K. A. TGF-beta1, GDF-5, and BMP-2 stimulation induces chondrogenesis in expanded human articular chondrocytes and marrow-derived stromal cells. *Stem Cells* **33**, 762-773, doi:10.1002/stem.1890 (2015).
- 30 Huang, B. J., Huey, D. J., Hu, J. C. & Athanasiou, K. A. Engineering biomechanically functional neocartilage derived from expanded articular chondrocytes through the manipulation of cell-seeding density and dexamethasone concentration. *J Tissue Eng Regen Med* **11**, 2323-2332, doi:10.1002/term.2132 (2017).
- 31 Cissell, D. D., Link, J. M., Hu, J. C. & Athanasiou, K. A. A Modified Hydroxyproline Assay Based on Hydrochloric Acid in Ehrlich's Solution Accurately Measures Tissue Collagen Content. *Tissue Eng Part C Methods* **23**, 243-250, doi:10.1089/ten.tec.2017.0018 (2017).
- 32 Gonzalez-Leon, E. A., Bielajew, B. J., Hu, J. C. & Athanasiou, K. A. Engineering self-assembled neomenisci through combination of matrix augmentation and directional remodeling. *Acta Biomater* **109**, 73-81, doi:10.1016/j.actbio.2020.04.019 (2020).
- 33 Cox, J. & Mann, M. MaxQuant enables high peptide identification rates, individualized p.p.b.-range mass accuracies and proteome-wide protein quantification. *Nat Biotechnol* **26**, 1367-1372, doi:10.1038/nbt.1511 (2008).
- 34 Makris, E. A., MacBarb, R. F., Paschos, N. K., Hu, J. C. & Athanasiou, K. A. Combined use of chondroitinase-ABC, TGF-beta1, and collagen crosslinking agent lysyl oxidase to engineer functional neotissues for fibrocartilage repair. *Biomaterials* **35**, 6787-6796, doi:10.1016/j.biomaterials.2014.04.083 (2014).
- 35 Link, J. M., Hu, J. C. & Athanasiou, K. A. Chondroitinase ABC Enhances Integration of Self-Assembled Articular Cartilage, but Its Dosage Needs to Be Moderated Based on Neocartilage Maturity. *Cartilage*, 1947603520918653, doi:10.1177/1947603520918653 (2020).
- 36 Bruckner, P. & van der Rest, M. Structure and function of cartilage collagens. *Microsc Res Tech* **28**, 378-384, doi:10.1002/jemt.1070280504 (1994).
- 37 Cremer, M. A., Rosloniec, E. F. & Kang, A. H. The cartilage collagens: a review of their structure, organization, and role in the pathogenesis of experimental arthritis in animals and in human rheumatic disease. *J Mol Med (Berl)* **76**, 275-288, doi:10.1007/s001090050217 (1998).

- 38 Eyre, D. R., Wu, J. J. & Woods, P. E. The cartilage collagens: structural and metabolic studies. *J Rheumatol Suppl* **27**, 49-51 (1991).
- 39 Bielajew, B. J., Hu, J. C. & Athanasiou, K. A. Collagen: quantification, biomechanics and role of minor subtypes in cartilage. *Nat Rev Mater* **5**, 730-747, doi:10.1038/s41578-020-0213-1 (2020).
- 40 Sugrue, S. P. *et al.* Immunoidentification of type XII collagen in embryonic tissues. *J Cell Biol* **109**, 939-945, doi:10.1083/jcb.109.2.939 (1989).
- 41 Wessel, H. *et al.* Type XII collagen contributes to diversities in human corneal and limbal extracellular matrices. *Invest Ophthalmol Vis Sci* **38**, 2408-2422 (1997).
- 42 Oh, S. P., Griffith, C. M., Hay, E. D. & Olsen, B. R. Tissue-specific expression of type XII collagen during mouse embryonic development. *Dev Dyn* **196**, 37-46, doi:10.1002/aja.1001960105 (1993).
- 43 Walchli, C., Koch, M., Chiquet, M., Odermatt, B. F. & Trueb, B. Tissue-specific expression of the fibril-associated collagens XII and XIV. *J Cell Sci* **107 (Pt 2)**, 669-681 (1994).
- 44 Gregory, K. E., Keene, D. R., Tufa, S. F., Lunstrum, G. P. & Morris, N. P. Developmental distribution of collagen type XII in cartilage: association with articular cartilage and the growth plate. *J Bone Miner Res* **16**, 2005-2016, doi:10.1359/jbmr.2001.16.11.2005 (2001).
- 45 Murphy, M. K., Masters, T. E., Hu, J. C. & Athanasiou, K. A. Engineering a fibrocartilage spectrum through modulation of aggregate redifferentiation. *Cell Transplant* **24**, 235-245, doi:10.3727/096368913X676204 (2015).
- 46 Huwe, L. W., Sullan, G. K., Hu, J. C. & Athanasiou, K. A. Using Costal Chondrocytes to Engineer Articular Cartilage with Applications of Passive Axial Compression and Bioactive Stimuli. *Tissue Eng Part A* **24**, 516-526, doi:10.1089/ten.TEA.2017.0136 (2018).
- 47 Andrzejewska, A. *et al.* Multi-Parameter Analysis of Biobanked Human Bone Marrow Stromal Cells Shows Little Influence for Donor Age and Mild Comorbidities on Phenotypic and Functional Properties. *Front Immunol* **10**, 2474, doi:10.3389/fimmu.2019.02474 (2019).
- 48 Martin, I., Vunjak-Novakovic, G., Yang, J., Langer, R. & Freed, L. E. Mammalian chondrocytes expanded in the presence of fibroblast growth factor 2 maintain the ability to differentiate and regenerate three-dimensional cartilaginous tissue. *Exp Cell Res* **253**, 681-688, doi:10.1006/excr.1999.4708 (1999).
- 49 Barbero, A., Ploegert, S., Heberer, M. & Martin, I. Plasticity of clonal populations of dedifferentiated adult human articular chondrocytes. *Arthritis Rheum* **48**, 1315-1325, doi:10.1002/art.10950 (2003).
- 50 Hsieh-Bonassera, N. D. *et al.* Expansion and redifferentiation of chondrocytes from osteoarthritic cartilage: cells for human cartilage tissue engineering. *Tissue Eng Part A* **15**, 3513-3523, doi:10.1089/ten.TEA.2008.0628 (2009).
- 51 Chieppa, M. N. *et al.* Modeling amyotrophic lateral sclerosis in hSOD1 transgenic swine. *Neurodegener Dis* **13**, 246-254, doi:10.1159/000353472 (2014).
- 52 Lee, J. K. *et al.* Tension stimulation drives tissue formation in scaffold-free systems. *Nat Mater* **16**, 864-873, doi:10.1038/nmat4917 (2017).